DEVELOPMENT OF GEOTECHNICAL GROUND MODELS FOR SLOPE INSTABILITY, EASTERN SIDE, TAKAKA HILL, TASMAN DISTRICT

A thesis

Submitted in partial fulfilment of the requirements for the degree of

Master of Science in Engineering Geology

at the

University of Canterbury

By

Christine Prasad

2020

Abstract

State Highway 60 (SH60) over Takaka Hill in Tasman District has a long history of damage and closure from rainfall-triggered slope failures. Extreme rainfall from Ex-tropical cyclone Gita on 20th February 2018 triggered numerous translational soil slides on the southern side of Takaka Hill resulting in a series of debris flows that damaged SH60 near Riwaka. Scour erosion of road seal, damage to culverts, and failure of embankment sections led to complete closure of the road for five days, preventing all road access to the Takaka- Collingwood region. The road continues to be reduced to a single lane with traffic control more than two years after the event as repairs are ongoing.

A programme of geomorphic mapping, geophysical profiling, and both *in-situ* and laboratory geotechnical testing was carried out to characterise the 2018 debris flows and investigate the hazard from rainfall-triggered slope failure and debris flows on Takaka Hill. Three stream catchments, on the lower slopes of the southern side of Takaka Hill, were the focus of this investigation. These are underlain by differing bedrock: granite, schist and a basic igneous suite.

Historical records indicate an approximately 30-year recurrence for major events resulting in road closure for ≥ 5 days. The main types of rainfall-triggered failures are culvert blockage, shallow soil slides and debris flows. Smaller failures resulting in temporary road closures occur more frequently.

Extreme rainfall events, often following periods of protracted rainfall trigger shallow translational soil slides in colluvial and residual soil profiles. Failure planes are generally shallower than 5 m. The debris from these failures enters the adjacent drainage courses and is then remobilised as channelised debris flows. The soil slide source colluvium is matrix supported with clasts up to boulder size. Pre-2018 debris flow deposits exposed in stream banks are 1 – 2 m in thickness. Geophysical profiling indicates up to 10 m of accumulated debris flow material in the debris fans on the lower slopes of Takaka Hill, indicating long-term debris flow activity in the area.

Geotechnical characterisation of the colluvial soils in the slide source areas, the debris flow materials from 2018 and prior debris flow events, as well as the weathered bedrock and residual soil profiles encountered in the study area were used to develop detailed engineering geological profiles for the Takaka Hill area. These will provide the basis for any future slope stability analysis.

Acknowledgements

This research would not have been possible without funding from New Zealand Aid Scholarship. Thank you for giving me this opportunity to further my studies. Thank you Nina Hannuksela from the scholarship team for her continuous support.

I would like to express my utmost gratitude to my supervisory team: Clark Fenton (primary supervisor, University of Canterbury), David Bell (co-supervisor, University of Canterbury), and Glenn Stevens (associate supervisor, Tasman District Council). A special thank you to David Bell for his guidance in the last 2 months of writing. Your dedication to help students is applaudable.

Thank you, Glenn Stevens for your continuous support from the very beginning of the project, providing me with data and assisting me with the geophysical field survey. To Tasman District Council, thank you for the financial support for fieldwork.

Thank you, Sean Rees, for your continuous support and advice on soil mechanics concepts and laboratory testing. I would like to thank my friends, Katherine Yates and Romy Ridl, (PhD students) for answering my questions on soils and rocks, and for the encouraging words.

Thank you to the landowners (Steve Ryder and Stephen Tonson) for allowing me to map and collect samples for laboratory testing. To New Zealand Transport Agency and Beca, thank you for providing funding and core samples for laboratory testing.

Thank you to the University of Canterbury geotechnical team: Cathy Higgins, Chris Grimshaw, Matt Cockcroft, Rob Spiers, Sarah Pope, John Southward and Sacha Baldwin.

Thank you to my friends and family for the continuous support. Special thanks to Jessica Boyd for assisting with the geophysical field survey and final formatting. My office and lab buddies Jessica Fensom and Laura Gnesko, thank you for the great company and support.

Last but not least, thank you to my husband Satbir Singh, for coming with me to New Zealand and for your continuous support. Also thanks for being a great field assistant, it would have been difficult to carry all those samples by myself.

Table of Contents

List of Figures

List of Tables

Chapter 1: Introduction

1.1 Context

State Highway 60 (SH60) over Takaka Hill experienced significant damage from debris flows triggered by the passage of Ex-tropical Cyclone Gita in February 2018. SH60 is a critical lifeline road link for residents of Golden Bay, as well as being a popular tourist route (Figure 1.1).

The passage of Ex-tropical Cyclone Gita on 20th February 2018 caused rainfall in excess of 180 mm in a 24-hour period, as recorded at Woodmans Bend, Motueka. This extreme rainfall triggered numerous shallow soil slides and debris flows, causing extensive damage to SH60 on the Motueka side of the Takaka Hill. The road was completely closed for five days, stranding both tourists and residents, and more than two year later parts of the road are still restricted to a single lane and traffic control while repairs are being carried out.

SH60 has a history of road closures from rain-triggered slope instability on the Takaka Hill. New Zealand Transport Agency (NZTA) maintenance records show an average frequency of five events per year. Ex-tropical cyclone Gita was an 'extreme' weather event, although the exact rainfall at the area of greatest damage is unknown as the nearest rain gauge rain gauge was located 4 km away. The magnitude and widespread nature of the debris flows, together with the consequent damage to the road corridor, was similar to a storm event in 1990, when 224 mm fell in a 24-hour period. The impact of Ex-tropical cyclone Gita, along with historical debris flow activity in the region, indicates that this is an ongoing hazard that may be exacerbated by increased frequency of extreme weather events due to climate change. Improved slope stabilisation and stormwater control measures are important given the critical nature of SH60 in providing access for the ~5,000 residents of Golden Bay, which may treble during peak tourist season (November to March) due to visitors.

Despite the region being affected by a number of rainfall-triggered slope failures in the past, to date there has been no detailed study of the landslide hazard. This thesis examines the slope instability triggered by the passage of Ex-tropical cyclone Gita in order to develop an engineering geological evaluation of the failure mechanisms. This understanding is used to suggest approaches for future management of SH60.

1.2 Project area

1.2.1 Location

The field area for this study is located in Tasman District in the northwest part of the South Island, New Zealand. Shown in Figure 1.2, the regional study area outlined in yellow covers approximately 15 km^2. The red polygon bounds the area of detailed analysis for the 2018 debris flows. Three drainage catchments were selected as they are the source areas for debris flows directly affecting SH60 and are under different bedrock lithologies. These drainage courses are underlain by the three principal bedrock lithologies of Ordovician to Cretaceous age found in the area. The oldest unit is the Onekaka Schist, comprising biotite schist and interlayered quartzite. The Devonian-age Undifferentiated Riwaka Igneous Complex consists of mafic and ultramafic igneous rocks, and the biotite-rich Separation Point Granite is widely exposed in north-west Nelson.

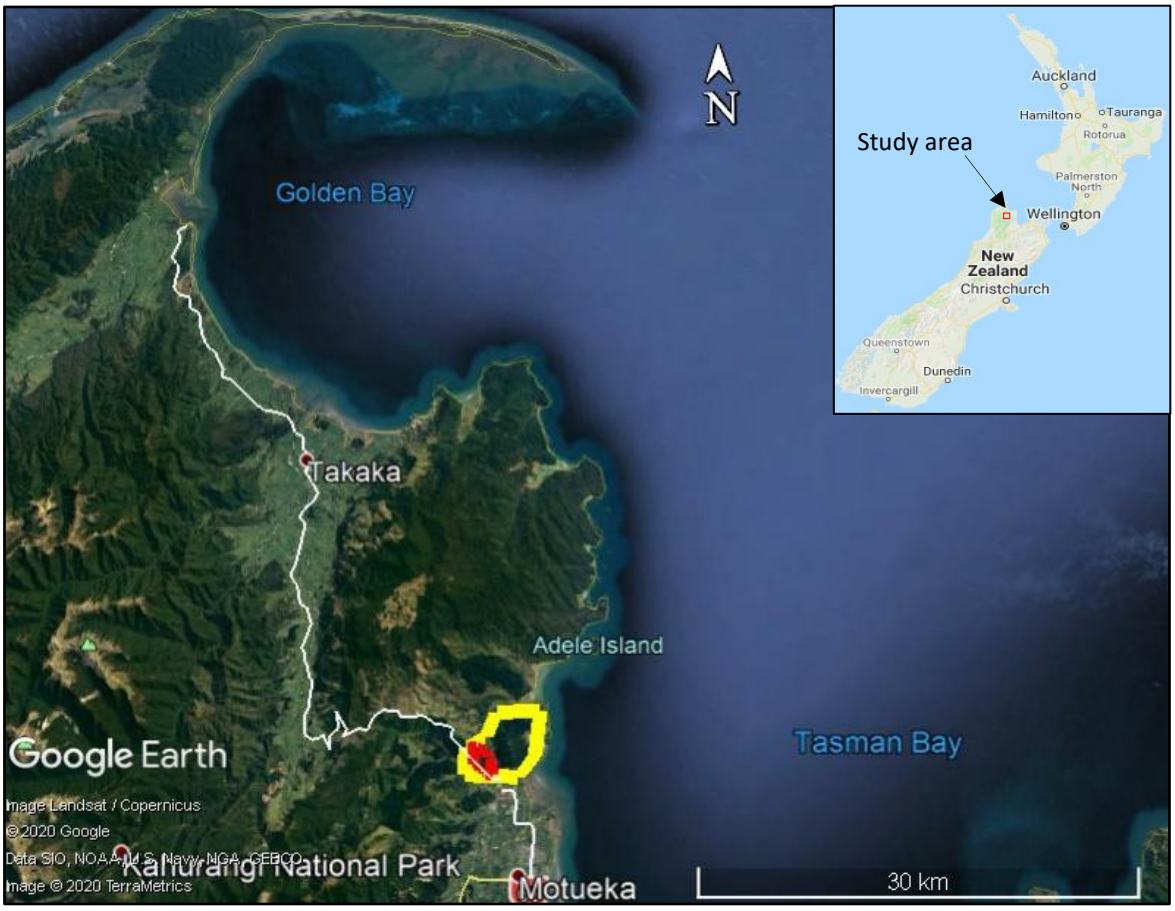

Figure 1.1: Location of Golden Bay. SH60 highlighted in white. The regional study area is outlined in yellow. Source: Google Earth (2019)

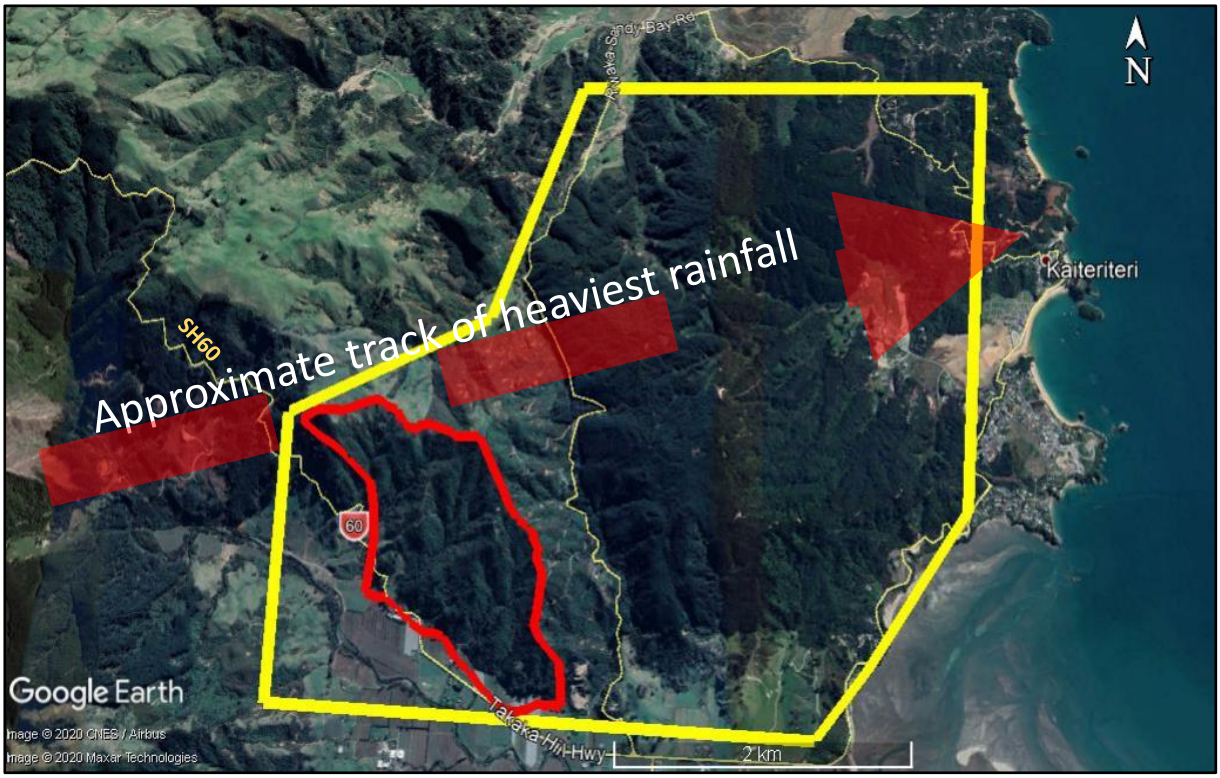

Figure 1.2: Location of Takaka Hill study area. The red polygon bounds the area of detailed catchment analysis for the 2018 debris flows. The yellow polygon indicates the extent of the regional debris flow study, including pre-2018 events. SH60 and the Riwaka-Sandy Bay Road, both damaged in 2018, are shown. Source: Google Earth (2019)

1.2.2 Regional Geological Setting

The northwest (NW) Nelson region lies to the west of the active Australian-Pacific plate boundary (Figure 1.3), which extends through the Hikurangi Trough off the East Coast of the North Island and continues along the West Coast of the South Island. The plate boundary is a transpressional system. Across the Tasman District, this is expressed as a series of NW-striking folds and thrust belts.

In New Zealand the basement rocks are divided into the Western and Eastern Province, separated by the Carboniferous-Cretaceous Median Tectonic Zone. Both are divided into discrete tectono-stratigraphic units (Muir et al., 1995; Rattenbury et al., 1998). The Eastern Province consists of arc volcanic rocks, arc-derived sedimentary sequences, and accretionary complexes of Permian and Mesozoic age, representing products of convergent margin tectonics (Muir et al., 1995). The Western Province is a fragment of Gondwana and comprises Cambrian -Devonian Takaka Terrane and Ordovician Buller Terrane (Muir et al., 1995; Turnbull et al., 2017).

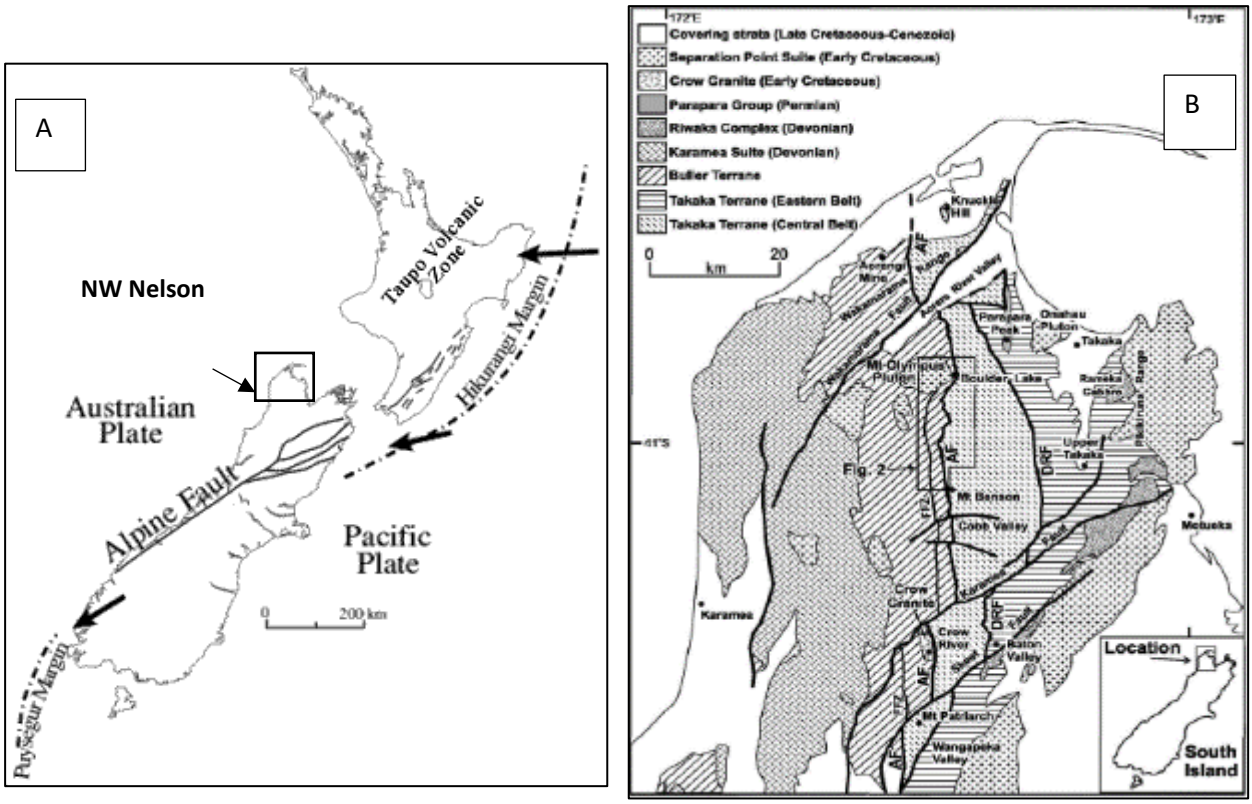

Figure 1.3: Tectonic setting of NW Nelson in New Zealand. Source: (University of Otago, n.d.) (B) Generalised geology of NW Nelson region (Jongens, 2006).

The study area is in the Western Province and is underlain by rocks of the Takaka Terrane. The Takaka Terrane is separated from the Buller Terrane by the north-striking Anatoki Fault (Jongens, 2006). The Anatoki Fault is the most important structure in the basement rocks of NW Nelson, and it is typically marked by a conspicuous but narrow zone of breccia, mylonite and cataclasite. Along the entire length of the Anatoki Fault there is a clear separation of the two terranes, although the sense of movement along the fault has varied with time and there have been several periods of reactivation. The two terranes were originally an appreciable distance apart, probably hundreds of kilometres, as suggested by their histories and tectonic settings (Rattenbury et al., 1998). Amalgamation of the two terranes most likely occurred in the Early to Middle Devonian period, prior to the Karamea Granite and Riwaka Complex emplacement (Rattenbury et al., 1998; Turnbull et al., 2017).

The Takaka Terrane includes at least two major depositional cycles: a Cambrian volcanic arc assemblage, and a Late Cambrian to Early Devonian passive marine succession (Jongens, 2006; Rattenbury et al., 1998). The western part of the terrane, between the Anatoki Fault and Devil River Fault is largely confined to an arc-related sequence which includes the Haupiri Group and Devil River

Volcanics Group. The Haupiri Group is restricted to the sedimentary part of volcano-sedimentary sequence, and includes the oldest rocks dated by fossils in New Zealand. All volcanic and plutonic rocks of the Cambrian to early Ordovician age are part of the Devil River Formation (Rattenbury et al., 1998).

The eastern part of the terrane comprises the passive margin sequence composed of the Mount Arthur and Ellis Groups (Rattenbury et al., 1998). A major change in the depositional regime at the base of the Mount Arthur Group is marked by the onset of carbonate deposition in the Late Cambrian to Early Ordovician. The eastern side of the Takaka Terrane limestone, significantly altered to marble with calcareous mudstone and sandstone and some dolomite bands, is mapped as the Arthur Marble: the western part is mapped as Summit Limestone. The Ellis Group, consisting of thin to thick bedded quartz sandstone, quartzite and siliceous siltstone, overlies the Mount Arthur Group. In the Pikikiruna Range, the metamorphosed Ellis Formation is mapped as **Onekaka Schist** (Johnston, 1974).

The long-lived plate subduction along the eastern Pacific Gondwana margin resulted in Western Province plutonism (Turnbull et al., 2017). The I and S type plutons intrude on the early Palaeozoic Buller and Takaka terranes (Mortimer et al., 1999). The Takaka Terrane is intruded on by the Late Devonian gabbros, diorites, and pyroxenites of the **Riwaka Complex**, whereas the Buller Terrane is mostly intruded on by the late Devonian Karamea Batholith, which are mainly S-type (metasedimentary supracrustal melt) granites (Jongens, 2006; Rattenbury et al., 1998; Turnbull et al., 2017). Both terranes have occurrences of minor contemporaneous I type (meta-igneous intracrustal melts) of Paringa Suite plutonism (Turnbull et al., 2017).

The final stage of magmatism of an extensive arc system, located on the SW Pacific margin of Gondwana during the Mesozoic, is represented by **Separation Point Batholith** in the early Cretaceous. The Separation Point Batholith comprises granite and granodiorite plutons intruded into the lower Palaeozoic Takaka rocks and Riwaka Complex intrusives (Muir et al., 1995; Rattenbury et al., 1998).

Three bedrock lithologies in the study area are as follows: Onekaka Schist, Undifferentiated Riwaka Igneous Complex and Separation Point Suite (also known as Separation Point Granite). For the purpose of this thesis, the Separation Point Suite was called Separation Point Granite. The mapped bedrock geological units in the study area are summarised in Table 1.1 below.

Table 1.1: Summary of bedrock units in the study area (GNS Web Map, 2012; Rattenbury et al., 1998).

Stratigraphic Name	Description
Separation Point Granite (SPG)	Granite and granodiorite
Undifferentiated Riwaka Igneous Complex (URIC)	Undifferentiated gabbro, diorite, pyroxenite, peridotite and amphibolite
Onekaka Schist (OS)	Biotite-muscovite schist with metaquartzite bands

1.2.3 Vegetation and Land use

Vegetation in the catchment area consists of mainly grassland and gorse shrub (Figure 1.4), however, during field investigation it appeared to be leptospermum and fern. The data is from 2015 LINZ Cover databases, the latest vegetation cover map available. The regional study area is covered with exotic forest and scrub. Towards the north east side of this area (exotic forest and scrub) it is mostly underlain by Separation Point Granite with commercial production forest. The other commercial land use practices are agriculture (sheep grazing) and horticulture.

Figure 1.4: Vegetation cover map of the study area, with the detailed catchment in red. From LINZ Cover Database (2015).

1.3 Climate and Hydrology

Although rainfall is fairly uniformly distributed across the year, February and March are generally the driest months, whereas winter and spring are the wettest periods (Figure 1.5). Annual rainfall in parts

of the Tasman Mountains exceeds 6000 mm (Macara, 2016), and over the last thirty years the average annual rainfall at Takaka, recorded at the Riwaka meteorological station, is 1389 mm (Opus, 2001).

Interpretations of climatic data for any rainfall station need to be made with caution, including areas such as the extremely rugged Takaka Hill, which is subject to significant variations in rainfall and has pronounced windward and leeward slopes (Opus International Consultants Limited, 2001).

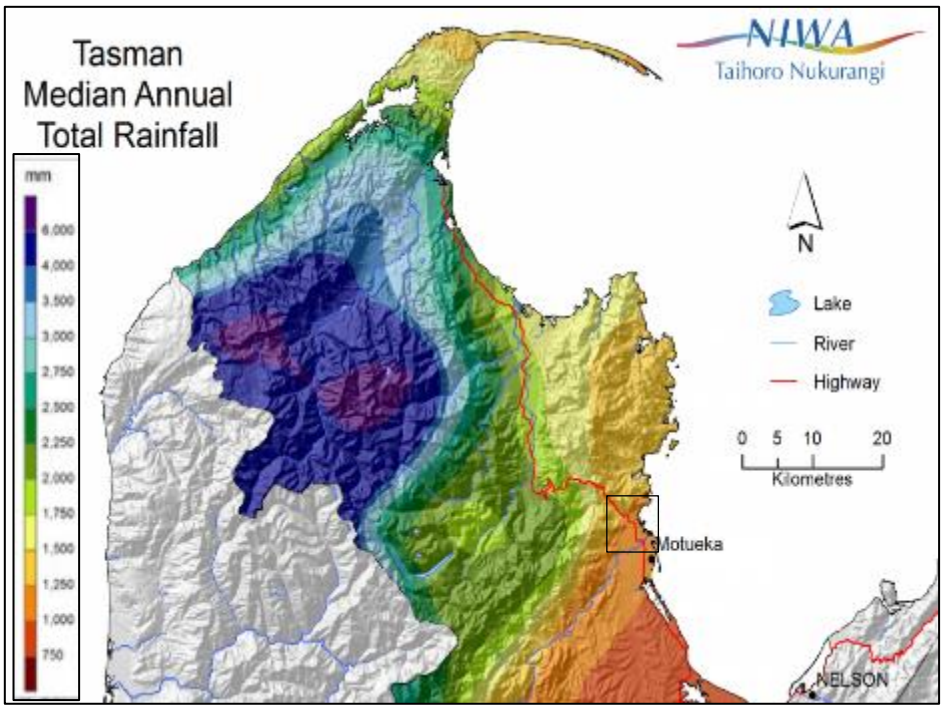

Figure 1.5: Nelson and Tasman median annual rainfall. The study area is outlined in black. The area receives around 1250 mm – 17500 mm annually. Source: (Macara, 2016).

1.3.1 Rainfall Characteristics

SH60 has been reduced to one lane during rainstorms on average five times annually for varying periods due to slips (MWH, 2009; Opus International Consultants Limited, 2001)The road is totally closed for only a few hours once a year due to slips (Opus International Consultants Limited, 2001). Historic rainfall triggered slides and flows in the study area will be discussed in Chapter 2.

Rainfall was the major trigger for the debris flows and slides in February 2018. Rainfall measured at Woodmans Bend near Motueka (Site 1 in Figure 1.6) during Ex-tropical Cyclone Gita exceeded 180 mm for a 24 hour period. The rainfall from Ex-tropical cyclone Gita was localised, but with very few rainfall measurements recorded. Actual rainfall levels and intensities in the most affected areas would have been higher than those recorded. Three rainfall data locations are shown in Figure 1.6. Site 1 recorded 126 mm / 24 hours; Site 2 recorded 183.2 mm / 24 hours; and Site 3 recorded 171.5 mm / 24 hours.

There were no rain gauges in the areas of greatest damage on the Takaka Hill. From personal communication with residents in the study area, debris flow activity started at around 5 pm on 20th February.

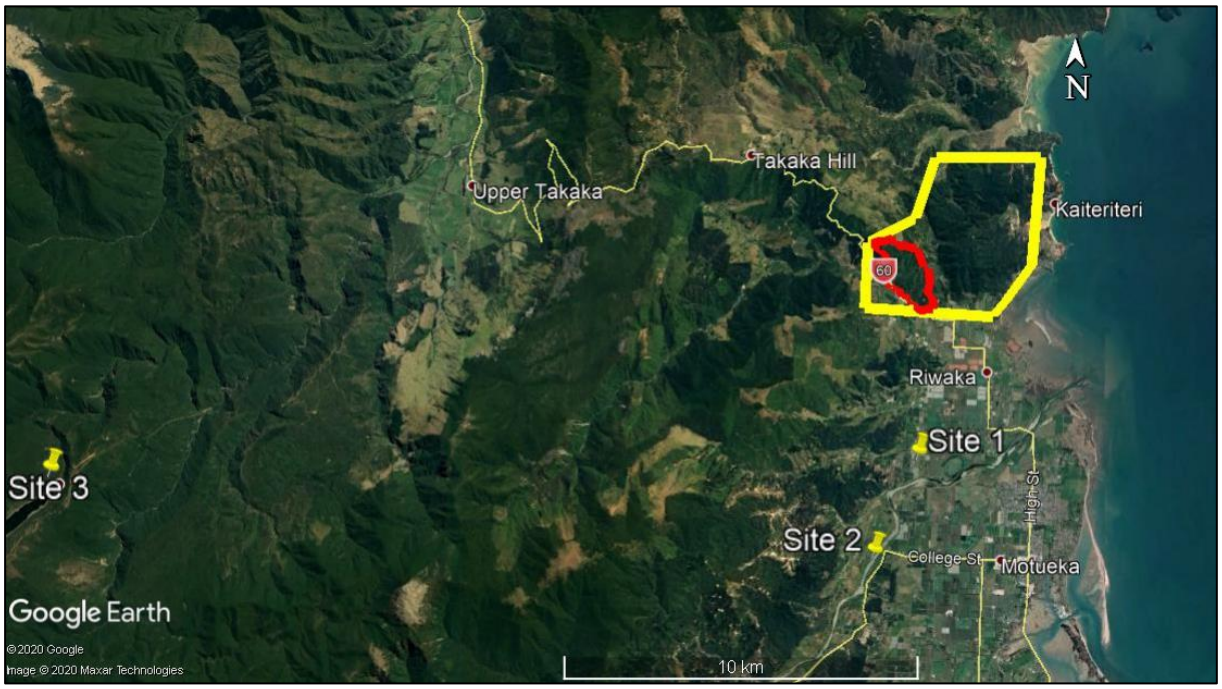

Figure 1.6: Location of sites where rainfall data was taken.

About two and a half weeks prior to Ex-tropical cyclone Gita, the region experienced heavy rainfall from the passage of Ex tropical cyclone Fehi on 1st February 2018, and the Tasman region experienced storm surge and flooding (National Institute of Water and Atmospheric Research [NIWA], n.d). Figure 1.7 shows the rainfall distribution for the month of February 2018.

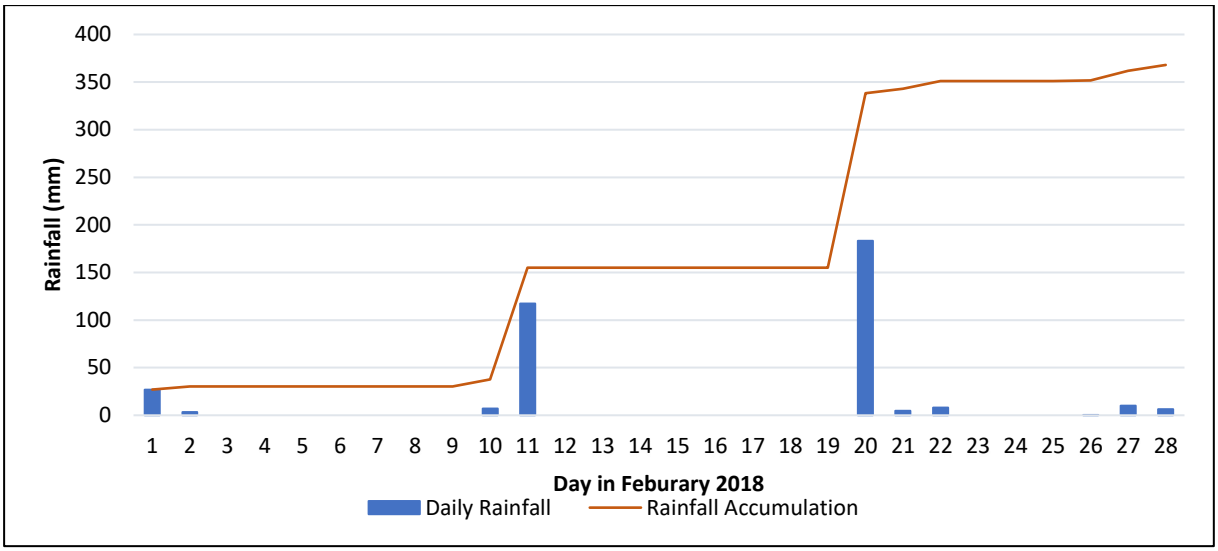

Figure 1.7: Rainfall accumulated for the month of February 2018 is shown by the orange line. The daily documented rainfall for February is displayed in blue. Data was recorded at the Motueka Woodman's Bend site (Figure 1.6) and supplied by Tasman District Council.

1.4 Geology and Geomorphology of Study Area

The geology of the study area is complex, with multiple faults and geological units (Figure 1.8). The Pikikiruna and Pisagh Faults are the major faults in this area, and, according to the GNS active faults database, these faults are inactive (Page et al., 2012). In the study area the Takaka Hill comprises a series of steep catchments in which debris was mobilised during Ex-tropical cyclone Gita in 2018. The main catchments are intersected by tributary channels, and the slope angles are steep (ranging between 15° and 40°). Three different basement lithologies have been identified: Onekaka Schist, Undifferentiated Riwaka Igneous Complex, and Separation Point Granite (Table 1.1). The main rock types are schist, gabbro, and granite/granodiorite respectively.

Quaternary alluvial fan deposits are prominent on the southern flanks of the Takaka Hill, draining into the Motueka and Riwaka River valleys (Rattenbury et al., 1998). The uneven fan surfaces with large boulders at low elevations in the study area suggest a debris flow history. Pre-2018 debris flow deposits are exposed along the banks in all mapped channels and are both clast and matrix supported. Clasts vary in composition, are sub- angular to sub-rounded, well graded and poorly sorted with chaotic matrix structure.

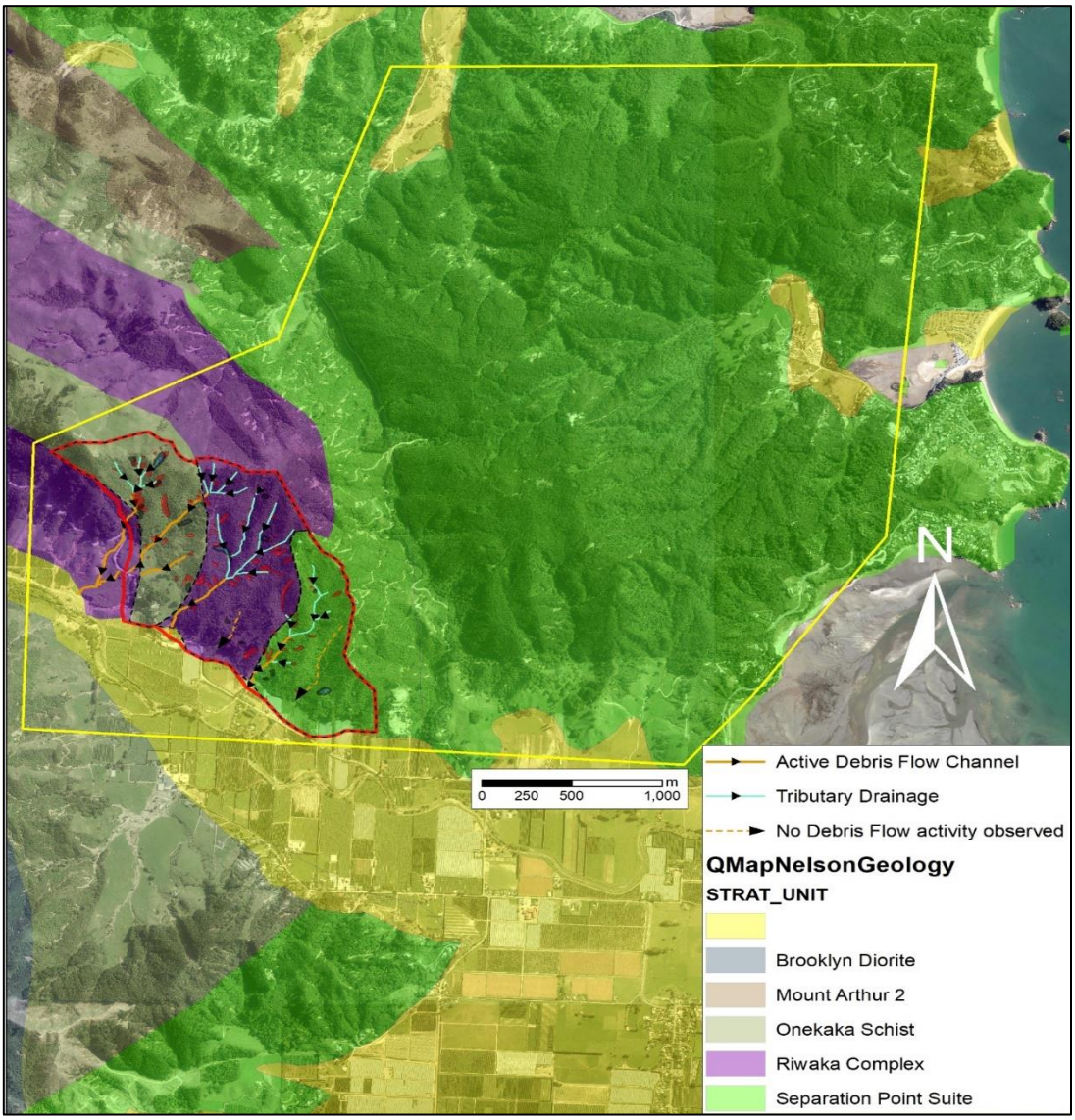

Figure 1.8: Simplified geology and geomorphology of the study area. The geology map is sourced from GNS Web Map (2012).

1.5 Thesis Aim and Scope

Previous slope failures along SH60 over Takaka Hill triggered by heavy rainfall are documented, but this area has not been studied in detail to understand the debris flow hazard. The present research examines in some detail the shallow landslides and debris flows developed on all three lithologies, with a view to providing an engineering geological evaluation of the failure mechanisms and their implications for future management of SH60 and immediately adjacent areas. A key focus is the nature of landsliding in all three lithological units, the relationship to slope angle and matrix clay content, and the controls exerted by sliding at the colluvium-completely weathered bedrock/residual soil interface by infiltration of water. As a result, three catchment areas in three different bedrock lithologies were selected for detailed study.

In summary the aims of the research were to:

- Identify and map landslides ("slips") and debris flows caused by Ex-tropical cyclone Gita.
- Quantify the debris flow magnitude and frequency on Takaka Hill.
- Determine pertinent geotechnical properties of the slope-forming materials.
- Consider implications of the ground models for future management of the SH60 corridor.

1.6 Thesis Organisation

This thesis consists of seven chapters:

- Chapter 2 discusses the past slope instability in the study area.
- Chapter 3 describes the field investigations, including engineering geomorphological mapping, remote sensing, soil sampling and *in situ* testing and geophysical surveys.
- Chapter 4 discusses the geotechnical characteristics of the debris flows and the colluvial source material derived from laboratory tests.
- Chapter 5 presents a geotechnical characterisation of the bedrock source areas and the influence of weathering.
- Chapter 6 presents a synthesis of the various geotechnical investigations, presenting a model for debris flow generation. Recommendations for future management of SH60 are also discussed.

1.7 Terminology Adopted

The soil and rock observed in this study often show diffuse and gradational contacts between the differing units. Similarly the distinction between colluvium, soil slides and debris flows, *sensu stricto,* is often difficult to discern, as the mechanism of failure often display a transition from one mode to another. In order to distinguish between the differing slope materials and the modes of failure, the terminology detailed in the following sections was adopted.

1.7.1 Weathering Profile

During the initial field investigations (see Chapter 3) a generalised soil profile was developed to indicate the relationships among the different soil units encountered on the Takaka Hill (Figure 1.9) from outcrop logging in the study area. This is based on observations from detailed soil profile logs recorded across the study area.

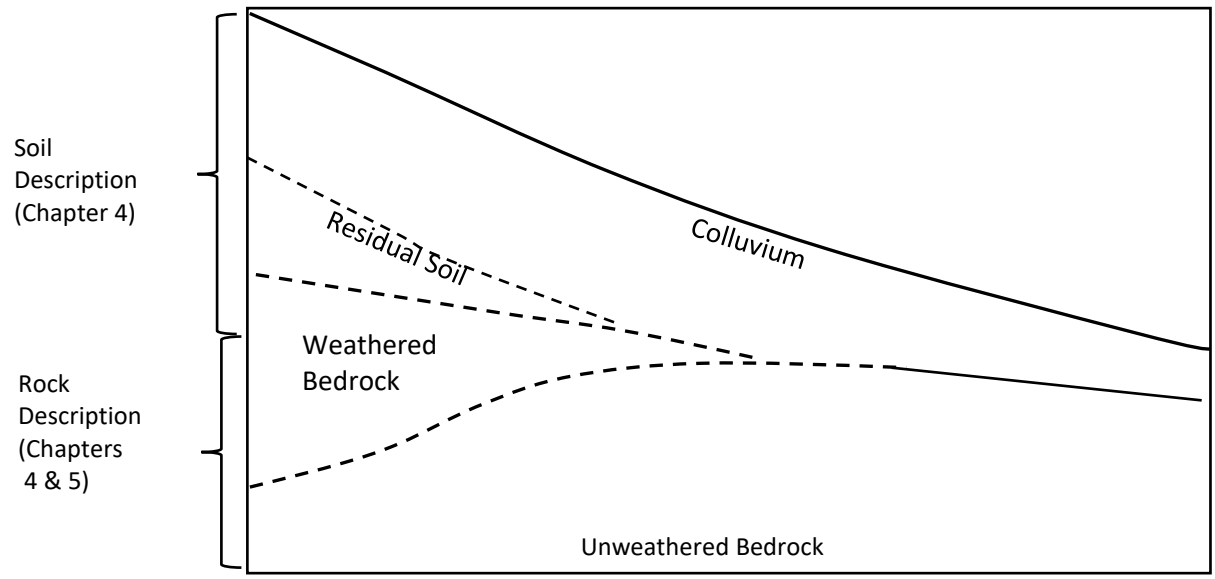

Figure 1.9: Schematic diagram showing relationships among soils found in the study area. Dashed lines indicate gradational or diffuse contacts.

Colluvium is used to describe generally widely graded (and sometimes gap graded) soils covering a slope, the formation of which has involved transportation and deposition by mass wasting processes. Colluvial soil may be derived from the underlying bedrock, the residual soil developed on that bedrock or from prior transported material that has been remobilized by slope processes. The colluvial soils in the study area are divided into two categories: those soils activated as soil slides, and debris flows in 2018 and pre-2018 deposits. The distinction between individual soil units is not always clear, as the contacts are often gradational (Figure 1.9).

The following terms are adapted from (New Zealand Geotechnical Society, 2005) soil and rock description standards to describe the bedrock and residual soil units encountered in the study area:

- **Residual Soil (RS)** is where the rock has completely disaggregated to a soil. It is often difficult to determine whether an exposure is residual soil, with no remnant components of the parent bedrock, or if some remnant mineral grains are present, thus indicating **Completely Weathered Rock (CW).** Thus, a range of definitions is used, and the composite term **CW-RS** is often applied.
- **Highly Weathered Rock (HW)** is distinguished from CW by the presence of some unweathered or slightly weathered rock. By definition more than half the weathered rock mass is altered to soil.
- **Moderately Weathered Rock (MW)** is material that is significantly weakened, and part may have been altered to engineering soil. The composite term MW-HW is used where it is not clear if either term is more appropriate, and where there is evidence of significant alteration to engineering soil in parts of the rock mass.

- **Slightly Weathered Rock (SW)** is distinguished from **Unweathered Rock (UW)** based on the presence of minor alteration along discontinuities (commonly ferrous oxide staining) but no significant reduction in overall material strength.

For the purposes of this thesis, HW, CW and RS are considered to be engineering soil because of the extent of alteration and intact (mass) strength reduction. These materials are discussed in Chapter 4. The less weathered rock (HW, MW, SW and UW) are discussed in Chapter 5.

1.7.2 Slope Movement Terminology

Slope failures are classified according to Cruden and Varnes (1996). A debris slide is defined as "downslope movement of a soil or rock mass occurring dominantly on surfaces of rupture or on relatively thin zones of intense shear strain". A debris slide may develop into debris flow due to displaced material loosing cohesion, the addition of water or encountering steeper slopes. Channelised debris flows are simply debris flows constrained by channel topography (Cruden & Varnes, 1996)

Shallow slope failures in colluvium and the underlying weathered rock profiles are common in the study area. The main debris slides involve translational failure within colluvium or at the residual soil - colluvium contact, and sometimes extending to the interface between weathered and unweathered rock.

The mechanism of failure involves rapid infiltration of rainwater into highly permeable (probably already saturated) colluvial slopes. This increases pore pressure, reduces effective stress and leads to shear failure. The resultant soil slides enter the drainage systems, where addition of further water from excessive storm runoff causes channelised debris flows. Both slides on slopes, changing to fluid behaviour, and mobility of channelised debris flows are the key issues within the study area on the Takaka Hill (Figure 1.10).

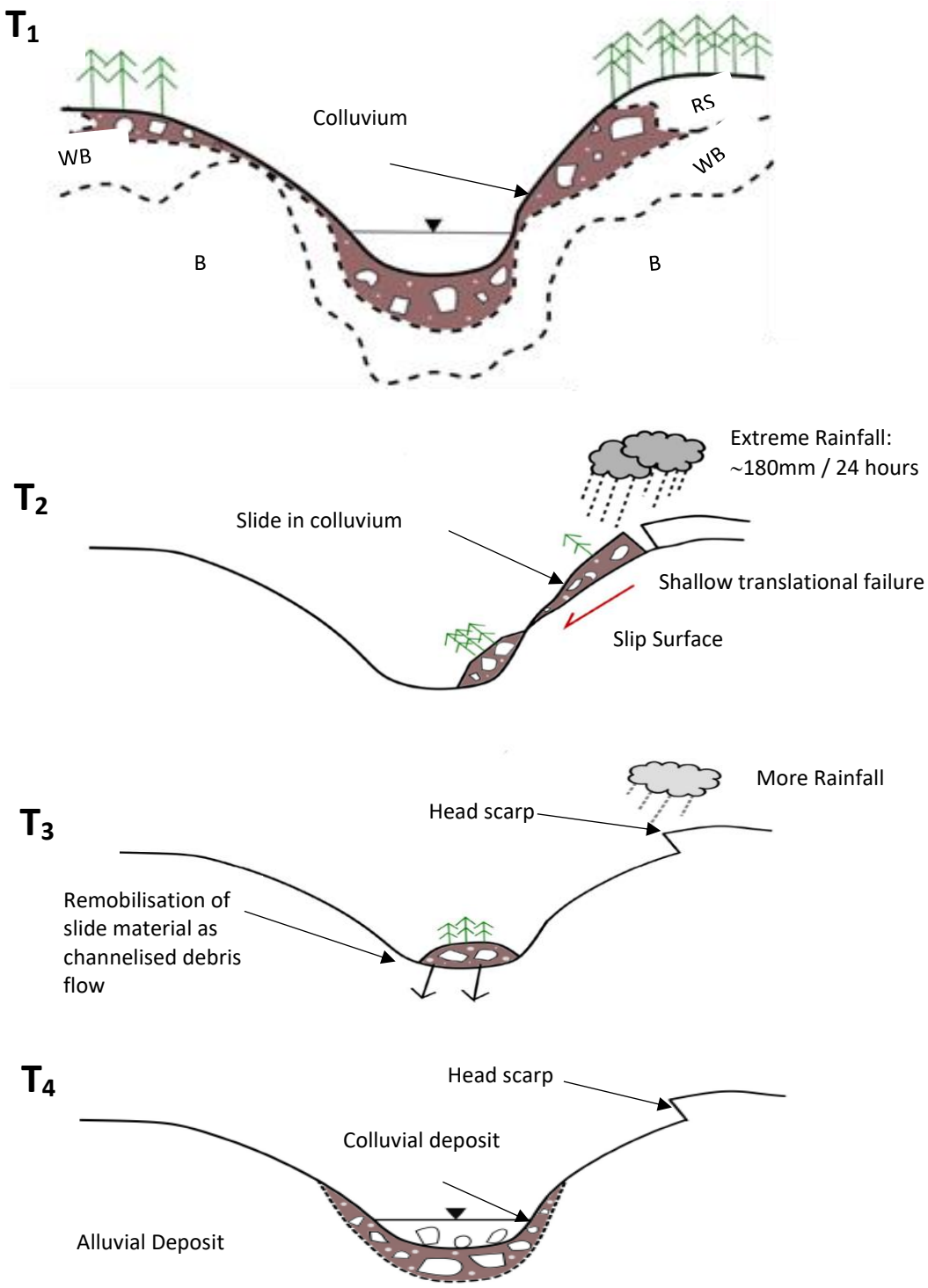

Figure 1.10: Schematic sketch of channel from Pre-2018 to 2018 Event. RS: Residual Soil; WB: Weathered Bedrock; and B: Unweathered bedrock. T1: Pre-2018 slope geometry. The diagram has been simplified and does not show different debris flow events. T2: Ex-tropical cyclone Gita event. The rapid infiltration of rainwater into colluvial slopes above drainage. The main soil slides are translational failure in colluvium at or near the bedrock or residual soil – colluvium contact. T3: These slides enter the drainage and, with the addition of further moisture from excessive runoff during the rainstorm, fluidise to form channelised debris flows. T4: Present slope geometry with thicker colluvial deposit.

Chapter 2: History of Slope Failures on Takaka Hill

2.1 Introduction

The overall objective of this research is to gain a better understanding of the debris flow hazard along the State Highway (SH) 60 corridor on the eastern side of Takaka Hill. As well as investigating the 2018 failures, it is also important to understand the characteristics of past slope instability. This requires identification of source areas (soil slide scars), estimating their approximate age, and summing the areas of each age category to estimate the size of previous events. This chapter focuses on SH60 including discussion of the physical characteristics of the highway over Takaka Hill and the historical failures along SH60 on both sides of the summit. This chapter also discusses the failures on adjacent slopes underlain by Separation Point Granite, specifically, along the Kaiteriteri-Riwaka road and the Riwaka-Sandy Bay road (Figure 2.1). Much of the data discussed in this chapter are taken from the National Institute of Water and Atmospheric Research (NIWA), and from unpublished geotechnical consulting reports. The focus of this research is on the eastern side of Takaka Hill, where most damage occurred during Ex-tropical cyclone Gita in February 2018.

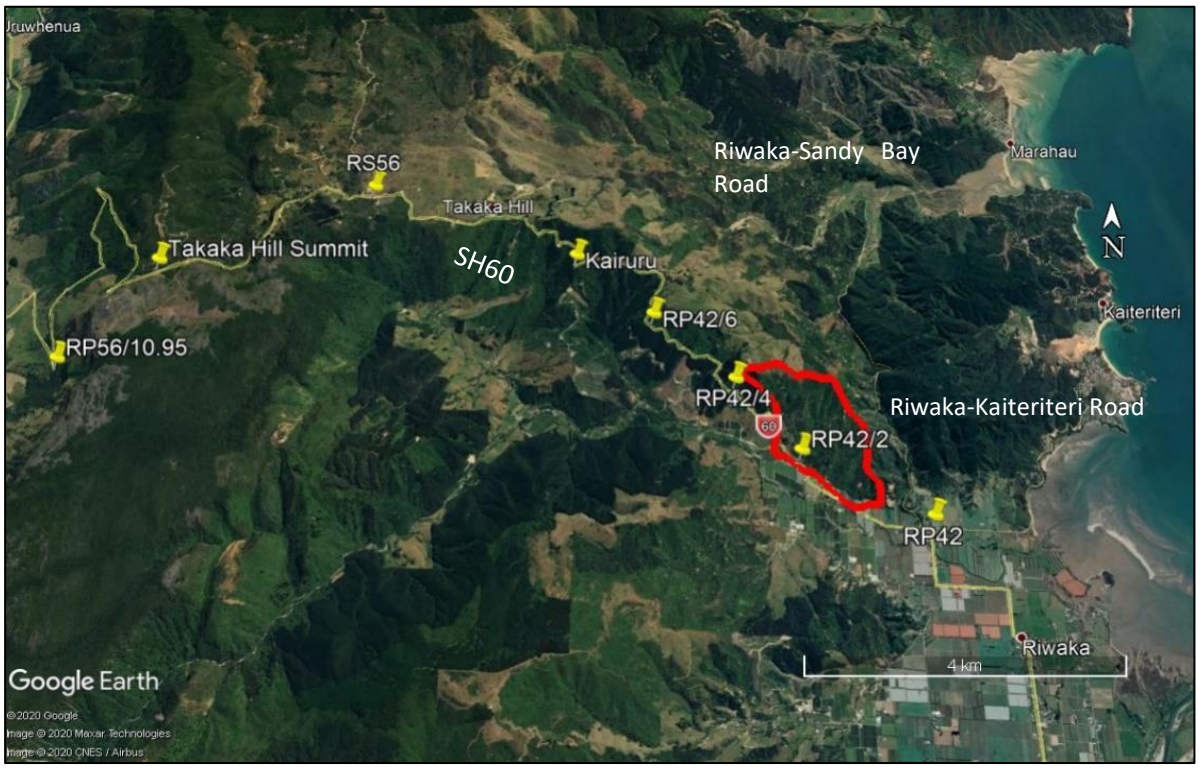

Figure 2.1: Location of State Highway (SH) 60. The RP numbers in the Figure are referred to in the text. SH60 starts at the T junction at RP42, and the subsequent numbers are in kilometres from RP42 (e.g. RP42/2 is 2 km from RP42). The red box is the detailed catchment area being studied. SH60 continues after RS56 56/10.95 towards Takaka. Source: Google Earth (2019).

2.2 Construction of SH60

Between 1856 and 1863, the bridle track route over Takaka Hill varied, as shown in Figure 2.2. This was due to slumpage and decisions to improve the gradients. In 1886 the alignment of the present SH60 was surveyed. The road was constructed to be suitable for horse drawn coaches (Figure 2.3), and was 4m in width (Turley, 2009). The Public Works Department let the contract for construction during 1886 and early 1887. SH60 was completed in late 1887 (MWH, 2009).

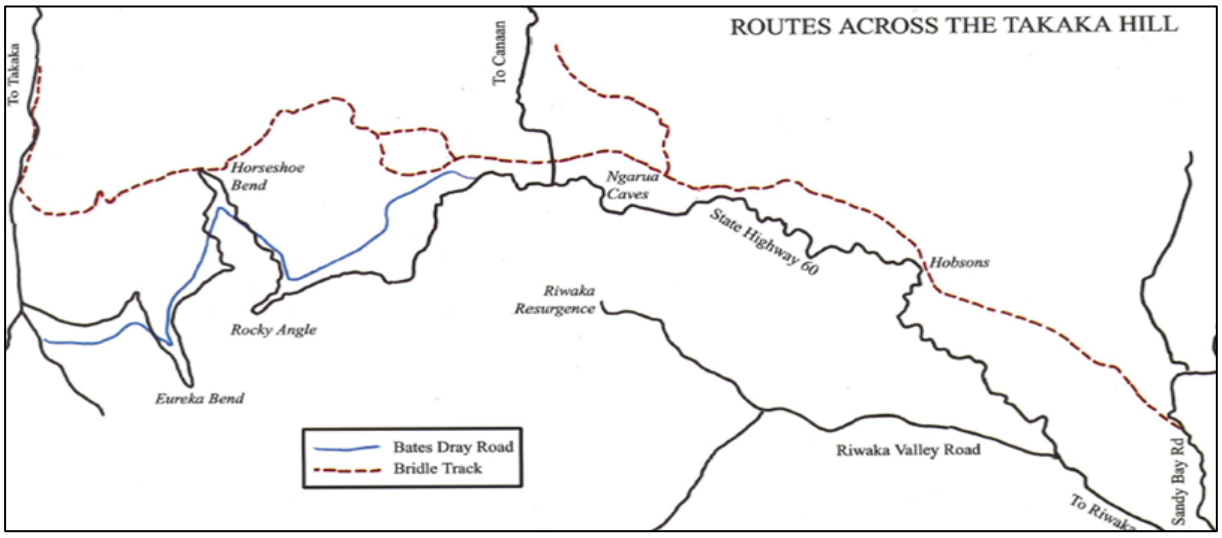

Figure 2.2: The routes across Takaka Hill. Source: (Turley, 2009).

Figure 2.3: Coach carrying passengers along SH60; date unknown. Source: (Turley, 2009).

In the 1930s widening was carried out using manual labour and small bulldozers, and in the 1950s tar sealing commenced (Turley, 2009). This was done using a single seal width of 3 m, with 1 m wide gravelled shoulders on each side of the road (MWH, 2009). With the introduction of national standards in the 1950s, as well as budget availability and priorities, the road was improved (Opus International Consultants Limited, 2014; Turley, 2009). Inspection of the road by the National Roads Board was carried out every five years to consider ongoing maintenance and improvements. This resulted in improved drainage in 1988 and 1989 (Turley, 2009). By the year 1990, the road was on the current alignment (Opus International Consultants Limited, 2014).

Opus International Consultants Limited (2014) state that "Takaka Hill can be considered as starting at RP 42/2.05 on the Nelson side and going to RP56/13.85 on the Golden Bay side". The 25 km long Takaka Hill section of State Highway 60 is mountainous, with steep hillside slopes above and below the highway, and it crosses a number of steep gullies, cutting through the ridges between the gullies (Opus International Consultants Limited, 2001).

SH60 starts at the T-intersection where the traffic can either turn westward towards Takaka Hill and continues along the SH60 corridor or turn eastwards towards Kaiteriteri (Figure 2.1). Shortly before its intersection with the Riwaka Valley Road at RP42/2.00, SH60 begins to climb and, for the next 14km, it traverses the south eastern side of Takaka Hill to its summit at RP56/4.02 (Opus International Consultants Limited, 2001).

The report on Takaka Hill Management by Opus International Consultants Limited (2001) states that the present road follows a practical route, and that any significant deviation from this route would be geometrically unacceptable for significant portions of the road length. The detailed catchment area in this study is located approximately between RP42/2 and RP42/4.5 (Figure 2.1).

2.3 Slope Instability affecting SH60

2.3.1 Historical Instability

Heavy rainfall and resulting runoff have always been an issue on Takaka Hill. Since SH60 was completed in 1887, it has only been blocked once by an earthquake, when the 1929 Murchison Earthquake caused rockfalls to the east of Takaka Hill summit (Figure 2.1). However SH60 has been partially blocked due to rainfall-triggered slope failures on an average of five times annually (MWH, 2009). During these frequent slope failures, SH60 is often reduced to one lane with traffic control. The time required to reopen the road depends on the location, safety issues, weather conditions and available resources.

Approximately once a year for a few hours only, the road totally closes due to slips (Opus International Consultants Limited, 2001).

Upgrading of Takaka Hill highway, including road repairs and widening, has been documented since the 1960s. The combination of steep mountain slopes, varied rock types and high rainfall on Takaka Hill caused ongoing maintenance problems in the early 1980s. In the past, the short term solution involved sidecasting of slip debris (Turley, 2009).

Most of the reports evaluated use the term "slips", and no differentiation is made between soil slides and debris flows, or a combination of both. The geotechnical report and landslips remedial works report provided by the New Zealand Transport Agency (NZTA) covers the period 2000-2019. The reports were mostly done by consultants: Opus International Consultants, MWH (Montgomery Watson Harza), and GEOadvise Ltd. Each were contracted to perform site investigations and/or provide remedial measures design along SH60. Most of the rainfall data is taken from the NIWA Historic Weather catalogue, which records major weather events over the last 200 years. The information in this catalogue has been collated from various sources, including newspaper reports, journals, books and databases (National Institute of Water and Atmospheric Research [NIWA], n.d). Slips up to 1887 have been recorded for Takaka Hill area, and incorporated into Table 2.1, although some events may have been missed due to a lack of available data. The report shows that there are three main types of failures over Takaka Hill: culvert blockage, shallow soil slides and channelised debris flows.

Table 2.1 shows the historical slope instability along SH60 on both sides of Takaka Hill, and on the adjacent hills underlain by Separation Point Granite. It highlights the events that caused significant damage to SH60. It should be noted that there were other rainfall events that caused major damage in the Nelson-Tasman region, but only minor damage to SH60 over Takaka Hill. For instance, although the storm event on 15th December 2011 was significant for the region, it caused minor damage along SH60 (Figure 2.4). The following discussions in this section relate to rainfall-triggered soil slides and debris flows in the study area i.e. the eastern side of Takaka Hill.

Figure 2.4: Example of damage to SH60 caused by a slip on the western side of Takaka due to a storm event in December 2011. Photo provided by the Tasman District Council.

Table 2.1: Failures in the study region. The damage caused to SH60 by these events was not as extensive as the 1956/1957? 1990, and 2018 events.

Date	Location	Type of Failure	Triggering Rainfall	Description	References
3 to 7 February 1877	Tasman-Nelson	Slips	no data	"The intense rainfall generated a huge number of slips."	(NIWA, n.d.)
25 July 1948	Takaka Hill	Slips	70.4 mm/24 hours	"The main damage occurred at Takaka Hill where two slips blocked the road."	(NIWA, n.d.)
26-30 May 1949	Takaka Hill	Slips	361 mm/4 days	"Large slips came down Takaka Hill on the 30th. The road was impassable for two days on 30th"	(NIWA, n.d.)
5-8 March 1954	Takaka Hill	Slips	76.2 mm/24 hours	"There were numerous slips on Takaka Hill and a large subsidence blocked the road to Upper Takaka."	(NIWA, n.d.)
1956	SH60	Slips	Rainfall	SH60 impassable for one week. Date unknown	(Turley, 2009)
12-18 April 1957	Takaka Hill	Slips & debris burst	456 mm/7 days	Numerous slips	(NIWA, n.d.)
8-12 July 1983	(SH60)	Slips	462 mm/48 hours	"Takaka Hill Road (State Highway 60) was closed by slips."	(NIWA, n.d.))
21 October 1983	SH60	Slip	60.1 mm/24 hours	"Takaka Hill Road closed by a slip near the Eureka bend"	(NIWA, n.d.)
12 March 1988	SH60	Slips	150.3 mm/24hour	"Several new slips came down on Takaka Hill, one slip covering most of the road on the Takaka side".	(NIWA, n.d.)
11-13 August 1990	RP42/2 to RP42/7	Slips	349 mm/72 hours 224 mm/24 hours	Road closed for 1 week	(MWH, 2009)
July 2000	SH60	Landslide	-	Heavy rainfall and a blocked culvert caused a slope failure along a 50-metre section of SH 60 on Takaka Hill west of Nelson, making the state highway hazardous to road users.	(New Zealand Geotechnical Society, 2003)
14-15 April 2008	Riwaka-Kaiteriteri road	Slips	93.2mm/24 hours	Small slips recorded	(NIWA, n.d.)
23-25 November 2008	SH60	Slips	79.4/3 days	SH60 from Riwaka to Collingwood was closed because of a slip on the Takaka side of Takaka Hill, cutting off Golden Bay. Takaka Hill and Takaka Valley Roads were closed overnight on the 24th.	(NIWA, n.d.)

14 May 2010	Hills underlain by SPG	Landslides	58 mm/24 hours	Minor slips recorded in Kaiteriteri and Riwaka Valley, however no records of slips over SH60	(Page, 2013; NIWA, n.d.)
15 December 2011	Takaka and Hills underlain by SPG	Slips	In Takaka, nearly 400 mm was recorded in just 24 hours	More than 200 landslides occurred across the region, with Collingwood, Cable Bay, Totaranui and Ligar Bay isolated due to landslides cutting off access roads to those areas. In Nelson and Pohara, 160 and 30 houses respectively were evacuated due to flooding or landslides. The landslides and debris flow originated in steep hills underlain by Separation Point Granite (SPG). "Collingwood was inaccessible as SH60 was closed past Takaka".	(Macara, 2016; Page, 2013) (NIWA, n.d.)
21 April 2013	(1) Riwaka Valley (2) SH60 Takaka Hill RP42/7.07	(1) Debris flow (2) Shallow landslip	(1) The preceding 2-hour rainfall was 127 mm	(1) A high intensity rainstorm generated a debris flow in the Riwaka Valley. In this instance, the debris flow originated in secondary indigenous scrub/forest and on Riwaka Complex Gabbro, with an hourly maximum of 34.3 mm immediately preceding the debris flow. (2) The northbound shoulder of SH60 was eroded	(1) (Page, 2013) (2)(Opus International Limited ,2016; NIWA, n.d.)
15-17 June 2013	Motueka area	Landslides and debris flows	Otuwhero Inlet:180mm/24hours Marahau Valley:290mm/24 hours	"Landslides struck a house at Otuwhero Inlet, killing the woman occupant. Many roads were blocked by landslides and debris flows between Marahau and Kaiteriteri, in the Riwaka and Brooklyn Valleys, and along the west bank of the Motueka River as far south as Rocky River. A salmon farm at Anatoki west of Takaka was badly damaged by a debris flow."	(Page, 2013)
23 March to 24 March 2016	RP:42/4.85 South-east flank of Takaka -4.8 km northwest of Riwaka Bridge on SH60	Underslip	210mm/24hours at Moss Bush 220mm/24hours at Riwaka North	The total length of the slip was 12m temporarily reduced to one lane	(GEOadvice Limited, 2016) (NIWA, n.d.)
20th February 2018	RP42/2230 to RP42/5620.	Soil slides and debris flow	180mm/24 hours	SH60 was closed on 20 February and reopened with restrictions on 25 February	(NIWA, n.d.)

2.3.2 Note on Terminology

The mass movement classification scheme of Cruden and Varnes (1996) has been adopted in this study to describe the slope failure types and mechanisms (Table 2.2). The terminology follows Varnes (1978), where the emphasis is on the type of movement and type of material. In the later classification, the sixth type of movement – complex landslide – has been dropped from the formal classification scheme (Cruden & Varnes, 1996). In fact the 2018 Gita failures were a combination of sliding and flowing due to the intense rainfall.

Two types of mass movement have been identified in the study area: shallow translational soil slides and channelised debris flows. For consistency, a slight modification to the Cruden and Varnes classification has been adopted: the term “debris and earth slide”, is termed “soil slide”. The slide material is generally described gap-graded soil consisting of boulder and cobbles in a fine grained matrix, and materials in the slide source area are heterogeneous (refer to Section 1.7 in Chapter 1 for further discussion of terminology).

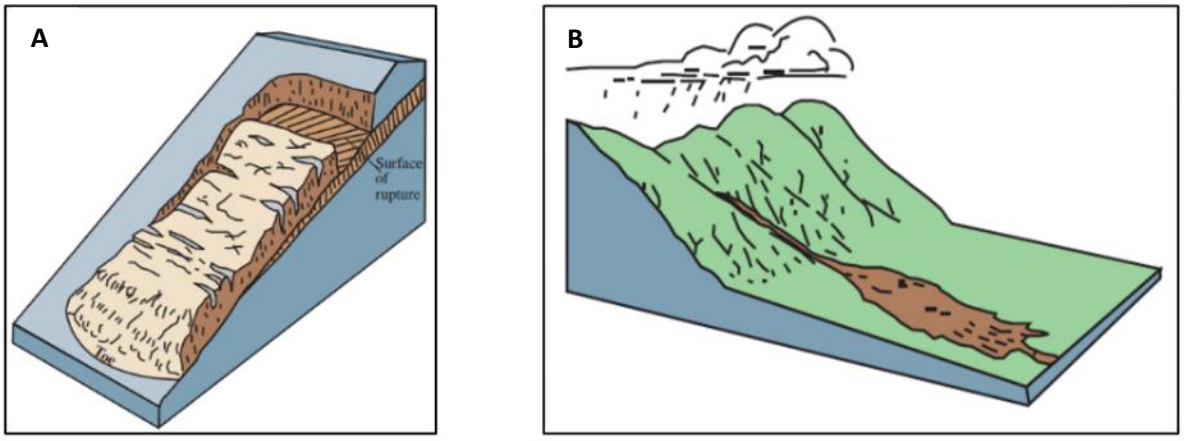

Figure 2.5: (A) Translational Failure (B) Debris flow. Source: (Cruden & Varnes, 1996).

Table 2.2: Varnes and Cruden classification for mass movement (Cruden & Varnes, 1996). The type of movement important to the study area has been highlighted in green.

Type of Movement	Type of Material		
	Bedrock	Engineering Soil	
		Predominantly Coarse	Predominantly Fine
Fall	Rock fall	Debris fall	Earth fall
Topple	Rock topple	Debris topple	Earth topple
Slide	Rockslide	Debris slide	Earth slide
Spread	Rock spread	Debris spread	Earth spread
Flow	Rock flow	Debris flow	Earth flow

There are three principal documented events recorded that resulted in extensive damage to SH60 over Takaka Hill, with road closure for a period of 5 days or more and requiring major repair works. These occurred in 1956/7, 1990 and 2018, and have been highlighted in Table 2.2.

2.3.3 1956/7 SH60 Closure

Turley (2009) recorded a slip in 1956 at Ryder's Dip (RP42/7.07) caused by heavy rainfall, extending for approximately 400 m midway between Kairuru and the bottom of the eastern side of the Hill (Figure 2.1). SH60 was impassable for a week following this storm event (MWH, 2014). However, the National Institute of Water and Atmospheric Research (National Institute of Water and Atmospheric Research [NIWA], n.d) records numerous slips on Takaka Hill on 12th to 18th April 1957, coincident with heavy rainfall (456 mm in 7 days) and with no records of slope failure in 1956. In fact no spikes in rainfall are found in 1956, therefore indicating that the event most probably occurred in April 1957. However, it could also be that the slip occurred as a result of prolonged rather than high intensity precipitation in 1956, and the records are inadequate to resolve the date.

With reference to Figure 2.6, it can be observed that the slip has taken the outer part of the road. The fill batter erosion from failure is undermining the road embankment. The channelised flow at the bottom of the slope can be seen. To remediate the failure a bench had to be cut above the failed area to allow remediation of SH60. The old landslide feature is identified from the hummocky surface (Figure 2.6).

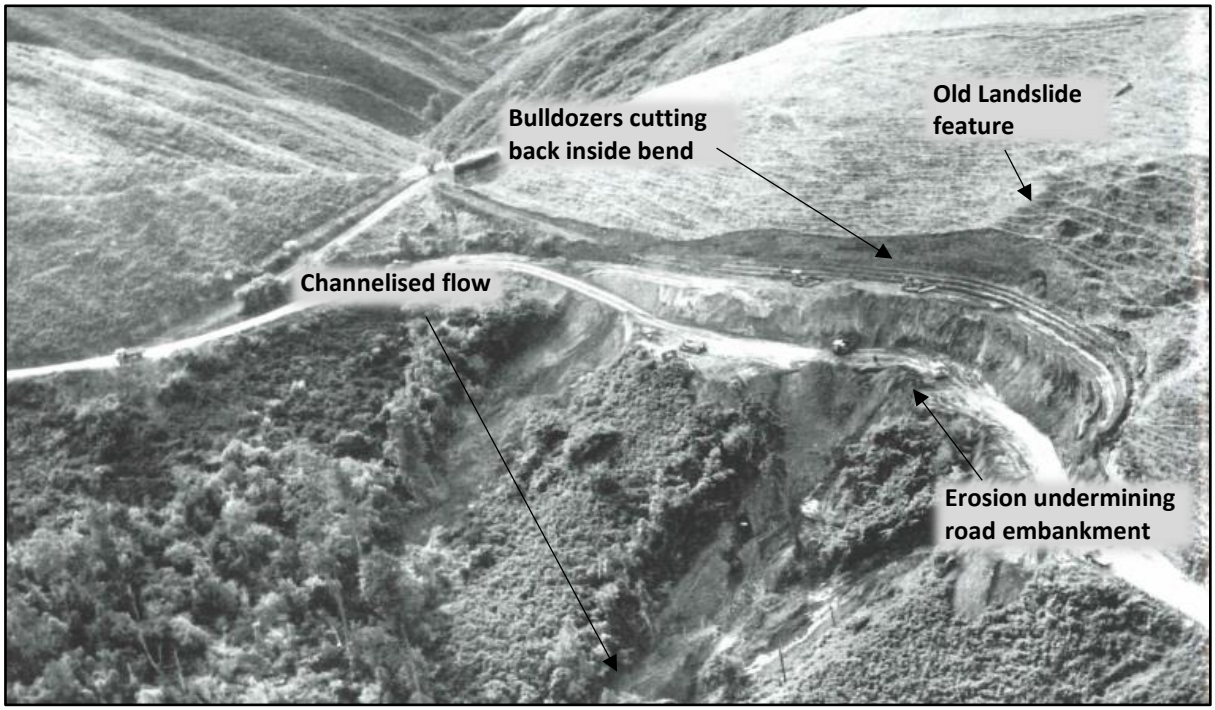

Figure 2.6: Historical photo of SH60 after 1956/1957 storm event. Source: (Turley, 2009).

2.3.4 August 1990 SH60 Closure

Prior to Ex-tropical cyclone Gita in 2018, one of the worst debris slide-flow events was recorded in 1990 when the road was closed for one week, as reported by the civil engineering company (MWH, 2009). The most damage was between Kairuru and the bottom of the Hill on the Riwaka side (RP 42/2 to RP 42/7, refer Figure 2.1). The storm occurred from 11-13th August 1990, and over 700mm of rainfall was recorded in the nearby Riwaka Valley, with 250mm on the final night. The Riwaka side of the highway was littered with more than 80 landslips, washouts and blocked culverts (Turley, 2009). The total cost to fix the road following the 1990 event was in the order of NZD 2 million (Opus International Consultants Limited, 2001).

With reference to Figure 2.7 debris flows from the 1990 event can be observed in colluvial soil. The slope was vegetated with grass and shrubs and, the channelised debris flows initiated from shallow translational slide failures on the steep slope. The runout was to the flat ground at the base of the hillslope. Figure 2.8 shows soil slide on the outer bank of SH60 scouring, with the road corridor at another location.

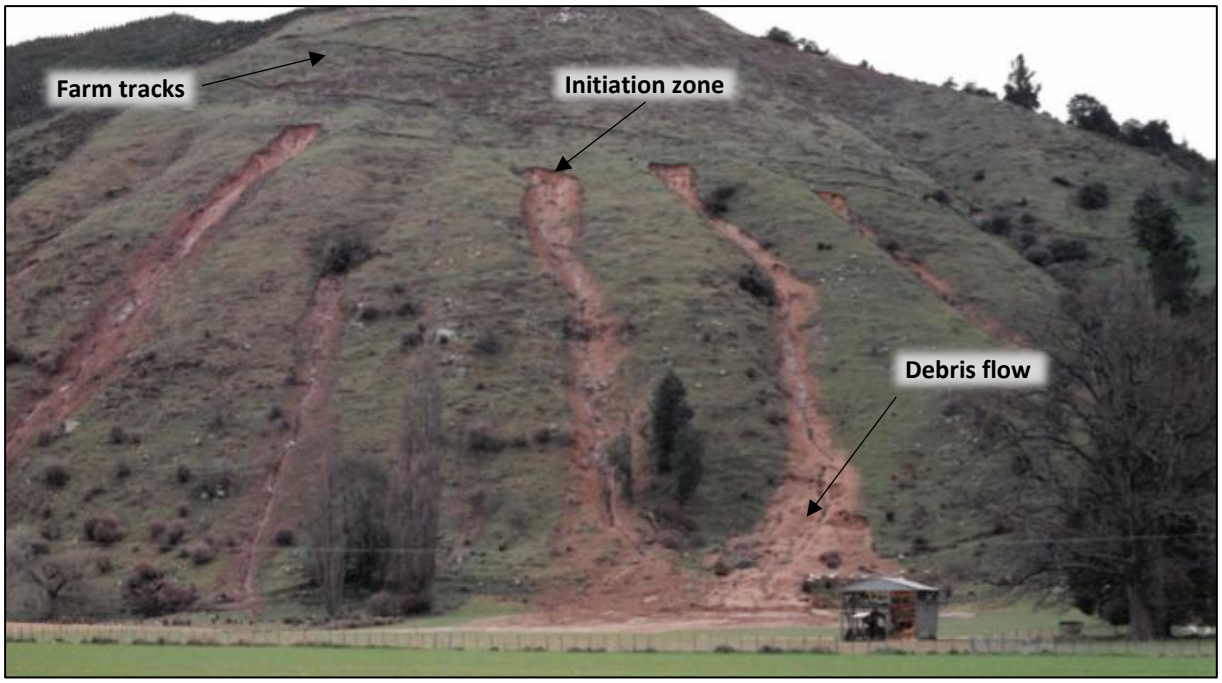

Figure 2.7: Debris flow caused by the 1990 storm in the study area. Photo Supplied by Tasman District Council.

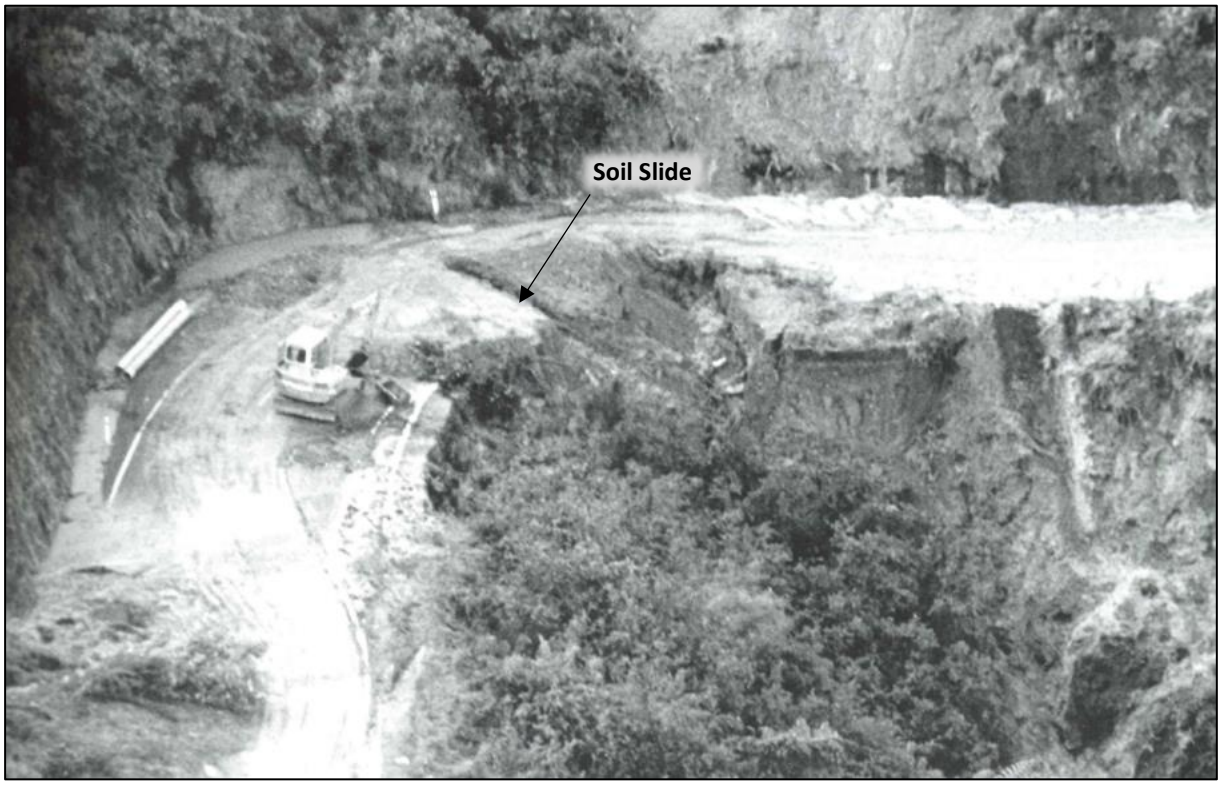

Figure 2.8: SH60 damaged by slips in August 1990. Source: (Turley, 2009).

2.3.5 Ex-Tropical Cyclone Gita (February 2018) SH60 Closure

The passage of Ex-tropical Cyclone Gita on 20th February 2018 caused significant damage (resulting in complete road closure of SH60 for 5 days. The road was opened to essential traffic for limited hours

on 25th February and fully opened to one lane traffic on 7th April (NIWA, n.d.). Two types of mass movement were again observed in the study area: shallow translational soil slides and channelised debris flows. The failures occurred between RP42/2.2 and RP42/5.6 (Figure 2.1).

Figure 2.9 shows channelised debris flows affecting the SH60 corridor. Shallow translational soil slides were feeding into the channel. The debris flow deposit and overflow of deposit can be seen. The channelised debris flow comprises up to boulder size clast and tree debris. The debris flow caused undercutting and failure of the road embankment. There was a culvert at the bottom of the gully and boulders would have blocked the culverts as the design of the culvert was not adequate for the large scale debris flow event. The blockage of the culvert caused overtopping, leading to significant damage to the highway. There is also small scale channelised debris flow forming next to Channel 3.

Figure 2.9: (A) Deposits and erosion from a channelised debris flow triggered by Ex-tropical cyclone Gita in February 2018. Photo provided by GEOadvise Limited (B) Enlarged image showing erosion and inundation from debris flows causing undermining the road embankment. Source: (Stuff.co.nz, 2018).

2.4 Pre-2018 (Gita) Remote Sensing Data

2.4.1 Remote Sensing Data

This section is limited to the eastern side of Takaka Hill, where most damage occurred on SH60, and which the focus of this research is. This section discusses the changes in geomorphology in the 70 year period before the 2018 Gita event. The earliest photo available for the area is 1940 but the image has been damaged. The landscape appears to be similar in the 1940 and 1947 aerial photographs, and the 1947 aerial imagery (Figure 2.10) has been used as the baseline from which historic geomorphological changes could be evaluated.

To identify the source areas and the extent of the damage caused in landslide-generating events prior to 2018, a range of imagery was used (Table 2.3). Only selected aerial images were analysed in detail. However other aerial images was consulted to make some general observations. From the year 1967 onwards, it was observed that vegetation is well established on the eastern side of Takaka Hill.

Table 2.3: Summary of remote sensing data used for detailed analysis.

Year	Type	Data Source	SN number
27 March 1947	Aerial Photography	Tasman District Council	379
19 May 1958	Aerial Photography	http://retrolens.nz and licensed by LINZ CC-BY 3.0.	1075
1989	Aerial Photography	Tasman District Council	-
10 December 1991	Aerial Photography	Aerial Surveys Limited	11897B
2016	LiDAR	Koordinates	-
17 February 2017	Aerial Photography	Google Earth	-
22 February 2018	Aerial Photography	Tasman District Council	-

2.4.2 1947 Aerial Imagery

The 1947 aerial image is of comparatively low resolution, but a number of observations can be made (Figure 2.10). The 1947 aerial image shows shallow soil slides on non-vegetated slopes, which are represented by the white coloured patches and marked by purple coloured polygons. There are few soil slides (0.7 % of the catchment area outlined in red). The 1948 image shows shallow soil slides up to 100 m long and 50 m wide in the bare ground.

The area is not forested except for a few pockets of vegetation observed on the lower slopes. There is a lot of bare ground which was presumably cleared for pastoral farming. There is a series of gullies and deeply incised valleys showing a long history of erosion and incision in the area. The debris fan deposits on the eastern side of the study area (Channel 1) suggests some recent activity, while Channel 2 and

Channel 3 shows an older debris fan deposits (Figure 2.10). The soil slides, fan deposit, headscarps, and deeply incised gullies all indicate that the slope instability issues have been ongoing.

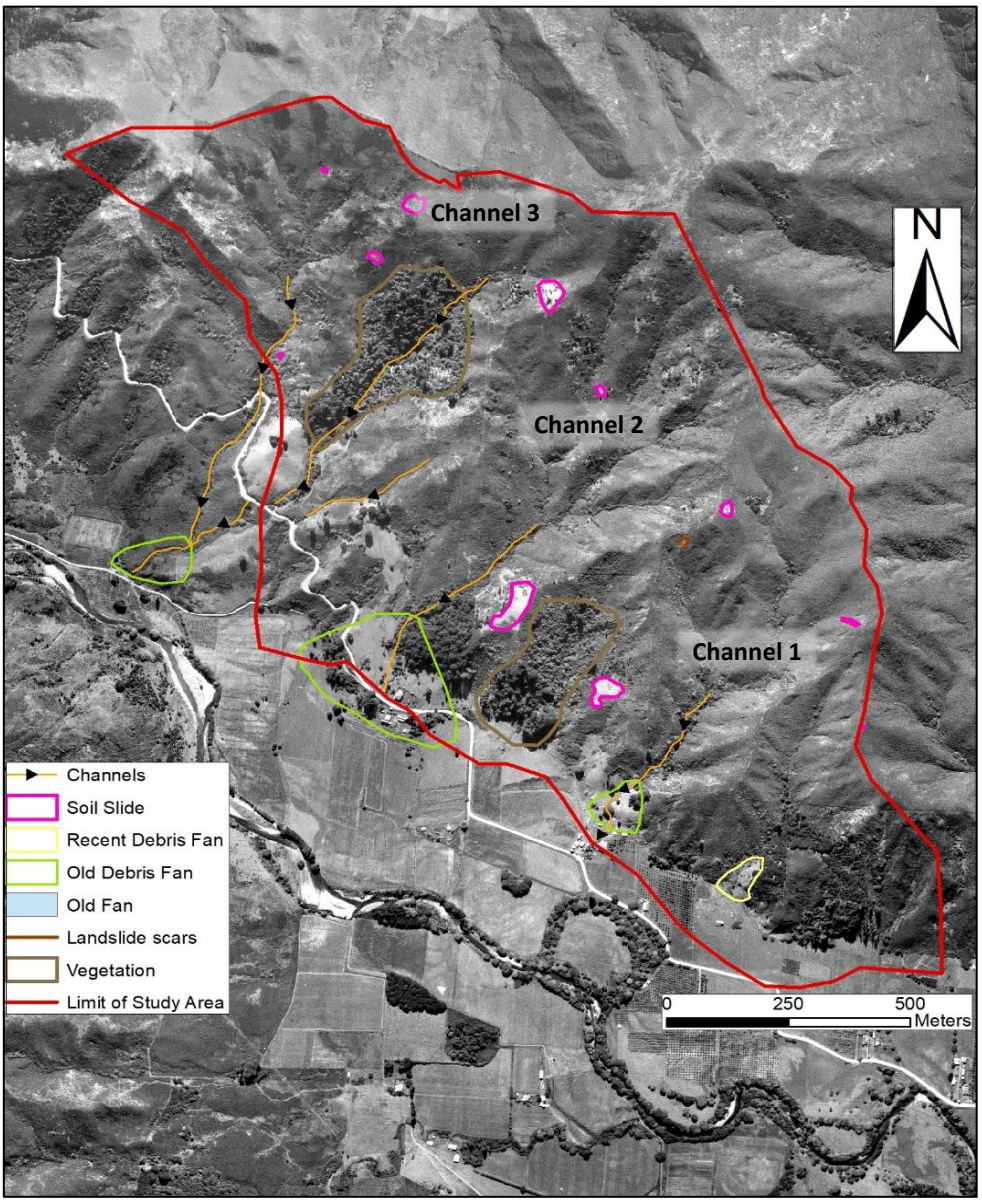

Figure 2.10: 1947 aerial image of the detailed catchment study area. Aerial Imagery provided by the Tasman District Council.

2.4.3 1958 Aerial Imagery

Between 1947 and 1958 the vegetation regrowth suggest cessation of farming activities. There is no major soil sliding evident in the study area. However, a few shallow soil slides (outlined by green polygon) on slope suggests continuing problems for SH60 (Figure 2.11). The shallow soil slides are on scrub covered vegetation.

As discussed in Section 2.3.3, slope failures in 1956/57 cut off SH60. The aerial image has been taken in May 1958 after the storm events. The soil slides are probably generated from these storm events. The coverage for 1958 aerial imagery is only for eastern part of Takaka Hill.

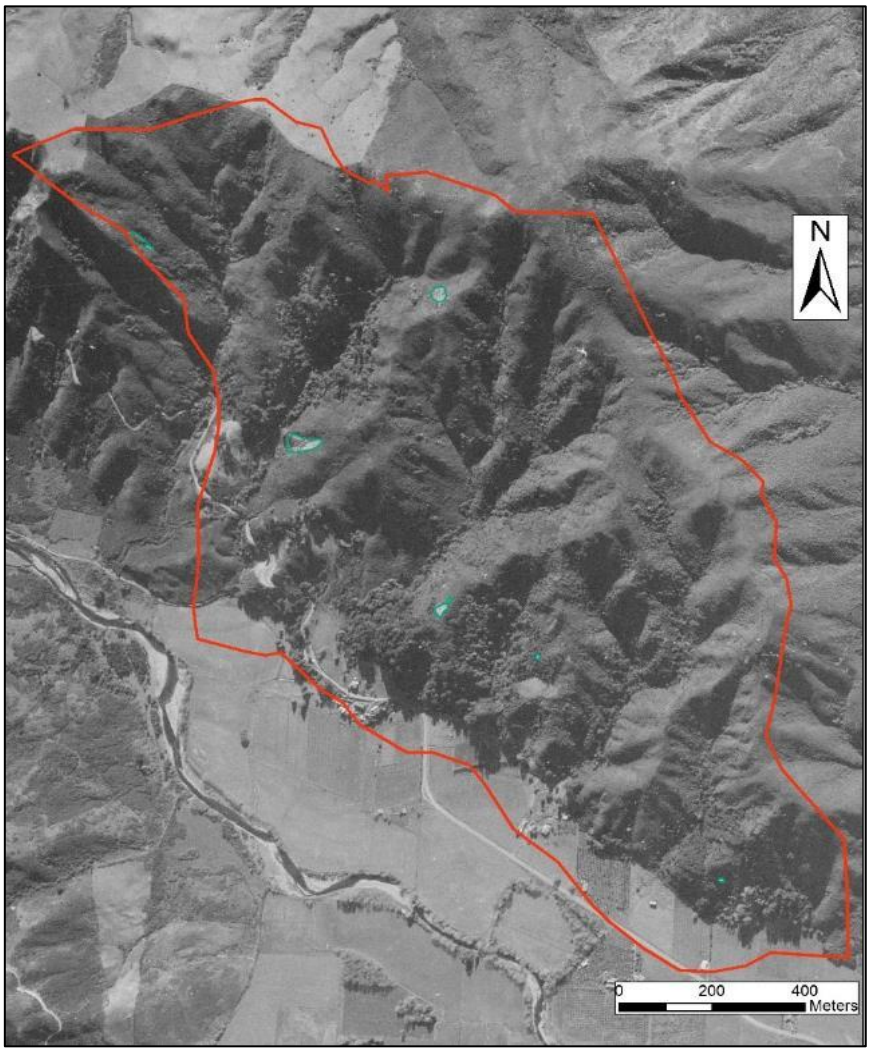

Figure 2.11: 1958 Historical image. Green polygon outlines soil slides in detailed catchment area. Source: http://retrolens.nz and licensed by LINZ CC-BY 3.0.

2.4.4 1989 and 1991 Aerial Imagery

The 1989 aerial image (Figure 2.12 A) shows the slopes covered with vegetation, whereas in 1947 the vegetation was not well established. In the 41 year time period, the vegetation has become well established, representing cessation of farming. In the detailed catchment area in the 1989 aerial image, outlined by the red polygon, there is one zone of instability; however there are few soil slides (marked by green polygon) observed outside the catchment boundary.

The 1991 aerial image (Figure 2.12 B) shows soil slides marked by blue polygons. The aerial image was the only coverage available for the study area, and the only image available after the 1990 event. The failures range in size up to 120m long and 30 m wide (Figure 2.12 B). The soil slides were in vegetated slope cover and the majority of the soil slides were concentrated on areas of high relief.

The total area of slides identified in 1991 aerial image in the detailed catchment area is 11,000m^2. This is 0.8% of the detailed catchment area. The failures are more on the western catchment area than the eastern side. Although the area has well established vegetation, the area has experienced soil slides. The 1991 image is the earliest image taken after the August 1990 storm event, and reports state that the eastern side was affected. The drainage in the 1991 aerial image shows bare ground representing a debris flow path which was covered with vegetation in the 1989 aerial image. It should be noted that there was a greater increase in soil slides outside the detailed catchment between 1989 and 1991, presumably due to the 1990 event.

2.4.5 2016 LiDAR

The author of this thesis presented some of the results of this research in a conference paper. (Prasad & Fenton, 2020) noted:

> "Analysis of the 2016 LiDAR image identified a series of slope failures within the tributary channel catchments (Figure 2.13.). Based on the relative 'freshness' of the geomorphic expression of these features, they were classified into three categories: fresh (recent), historical, and prehistoric source zones. The fresh source zones are active sources of debris and are represented by prominent rough surfaces on the LiDAR imagery. The historical and prehistoric sources show decreasing sharpness of landslide geomorphology. The three categories indicate repeated instability in the catchment area." (p.895)

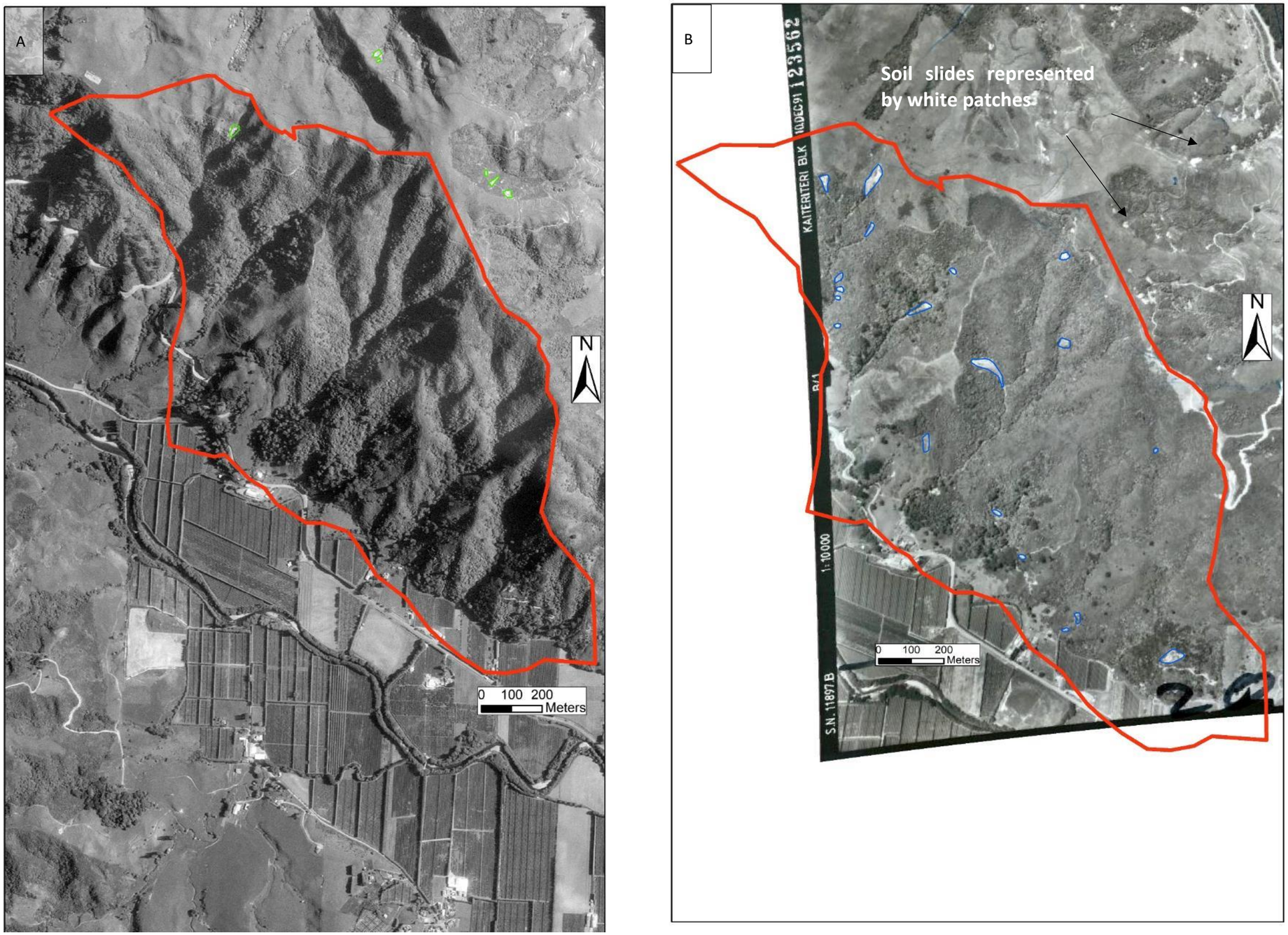

Figure 2.12: Historical images identifying geomorphological changes before and after the 1990 storm event. (A) 1989 aerial image. The green polygon represents soil slides. Aerial Imagery provided by the Tasman District Council (B) December 1991 aerial image; this is the only coverage of the area in 1991. The blue polygons represent slides generated in 1990. Aerial Imagery supplied by Aerial Surveys Limited.

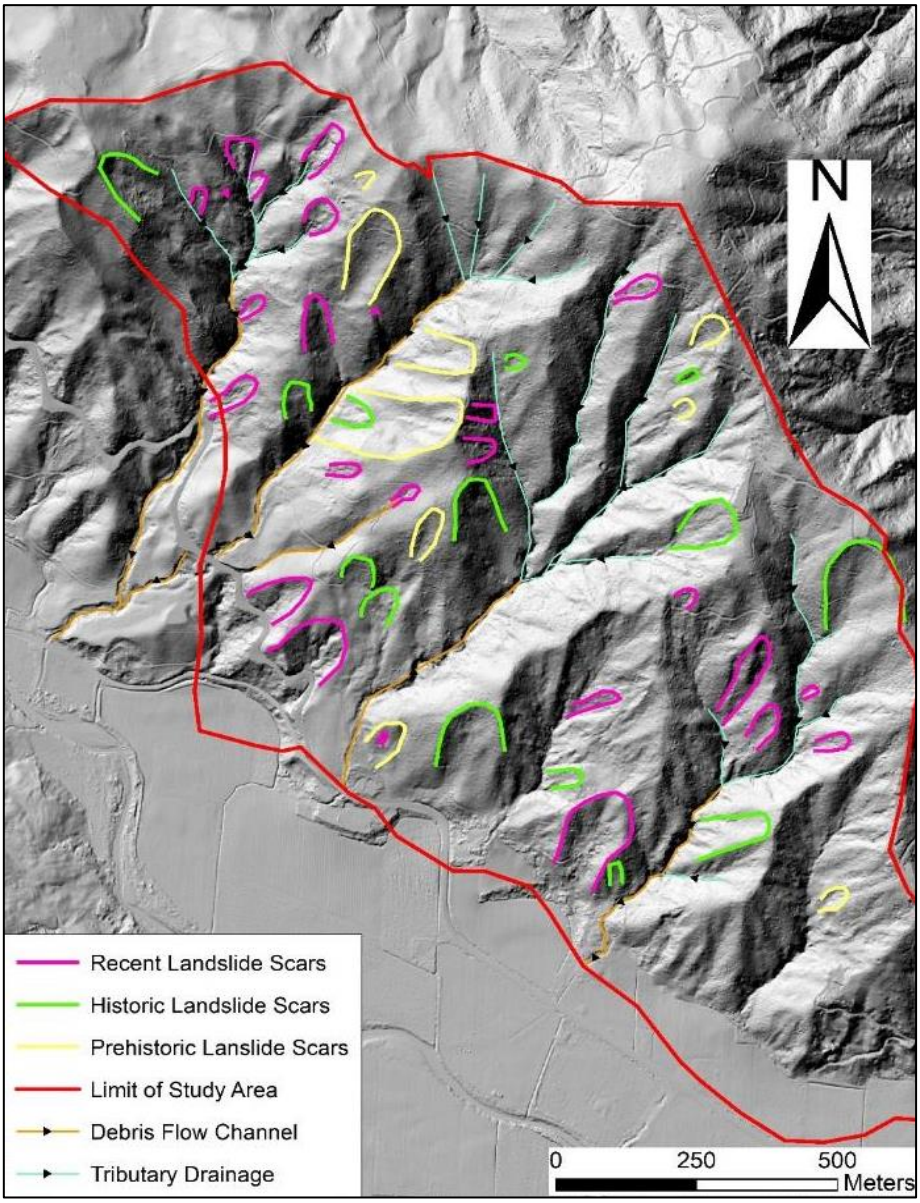

Figure 2.13: Hillshade model using 2016 LiDAR data. Soil slope failures are identified from common landslide geomorphological features, including hummocky ground, head scarps and fissures. Source: (Land Information New Zealand, 2018).

For this study, the fresh zones are considered to represent a time period from 1990 until 2016 (the date this LiDAR is taken). The historic landslide scars are thought to be from when the road was constructed in 1887 until 1990. Prehistoric landslide scars refer to pre 1887, before the road was constructed. The LiDAR analysis shows that instability is an ongoing issue. From the LiDAR analysis, there are more recent failures compared to historic and prehistoric landslide scars (Figure 2.13).

2.4.6 Pre-Gita 2018 Aerial Imagery

The aerial image taken on 17th February 2018, 3 days prior to the 2018 Gita storm event, shows only one small zone of instability underlain by Undifferentiated Riwaka Igenous Complex (Figure 2.14). This had an area of 125 m^2 and was approximately 25m by 5m. Prior to the 2018 event, the study area was well vegetated with native plants. In fact, the 2018 aerial image appears to be substantially more vegetated compared to the 1989 aerial image. There may be some zones of soil failures that are not visible due to the shadowing effect of trees.

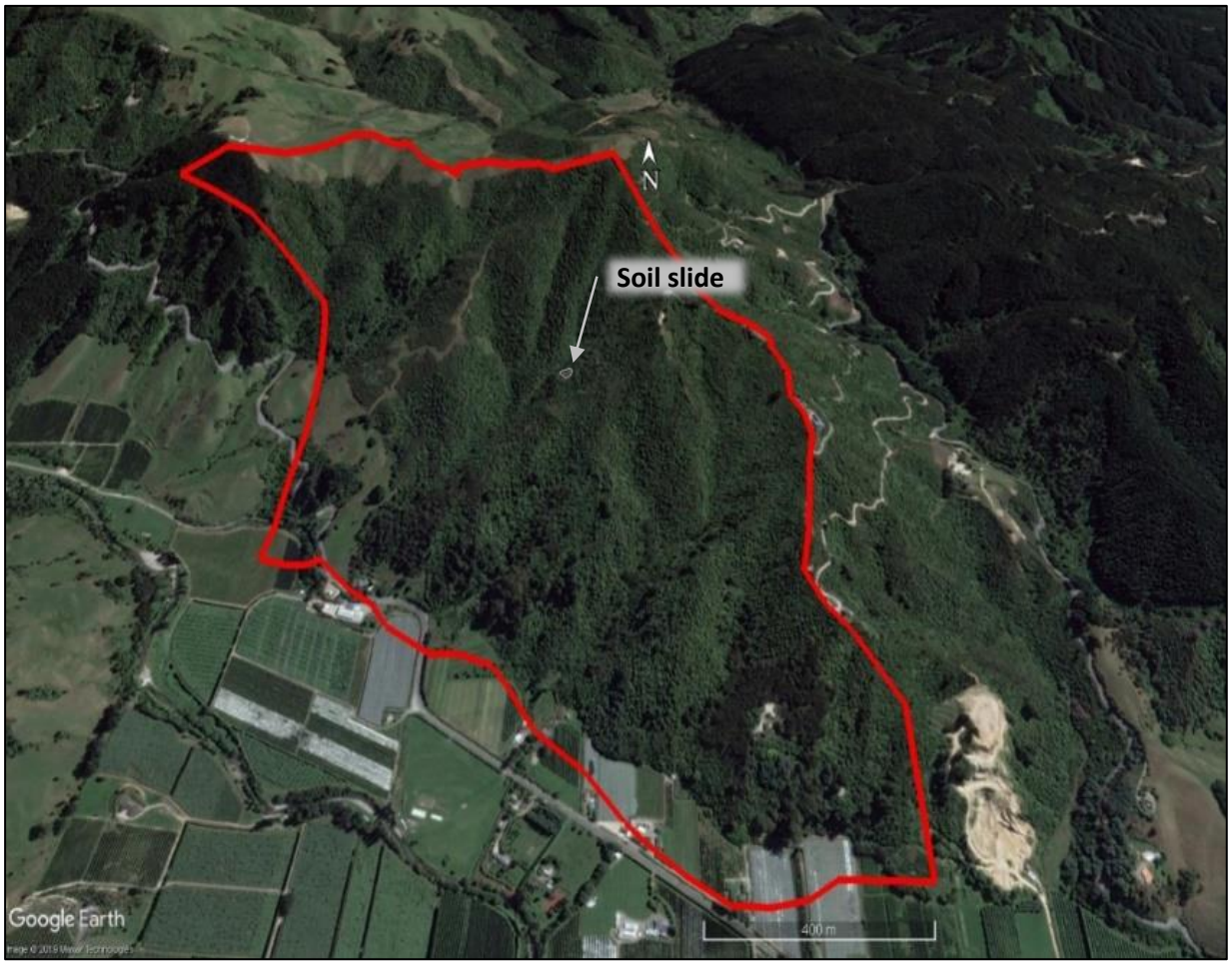

Figure 2.14: Aerial image taken on 17 February 2018, 3 days before the Ex-tropical Cyclone Gita hit. One zone of instability is noticed, outlined in white. There are no obvious zones of instability within the area of greatest impact from Ex-tropical Cyclone Gita. Source: Google Earth (2019)

2.5 Ex-Tropical Cyclone Gita (2018) Damage

Figure 2.15 shows shallow translational soil slides and channelised debris flow caused by Ex-tropical Cyclone Gita, on 20th February 2018. The soil slides is up to 200m long and 70 wide. The majority of these slides are immediately adjacent to the active drainage channels, therefore following a small

amount of displacement, the failed material becomes entrained in the channel and becomes the source for debris flow activity.

The channelised debris flows has a long runout distance from the source areas, depositing material on the lower slopes and pre-existing fan areas. Channel 1 and Channel 2 deposited debris on SH60 but did not cause extensive damage to SH60. However, both channels damaged the houses along its path. Debris flow in Channel 3 caused significant damage to SH60 as shown in Figure 2.15. Most of the damage occurred on the eastern side of Takaka Hill reducing SH60 to one lane. The one lane road starts 100m from channel 2 and continues for 1.5 km towards Takaka side of SH60.

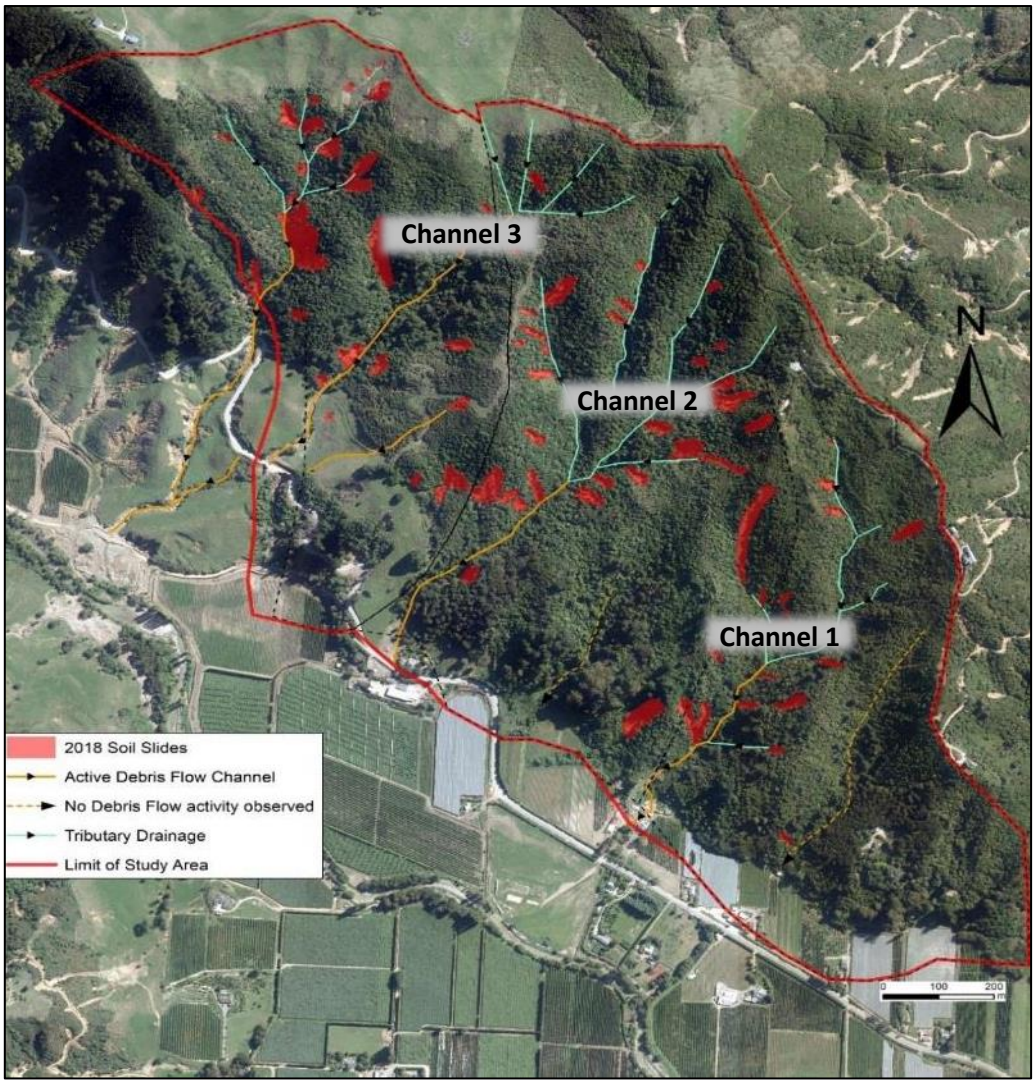

Figure 2.15: Slope instability identified in the February 2018 event. Aerial photo taken on 22nd February 2018, 2 days after Ex-tropical Cyclone Gita. Aerial image supplied by Tasman District Council.

The aerial imagery taken 2 days after Ex-tropical cyclone Gita was used to map areas of eroded open ground which represented soil slides. The total soil slides in the detailed catchment area (outlined in

red) is 77,300m^2, which is 5% of the catchment area. The failures are greater on the western side of the catchment area than on the eastern side. In the catchment area the majority of the slope failures are in vegetated ground.

2.6 Comparison of 1990 and 2018 Events

2.6.1 Geological Controls

The study area is underlain by Onekaka Schist, Undifferentiated Riwaka Igneous Complex and Separation Point Granite. The soil slides in both 1990 and 2018 have been overlain against the geological map from GNS (GNS Web Map, 2012).

The area of soil slides was calculated and divided by the total area of the individual geologic units within the detailed catchment area boundary, as shown in Figure 2.16. The soil slides underlain by Onekaka Schist bedrock is higher (1%) than the Undifferentiated Riwaka Igneous Complex. The area of soil slides sourced from Undifferentiated Riwaka Igneous Complex and Onekaka Schist bedrock are three times as much as the Separation Point Granite derived soil. In both years, 1991 and 2018, the soil slides are higher in soil underlain by Onekaka Schist measured in the detailed catchment area. Although the rainfall records were three times more in 1990 event compared to Ex-tropical cyclone Gita in 2018, the soil slides were significantly higher in 2018 event.

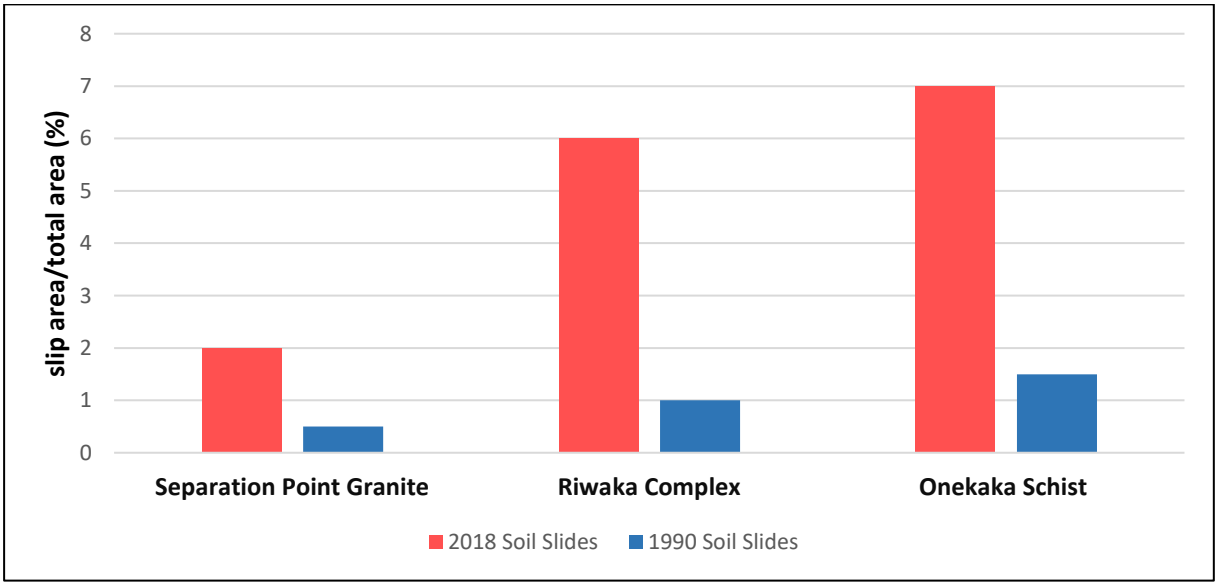

Figure 2.16: Percentage of soil slides in the detailed catchment study area in each bedrock.

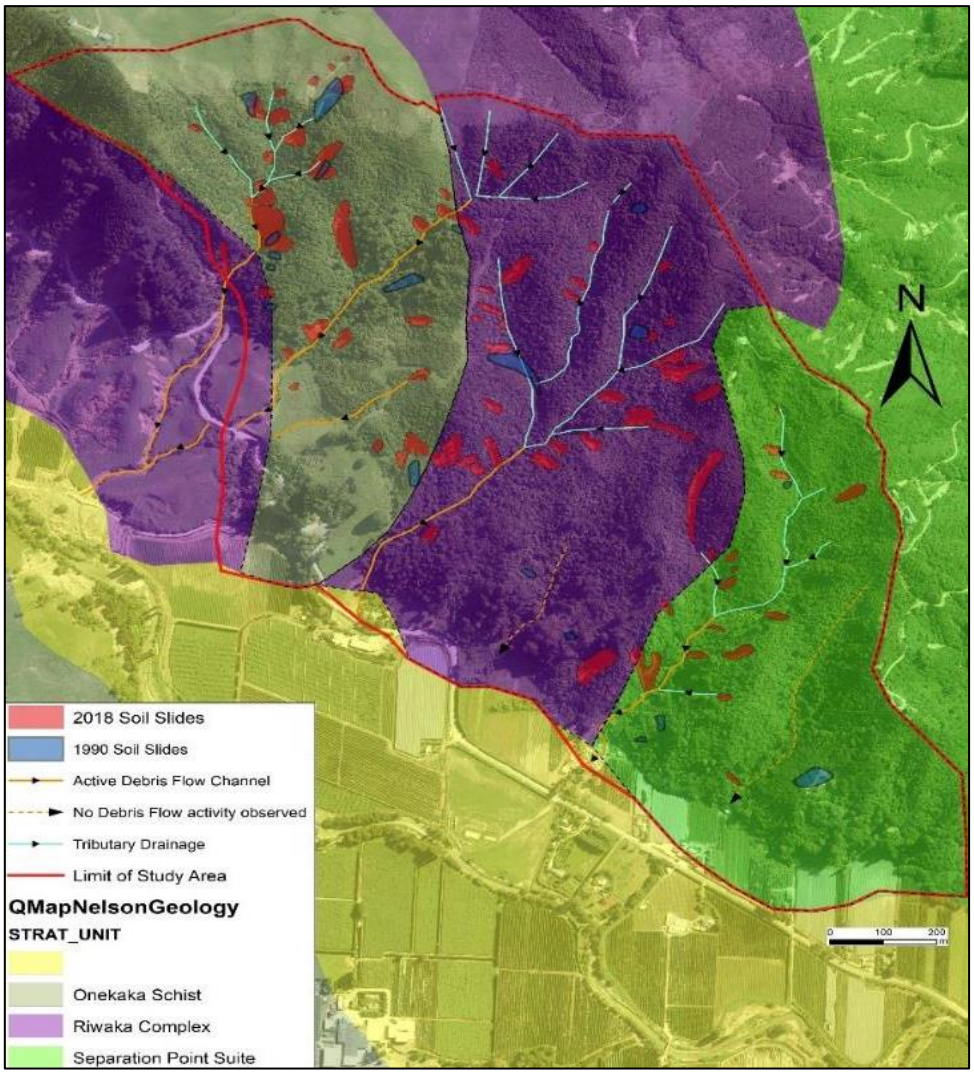

Figure 2.17: Post-Gita aerial image taken 2 days after the 2018 Gita event. The soil slides identified in 1991 and 2018 aerial image are overlain against the Qmap Geological map (GNS Web Map, 2012).

2.6.2 Topography Controls

Figure 2.18 shows the slides against slope angles derived from the 2016 Digital Elevation Model (DEM). It shows that all soil slides in 1990 and 2018 are concentrated in steepest slopes. The majority of the soil slides occurred on a 30° to 40° slope. No differences were identified between 1990 and 2018 soil slides on slope.

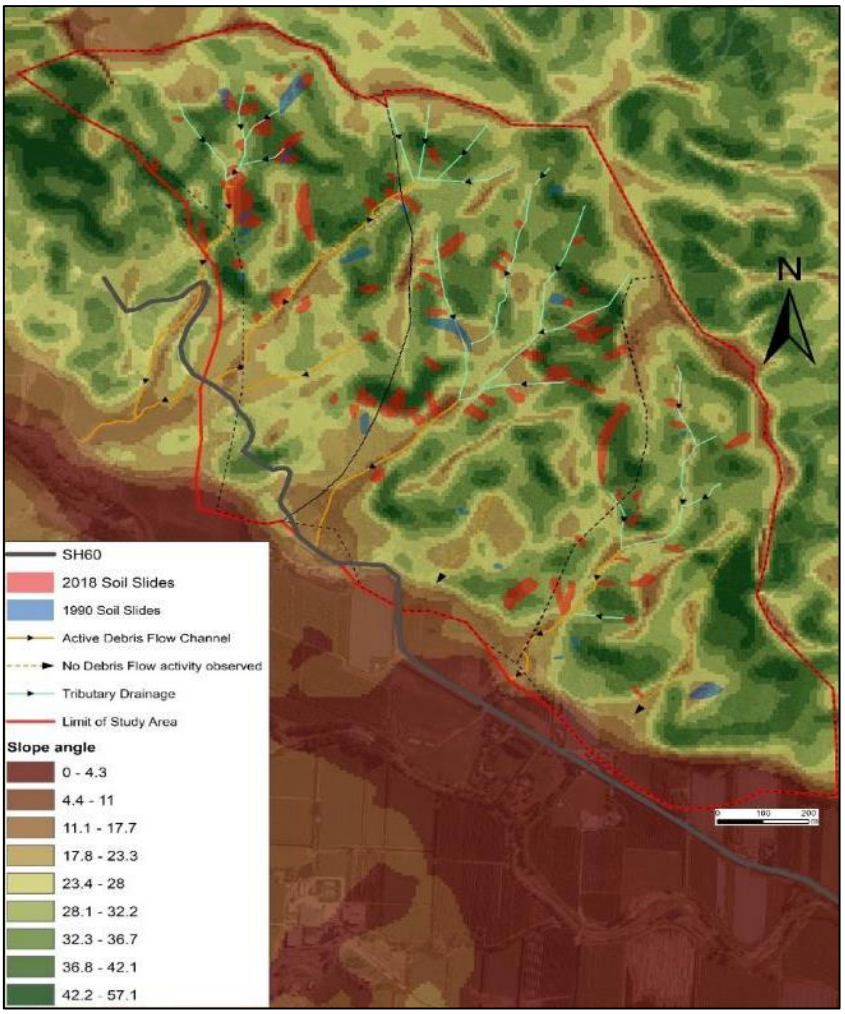

Figure 2.18: Soil slides in 1990 and 2018 plotted against slope angle derived from the 2016 DEM. Source: (Land Information New Zealand, 2018).

2.6.3 Overall Comparison

The total area of slope failures for 1991 is 11,000m^2, whereas the 2018 events generated a total of 65,000m^2 in (Figure 2.17). The 2018 event generated 6 times more slides compared to the 1990 event. Out of the 14 soil slides identified in the 1991 aerial image, 4 soil slides occurred in the same area as the 2018 soil slides, as seen by the overlapping polygons in Figure 2.17. In both the 1990 and 2018 soil slides, the majority of the failures along SH60 occurred in Onekaka Schist and Undifferentiated Riwaka Igneous Complex.

The source zones identified from the 2016 LiDAR were compared with the areas of soil slides identified in the 2018 aerial image and 1991 aerial image. Approximately 10% of the soil slides in 1991 and 35% in 2018 (Gita) were located in existing areas of instability in the LiDAR image (Figure 2.19). Therefore there were 65% new zones of instability in Ex-tropical cyclone Gita event in 2018.

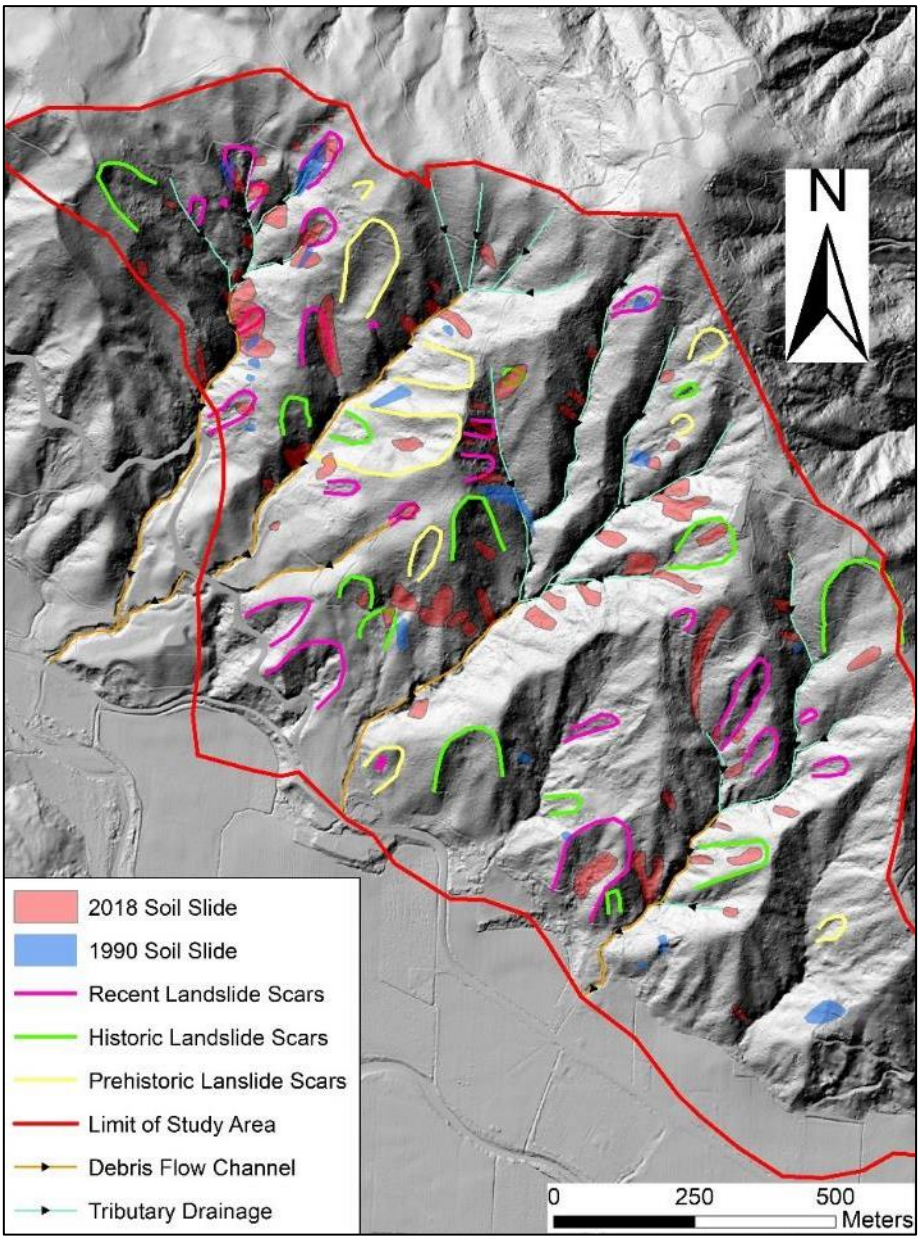

Figure 2.19: Hill shade model using 2016 LiDAR data. The 2018 soil slides triggered by Ex-tropical Cyclone Gita and soil slides identified in the 1991 image are superimposed on the areas of slope instability mapped using pre-2018 LiDAR data. Source: (Land Information New Zealand, 2018)

2.7 Magnitude-Frequency Relationships

Figure 2.20 is plotted from 1944 to 1955, Figure 2.21 from 1956 to 1989, and Figure 2.22 from 1990 to 2018. The rainfall data has been provided by NIWA and is taken from site 1 in Figure 1.5(4 km from the study area). The red star shape represents principal events leading to road closure for ≥ 5 days, and the yellow polygon outlines the small scale “slips” recorded in Table 2.1. From the plots it is observed that, where rainfall exceeds 360mm for the month, major events have been recorded. The exception

is 1944, where no record was found of any instability. The limitations of the data are that most of the slope failures in various reports have been identified as “slips”.

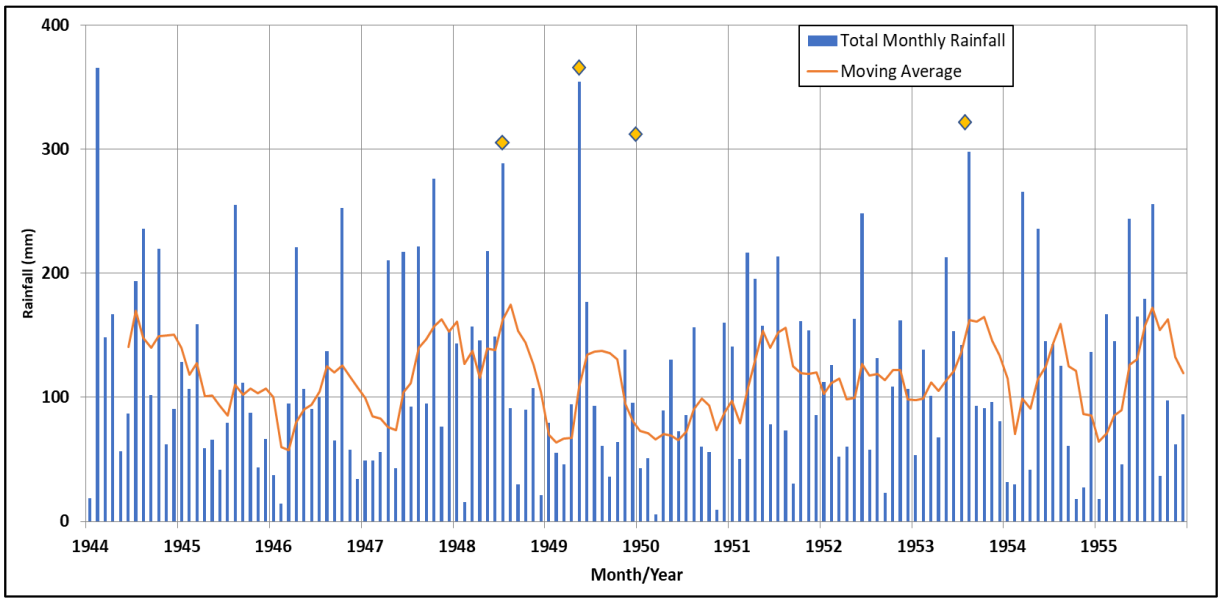

Figure 2.20: Plot of monthly rainfall data and known debris flows causing extensive damage along SH60 for periods 1944-1955. Vertical lines refer to months (Jan-Dec) in each year. For each time interval a moving total (at 6-month intervals) has been created. Rainfall data from NIWA (2018).

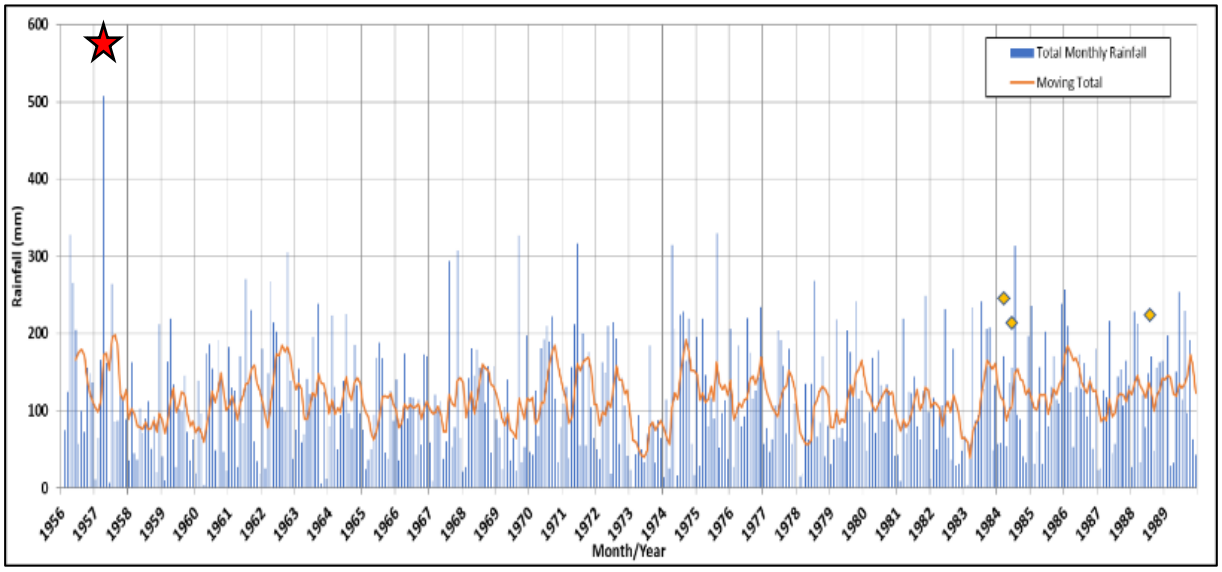

Figure 2.21: Plot of monthly rainfall data and known debris flows causing damage along SH60 for periods 1956 - 1989. Vertical lines refer to months (Jan-Dec) in each year. For each time interval a moving total (at 6-month intervals) has been created. Rainfall data from NIWA (2018).

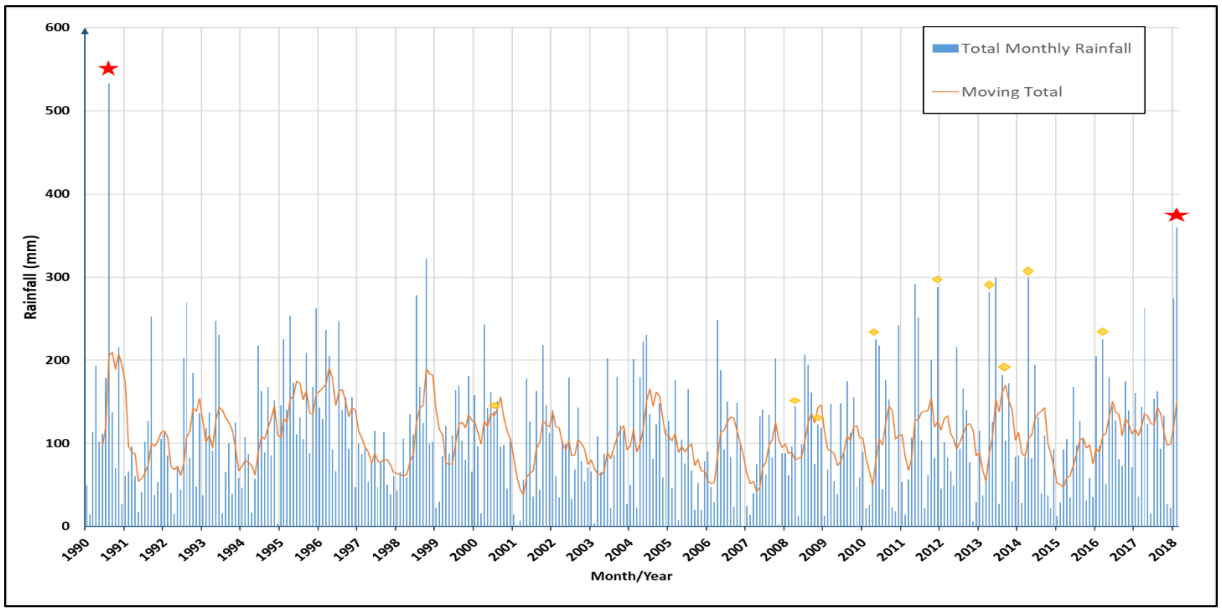

Figure 2.22: Plot of monthly rainfall data and known debris flows causing damage along SH60 for periods 1990-2018. The two largest damaging debris flow events correlate with the two greatest rainfall events in 1990 and 2018. Vertical lines refer to months (Jan-Dec) in each year. For each time interval a moving total (at 6-month intervals) has been created. Rainfall data from NIWA (2018).

The highest rainfall recorded was for August 1990, followed by April 1957, February 1944 and then February 2018. With the exception of 1944, slope instability (soil slides and debris flows) has been recorded for these time periods, as well as road closures of more than 5 days. This shows a frequency of approximately 30 years for large scale events resulting in significant damage to SH60. Although no damage to SH60 due to slips has been recorded in the NIWA historic catalogue in 1944, it does record a period of heavy rainfall in February 1944, where rainfall records were 149mm/24 hours. The 1947 aerial image shows soil slides and recent debris flow fan deposits, indicating some soil instability in 1947 or prior. There may be have slope failure that did not particularly impact SH60.

About 270mm was recorded in January 2018 before Ex-tropical cyclone Gita. The antecedent moisture level in the soil may have been high and the soil would have been in a partially saturated condition prior to the storm event.

2.8 Conclusions

The three principal events (1956/7, 1990 and 2018) correspond to extreme and prolonged rainfall activity as shown by the rainfall plots. The shallow soil slides observed in the 1991 image are interpreted as soil slides triggered by the August 1990 storm event. Again in the 2018 Gita event, SH60 on the eastern side of Takaka Hill was affected. The landowner living next to Channel 2 confirms that

debris flows occurred in 1990 (Sue, personal communication, October 2019) and Channel 2 was also activated in the 2018 storm event.

Before the 1990 storm event, the slopes were covered with vegetation as seen in the 1989 image. It is also observed that vegetation was well established before the 2018 Gita event. This shows that the slope failures occurred regardless of vegetation cover.

From the three known debris flow events in 1956/7, 1990 and 2018, the following conclusions could be drawn:

- The return period for these large-scale events is approximately 30 years.
- Only some of the failures occurred in areas of previous instability, the new failures presumably being first time failures.
- The amount of vegetation cover does not appear to influence slope stability greatly.
- There are more failures in soils overlying Onekaka schist and Undifferentiated Riwaka Igneous Complex bedrock than Separation Point Granite because that geological unit does not outcrop on SH60.
- Outside the study area (away from SH60) there were numerous failures observed in Separation Point Suite from post Cyclone Gita aerial photos.

It is not known whether this is due to the geotechnical properties of these soils or a function of local variation in rainfall. An attempt has been made to understand the geotechnical properties of the soils in the study region, and their relationship to failure is discussed in Chapter 4.

Chapter 3: Engineering Geology Investigations

3.1 Introduction

The debris flows triggered by Ex-tropical cyclone Gita in 2018 occurred in an area underlain by differing bedrock lithologies (Undifferentiated Riwaka Igneous Complex, Separation Point Granite and Onekaka Schist), as shown in Figure 1.8 (Chapter 1). The present chapter describes the field investigations performed in order to investigate the relationship between bedrock lithology and the occurrence and types of slope failures. The investigations involved engineering geomorphic mapping, *in-situ* testing, subsurface profiling and collection of samples for geotechnical laboratory testing. The main objective of these investigations was to characterise the 2018 failure materials, and by studying the older failures and potential debris flow sources zones, develop an understanding of the ongoing hazard of State Highway 60 (SH60).

To repair damaged sites along State Highway 60 (SH60) following Ex-tropical cyclone Gita, New Zealand Transport Agency (NZTA) commissioned engineering consultant Beca to provide the design for remedial solutions (Beca, 2019). A drilling campaign was carried out in March and April 2019, and the author participated in the drilling programme on two of the sites adjacent to the area of detailed investigation for this study (Channel 3 catchment). The core from this drilling campaign was used for point load strength testing and Uniaxial Compressive Strength testing. The core samples were also used to prepare thin sections in order to evaluate the degree of weathering and hence evaluate the effect of weathering on rock strength. This is discussed in detail in Chapter 5.

3.2 Field Methodology

3.2.1 Desktop Study

Prior to beginning the field investigations a series of desk study activities, including synthesis of prior data and image analysis (Chapter 2), were performed to map the areas of damage from the 2018 storm and to identify areas of previous slope instability. The first activity was mapping of the soil slides (debris flow source areas) and the debris flow paths on the eastern side Takaka Hill triggered in 2018. This was accomplished using aerial imagery taken two days after the passage of Ex-tropical cyclone Gita (Figure 3.1). In addition, previous remote sensing data (aerial photographs and LiDAR imagery) were analysed to understand the nature of past slope instability and thus understand the hazard to SH60.

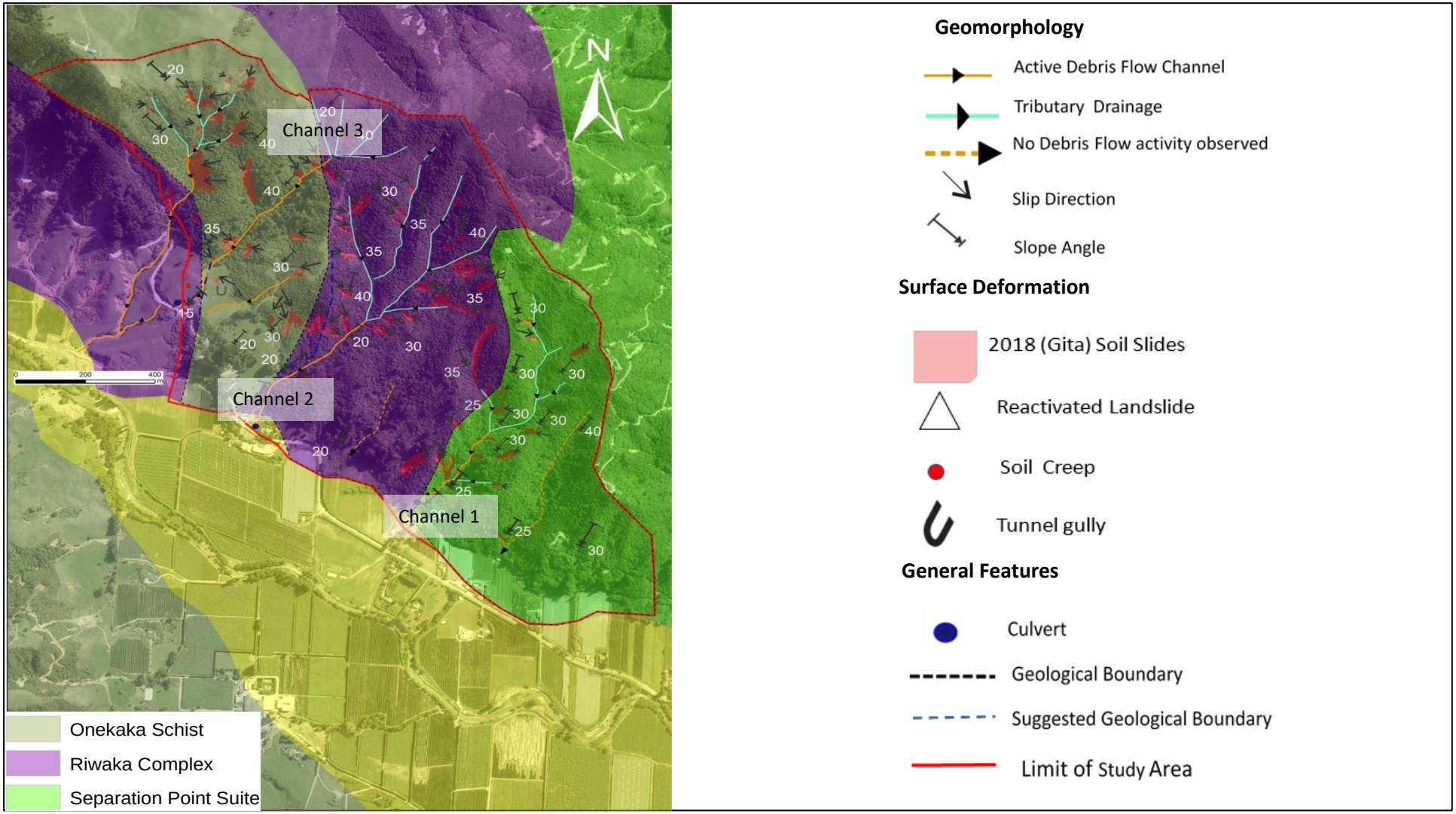

Figure 3.1: Engineering Geomorphology map of the detailed catchment area.

Following desktop studies, a reconnaissance survey was undertaken for site selection. The detailed catchment area outlined in red was selected for this thesis (Figure 3.1). The area was selected as there were channels that activated during activated during Ex-tropical cyclone Gita and were underlain by three bedrock lithologies. This will provide an insight into whether the bedrock has an influence on slope failure. During the reconnaissance survey channel width and channel height, as well as colluvium thickness, was measured every 20m in the three main debris flow channels. A generalized channel profile is presented in Appendix A.1.

3.2.2 Field Sampling

A programme of field investigation was planned which included face logging, *in-situ* testing, soil sampling and geophysical survey. As some of the channels are still blocked by debris from the 2018 debris flow activity, it was not possible to collect samples from all areas (Figure 3.2). This also limited the number of *in-situ* tests that could be performed.

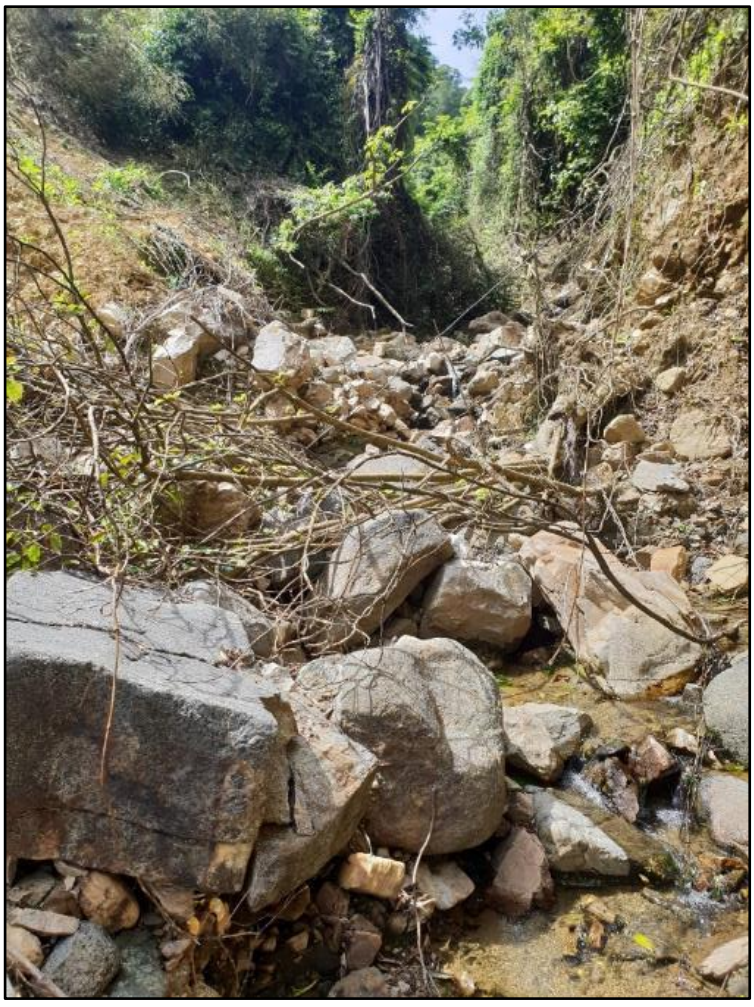

Figure 3.2: Channel 3 blocked by trees and boulders making it difficult to access the channel.

Both undisturbed tube samples and disturbed bulk samples were collected for classification tests and shear strength tests. The samples were collected from exposed stream banks in the channels and road cuts (refer to Figure 4.1, Chapter 4 for sample locations). The samples were collected from each weathering profile identified, from both 2018 debris flow sources areas and from the matrix of pre-2018 debris flow deposits. All samples were tightly bagged and sealed at the site to retain the moisture and they were kept in a storage container in the laboratory.

Undisturbed samples for soil density and hydraulic conductivity tests were collected using driven steel tubes. Tubes of 38mm diameter and 120mm length were used to collect samples for density testing. It was often difficult to drive a tube for its full length and some soils were too stiff/dense to allow any sample collection. In total 11 samples were collected for density testing. The tubes used for hydraulic conductivity test were 100mm in diameter and 110mm in length. Six complete samples were collected.

Attempts were made to collect larger, intact block samples using large diameter PVC pipe. However, this was not successful, as the soils disaggregated. Therefore, only bulk (disturbed) samples were collected for direct shear testing.

3.3 Engineering Geomorphology Mapping

Following detailed mapping from LiDAR and aerial photos, and reconnaissance survey, field mapping of the lithologies in each channel was carried out. Field observation of Ex-tropical cyclone Gita-induced slope failures was performed in detail. In order to quantify older debris flow volumes, stream bank sections were logged in detail (Section 3.4). As these exposures only provide a 2-D representation of past events, unit thickness was used as a proxy measurement for debris flow volume.

The main soil slides observed following Ex-tropical cyclone Gita occurred in 1-5 m thick colluvium at or near the completely bedrock or residual soil – colluvium contact. At times the failed mass extended into the completely weathered interface. The majority of failures were translational, on planar to slightly undulating slip surfaces. Exposures in the headscarps and lateral scarps of the failures show the colluvium to be mainly matrix supported, with predominantly boulder and cobble-size clasts in a fine-grained matrix. The matrix is silt with varying amounts of clay and sand. The larger clasts (boulders and cobbles) are sub-angular to sub-rounded, part of a widely or gap graded deposit showing random or chaotic internal structure.

Uneven surfaces on the lower slopes with large boulders at low elevations, prominent lobate, channel and levee surface morphology suggest that these are debris fans, indicating a long history of debris flow activity in the area. In fact, pre-2018 deposits are exposed in channel cut banks of all channels examined on Takaka Hill. At least two pre -2018 debris flow deposits were recognised along each of the channel banks in all three lithologies.

Shallow soil slides in colluvium above weathered bedrock were the main source of debris flows observed in all the debris flow channels activated in 2018. Other sources of debris were overlying vegetative material and weathered bedrock supplying sediments to the debris flow.

Within the main drainage landslides occur on slopes of 15° to 40° (Figure 3.1). The majority of these slides are immediately adjacent to the active drainage channel, therefore even with small amounts of displacement, the failed material becomes entrained in the channel and becomes the sources for debris flow activity.

The channelised debris flows from 2018 are characterized by long runout distances, hundreds of metres from the source area, depositing material on the lower slopes, on debris fans or on the Riwaka floodplain. Channel volumes were estimated to range from 6400 m^3 to 14000m^3 (refer to Appendix A.1 for calculation of volumes). Although the majority of the channelised debris flow material has been deposited on the lower slopes, an appreciable amount of material is still stored within the channels. The active drainage channels are filled with a mix of boulders, tree debris, and fine sand to gravel from previous debris flows as well as material from Gita. Figure 3.1 shows the geomorphology of the detailed catchment study area.

3.4 Exposure Face Logging

Both the 2018 and pre-2018 debris flow deposits were described according to geomorphological setting in channels. Channel 1 is underlain by Separation Point Granite. Channel 2 and Channel 3 is underlain by both Undifferentiated Riwaka Igneous Complex at the lower part of the slope and Onekaka Schist higher up the stream (Figure 3.1). Detailed descriptions and logs for all exposures mapped are presented in Appendix A.2. The logs show sample location. The description of exposure follows the New Zealand Geotechnical Society (NZGS) 2005 Guidelines (New Zealand Geotechnical Society, 2005).

3.4.1 Channel 1

Channel 1, underlain by Separation Point Granite (SPG) and has an average channel depth of 2 m as measured. This gives a volume of ~6,400 m^3 of deposit on stream banks along the main flow of the channel (active debris flow, orange line, Figure 3.1) from aerial imagery and width measured in the field. Appendix A.1 shows typical profiles of Channel 1 indicating the depth of colluvium and inferred bedrock contacts.

Moderately weathered SPG is exposed at the upper end of Channel 1. There were two major joint sets in both exposures. Figure 3.3 A shows moderately weathered SPG, at the upper end of Channel 1. The debris flow source areas identified from aerial photos could not be accessed due to steep tributary drainage channels at the top of the main channel. Two short and steep tributaries intersect the main channel and have scoured overlying sediments to bedrock (Figure 3.3 C). As such none of the debris flow slide sources areas identified in aerial image could be accessed. Samples were therefore collected along the Riwaka-Kaiteriteri road cut (S2) where shallow soil slides occurred above weathered SPG (Appendix A.2). This was considered representative of the channel geology. A drone survey was conducted in August 2019 over Channel 1 to identify any new slides that may have occurred after the February 2018 rainfall-triggered debris flows. No new soil slides were identified in the area of the drone survey. These results are presented in Appendix A.3.

The typical pre-2018 debris flow deposit overlying SPG is shown in Figure 3.4. At least three debris flow events have been identified in this exposure. The description of the three pre-2018 debris flow deposits are as follows: (A) clayey silt with occasional (1%) cobbles and gravel, firm, moist, high plasticity, poorly graded; (B) 20% boulders and cobbles – the matrix is silty sand with some gravel and minor clay; (C) 15% cobbles and boulders – the matrix is sandy gravel with minor silt and clay. In all pre-2018 debris flow events, the cobbles and boulders are sub-angular to sub-rounded quartzite and diorite rocks. The percentage of boulders and cobbles represents proportion in the fine grained matrix and not weight percentages.

Figure 3.3: (A) Moderately weathered SPG. Iron staining and closely to moderately spaced joint sets are prominent. (B) Completely weathered SPG. The inset shows an enlarged picture of the weathered bedrock). (C) Upper end of main channel 1 where two tributary channels intersect main channel and scour into bedrock.

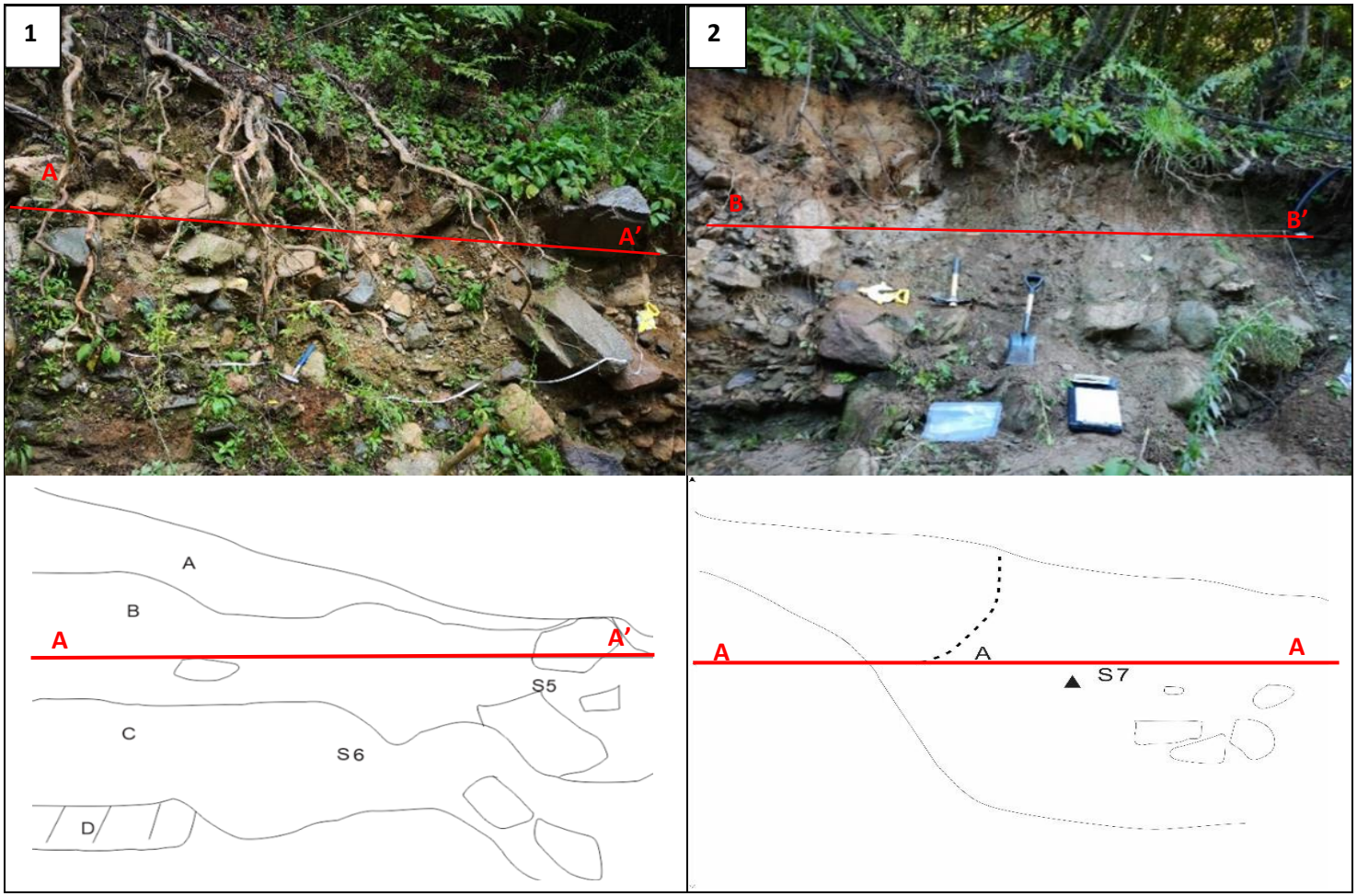

Figure 3.4: Pre-2018 Debris flow deposit underlain by Separation Point Granite. The interpretation are shown below each exposure. 1: Highly weathered granodiorite (D) is overlain by at least 3 different debris flow events (A-C). 2: Another exposure showing locations of in-situ test locations. The triangle represents shear vane. The locations of sample collection are represented by S (Sample). Hammer for scale.

3.4.2 Channel 2

Undifferentiated Riwaka Igneous Complex (URIC) mostly underlies the lower slopes (Figure 3.1). Figure 3.5 shows a typical pre-2018 debris flow deposit in the Channel 2 bank. Five pre-2018 deposits have been identified in this exposure above weathered gabbro. The description of the five pre-2018 debris flow deposits are as follows: (A) 30 % boulders of felsic and mafic igneous rock, sub angular, unweathered to slightly weathered in a sandy matrix; (B) 7% boulders and cobbles of mafic and felsic igneous rock sub angular to sub rounded – matrix supported – silty sand with minor gravel, moist, no plasticity, very stiff; (C) 15% boulders and cobbles, mostly mafic rock with some quartzite, sub angular to sub rounded, unweathered to slightly weathered in sandy matrix; (D) Stratified gravelly debris flow deposit in a sandy silty matrix – gravels – unweathered to moderately weathered gravels of mafic and quartzite rocks – bulk sample collected, S12; (E) 20% boulder and cobbles, sub rounded to sub angular igneous rock, mostly gabbro in a sandy matrix.

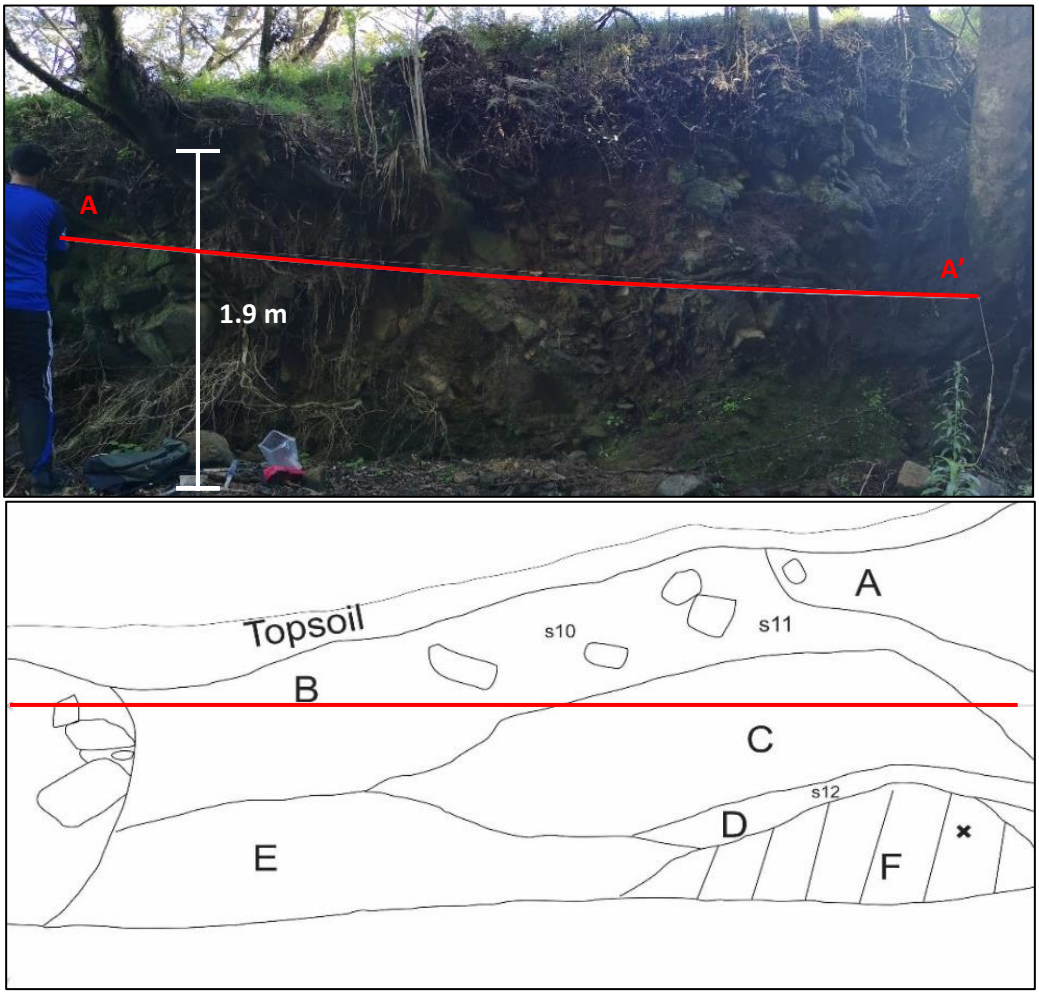

Figure 3.5: Pre 2018 debris flow deposit - 1 is without interpretation, and 2 is with interpretation. At least 5 debris flow events (A-D) have been identified above highly weathered bedrock (F). The "x" represents Schmidt hammer tests. Bulk samples s10 and s 11 were collected.

A soil slide material up to 5 m overlying residual soil to completely weathered URIC bedrock has been identified in Channel 2 (Figure 3.6). A drone survey was also conducted above Channel 2 and no new slides after Ex-tropical cyclone Gita were identified (refer to Appendix A.3 for drone image).

Figure 3.6: Soil slide in approximately 5 m thick colluvium (A and B) located in Channel 2 above URIC. Failure is translational on a slip plane subparallel to the ground surface at the contact with weathered URIC bedrock, marked by orange dashed line(C) is completely weathered to residual soil and (D) is highly weathered URIC bedrock. The failed material has fallen into the active drainage channel (E). Shear vane measurements were taken on weathered bedrock. The colluvium was too hard to drive the shear vane in.

While mapping channel 2, Onekaka Schist bedrock was identified (Figure 3.7), which has been marked as URIC 1:250,000 Geology map (GNS Web Map, 2012). A geological boundary suggestion is shown in Figure 3.1.

Figure 3 7: Onekaka Schist outcrop in Channel 2.

3.4.3 Channel 3

The lower part of Channel 3 is underlain by URIC bedrock, and Onekaka Schist bedrock underlies the colluvium approximately 180m above SH60 (Figure 3.1). The slide occurred at the contact between Onekaka schist and Riwaka Complex (Figure 3.8). A geological boundary suggestion is shown in Figure 3.1 which is different from the 1: 250,000 Geological map (GNS Web Map, 2012). The weathering profile in Onekaka Schist was different from the Separation Point Granite and Undifferentiated Riwaka Igneous Complex, in that it was clay -rich with angular gravel. The derived residual soil was highly plastic. The mapping of Onekaka schist bedrock in Channel 3 was limited as the slides were further up the channel, and trees and boulders blocked the channel, making it difficult to gain access up the channel.

Figure 3 8: Soil slide in approximately 1m thick colluvium located in Channel 3. Failure is translational on an undulating surface. The contact between Onekaka schist (OS) and Undifferentiated Riwaka Igneous Complex (URIC) is seen. The colluvium (S13) consists of 12% cobbles. Matrix silty clay, dark brown, soft, moist, medium plasticity. The Onekaka Schist (S14): completely weathered to residual soil, orange brown, silty CLAY with some gravel, moist, high plasticity. Gravel: angular, slightly weathered quartzite. The URIC (S15): completely weathered to residual soil, dark brown with some visible black minerals, clayey SILT, moist, low plasticity. Tube and bulk samples were collected for colluvium and both weathered bedrocks.

Figure 3.9: Pre-2018 debris flow deposit. The red area is the slide visible in Figure 3.8

Along with the observation of soil slides and pre-2018 debris flow deposits, other geomorphological indications of slope movement, including tunnel gullying and soil creep terracettes (Appendix A2), were observed on the slopes underlain by Onekaka Schist and Undifferentiated Riwaka Igneous Complex next to the channel 3 (Figure 3.1 shows the location of these deformations).

3.5 Geophysical Surveys

3.5.1 Survey Design

Geophysical lines were conducted on a debris fan next to Channel 2, which is underlain by Onekaka Schist and Undifferentiated Riwaka Igneous Complex bedrock (Figure 3.10). The primary objectives of the geophysical survey were to provide a better understanding of the geometry and hence the volume

of prior debris flow events, as the profiles of prior debris flows obtained from outcrop face logging are only in 2D. Another objective was to identify colluvium and bedrock contacts.

A total of three lines were run, one across the axis of the debris fan and two perpendicular to the axis in the same line. Methods included both Multi-channel Analysis of Surface Waves (MASW) and Ground Penetrating Radar (GPR). *In-situ* tests including dynamic cone penetrometer (DCP) and double ring Infiltrometer (Figure 3.10) were conducted along the geophysical lines: the results are discussed in Section 3.6.

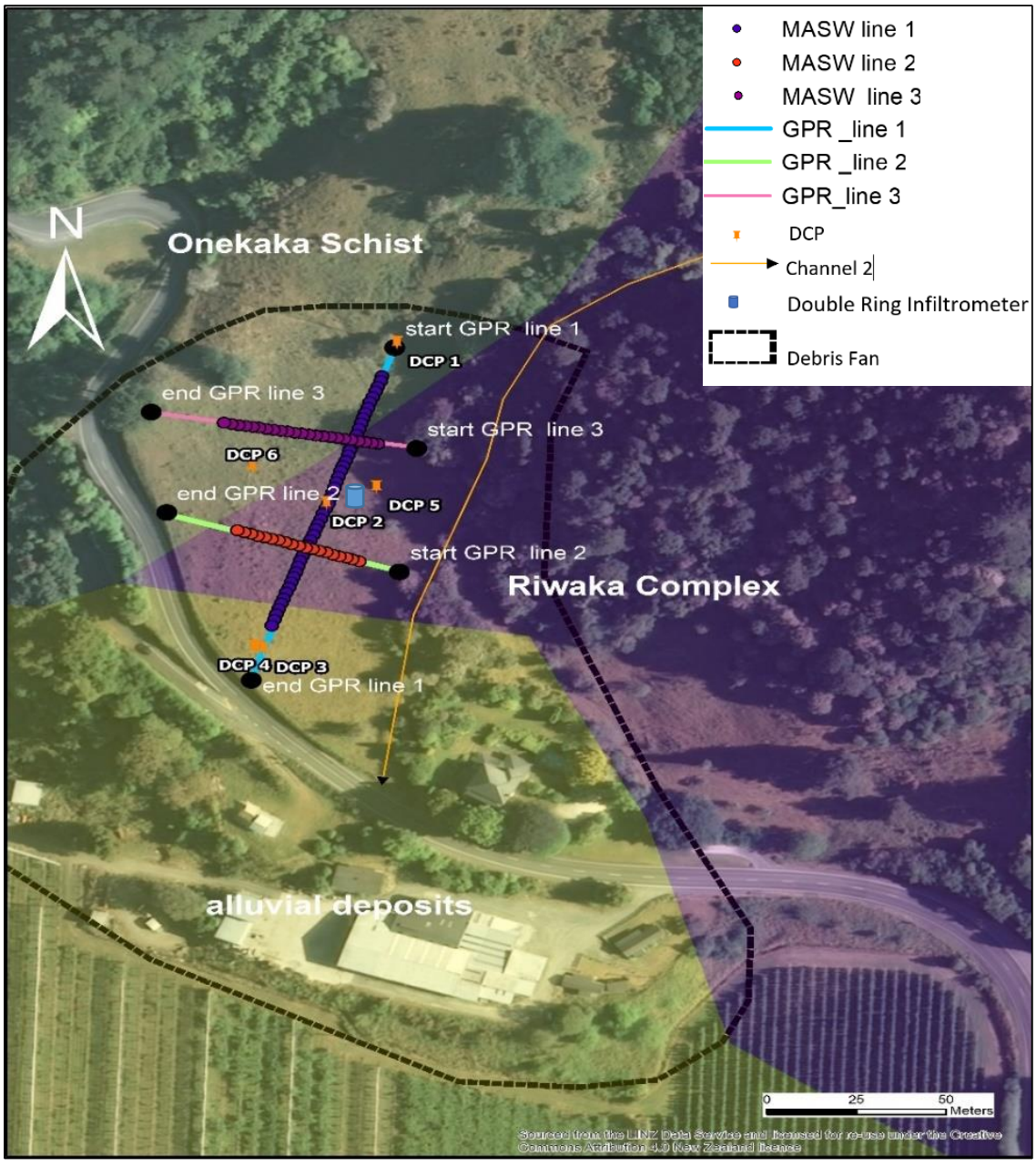

Figure 3.10: Location of subsurface and in situ testing sites. The GPR lines are slightly longer than the MASW lines. Geological contacts are taken from QMAP Nelson (GNS Web Map, 2012).

3.5.2 Multi-Channel Analysis of Surface Waves

MASW is a non-invasive method used for shallow subsurface profiling. It evaluates the ground by measuring shear wave velocity (Vs) in the subsurface. As well as providing information on the subsurface structure, Vs can also be used to determine material density and stiffness.

The maximum depth range for MASW survey is 10-30 meters, but varies with different sites and sources of data acquisition used (Park Seismic LLC, 2006). The MASW survey method was carried out in three steps: acquiring data, extracting dispersion curves, and inversion of generated dispersion curves. The raw data was processed by Christian Ruegg (Southern Geophysics) using SurfSeis software. Each record from the field was used to generate a dispersion image using the f-k transformation method, followed by extraction of a dispersion curve from the image. Inversion was carried out on the dispersion curve to create a 1-D (depth) Vs Profile.

MASW line 1 (along the axis of fan) was 93m in length and the lines running perpendicular to the MASW line 1 were 33m (MASW line 2) and 43m (MASW line 3) in length. The seismic waves were generated using a 4 kg sledgehammer and a 10m shot offset. An impact plate was placed to improve signal coupling. Four shots were stacked at each measurement location. The resulting signals were recorded by 24 vertical low frequency (2.5Hz) geophones spaced every 1m. Two-meter line movements in a north –south direction (from top to bottom of the channel) were performed along the axis of the fan. The perpendicular lines were run in east-west direction.

An exposure along SH60 at the bottom of the fan were used to assist with data interpretation (Figure 3.11). The typical values mentioned above and DCP data (*in-situ* tests discussed in next section) were also used for interpretation. A case example presented by Park (2016) include a Vs 100 m/s - 300 m/s, indicating soft soil and bedrock velocities that include 300 m/s - 1000 m/s, indicating bedrock with different weathering grades. Another example included velocities of bedrock at 1000 m/s - 1500 m/s, which was interpreted as slightly weathered rock (Park, 2006). The National Earthquake Hazard Reduction Program (NEEHRP) provides typical shear wave velocity (Vs) values for soil and rocks: Soft clay soil - <180 m/s; Stiff soil - 180 m/s to 360 m/s; Very Dense Soil and Soft Rock - 360 m/s to 760 m/s; Rock - 760 m/s to 1500 m/s; and Hard rock - >1500m/s (Park, 2006).

The processed MASW data with interpretation is presented in Figure 3.12. The maximum depth of penetration was up to 30m. The shear wave velocity increases with depth and ranged from 100 m/s to 1500m/s. The processed MASW profile shows a gradation of shear wave velocity (Vs). Table 3.1 shows the interpretation of the shear wave velocity.

Figure 3.11: Exposure at the bottom of geophysical line 1. Approximately 3 m of debris flow deposit consisting of boulder and cobbles in a fine grained matrix. At least two units are observed: (A) Approximately 2% cobbles and boulder (B) Approximately 7% cobbles and boulders.

Table 3.1: Shear wave velocity interpretation.

Shear wave velocity, V_s (m/s)	**Description**
100-400	Colluvium
400-600	Completely weathered bedrock to residual soil
600-1000	Highly weathered to moderately weathered bedrock
>1000	Slightly weathered to unweathered bedrock

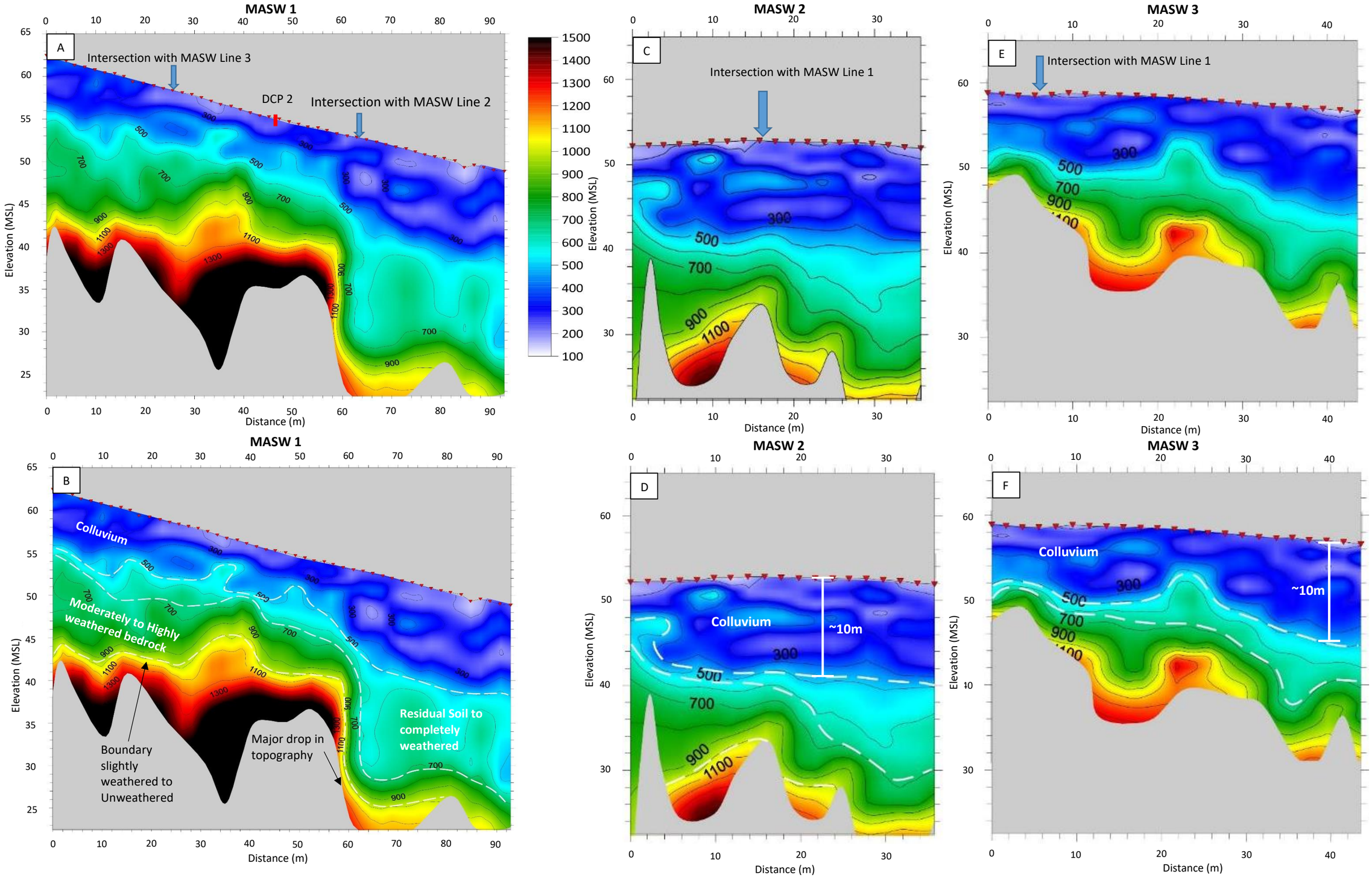

Figure 3.12: Processed MASW results for the 3 lines. MASW line 1 shows the locations of DCP 1. A through F are the processed MASW results. A, C and E are without interpretation, while B, D and F are with interpretation. The grey colour at the bottom of each Figure indicates no penetration.

Along MASW line 1, where the DCP 2 test was carried out (Figure 3.12 A), shows that the Vs changes from 200 m/s to 300 m/s. This is also reflected in the DCP data (Section 3.6) where the soil shows a loose to dense type behaviour with increasing depth. Along MASW line 1, the thickness of colluvium increases towards the bottom of the fan, as it was expected. This profile is interpreted as showing colluvium thickness varying between of around 6 m on the upper slope, thinning to 2 m on the mid-slope, before suddenly thickening to 9 m towards the base of the slope. This sudden thickening of the colluvial sequence could possibly be infilling an erosional bedrock hollow. Lines 2 and 3 which run transverse to the fan axis show colluvium varying between 6 m and 10 m. The interpreted bedrock profile also shows a number of step-like erosional features (Figure 3.12).

3.5.3 Ground Penetrating Radar

Ground Penetrating Radar (GPR) uses an electromagnetic pulse and record reflections from interfaces with differing dielectric properties. This is another non-invasive method to get subsurface information. The transmitter antenna sends electromagnetic waves into the ground and the reflected waves are received by the receiver antenna. This information travels to computer equipment via fibre optic cables, and computer equipment translates information into a picture on the screen (Jol & Bristow, 2003). The antennae frequency of 100 MHz was used for the survey. Using common mid-point (CMP) method, the velocity was calculated to be 0.06 m/ns.

The GPR survey was also conducted along with the MASW profiles to provide further detail of the subsurface structure. Although the GPR profiles were limited to the upper 6 m, they provide a reasonable picture of the debris fan architecture. GPR survey data was subject to minimal processing. Other than filtering to remove air arrivals and correcting for topography, the profiles presented are of raw field data.

In the GPR Line 1 data, the upper slope is marked by a series of planar, slope-parallel units probably representing sheet wash colluvium. The mid slope shows a buried debris channel. The chaotic reflections (overlapping diffractions) in the lower slope indicate a concentration of boulder material. This architecture is typical of many debris' flows. The linear feature in GPR line 1 is interpreted to represent debris flow events (marked by different colours in the mid-slope). The DCP placed at the start of GPR Line 1 shows up to 1.5 meters depth, where the DCP could not be penetrated any further. This is most likely due to bedrock as GPR does not show any signal at that depth (Figure 3.14). The two GPR lines (Figure 3.15 and Figure 3.16) running perpendicular to the fan axis also show similar chaotic structure. A buried channel is observed in Line 3 (Figure 3.16).

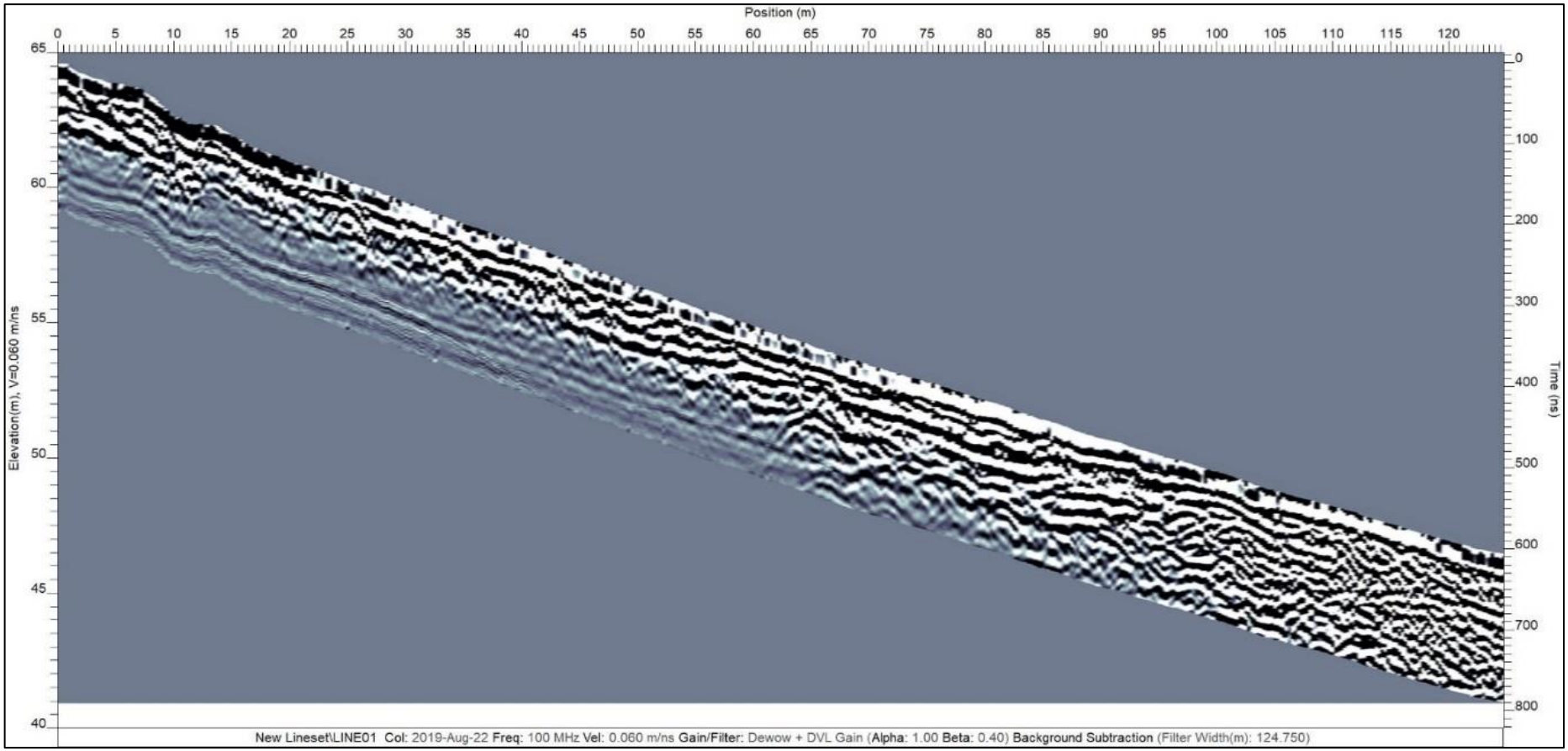

Figure 3.13: Raw GPR data of Line 1.

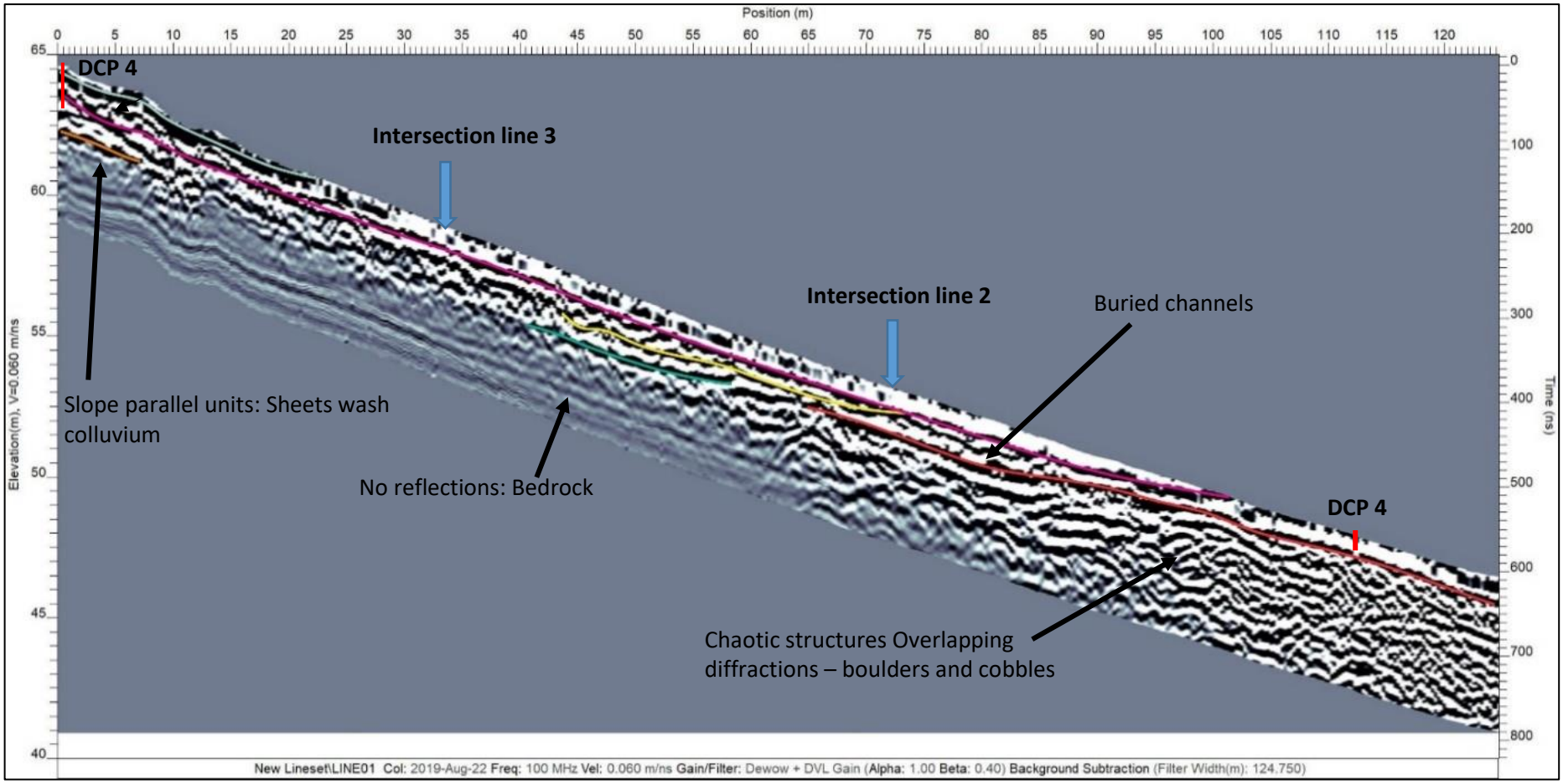

Figure 3.14: Interpreted GPR data of the longest Line, 1, along the debris fan. The red lines indicate the location of two DCP tests conducted along the GPR extent. The Blue arrows show the intersection of GPR lines 2 and 3.The linear featured marked by different coloured lines is interpreted to be different debris flow events.

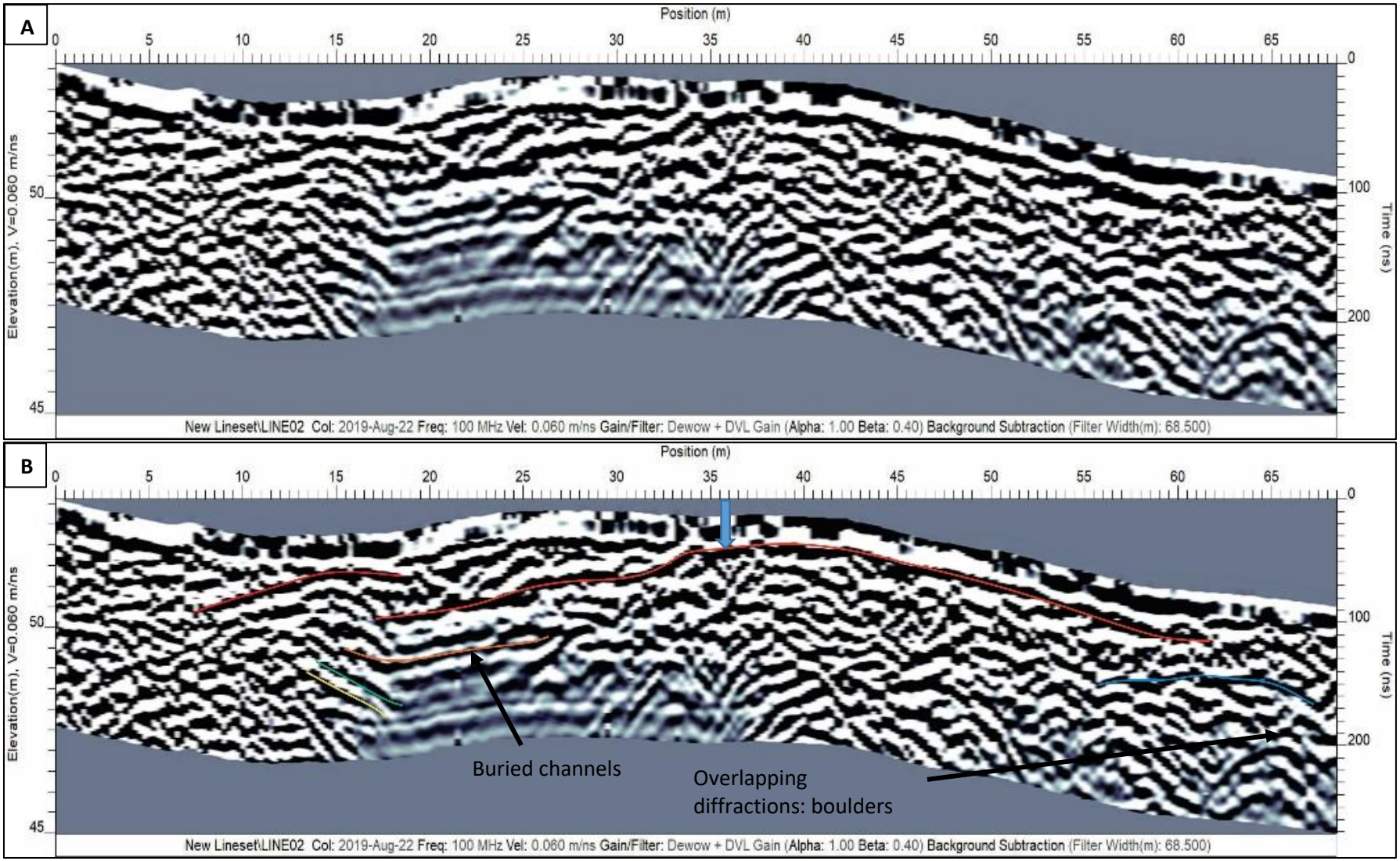

Figure 3.15: A) Raw GPR data of Line 2. B) Interpreted GPR data of Line 2. The blue arrow indicates the intersection of GPR line 1.

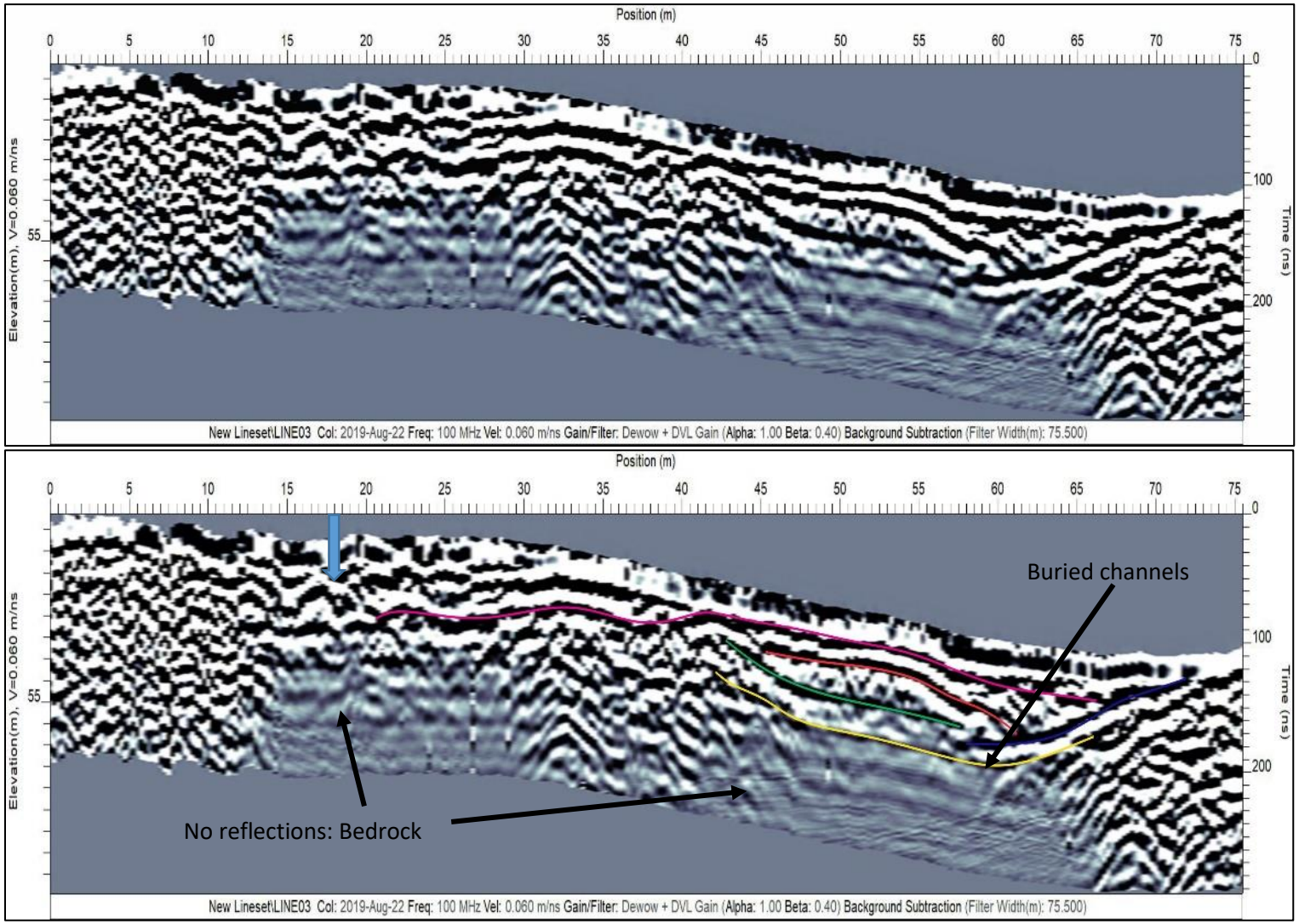

Figure 3.16: A) Raw GPR data of Line 3. B) Interpreted GPR data of Line 3. The blue arrow indicates the intersection of GPR line 1.

3.5.4 Synthesis of Subsurface Data

The GPR and MASW lines show a sequence of fan-deposited colluvium (pre-2018 debris flow deposit) ranging from 3 m to 10 m thickness. A roadside exposure at the margin of the geophysical survey area confirms the presence of at least 3 m of colluvium (Figure 3.11).

Using both the subsurface geophysical data and geomorphological mapping the total volume of deposited fan-derived colluvium can be estimated. The area of the fan surface was estimated to be 42000m^2 (Figure 3.10). The average thickness of colluvium from the geophysical survey is 6 m. This gives an estimated volume of 250,000 m^3 for pre-2018 debris flow deposit.

When the MASW and GPR data on the same survey lines are compared (Figure 3.17). It is observed that the channel in the GPR line 1 is coincident with the bedrock 'step' on the MASW Line 1.

The zone of no reflection in GPR lines 2 and 3 was initially interpreted as bedrock (Figure 3.15 and Figure 3.16). However when compared with MASW lines (Figure 3.18) it appears that this is most likely an area of saturated colluvium.

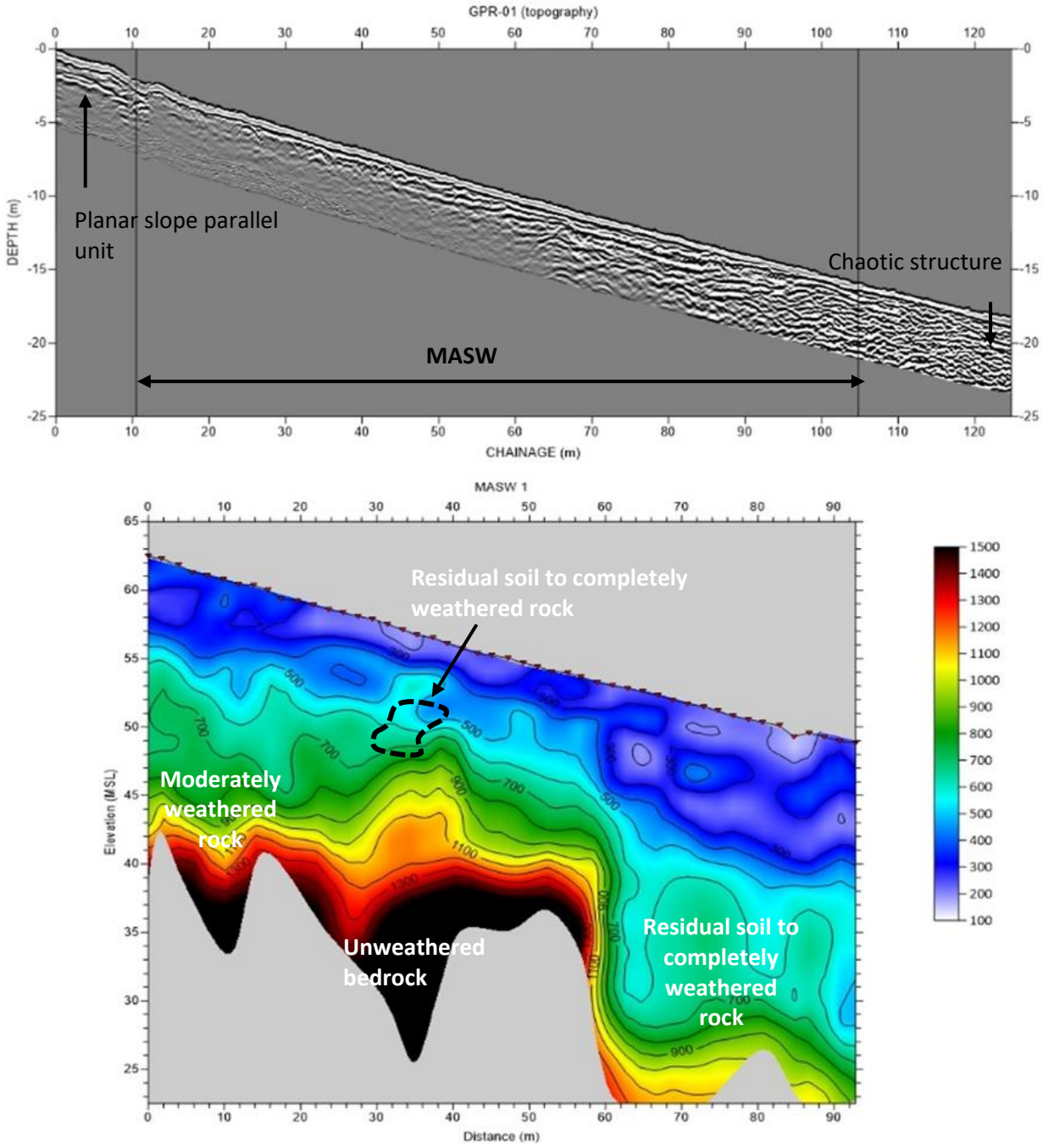

Figure 3.17: GPR line 1 (top) and MASW line 1 (bottom) profiles along the axis of the debris fan.

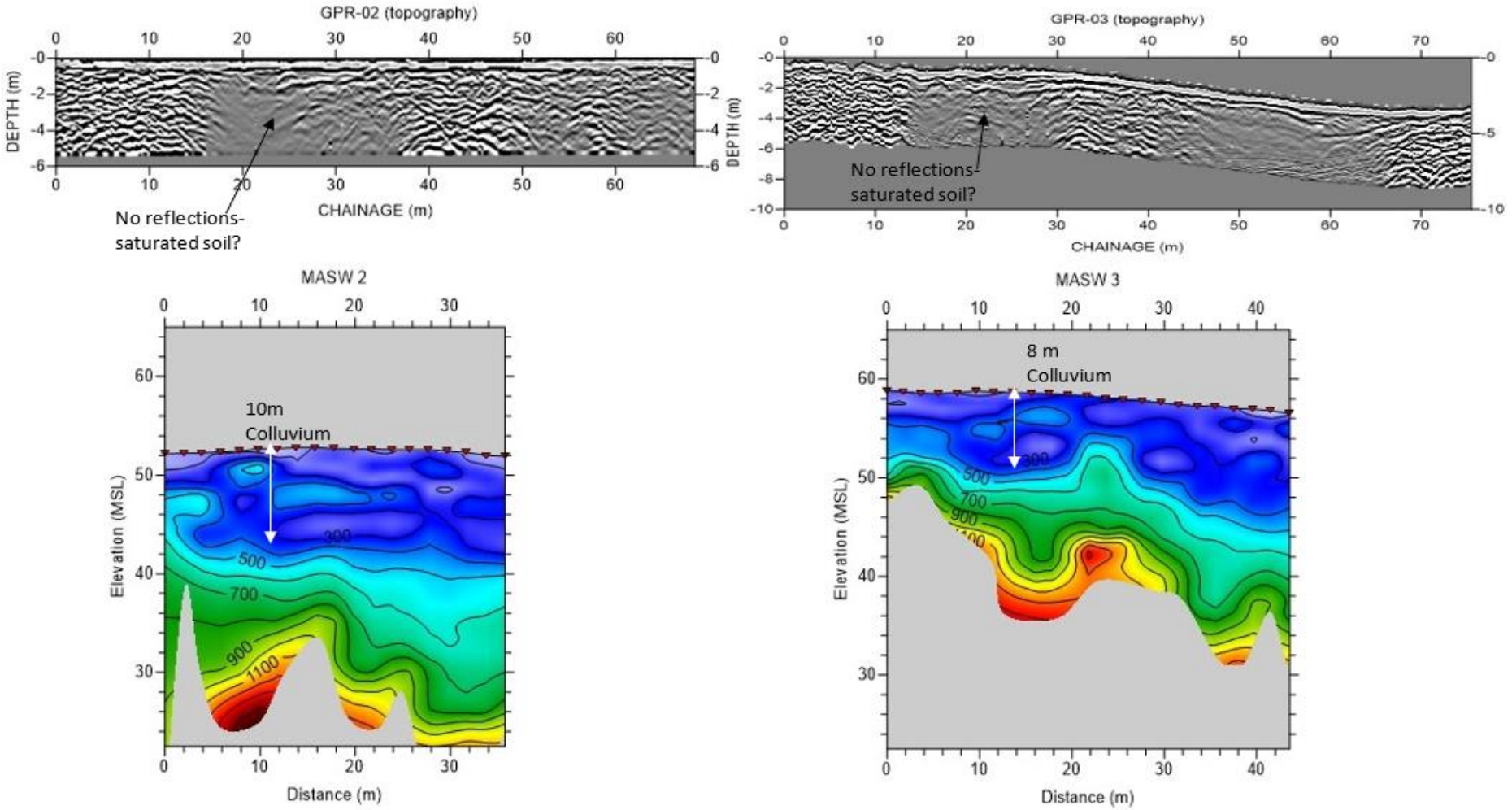

Figure 3.18: GPR line 2 and 3 (top) and MASW line 2 and 3 (bottom) profiles along the axis of the debris fan.

3.6 *In-situ* Geotechnical Testing

3.6.1 Testing Methodology

To characterise the colluvium, *in-situ* tests were carried out. *In-situ* testing was conducted where appropriate and when sites could be accessed safely. For most exposures, the soil was stiff and dense making it difficult to use *in-situ* testing equipment such as shear vane. The Schmidt hammer was used to test the strength of rock, and those results are discussed under geotechnical characteristics of rock in Chapter 5.

The *in-situ* testing for soil included shear vane, Scala penetrometer and Double ring Infiltrometer. Shear vane was used for undrained shear strength for soil exposures. Scala penetrometer and double ring Infiltrometer locations were adjacent to the Geophysical lines next to Channel 2 underlain by Undifferentiated Riwaka Igneous Complex and Onekaka Schist (Figure 3.10).

3.6.2 Shear Vane results

The pocket shear vane was used to measure the undrained shear strength of soil including colluvium from debris flow source areas, pre-2018 debris flow deposits and underlying completely weathered bedrock to residual soil. The shear vane testing was conducted in places where outcrop face logging was carried out, and the locations of shear vane are shown in Appendix A.2. This test is suitable for soft to medium cohesive soil. As the soils are rather granular in nature, the results are of low reliability. There were places where the soil was too hard and/or too granular for the shear vane to work, therefore no reading is available for the identified profile.

The lowest values were found in the pre-2018 debris flow deposit, Sample 16, where the soil fraction was predominantly silt with some sand, clay and trace gravel. It was described in the field to be soft, whereas shear vane gave a range of values from 19-44 kPa. The terms used are from the descriptions in the New Zealand Geotechnical Society (2005) rock and soil field guide. The differences between readings and field assessments are shown in Table 3.2. The values should be treated with caution because, as mentioned, the soils were heterogeneous, and presence of coarse fraction affects the results.

Table 3.2: In-situ strength test results.

Sample number	Bedrock	Geomorphic Setting	Average Undrained shear strength (kPa)	Term	Range	Field assessment
2	SPG	Road cut	70	Stiff	48-79	Can be indented by thumb pressure
7	SPG	1	49	Firm	37-58	Can be indented by thumb pressure
9	URIC	2	47	Firm	21-76	Can be indented by thumb pressure
13	OS	3	38	Firm	23-48	Easily indented by fingers
16	URIC	3	37	Firm	19-44	Easily indented by fingers
18	OS	Adjacent to channel 3	67	Stiff	38-79	Can be indented by thumb pressure

3.6.3 Scala Penetrometer Testing

To combat the problem of using shear vane for granular soil, a dynamic cone penetrometer (DCP also known as the Scala penetrometer) was used to estimate soil strength with depth. The DCP tests were done on colluvium deposit along the geophysical lines. The location of the DCP tests is shown in Geophysical Section 3.5. 6 DCP tests were conducted and only one location reached a maximum depth of 2.17 m as it could not go any deeper due to rebound. The issue with testing this soil was encountering boulders at shallow depth, which was expected based on outcrop exposures. Figures 3.19 to 3.23 show the DCP results. The graphs shows the cumulative number of blows with the corresponding depths of penetrations, and the tables below graphs show the interpretation of each DCP.

Figure 3.20 shows the DCP result for the test that reached the greatest depth (DCP 2), and Figure 3.21 shows the test conducted at the bottom of the geophysical line above the exposed face (DCP 3 and DCP 4). For DCP 2 (Figure 3.16), from ground surface to 1200mm, the result is 2 blows/100mm, which is representative of loose soil. An interval is seen between 1200 and 1900 mm which is also constant but having much higher penetration resistance with, an average of 11 blows/100mm. From 1900 mm to 2200 mm the bearing again increases linearly with an average of 30 blows/100mm, representing very dense soil. This increasing density with depth is also shown in the geophysical results (Figure 3.12,

Line 1). The soil could not be penetrated any deeper than this due to high penetration resistance which probably represents boulders.

All DCP data was terminated due to high resistance, which is interpreted to be from large clasts (boulders or cobbles) or bedrock as seen from exposures and geophysical survey results. At the bottom of the geophysical line (above DCP 3 and DCP 4), along the highway, at least 3 m of colluvium was exposed. DCP 3 and DCP 4 were conducted 1 m from each other due to obstruction at shallow depth (Figure 3.21). From ground surface to 350 mm, an average blow of 6 blows/100mm is interpreted, which is equivalent to dense type soil. A stream exposure located 20 m from DCP 5 shows at least 2m of colluvium above completely weathered bedrock. The aim of the DCP was to understand the behaviour of soil above this weathered bedrock and the data obtained are consistent with the observed profiles in stream banks and cut faces.

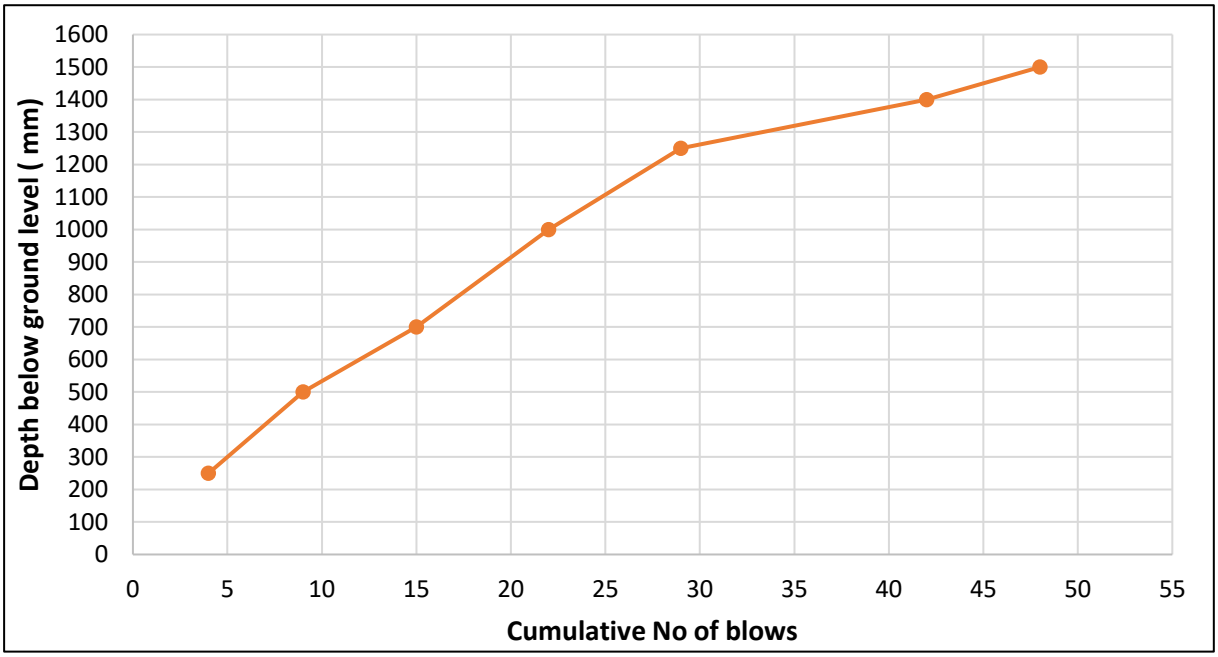

Figure 3.19: DCP results for the test at the top of the geophysical line.

Table 3.3: Interpretation of the DCP 1 results.

DCP	Depth (mm)	Average blows/100mm	Descriptive term	Notes/Interpretation
1	250-500	2	Loose	
	500-700	3	Loose	
	700-1000	3	Loose	
	100-1250	3	Loose	
	1250-1500	8	Dense	High resistance - could not penetrate deeper - Bedrock

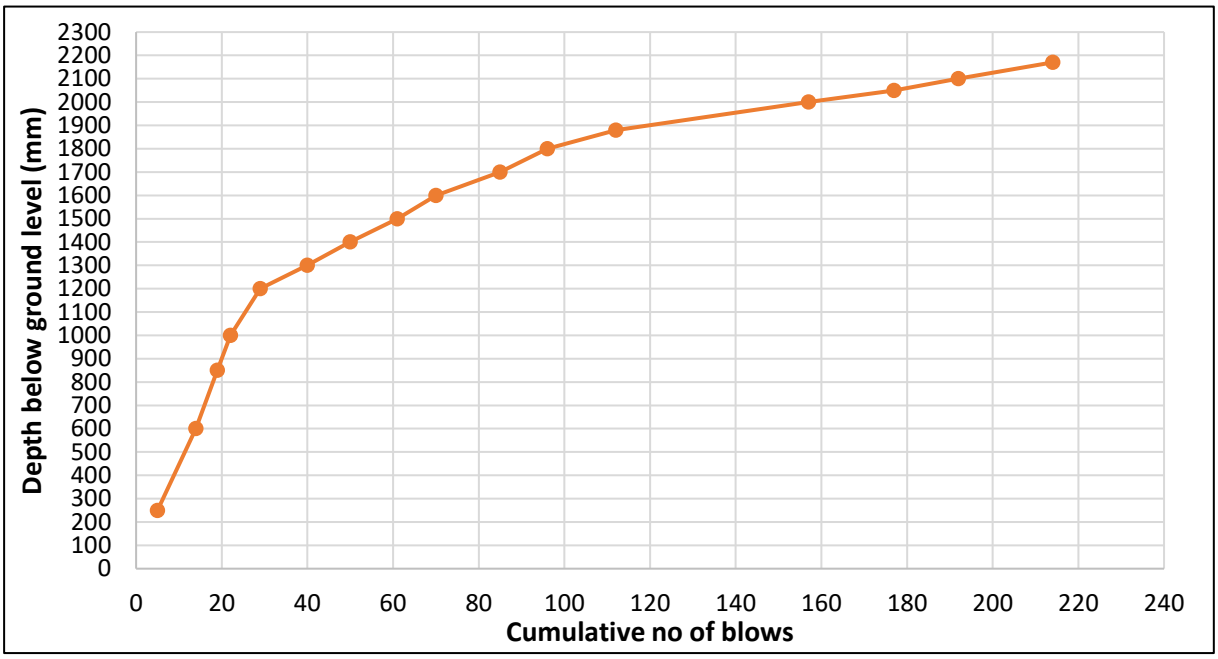

Figure 3.20: DCP 2 results for the test that reached the greatest depth.

Table 3.4: Interpretation of the DCP 2 results.

DCP	Depth(mm)	Average blows/100mm	Descriptive term	Notes/Interpretation
2	250-1200	2	Loose	
	1200-1900	16	Dense	
	1900-2170	30	Very dense	High resistance-could not penetrate deeper

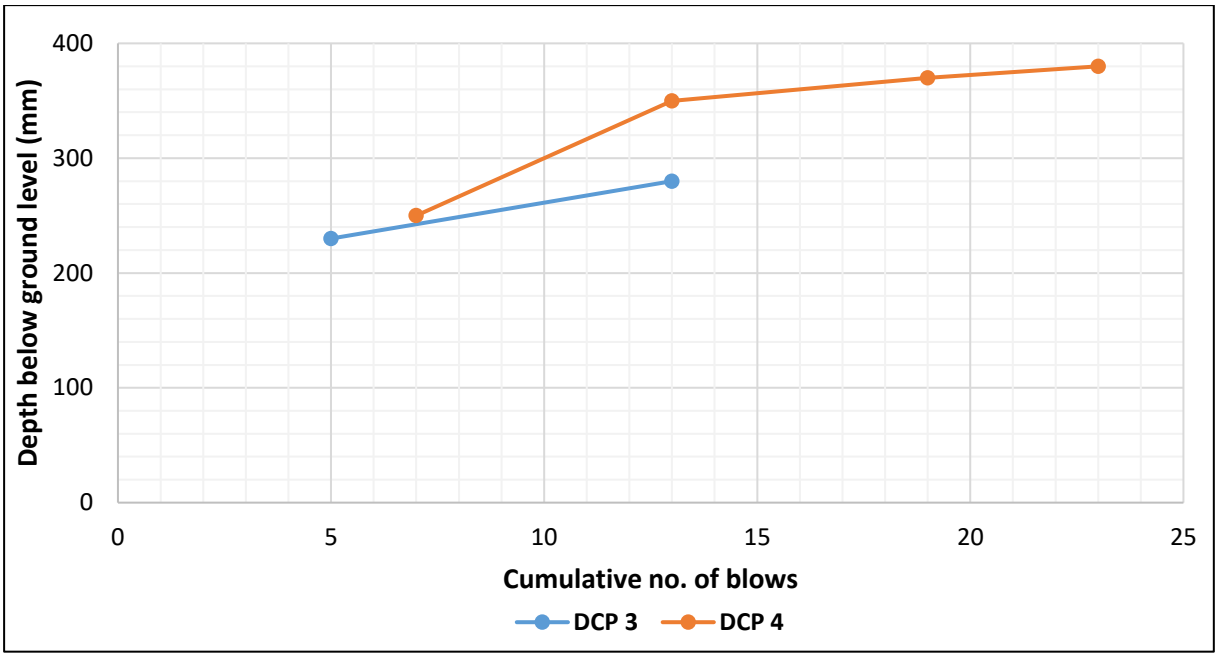

Figure 3.21: DCP 3 and 4 results for the tests at the bottom of the geophysical line above the outcrop that showed at least 3 m of colluvium (in Figure 3.11).

Table 3.5: Interpretation of the DCP 3 and 4 results

DCP	Depth (mm)	Average blows/100mm	Descriptive term	Notes/Interpretation
3	<100mm			High resistance-could not penetrate deeper
4	250 - 350	6	Medium dense	Terminated at 380mm due to high resistance. From 350-380, the gradient steepens and indicated dense soil

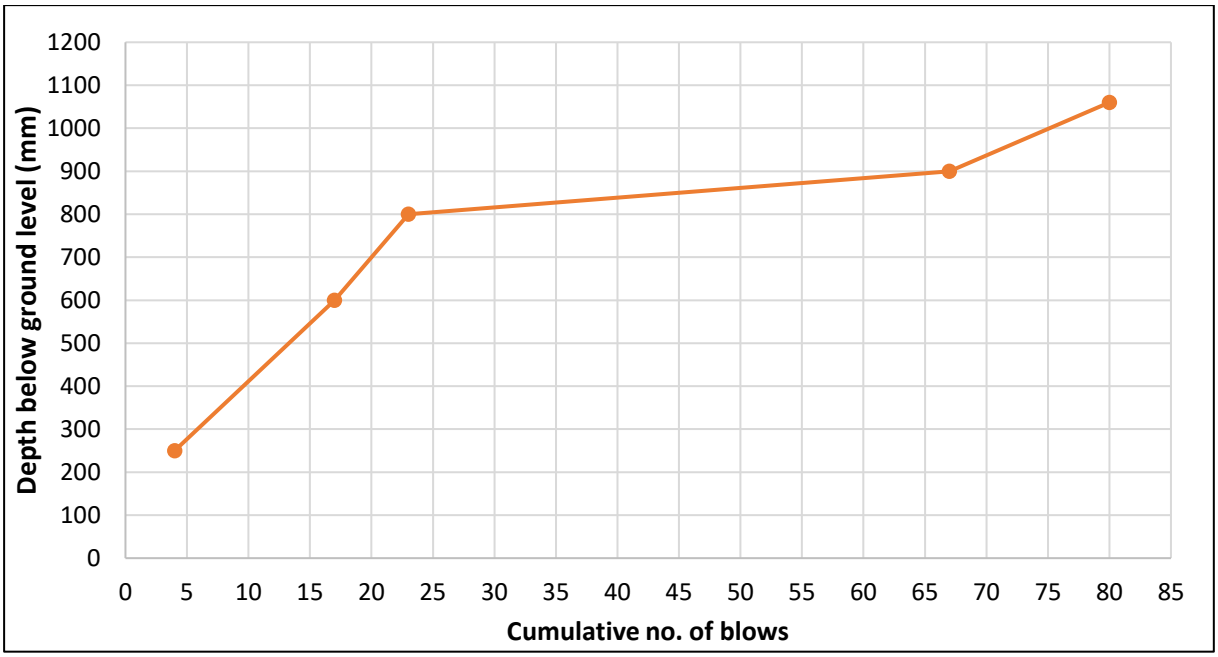

Figure 3.22: DCP 5 results.

Table 3.6: Interpretation of the DCP 5 results.

DCP	Depth (mm)	Average blows/100mm	Descriptive term	Notes/Interpretation
5	250-600	3	Medium dense	
	600-800	3	Medium dense	
	800-900	44	Very dense	
	900- >1060	8	dense	High resistance-could not penetrate deeper

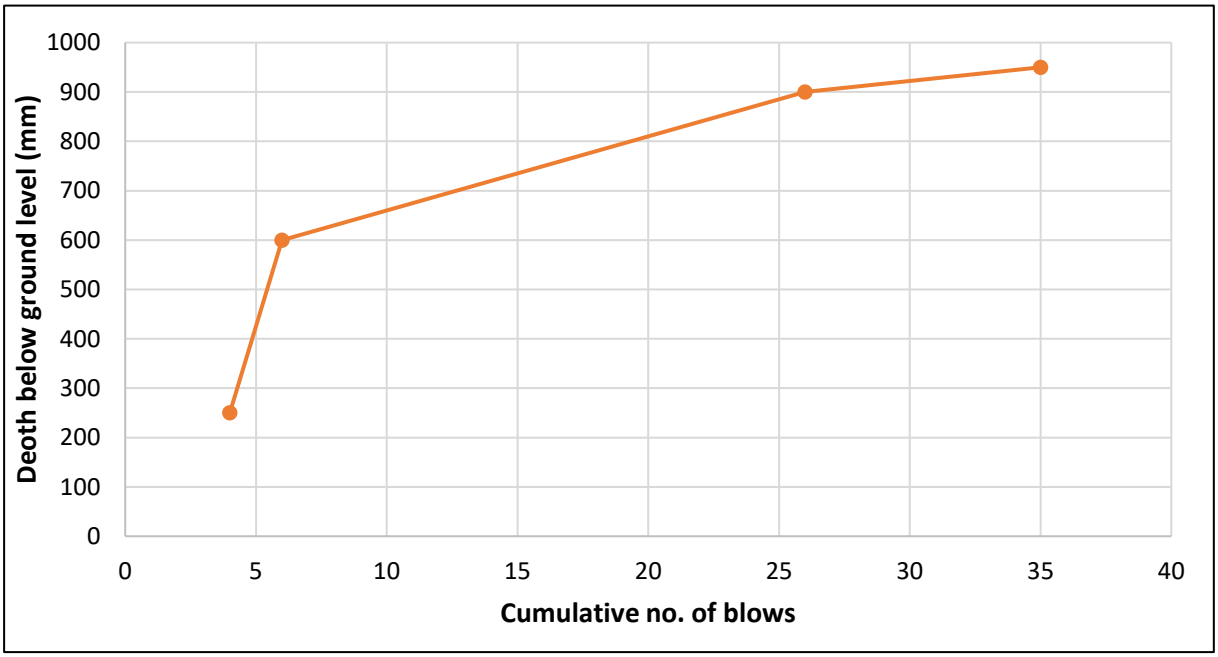

Figure 3.23: DCP 6 results.

Table 3.7: Interpretation of the DCP 6 results.

DCP	Depth (mm)	Average blows/100mm	Descriptive term	Notes/Interpretation
6	250-600	1	Loose	
	600-850	6	Medium dense	
	850-950	11	Dense	High resistance-could not penetrate deeper

3.6.4 Infiltration Ring Testing

A double ring Infiltrometer was used in the field to measure the infiltration rate. The equipment was placed in the geophysical survey area (Figure 3.10). The setting up of the ring was done according to (ASTM-D3385, 2019). The measurement was done differently to ASTM-D3385, 2019 standards, and followed the method outlined in Eijkelkamp (2018) as it was a more straight-forward test to conduct in the field (refer to Appendix A.4 for detailed methodology).

The average infiltration rate for the inner ring was calculated to be 13 mm/hr, which is typical of loam (sand, silt and smaller fraction of clay) type soil (Eijkelkamp, 2018). The soil collected at shallow depth (<100mm) had an engineering geological description of sandy silty clayey mix with some minor fine to medium gravel, dark brown, firm, moist, and of high plasticity (New Zealand Geotechnical Society, 2005). The particle size distribution showed silt and sand to be the predominant fraction with minor (>5%) clay and gravel (S19).

It can be observed from the graph that the initial infiltration rate is high but decreases rapidly within an hour, reaching a steady value (Figure 3.24). This is the expected behaviour of the test; with time the soil will become more saturated and infiltration rate will drop. As such, the steady value is of the most interest (Sanders, 1998). The sample collected near the test site showed soil to be silty sand with minor clay fraction. An infiltration rate of 13mm/hours is considered low infiltration rate by Tideman (1996).

One of the factors affecting the infiltration at the soil surface was vegetation and antecedent moisture content. Two days prior to the survey, the region had some rain and the soil were observed to be moist at the time of the test.

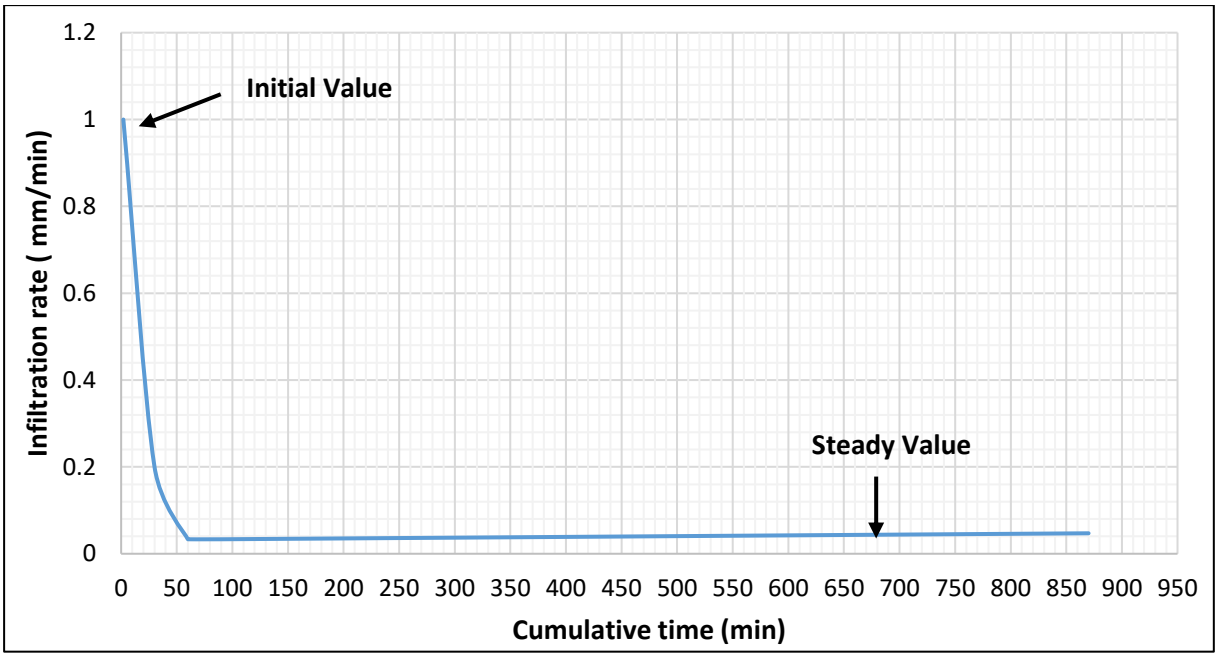

Figure 3.24: Infiltration curve. The infiltration rate declines as infiltration proceeds, reaching a steady value.

3.7 Synthesis

The Takaka Hill is prone to shallow translational soil slides triggered by extreme rainfall events (>180mm in 24 hours). Field investigations have identified two types of mass movements in 2018: shallow translational soil slides and channelised debris flow. Most of the soil slides occurred on slopes of 30° to 40°.

Debris flow sources are located in both colluvium and completely weathered bedrock to residual soil. Many debris flows also include local vegetation. The colluvium is predominantly gap-graded, mainly comprising large boulders in a fine-grained matrix (silty sandy clay mix). The pre-2018 debris flow deposits exposed along stream banks in all three channels show that these events have been ongoing throughout recent geological history.

In each channel, the accumulated thickness of pre-2018 debris flow deposit in stream banks varies from 0.5 m to 10 m. The average accumulated debris thickness was 2 m for Channel 1, 4 m for Channel 2, and 3 m for Channel 3. Subsurface geophysical profiling using MASW and GPR was used to determine the nature of pre-2018 events. Up to 10 m of pre-2018 debris flow deposits were interpreted to have accumulated at the bottom of the fan adjacent to Channel 2.

These data indicate that rainfall-triggered slope instability and debris flow activity like that experienced in 2018 is not new to the study area. The frequency of large- scale rainfall-triggered slope failures is estimated to be once every 30 years.

Chapter 4: Geotechnical Characterisation of Soils

4.1 Introduction

This chapter discusses the laboratory geotechnical characterisation of the colluvium, residual soil and completely weathered bedrock found in the study areas on Takaka Hill. The main objective of the laboratory testing programme was to characterise the soils' physical and strength parameters.

During the initial mapping programme (Chapter 3), at least two soil sample sites were selected to represent each bedrock lithology. Soil samples were collected from the following settings (Figure 4.1; Table 4.1):

- 2018 debris flow sources areas (referred to as 2018 (Gita) in the text)
- pre-2018 debris flow deposits
- highly to completely weathered to residual soil (weathered parent bedrock)

The 2018 (Gita) debris flow source areas include slides in colluvium. For Channel 1 underlain by Separation Point Granite, it was not possible to access the debris flow source areas (Chapter 3). Similar material was sourced from (Sample number 2) above weathered granite along the Riwaka-Sandy Bay road (Figure 4.1 for location) and have been grouped together with 2018 (Gita).

As mentioned in Chapter 1, the highly weathered bedrock, completely weathered bedrock and residual soil (collectively referred as weathered bedrock in this chapter) are regarded as engineering soil because of the extent of alteration and intact (mass) strength reduction. The colluvium and weathered bedrock are grouped together in this chapter as they have similar "soil like" characteristics. Appendix A.2 shows the locations of the samples collected with respect to the weathering profile identified at each site.

Particle size distribution, Atterberg limits, bulk and dry density, specific gravity, void ratio, and hydraulic conductivity were determined for soil samples. In order to assess the strength of each, a series shear strength tests were also conducted. The results of each test have been divided into 3 parts: pre-2018, 2018 (Gita), and weathered bedrock.

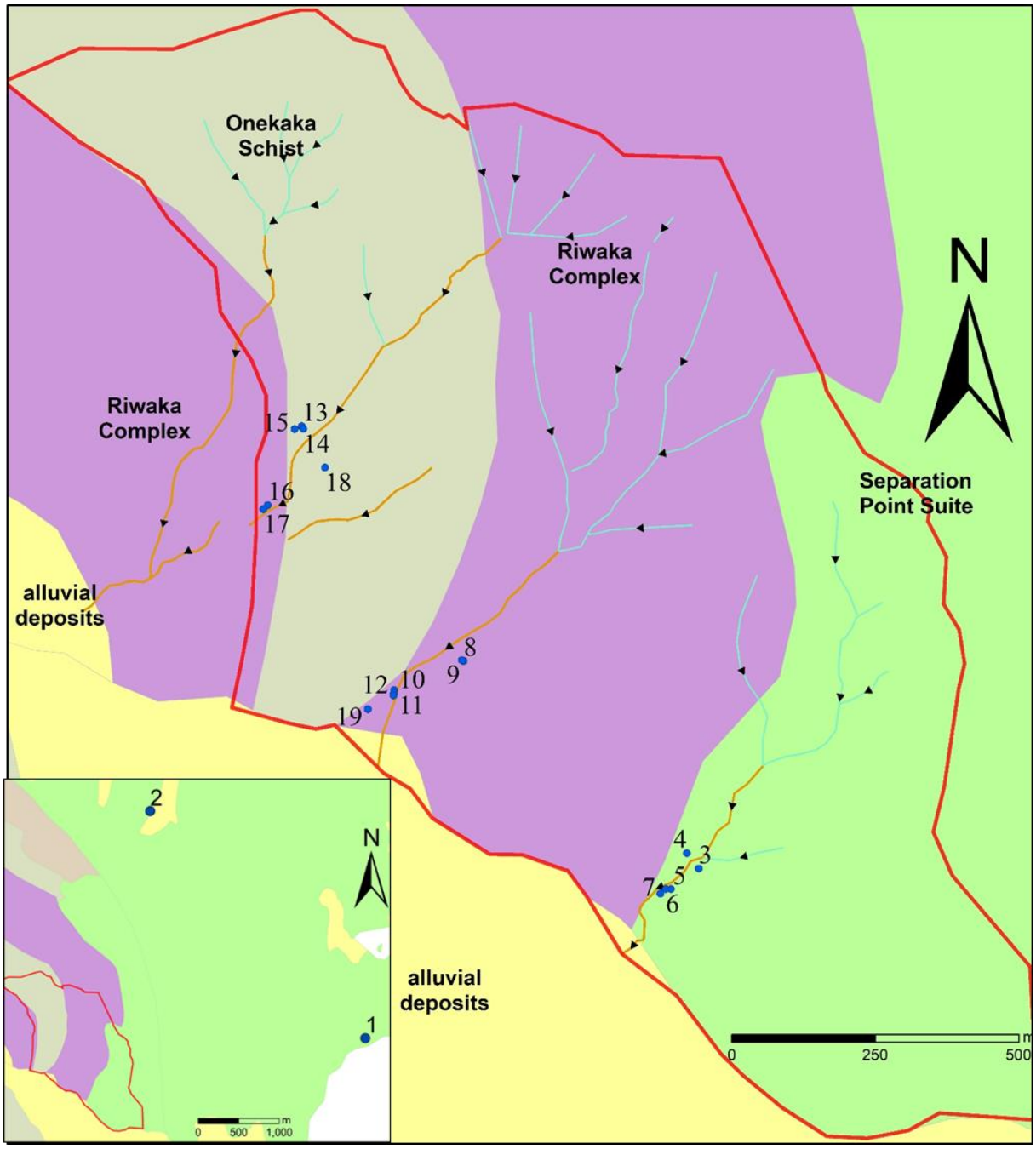

Figure 4.1: A simplified geological map of the Takaka Hill study area showing sample localities (blue circles). Source: (GNS Web Map, 2012).

Table 4.1: Summary of soil sample locations and material collected. Tests carried out indicated by (✓). PSD=Particle Size Distribution.

Sample number	Description	Parent Bedrock	Geomorphic Setting	Log number * refer to Appendix A.2	Atterberg Limits	PSD	*In-situ* Density & water content	Specific Gravity	Hydraulic Conductivity	Direct Shear-box	Ring Shear
1	HW SPG	SPG	Road cut		✓	✓	✓	✓	✓	✓	
2	2018 Soil slide	SPG	Road cut		✓	✓	✓	✓		✓	✓
3	Pre-2018 debris flow deposit	SPG	Channel 1	log 1		✓					
4	RS-CW SPG	SPG	Channel 1			✓	✓		✓	✓	
5	Pre-2018 debris flow deposit	SPG	Channel 1	log 2		✓					
6	Pre-2018 debris flow deposit	SPG	Channel 1			✓				✓	✓
7	Pre-2018 debris flow deposit	SPG	Channel 1	log 3	✓	✓	✓			✓	✓
8	2018 debris flow source area	URIC	Channel 2	log 4	✓	✓	✓	✓	✓	✓	✓
9	CW –RS URIC	URIC	Channel 2			✓	✓		✓	✓	
10	Pre-2018 debris flow deposit	URIC	Channel 2	log 5		✓		✓			
11	Pre-2018 debris flow deposit	URIC	Channel 2			✓				✓	
12	Pre-2018 debris flow deposit	URIC	Channel 2			✓					
13	2018 debris flow source area	OS	Channel 3	log 6	✓	✓	✓	✓		✓	✓
14	2018 Slide CW-RS OS	OS	Channel 3			✓	✓	✓	✓	✓	
15	CW-RS URIC	URIC	Channel 3			✓	✓	✓			
16	Pre-2018 debris flow deposit	URIC	Channel 3	log 7	✓	✓	✓	✓		✓	✓
17	Pre-2018 debris flow deposit	URIC	Channel 3			✓				✓	
18	2018 Reactivated Landslide	OS	Adjacent to Channel 3			✓					✓
19	Fan deposit	OS	Adjacent to Channel 2			✓		✓	✓		

4.2 *In-situ* Moisture Content and Atterberg Limits

4.2.1 Testing Methodology

The moisture content of a soil is the most frequent physical and mechanical determined characteristic, and is important as the amount of water in soils can influence the behaviour of the soil (Head & Epps, 2014). Atterberg limits are used to characterise the fine fraction (<425µm) of a soil. The liquid limit, plastic limit and plasticity index are used individually or collectively to correlate with engineering behaviour, including compressibility, permeability, compatibility, shrink-swell, and shear strength (ASTM D4318, 2017). The Atterberg limits are a good indicator of the type of clay mineral, and hence a good indicator of the engineering properties of the soil (Barnes, 2000).

The Atterberg limits of the soil samples were determined in accordance with the procedures of New Zealand Standards (NZS) 4402: 1986, Tests 2.2, 2.3 and 2.4. The soil was wet sieved through a 425µm sieve, as it was difficult to remove all larger particles by hand. Excess water was removed by pouring water from the surface of the suspension and by evaporation at less than 30°C. During evaporation, the soil was stirred frequently to prevent over drying on the sides of the dish. It took at least five days to evaporate excess water from the samples. The liquid limit was determined using the Casagrande method.

The *in-situ* moisture content was determined in accordance with the procedure described in NZS 4402: 1986, test 2.1. The soil was tight sealed, brought to the laboratory, and the moisture was determined before wet sieving. A correction to the moisture content was applied as all soil contained sand and/or gravel particles and the testing was carried out on sub-samples passing through 425µm sieve (Barnes, 2000). The equation used for the correction factor was taken from Barnes (2000) was as follows:

$$W = \frac{w_n}{P} \times 100 \qquad \text{Equation (1)}$$

Where, W Percentage (%) of corrected moisture content (moisture content of the portion of the sample without the gravel and sand).

w_n Percentage of moisture in the whole sample.

P Percentage of water passing the 425µm sieve for comparison with the Atterberg limits (determined from PSD).

4.2.2 Results

Figure 4.2 shows plasticity index (PI) and liquid limit (LL) for the clayey silty soil samples plotted on the Casagrande chart. The results are tabulated in Table 4.2.

Soil collected from 2018 debris flow source areas (S8 and S13) in both Channel 2 and 3 had a liquid limit greater than 50, with a corresponding high plasticity index (15-25). On the plasticity chart in Figure 4.2, these samples plot below the A line and are classified as high plasticity silt. Whereas the colluvium soil derived from Separation Point Granite (S2) rock plots above the A line and is classed as low plasticity silt.

The pre-2018 deposits are low plasticity clay and high plasticity silt. The *in-situ* moisture content of all soil samples is close or above to its plastic limit.

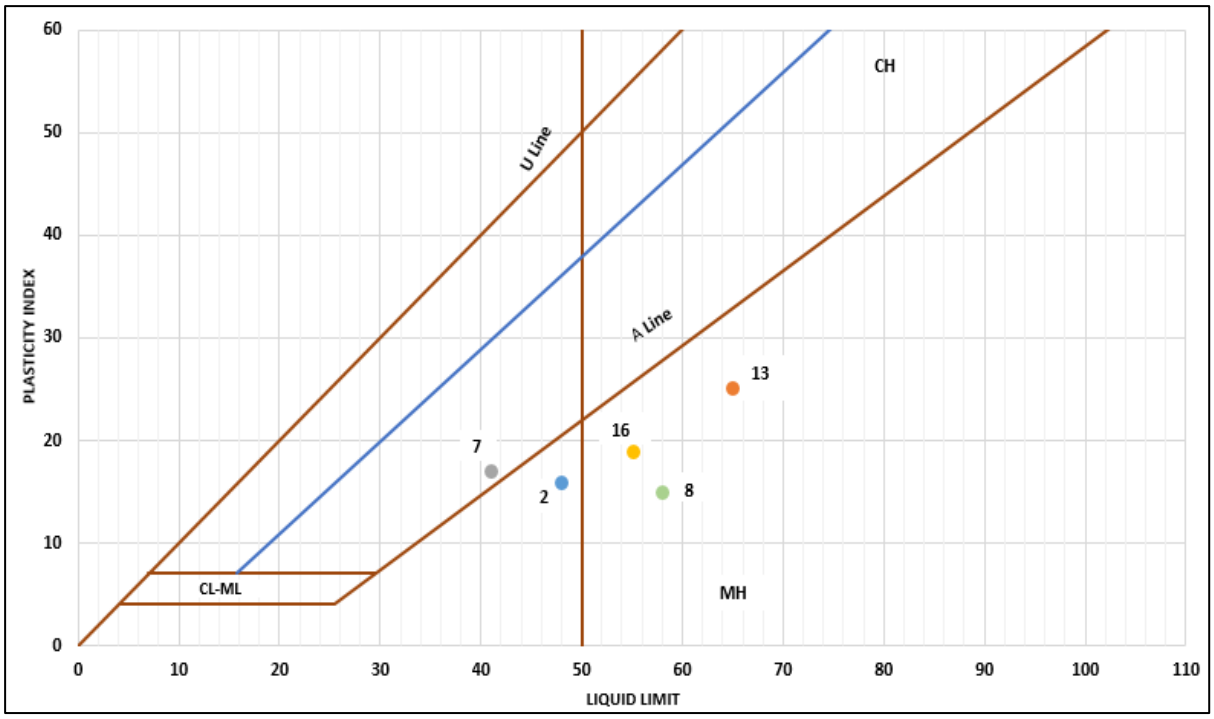

Figure 4.2: Casagrande Plasticity Chart. The different colour indicates samples numbers.

Table 4.2: Summary of results from Atterberg limit test and in-situ moisture content.

	Sample number	Parent Bedrock	Liquid Limit	Plastic Limit	Plasticity Index	*In-situ* Moisture Content
2018 (Gita)	2	SPG	48	32	16	32.5
	8	URIC	58	43	15	43.8
	13	OS	65	40	25	34.0
Pre-2018	7	SPG	41	24	17	31.4
	16	URIC	55	36	19	33.7

4.2.3 Activity

The Atterberg limit test was used to determine the classification of soil and some related properties. For soils with liquid limit of <50, the term lean is suggested (Bowles, 1979). The soils underlain by Separation Point Granite in both pre-and 2018 (Gita) fall in this category.

For soils with liquid limit above 50, the term “fat “ for clays is suggested (Bowles, 1979). Soils from source zones of the 2018 debris flow underlain by Undifferentiated Riwaka Igneous Complex bedrock have liquid limits above 50. Due to the similarity of engineering properties, kaolin clays tend to plot below the A line as inorganic silts (ML or MH) (Bowles, 1979). Most soils plot in the MH zone and may contain kaolinite clay, which is the least active clay mineral.

The results from Atterberg limits and particle size distribution can be used to calculate the activity. The plasticity index from the Atterberg test and clay fraction from the particle distribution curve (less than 2 microns) are used. (Skempton, 1953) defines activity in the following ratio:

$$\text{Activity} = \frac{Plasticity\ index}{\%\ of\ clay\ content} \qquad \text{Equation (2)}$$

Skempton (1953) defined activity in three categories:

- Inactive clays: activity <0.75
- Normal clays: activity 0.75 -1.25
- Active clays: activity >1.25

Bowles (1979) gave typical values for three main groups of clay mineral: kaolinite 0.4 to 0.5; illite 0.5 to 1; and montmorillonite 1 to 7. Kaolinite is the least active, followed by illite with intermediate activity, and montmorillonite being the most active (Bowles, 1979).

Activity is a good indicator for volume change in the soil mass (Bowles, 1979). Using the measured plasticity index from the Atterberg limit and clay fraction from the particle size distribution (discussed in the next section), the activity was calculated (Table 4.3). All samples tested were classed as normal and inactive, with the exception of pre-2018 soil in Channel 3 (S16). The activity of the soil suggests that Samples 2, 7, 8, and 13 consist of illite and S16 consists of montmorillonite. An XRD analysis is recommended to determine the type of clay.

Table 4.3: Activity values calculated from Plasticity Index and Clay fraction measured from hydrometer test.

	Sample number	Parent Bedrock	Plasticity Index	Clay content (%)	Activity	Terminology
2018 (Gita)	2	SPG	16	22	0.7	Inactive
	8	URIC	15	20	0.75	Active
	13	OS	25	31	0.81	Normal
Pre-2018	7	SPG	17	17	1	Normal
	16	URIC	19	9	2.1	Normal

4.3 Particle Size Distribution

4.3.1 Testing Methodology

Particle size distribution (PSD) is a good indicator of engineering properties, including hydraulic conductivity and shear strength. During the field investigation, the debris flow source areas (2018 Gita soils) and Pre-2018 debris deposits were observed to be predominantly gap-graded material (Chapter 3), being described as cobbles and boulders in a fine grained matrix mostly of silt with varying amounts of clay and sand.

Particle size distribution of colluvium in 2018 (Gita), and Pre-2018 debris flow deposits and weathered bedrock, was determined in the field by visual estimation of the percentage of clasts (>60 mm) and matrix. Subsequently, the 'bulk' particle size distribution was determined from field photos using ImageJ software. ImageJ software was used for "photo sieving" for coarse-grained particles (Graham et al., 2005). The ImageJ analysis of particle size was done by a manual process of drawing the boundary around particles (cobbles and boulders). The software calculates the area of the cobbles and boulders, and by dividing this area by the total area of the selected deposit, the proportion of cobbles and boulders was found. This was correlated with estimates made in the field observations.

Particle size analyses in the laboratory were completed on size fractions finer than 60mm for samples collected from 2018 debris flow source areas (Sample 2, 8 and 13), including soil from a reactivated

slope failure (S18) , Pre-2018 debris flow deposits exposed in stream banks (Samples 3, 5, 6, 7, 9, 10, 11, 12, 16 and 17), including a fan deposit (S19); and weathered bedrock (Samples 1, 4, 9, 14, and 15). Particle Size Distribution usually does not include cobbles and boulders as they are removed in the field and an estimate made of their proportion (Barnes, 2000). The sieve analysis of particles including boulders and cobbles would require a large sample size – at least 50kg – which is not practical to bring into the laboratory. The fine fraction controls the soil behaviour and is therefore the critical fraction.

The samples were tested in accordance with NZ 4402:1986, using wet sieve (Test 2.8.1), dry sieve (Test 2.8.2), pipette (Test 2.8.3) and hydrometer (Test 2.8.4) testing. In addition, particle size analysis was also determined using a laser sizer. The soil samples that were tested in the laser sizer were subsampled from the direct shear test samples (detailed methodology outlined in Appendix B.1).

4.3.2 Test Results

Semi log plots of the results from wet sieve and hydrometer/pipette testing are presented in this sub-section. A table is attached to each graph to show the percentage of gravel, sand, silt and clay, as well as the field description. The individual test results are presented in Appendix B.1. According to(New Zealand Geotechnical Society, 2005), > 35% of soil passing 0.06mm is defined as fine soil. The silt and clay are described as particles finer than 0.06 mm and 0.002 mm respectively. The laboratory tests, including both particle size analysis and Atterberg limit, were used to give a soil name. The soil behaviour is likely determined by silt and clay if more than 35% is present (Barnes, 2000). The name assigned to each soil follows the NZGS classification(New Zealand Geotechnical Society, 2005).

Out of the 19 soils tested, 10 samples have more than 35% of particles passing the 0.06 mm sieve and are classed as fine soil. These fine soils are predominantly silt, with varying amounts of clay and sand. The lower and upper bounds for all samples is shown in Figure 4.3. Overall the samples are widely graded with variable fines content.

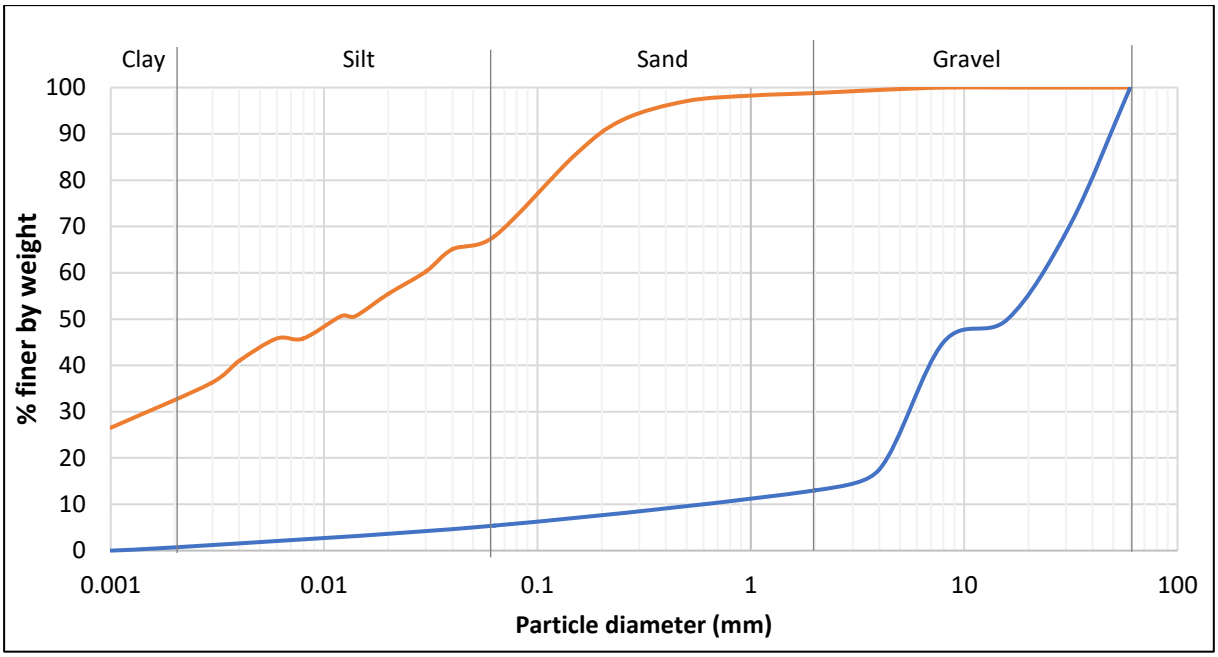

Figure 4.3: The upper and lower bounds for all 19 samples. The data were gathered from wet sieve, hydrometer, pipette and dry sieve. The data excludes particles greater than 60mm (i.e. cobbles and boulders).

4.3.3 Pre 2018 Debris Flow Deposit

The pre-2018 debris flow deposits were identified, and samples collected from stream bank exposures along the three channels. The soil samples collected from the matrix of pre-Gita deposits consist of a wide range of particle sizes. The deposit has silt and sand as the predominant sizes, and a few deposits comprising gravel as the major fraction. Out of the 9 pre-2018 soil samples collected, only 4 samples consist of more than 35% silt and clay and are classed as fine soils. The other 6 samples are coarse soils (Figure 4.4).

The clay fraction ranged from 3% to 20%. Seven out of nine samples consist of more than 10% clay. There is a variable amount of sand and gravel in the soil samples collected (Figure 4.4).

From the field observations, there is a variable proportion of boulders and cobbles ranging from 5% to 25%. In some debris flow deposits recognised, there were no cobbles and boulders identified.

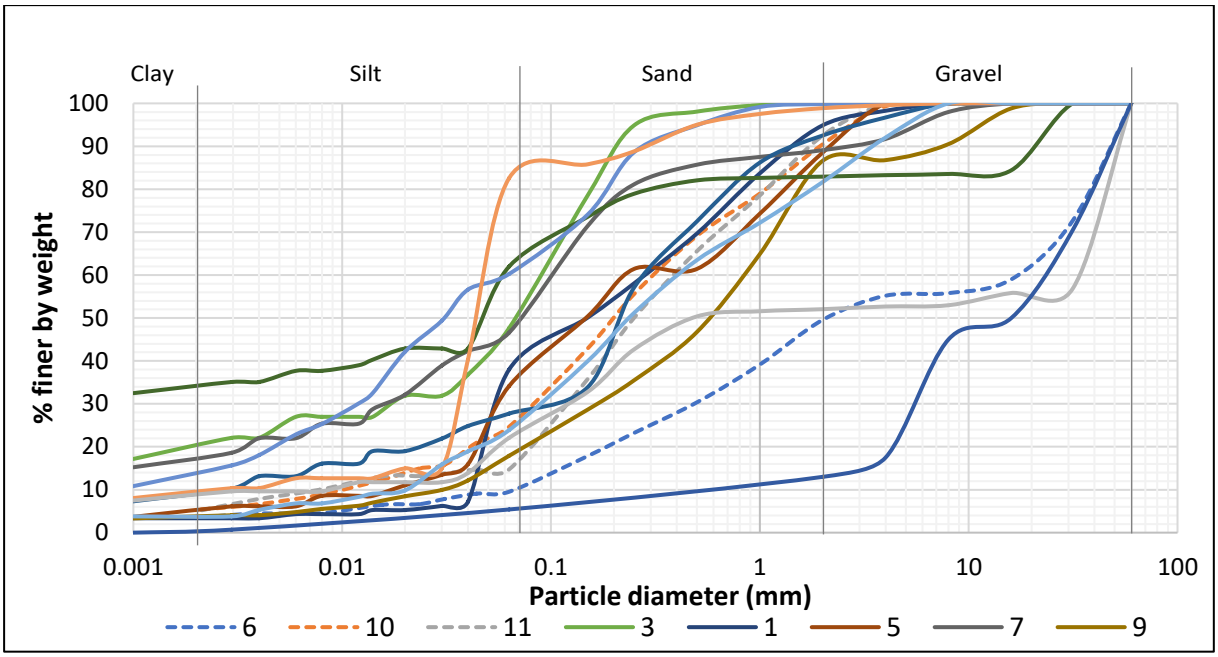

Figure 4.4: Particle size distribution for soils collected from Pre-2018 deposit. Refer to Table 4.1 for sample description and geomorphic location. The data were gathered from wet sieve, hydrometer, pipette and dry sieve. The pipette method was used for S6, S10, and S11, marked by dashed lines, while the hydrometer was used for the remaining samples.

Table 4.4: Summary results from field observations and laboratory testing of pre-2018 deposit. Note that the soil names are based on samples that have had the cobbles and boulders content removed.

Sample number	Field and ImageJ analysis		Laboratory testing				Soil Name
	Term	Proportion of fraction >60mm	Clay (%)	Silt (%)	Sand (%)	Gravel (%)	
3	Finer fraction	none	20	28	52	0	sandy SILT
5	Finer material with some cobbles and boulders	15% cobbles and boulders	5	29	54	11	silty SAND
6	Finer material with many cobbles and boulders	25% cobbles and boulders	3	7	40	50	Sandy GRAVEL
7	Finer material with occasional cobbles and boulders	5% cobbles and boulders	17	30	43	11	silty SAND
10	Finer material with some cobbles and boulders	7% cobbles and boulder	9	19	65	7	silty SAND
11	Finer material with some cobbles and boulders	7% cobbles and boulder	5	10	78	7	silty SAND
12	Finer material	no boulders and cobbles	3	4	8	85	GRAVEL
16	Finer material	none	9	74	16	1	sandy SILT
19	Finer material with some cobbles and boulders	15% cobbles and boulders	5	44	43	8	Sandy SILT

4.3.4 2018 (Gita)

The samples from source areas (Samples 2, 8 and 13) were predominantly silt (refer to Figure 4.5 and Table 4.5). All three samples consist of ≥20% clay fraction and variable amounts of gravel ranging from 2% to 32%. The highest clay fraction was 31%, where the underlying bedrock was Onekaka Schist. The clay and silt fractions were similar in Samples 2 and 13.

The soils collected from the reactivation area of colluvium (S18) are predominately gravel. The proportion of cobbles and boulders estimated from the field were 2% to 12%.

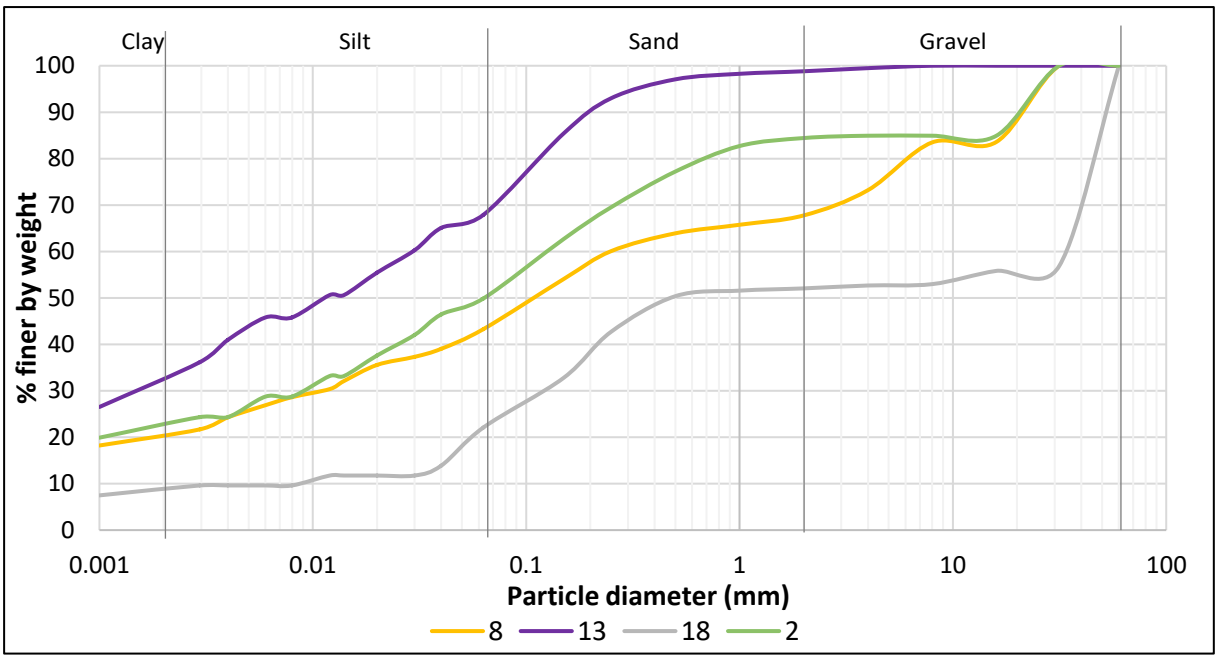

Figure 4.5: Particle size distribution for soils collected from 2018 (Gita) deposit. Refer to Table 4.1 for sample description and geomorphic location. The data were gathered from wet sieve dry sieve, and hydrometer.

Table 4.5: Summary results from field observation and laboratory testing of 2018 (Gita) debris flow source areas. Note that the soil names are based on samples that have had the cobbles and boulders content removed.

Sample number	Field and Image J analysis		Laboratory testing				Soil Name
	Term	Proportion of fraction >60mm	Clay (%)	Silt (%)	Sand (%)	Gravel (%)	
2	Finer fraction	None	22	28	35	16	clayey sandy SILT
8	Finer material with occasional cobbles and boulders	2% cobbles and boulders	20	23	25	32	gravely sandy clayey SILT
13	Finer material with some cobbles	12% cobbles	31	36	31	2	clayey sandy SILT
18	Finer material with minor cobbles	7% cobbles	9	13	30	48	Sandy GRAVEL

4.3.5 Weathered Bedrock

Highly weathered Separation Point Granite (SPG) (S1) collected from a road cut consists largely of gravel. The completely weathered SPG collected from Channel 1 is predominantly silt. The silt and sand sized particles observed in the sample were quartz minerals. Both highly and completely weathered SPG consist of ≤4% clay. The gravel fractions were variable. Highly weathered SPG bedrock consists of 48% gravel and the completely weathered to residual soil SPG consists of 1% gravel.

The completely weathered to residual soil Undifferentiated Riwaka Igneous Complex (URIC) bedrock consists of 3% clay in Channel 2, whereas completely weathered to residual soil URIC in Channel 3 consists of 13% clay.

The completely weathered to residual soil Onekaka Schist (S14) consists of the highest percentage of clay fraction and was described as silty Clay. Out of the 19 samples, S14 consist of the highest clay fraction.

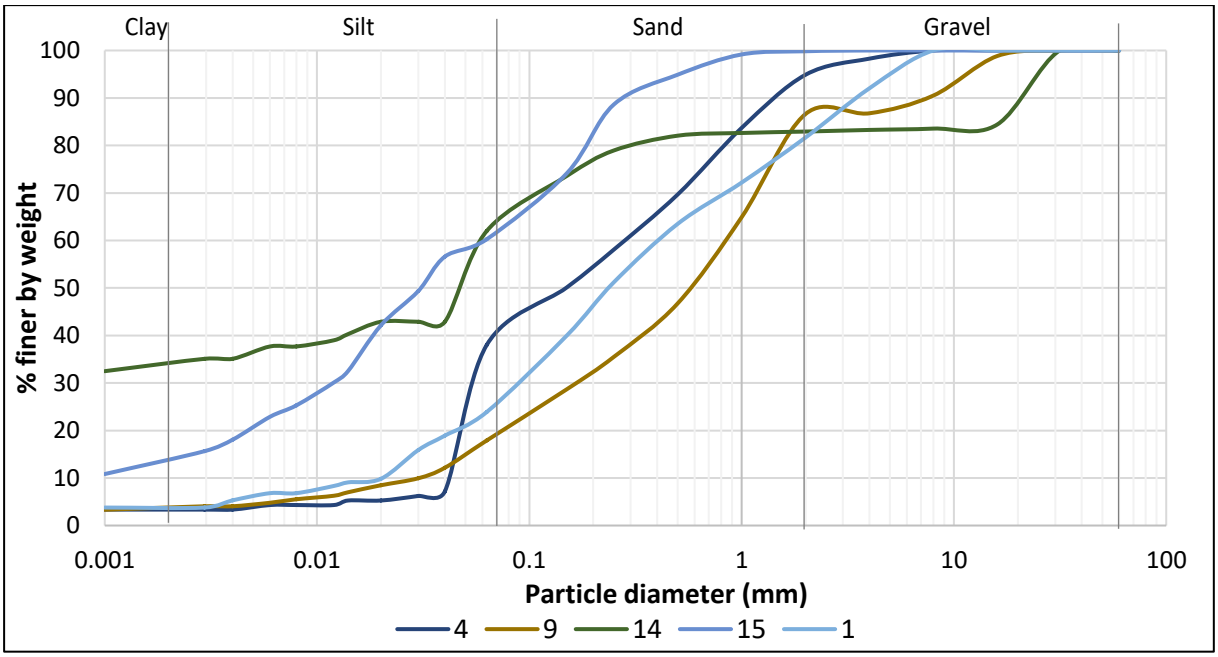

Figure 4.6: Particle size distribution for soils collected from residual to highly weathered bedrock. Refer to Table 4.1 for sample description and geomorphic location. The data were gathered from wet sieve and hydrometer and dry sieve.

Table 4.6: Summary results from field observation and laboratory testing. Note that the soil names are based on soil samples that have had the cobbles and boulders content removed.

Sample number	Field and Image J analysis		Laboratory testing				Soil Name
	Term	Proportion of fraction >60mm	Clay (%)	Silt (%)	Sand (%)	Gravel (%)	
1	Finer fraction	no coarse fraction	4	18	30	48	silty SAND
4	Finer fraction	no coarse fraction	3	80	57	1	sandy SILT
9	Finer material	no cobbles and boulders	3	15	69	13	silty SAND
14	Finer material	no cobbles and boulders	34	28	20	18	silty CLAY
15	Finer material	no cobbles and boulders	13	47	40	0	sandy SILT

4.4 Laser Sizer

4.4.1 Testing Methodology

This section shows results for only sand, silt and clay size fraction from laser sizer analysis and puts it with data obtained from hydrometer/pipette analysis. The hydrometer analysis data has been recalculated to include only sand (2 mm-0.06 mm), silt (0.06 mm-0.002 mm) and clay fraction (<0.002

mm). The main purpose of this test was to combat the problem of dealing with heterogeneous soil by having another method to determine the fines in the sample.

The results of laser and hydrometer/pipette were similar in identifying the major fraction for most samples, although the percentage of each differed. The major discrepancies between hydrometer/pipette and laser was in estimating the percentage of sand by laser sizer. The largest fraction identified by laser was 0.35 mm, medium sand.

The laser sizer detected a smaller clay fraction. However, it did confirm that the clay fraction in most samples is a minor fraction that is less than 12 %, as defined by (New Zealand Geotechnical Society, 2005). Only Samples 8, 13, and 14 had clay fractions of more than 15%, as detected by laser method.

4.4.2 Pre-2018 Debris Flow Deposit

There were major differences in Sample 11 where the pipette method was used, where silt was identified as the major fraction whereas in laser, sand was the major fraction. For Samples 3 and 7, the clay fraction identified by the laser was significantly lower compared to the hydrometer test.

Table 4.7: Finer fractions determined by laser sizer and hydrometer/pipette. The sample number with P is the result from the Pipette while the rest are from hydrometer.

Particle Size	**Sample number**						
	3	5	6P	7	10	11P	16
	Fraction determined by Hydrometer						
clay	19	3	6	19	9	5	8
silt	27	35	13	33	21	11	66
sand	55	61	81	48	70	84	26
	Fraction determined by Laser						
clay	3	3	4	9	3	4	4
silt	42	45	32	55	41	68	70
sand	55	52	64	36	55	28	26

4.4.3 2018 (Gita)

The clay fraction in all soil samples has been significantly less in laser size compared to hydrometer. For Sample 8, hydrometer analysis showed the subordinate fraction to be sand (37%), whereas the laser detected a lower percentage of sand. Both methods showed silt to be the major fraction.

Table 4 8: Finer fractions determined by Laser sizer and hydrometer.

Particle Size	Sample number			
	2	8	13	18
	Fraction determined by Hydrometer			
clay	22	31	34	13
silt	37	32	35	47
sand	41	37	31	40
	Fraction determined by Laser			
clay	6	17	11	6
silt	47	72	66	54
sand	47	11	24	39

4.4.4 Weathered Bedrock

Some discrepancies were noted in a few samples: for example, Sample 4 in weathered Separation Point Granite Channel 1. The hydrometer identified sand as the major component, whereas the laser identified silt. The laser sizer detected a significantly smaller fraction of clay in Sample 14.

Table 4.9: Finer fractions determined by laser sizer and hydrometer.

Particle Size	Sample number				
	1	4	9	14	15
	Fraction determined by Hydrometer				
clay	5	4	6	40	5
silt	25	37	15	35	56
sand	71	60	79	25	40
	Fraction determined by Laser				
clay	2	3	5	11	5
silt	31	59	48	67	45
sand	66	38	47	22	50

4.5 Other Soil Physical Parameters

4.5.1 Testing Methodology

The *in-situ* density of the debris flow source area, Pre-2018 debris flow deposit, and weathered bedrock were determined by the sampling tube method. A cylindrical tube of 35 mm diameter was driven into the soil by placing a piece of wood on the tube and hammering it into the soil. The test hole size is representative of the soil matrix, which is mostly fine grained soil (predominantly silt with varying clay and sand and minor gravel). It was not possible to collect tube samples in some exposures due to hard soil, and a few Pre-2018 deposits were gravel-dominated. The samples were tightly sealed using cling film.

The same samples were used to determine their specific gravity by both gas and water pycnometer. The specific gravity using gas pycnometer was conducted in accordance with ASTM D55050: 2000. All oven dried samples was pulverised using a mortar and pestle. The test was repeated using a water pycnometer. The specific gravity test using water pycnometer followed the procedure outlined in NZS 4402:1986, Test 2.7.1. A modification to this test was using a 250 ml pycnometer instead of 1 L. A separate test was performed on silt and clay fractions for samples to be used in hydrometer analysis calculation for the gas pycnometer.

The soil was assumed to be partially saturated at the time of collection due to its moist condition. Bulk density and specific gravity were used to calculate the degree of saturation and then the void ratio (in the partially saturated state).

4.5.2 Test Results

The results are tabulated in Table 4.10. The water content varied from 13.1 % to 30.8%. The highest bulk density was recorded for S13 (debris flow source area). A general trend that can be seen is that, as dry density increases, the void ratio decreases (Figure 4.7). The void ratio could be used to determine the properties of course and fine grained soils. All soils tested are classed as fine grained soil, with the exception of Sample number 1. The value of the void ratio for Sample number 1 suggests it is a loose soil. For fine grained soil, values above 1.3 indicate very soft soil, values between 1.0 - 1.3 indicate soft soil, and values between 0.7 - 1.0 suggest firm soil (de Vallejo & Ferrer, 2011)

The bulk density for pre-2018 debris flow deposits were 1.87 t/m^3 and 1.97 t/m^3, with dry density being 1.5 t/m^3 and 1.6 t/m^3. Both soils are classed as fine grained soil from the particle size distribution tests, and the void ratio indicated a soft soil (S16) and firm soil (S7).

The bulk density of the 2018 related slide ranged from 1.53 t/m^3 to 2.06 t/m^3, with dry density between 1.19 t/m^3 and 1.57 t/m^3. All the soil tested was classed as fine grained soil, as measured from particle size distribution tests. The value of the void ratio indicated the type of soil to be firm (S2 and S13) and soft (S8).

Table 4.10: Results from measured density, specific gravity, calculated degree of saturation, and void ratio.

	Sample number	Parent Bedrock	Water content (%)	bulk density (t/m³)	dry density (t/m³)	Specific Gravity	Degree of Saturation	Void ratio
Pre-2018	7	SPG	22.7	1.97	1.61	2.77	0.87	0.73
	16	URIC	25.0	1.87	1.52	3.03	0.74	1.03
2018 (Gita)	2	SPG	16.5	1.71	1.48	2.77	0.52	0.88
	8	URIC	28.3	1.53	1.19	3.03	0.55	1.55
	13	OS	30.8	2.06	1.57	3.05	1	0.94
Weathered bedrock	1	SPG/HW	15.3	1.56	1.35	2.64	0.42	0.95
	4	SPG/CW-RS	13.1	1.81	1.6	2.64	0.53	0.65
	9	URIC/CW-RS	20.1	1.82	1.51	3.03	0.61	1
	14	OS/CW-RS	13.1	1.72	1.52	3.05	0.39	1.01
	15	URIC/CW-RS	32.4	1.64	1.24	3.03	0.68	1.45

The weathered Onekaka Schist bedrock (S14) and Undifferentiated Riwaka Igneous Complex bedrock (S15) are classified as soft soil. The Undifferentiated Riwaka Igneous Complex at another location, S9 is classed as firm soil with a higher bulk and dry density.

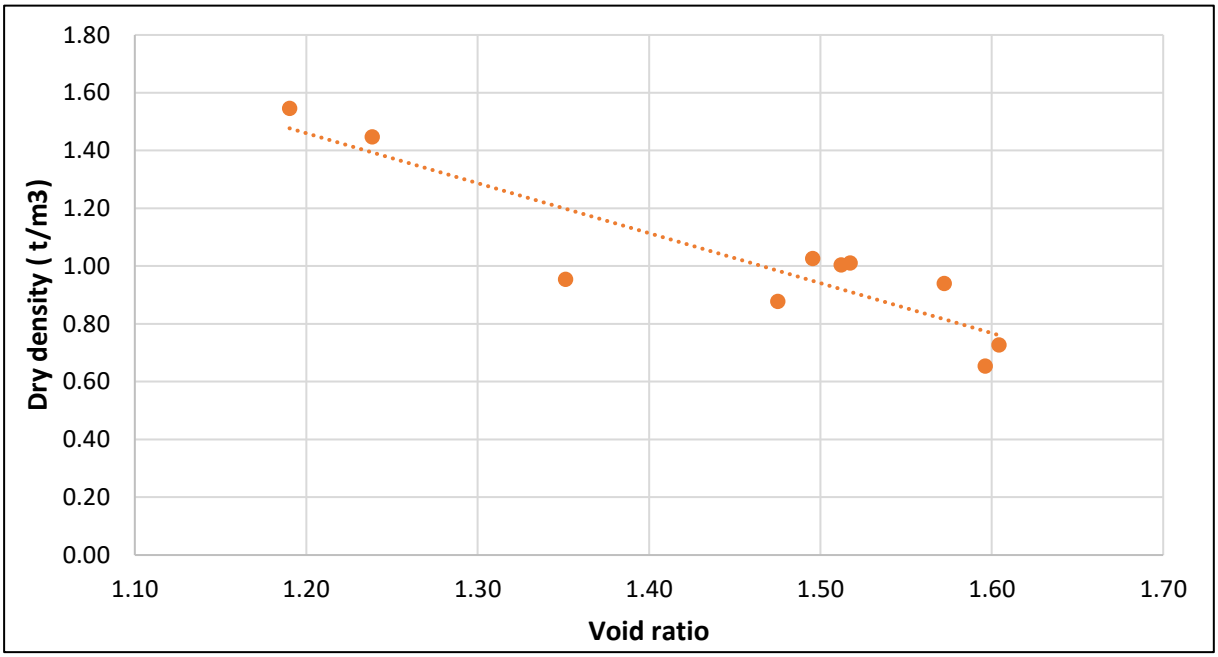

Figure 4.7: Relationship between void ratio and dry density for pre-2018, 2018 (Gita) and weathered bedrock.

4.6 Hydraulic Conductivity

4.6.1 Testing Methodology

Rainfall is the main trigger for the soil slides that result in debris flows. Understanding of the hydraulic conductivity (sometimes referred as coefficient of permeability) of the soil is deemed important. The

term hydraulic conductivity is a “measure of the ease with which a porous medium can transmit a fluid” (Sanders, 1998).

Soil samples were collected from pre-2018 fan deposit from (S19), 2018 source areas (S8 and S13), and weathered bedrock (S1, S4, and S9). The samples collected for testing were in tube, as discussed in Chapter 3.

The highly weathered Separation Point Granite was tested using the constant head method where the flow of water through sample is laminar. The procedure followed for this test was as described in British Standard (BS), BS1377: Part 5: 1990. This test is suitable for soil with less than 10% silt or clay (Barnes, 2000). It was initially thought that the weathered bedrock had a high proportion of gravel and sand, however during the test, the flow of water was slow and after conducting the particle size distribution on the sample, the percentage of clay and silt was 23%. This suggests the falling head test would have been more appropriate. However, this test still provided an approximate hydraulic conductivity of the sample.

All the remaining samples were tested using the falling head method. The visual inspection of soil to be tested indicated that it has more than 10% fines, and this was also confirmed by particle size distribution analysis. Therefore falling head method was used. The samples were kept in de-ionised water for more than 72 hours to allow saturation before the test. It was decided to measure the saturated hydraulic conductivity (k_s), as the saturated condition is the worst case condition. Sanders (1998) states that under saturated conditions, where pore space is saturated, and the presence of more water makes flow easier, as there is sufficient water to satisfy adhesion and cohesion while still allowing flow. The hydraulic conductivity of the saturated zone is generally substantially higher than that of the unsaturated zone. This is because in the unsaturated zone water passing through a dry pore space must overcome the adhesive and cohesive forces to pass through (Sanders, 1998).

The standard procedure for the falling heat test is not included in either the New Zealand standard or the British standard. The test was conducted using the test procedures used at the University of Canterbury and the methods outlined in Barnes (1995) and Sanders (1998). In this test, the standpipe measures head drop during the test. Refer to Appendix B.2, for the setup for the tests.

4.6.2 Test Results

Six samples collected in tubes were tested in the laboratory, two from each bedrock type. The results are similar (Table 4.11). The hydraulic conductivity is intermediate hydraulic conductivity range. Most

values obtained were in the range 10^{-5} to 10^{-6} mm/s. Both completely and highly weathered Separation Point Granite collected from Channel 1 and road cut had similar values from the two different test methods (the failing head and constant head tests).

Table 4.11: Hydraulic Conductivity result summary. Refer to Figure 4.1 for sample location.

	Sample number	Channel	Falling Head (m/s)	Constant Head (m/s)
Pre-2018	19	Fan deposit	2.07E-05	-
2018 (Gita)	8	2	3.56E-06	-
	13	3	1.94E-06	
Weathered bedrock	1	road cut	-	7.79E-06
	4		7.76E-06	-
	9	2	9.25E-05	-

The typical values for hydraulic conductivity for silt is in the range of 10^{-9} to 10^{-5} m/s; sand is 10^{-7} to 10^{-3} mm/s; and clay is 10^{-11} to 10^{-8} mm/s (Sanders, 1998). From the particle size distribution, the predominant fraction is silt and sand, and the calculated values for hydraulic conductivity fall in the 10^{-5} to 10^{-6} m/s range. The results from particle size distribution and measured hydraulic conductivity correlate well with each other, as well as with established correlations.

For the constant head permeameter test, one of the limitations is disturbance that occurs during sample preparation, which changes the microstructure and macrostructure and then tends to reduce the flow (Barnes, 2000). Although undisturbed specimens were used for the falling head permeameter test, potential for leakage is one of the main limitations which results in high values. This limitation of leak also applies to the constant head test (Barnes, 2000).

Another issue in the sample preparation was trying to get rid of all the air bubbles, especially for Sample 14. The trapped air bubbles in the sample can lead to lower values (Barnes, 2000; Bowles, 1979). There are some limitations for the tests for determining hydraulic conductivity, therefore the values should be considered as an estimate and not as absolute values.

4.7 Direct Shear Box Tests

4.7.1 Testing Methodology

The main objective of direct shear testing was to determine the shear strength of the reconstituted soil. The shear strength parameters from shear box testing are the effective friction angle (ϕ') and apparent cohesion (c'), which may be used for slope stability analysis. This testing measured the shear

strength of the soil by forcing a failure along a horizontal plane while being subjected to normal stress on the horizontal plane.

Coulomb (1776) described shear strength of soil along the failure plane as follows:

$$\tau_f = c + \sigma_n \tan \emptyset \qquad \text{Equation (3)}$$

Where τ_f Shear strength on the failure plane

c Cohesion

σ_n Normal stress

$\emptyset$ Effective friction angle

Shear strength testing was carried out in accordance with the method outlined in (ASTM-D3080/D3080M, 2011). Bulk soil samples collected in the field, including 2018 Gita related slide source areas, pre-2018 deposit, and weathered bedrock. The test was performed on reconstituted specimens, where soil of known volume was placed in the box on the perforated grid by tamping each layer (Figure 4.8). The samples were prepared to target a similar void ratio.

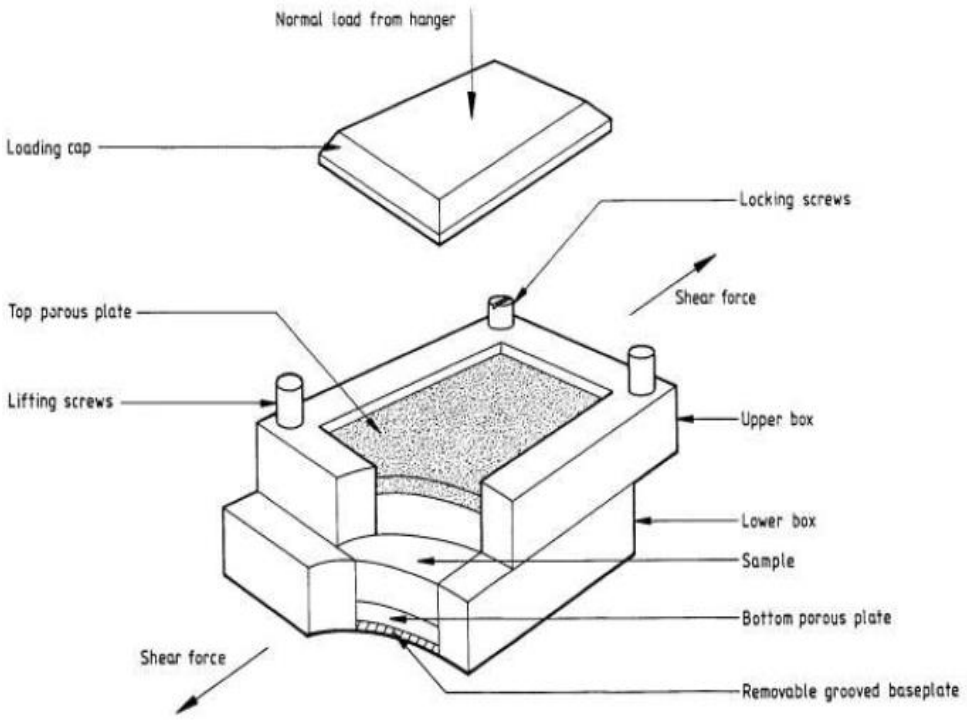

Figure 4 8: Soil Specimen setup. Source: (Controls Group, 2018).

According to ASTM-D3080/D3080M (2011) standard, generally three or more tests are performed on specimen from one soil sample. Each is performed at different normal stress at similar initial densities and void ratios. Each sample was divided into three subsamples to conduct the test under three normal stress: 10kPa, 20kPa, and 30kPa. These normal stresses were selected as the samples were collected at shallow depth (<5m) and do not appear to have been buried to any great depth. Only a soil fraction less than 4mm was used in the test. ASTM D3080 (2011) specifies that the thickness of the sample should not be less than six times the maximum grain diameter and the thickness of the shearbox was 24mm; hence particles finer than 4mm were used.

A consolidation period of 24 hours was applied to all samples. During consolidation, the normal stress that was used in the testing was applied. The shear box bowl was filled with water during consolidation, as the mechanism of failure is by infiltration of rainwater, resulting in soil slides. Moisture content was calculated before and after the test.

After consolidation, the graph of time versus vertical displacement was interpreted to see if the time of 24 hours would allow for complete consolidation. The graph (vertical displacement versus log time) was used to estimate the shear rate, which is the time required for failure to occur (as, for example, in Figure 4.9). The following equation was used to estimate time:

$$t_f = 50t_{50} \qquad \text{Equation (4)}$$

Where t_f Total estimated elapsed time to failure, in minutes.

t_{50} Time required for the specimen to achieve 50% consolidation under the maximum normal stress increment, in minutes.

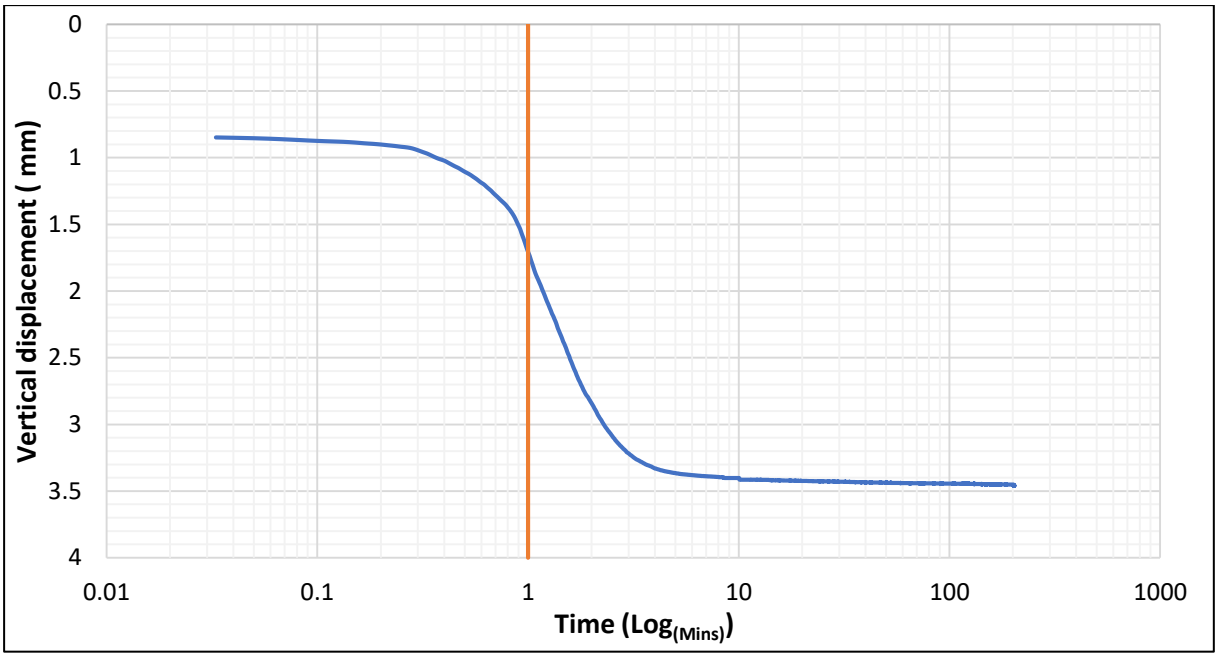

Figure 4.9: Graph displaying a typical calculation for colluvium (Sample 8) within a debris flow source area.

Figure 4.9 shows results of consolidation and time required to reach 50% consolidation for Sample 8, which is classified as SM according to the USCS classification (soil from slip source). In this case, using Equation (4) above, the t_f is calculated to be 50 min (1min*50), which is slightly less than the 60 min values given for SM type soil in the ASTM standard for the soil type. The displacement rate was estimated based on failure of the specimen being reached at 10mm of lateral displacement. Using the time estimated from the consolidation curve and 10mm lateral displacement, the displacement rate was calculated to be 0.2 mm/min for the example shown in the figure.

$$Rd = \frac{df}{t_f} \qquad \text{Equation (5)}$$

Where, Rd Displacement rate (meters per minute, m/min).

df Estimated relative lateral displacement at failure (mm).

However, a slower rate of 0.01mm/min was used. As the ASTM states, care should be taken if the time curve gives shorter times than the estimated values in the standard. The displacement speed of 0.01mm/min was used for sandy silt and silty sand soil. The soil was observed to be comprising high percentage of clay (i.e. S2, S7, S13, S14 and S16), so a slower rate of 0.006mm/min was used. This was also checked with the values of the displacement rate obtained from the consolidation curve.

As recommended in the standard, shearing was continued until the curve had a well-defined peak. In the absence of a well-defined peak, where the shear force increases monotonically, the sample was

continued to large deformation, up to 19mm horizontal displacement. The peak shear stress (Pascals, Pa) for each test was calculated using the following equation:

$$t_f = \frac{P}{A} \qquad \text{Equation (6)}$$

Where P Horizontal peak force (Newtons, N) measured by computer.

A Surface area of sample in meters squared, m^2.

The three data points were used to plot a graph of normal stress versus peak shear stress and a line of best fit was drawn. The graph was used to determine the effective friction angle (slope) and apparent cohesion (intercept).

4.7.2 Test Results

The effective friction angle for pre and 2018 (Gita) soil deposit ranged from 31° to 37°. The weathered bedrocks have a higher effective friction angle, all having a value of ≥ 40°, whereas the colluvium are in the 30° range. Appendix B.3 shows the results from the tests, including consolidation curves and shear stress versus horizontal displacement plot that was used to calculate peak shear stress for each test.

The void ratio was calculated for three soil specimens prepared from each bulk soil sample (refer to Appendix B.3 for void ratio calculation). For bulk Sample 13, the void ratio calculated for Test Specimen 2 (subjected to 20kPa normal stress) was significantly different from the void ratio for soil test specimen 1 (subjected to 10kPa normal stress) and 3 (subjected to 30kPa normal stress); therefore the effective friction angle and apparent cohesion was determined from specimens with similar void ratio (i.e soil specimen 1 and 3). For Soil Samples 14 and 16, one soil test specimen had a void ratio significantly different from the other two test specimens; therefore only 2 soil specimens were used to determine effective friction angle and apparent cohesion (Appendix B3 shows the details).

The *in-situ* void ratio estimated from the sampling tube method (Section 4.5) was slightly lower than all the other test specimens (with an exception for Sample 7). Therefore the expected effective friction angles for the soil *in-situ* would be slightly higher than those estimated from the laboratory testing, due to specimens tested in the laboratory being looser than the soil *in-situ,* suggesting the specimens were prepared in a slightly looser state. Therefore the calculated effective friction angle values would be slightly higher for the soil sample collected.

Some general observations from all three bedrock samples were that (1) soil at debris flow source areas has an effective friction angle in the 30°range and (2) all weathered bedrock (highly weathered bedrock to residual soil) has an effective friction angle of ≥ 40°.

4.7.3 Pre-2018 Results

The two pre-2018 soil sample deposits have an effective friction angle in the 30° range, with apparent cohesion of 8 and 13 (refer to Figure 4.10 and Table 4.12). Sample 16 has the highest cohesion out of all the soil tested and lowest effective friction angle.

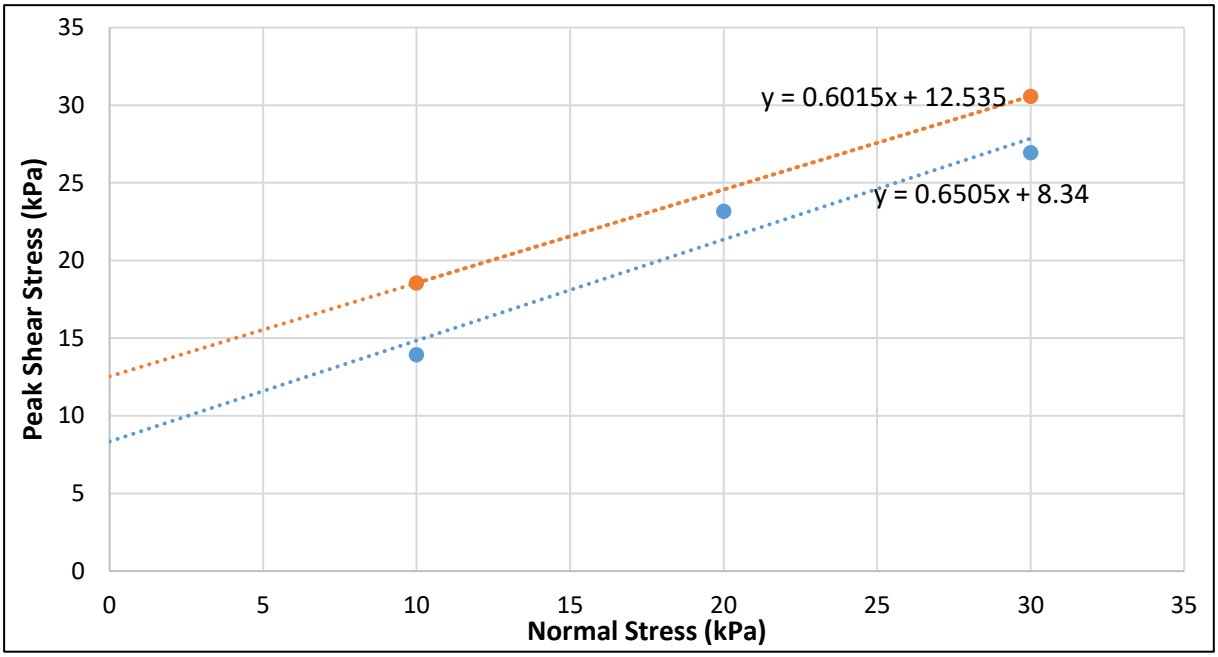

Figure 4.10: Direct shear test results for Pre-2018 deposit. The intercept represents the cohesion (c') and the slope the effective friction angle (ϕ'). The blue dotted line shows the results for sample 7 and the orange shows sample 16.

Table 4.12: Effective friction angle summary for pre-2018 soil samples.

Sample number	Normal Stress (kPa)	Peak Shear Stress (kPa)	Effective friction angle (°)	Cohesion (kPa)
7	10	13.9	33	8
	20	23.2		
	30	26.9		
16	10	18.6	31	13
	30	30.6		

4.7.4 2018-Gita related slides

The soil collected from debris flow source areas are in the 30° range (Refer to Figure 4.11 and Table 4.13). All samples are underlain by different parent bedrock. Sample 2 was underlain by Separation Point Granite, Sample 8 by Undifferentiated Riwaka Igneous Complex and Sample 13 by Onekaka Schist. The cohesion of the three soil samples are different. S2 and S13 have values for 5kPa and 4kPa respectively, whereas the S8 cohesion value is >50% higher than S2 and S13.

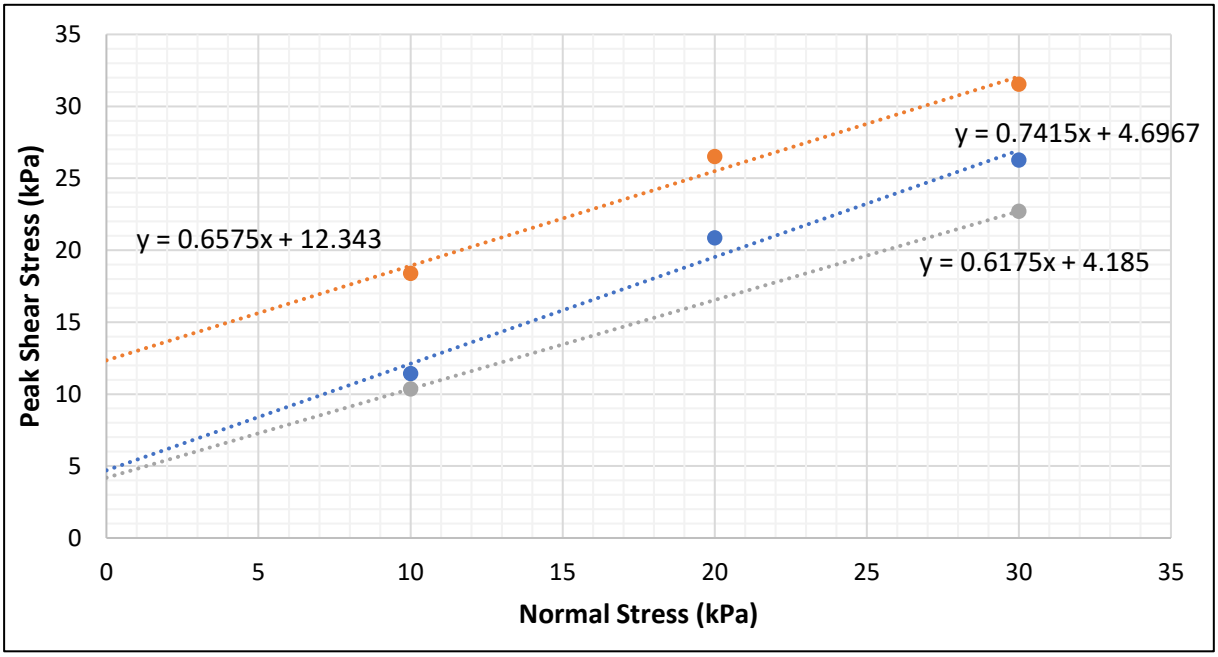

Figure 4.11: Direct shear test results for the 2018 event. The intercept represents cohesion (c') and the slope represents the effective friction angle (ϕ'). The blue dotted line is sample 2, the orange dotted line is sample 8 and the grey dotted line is sample 13.

Table 4.13: Effective friction angle summary for 2018 soil samples.

Sample number	Normal Stress (kPa)	Peak Shear Stress (kPa)	Effective friction angle (°)	Cohesion (kPa)
2	10	11.4	37	5
	20	20.9		
	30	26.3		
8	10	18.4	33	12
	20	26.5		
	30	31.6		
13	10	10.4	32	4
	30	22.7		

4.7.5 Weathered Bedrock

The weathered bedrock had the highest measured effective friction angle (Table 4.14). Although Sample 14 had a cohesion value of 6kPa, the measured effective friction angle was 40°. The sample appeared to contain a significant proportion (approximately 20%) of gravel particles in clayey soil. Sample 1 was highly weathered granite with a shear strength value of 46 degrees and Sample 4 was completely weathered granite to residual soil with a shear strength value of 42 degrees.

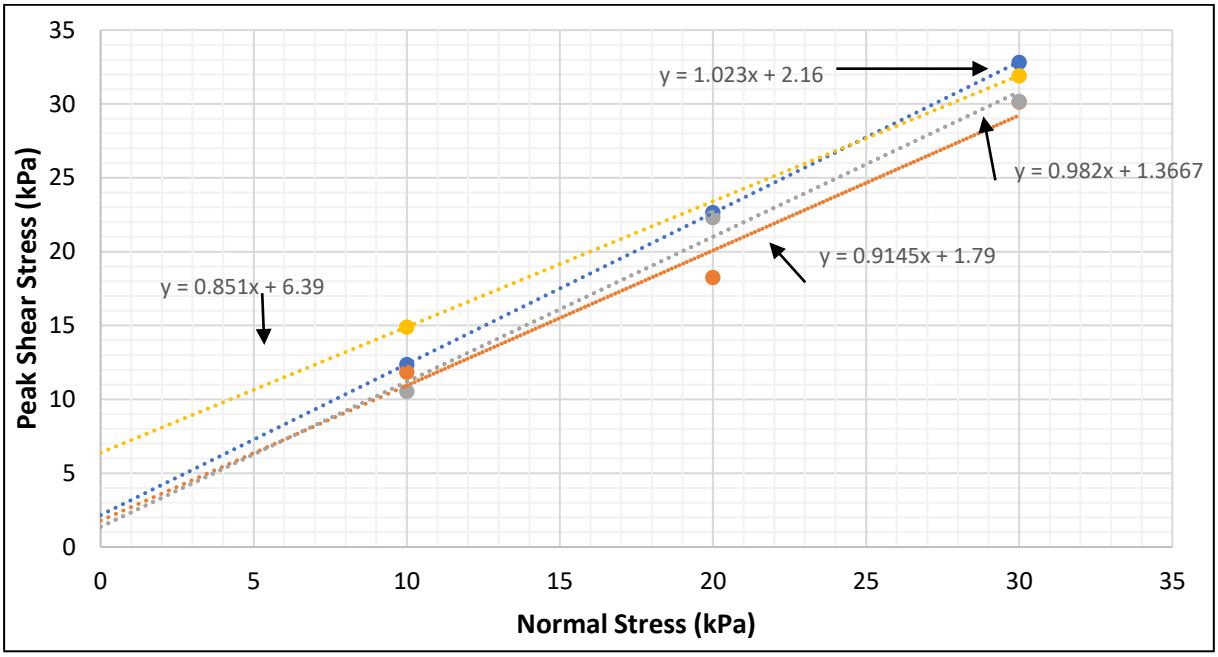

Figure 4. 12: Direct shear test results for weathered bedrock. The intercept represents the cohesion (c') and the slope represents the effective friction angle (ϕ'). The blue dotted line is sample 1, the orange dotted line is sample 4, the grey dotted line is sample 9, and the yellow dotted line is sample 14.

Table 4.14: Effective friction angle summary for weathered bedrock.

Sample number	Weathering Grade	Bedrock	Normal Stress (kPa)	Peak Shear Stress (kPa)	Effective friction angle (°)	Cohesion (kPa)
1	HW	SPG	10	12.4	46	2
			20	22.7		
			30	32.8		
4	CW-RS	SPG	10	11.9	42	2
			20	18.3		
			30	30.1		
9	CW-RS	URIC	10	10.5	44	1
			20	22.3		
			30	30.17		
14	CW-RS	OS	10	14.9	40	6

4.7.6 Discussion

The relationship between clay fraction and have effective friction angle is shown in Figure 4.13. A trend has been observed that the higher the clay fraction the lower the effective friction angle, but with the exception of Samples 2 and 14. In Sample 14 (weathered Onekaka Schist) and Sample 2 (colluvium soil above Separation Point Granite), there were significant proportions of gravel in a clayey soil which could have resulted in higher strength. Samples consisting of less than 5% clay have an effective friction angle above 40° (S1, S4 and S9). Samples consisting of 9 to 22% clay fraction have an effective friction angle in the 30° angle.

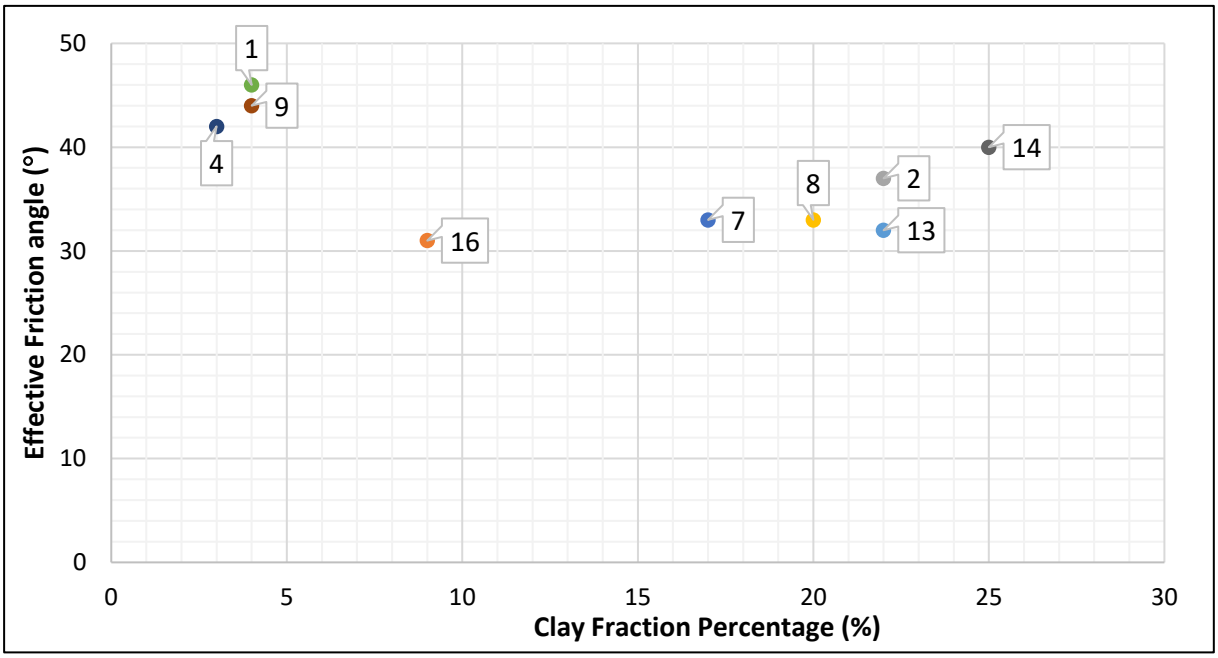

Figure 4.13: Clay fraction % and effective friction angle for soil tested in direct shear box. The data labels display the sample number.

The effective friction angle values in the 2018 (Gita slides) were higher in soil underlain by Separation Point Granite by 12% and 16%, compared to soils underlain by Undifferentiated Riwaka Igneous Complex and Onekaka Schist respectively. All the soil samples collected had silt as the predominant material with varying amounts of sand, clay and gravel.

The completely to residual soil for all three bedrock was tested. The effective friction angle was the highest in Undifferentiated Riwaka Igneous Complex, followed by Separation Point Granite and Onekaka Schist. The effective friction angle measured for Undifferentiated Riwaka Igneous complex was 5 % higher than Separation Point Granite and 10% higher than Onekaka Schist. The Separation Point Granite was 5% higher than Onekaka Schist bedrock. These are from only one test result

conducted in each type of soil therefore more tests needs to be conducted to confirm the strength relationships.

The values for the effective friction angle calculated from peak shear stress are high in general for the weathered bedrock. From the appearance of soil samples and from particle size distribution results, the predominant soil was silt and sand with more than 10% gravel inclusion and less than 5% clay (except for S14 where clay was the predominant material, but it consisted of more than 20% gravel). The sand and fine gravel were observed to be sub-angular, which gives greater interlocking leading to higher strength values (Bowles, 1979) compared with rounded material.

4.8 Ring Shear Testing

4.8.1 Testing Methodology

According to Skempton (1964), cited in Eid et al. (2016) a crucial parameter in evaluating the stability of pre-existing slip surfaces in new and existing slopes and the design of remedial measures is the "drained residual shear strength".

Residual shear strength has been performed on six remoulded samples using the Bromhead ring shear equipment. The main advantage of using this type of torsional ring shear apparatus over reversal direct shear test is that it shears the specimen continuously in one direction for any magnitude of displacement, allowing clay particles to be oriented parallel to the direction of shear and a residual strength condition to develop (Eid et al., 2016; Stark & Eid, 1994). The test assumes that cohesion is zero.

The procedure for the test followed BS1377: Part 7 1990. The test was conducted on samples passing the 2mm sieve. The inner and outer radius of the test specimen was 35mm and 50mm respectively. The initial thickness of sample was 5mm. A consolidation gauge was used to see the consolidation, and a graph of time versus consolidation was plotted to check if the soil had consolidated before the test. The test was run under different loads of 2kg, 3kg, and 4kg respectively, which is equivalent to 52kPa, 76kPa, and 100 kPa (normal stress). For every load increment, a shear plane was formed by using the handwheel on the equipment. The consolidation gauge was also used to check if there were sufficient samples remaining to carry out the test under three normal stresses.

The ring shear apparatus available at the University of Canterbury had a speed range of 44.5 mm/min to 0.02 mm/min. The test was run at 0.35mm/min as all soils were silt dominant, and at 0.012 mm/min

for reasons explained in the test results (Section 4.8.5). The test was stopped once it was observed from the graph that residual strength has been reached. Ring shear testing was performed at a slow test to ensure that no excess pore pressure is generated, therefore the soil took four to six weeks per sample. Due to the time limit for this thesis, the test was targeted to 2018 (Gita) soil and pre-2018 soil.

4.8.2 Test Results

The residual friction angle values range from 23° to 28°. The result from the test run at 0.35mm/min were slightly higher than initially expected. To confirm if the results were not due to shear speed rate, two samples were selected to be sheared at the slowest speed of 0.0178 mm/min. The test at 0.0178 mm/min took approximately 6 weeks per sample under three different normal stress.

4.8.3 Pre-2018 Deposits

The residual friction angle for pre-2018 soil samples ranged from 23.1° to 28.3° (Table 4.15). The samples are underlain by different parent bedrock. S6 and S16 is underlain by Undifferentiated Riwaka Igneous Complex (URIC), and S7 by Separation Point Granite (SPG) and in different channels (refer to Table 4.1 for locations and bedrock). Sample 7 and Sample 16 were also tested for effective friction angle, as discussed in Section 4.7. The residual friction angle for SPG derived soil was slightly higher than S6 and S16 underlain by URIC. The residual friction angle in soils overlying SPG is 18% higher than soils underlain by URIC.

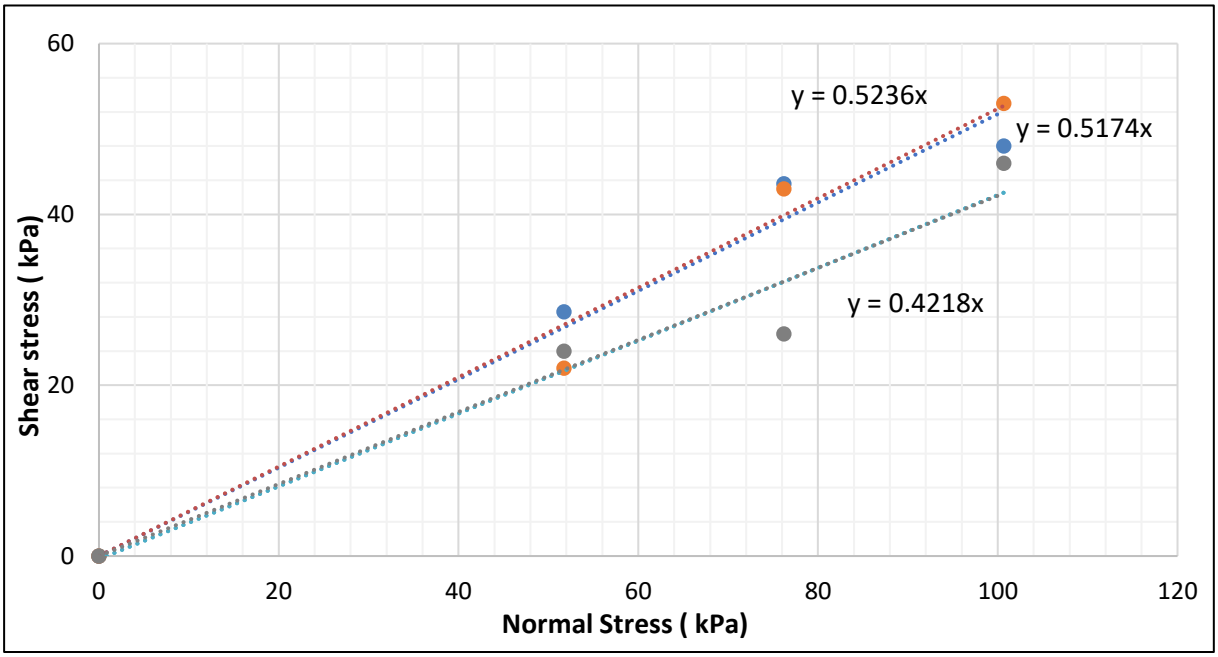

Figure 4.14: Residual friction angle results for pre-2018 soil samples. The blue dotted line is sample 6, the orange dotted line is sample 7, and the grey dotted line is sample 16.

Table 4.15: Summary results for ring shear tests for pre-2018 soil samples. The test was run at 0.35 mm/min.

Sample number	Normal Stress (kPa)	Shear Stress (KPa)	Residual Friction Angle
6	52	29	27.4°
	76	44	
	101	48	
7	52	30	27.6°
	76	45	
	101	53	
16	52	24	22.8°
	76	26	
	101	46	

4.8.4 2018 (Gita)

The soil had a range of residual friction angle values from 22.1° to 27.1° (Table 4.16). The residual friction angles are on average > 30 % lower than their effective friction angle measured in Section 4.7. The values of residual friction angles are similar to pre-Gita soil samples.

All samples tested are underlain by different bedrock. The residual friction angle was highest for soils underlain by Separation Point Granite, followed by Undifferentiated Riwaka Complex and Onekaka schist. The residual friction angle measured for soil underlain by Separation Point Granite is 14 % higher than soil underlain by Undifferentiated Riwaka Igneous complex and 21 % higher than soil underlain by Onekaka schist. The soil underlain by Undifferentiated Riwaka Igneous complex is 6% higher than soil underlain by Onekaka Schist bedrock. The results are from only one test result conducted for soils underlying each type of bedrock therefore, more tests need to be conducted to confirm the strength relationships.

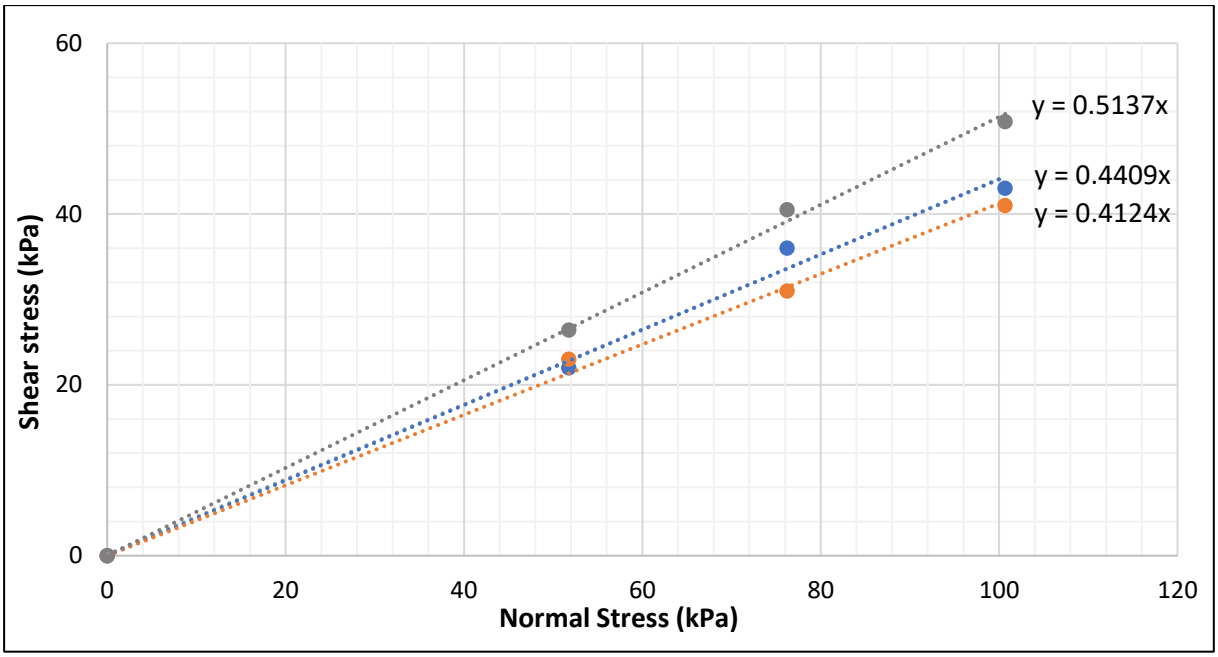

Figure 4. 15: Residual friction angle results from soil in Gita related slide. The blue dotted line is sample 8, the orange dotted line is sample 13, and the grey dotted line is sample 2.

Table 4.16: Summary results for ring shear tests for 2018 slide. The test was run at 0.02 mm/min.

Sample number	Normal Stress (kPa)	Shear Stress (kPa)	Residual Friction Angle
2	52	26	27.2°
	76	41	
	101	51	
8	52	22	23.8°
	76	36	
	101	43	
13	52	23	22.4°
	76	31	

4.8.5 Shear Rate

The test results on two colluvial soil samples at speeds of 0.01mm/min and 0.35mm/min are shown in Table 4.17. There is a 10% increase in residual friction angle when using 0.35 mm/min for Sample 8. For Sample 13, the residual friction angle was 19% higher in soil tested at 0.35 mm/min.

Table 4.17: Results of residual friction angle at two different shear rate.

Shear rate	S8	S13
0.02 mm/min	23.8°	22.4°
0.35 mm/min	26.2°	26.7°

4.8.6 Discussion

Residual friction angle for soil underlain by Separation Point Granite is greater than soil underlain by Undifferentiated Riwaka Igneous Complex and Onekaka Schist, by 14% and 21% respectively. The same was true for pre-2018 soil, where soil underlain by Separation Point Granite was 18% higher than soil underlain by Undifferentiated Riwaka Igneous Complex. However, more testing on soil needs to be conducted to confirm this trend.

Index properties such as clay fraction have been used to correlate with the residual friction angle by Skempton (1964), Borowicka (1965), and Binnie et al. (1967), cited in Sassa et al. (2007). According to this relationship of residual friction angle to clay fraction, the residual friction angle should decrease with increasing clay fraction. To test if the clay fraction had an influence on residual shear strength, a graph (Figure 4.16) has been plotted to check this relationship. From this graph, it is difficult to draw a clear relationship, as it would have been expected for S2, S7 and S8 to have a lower friction angle as they consist of higher clay fraction. One observation that could be made is that S13 had the highest clay fraction out of the six samples, and it has the lowest residual friction angle.

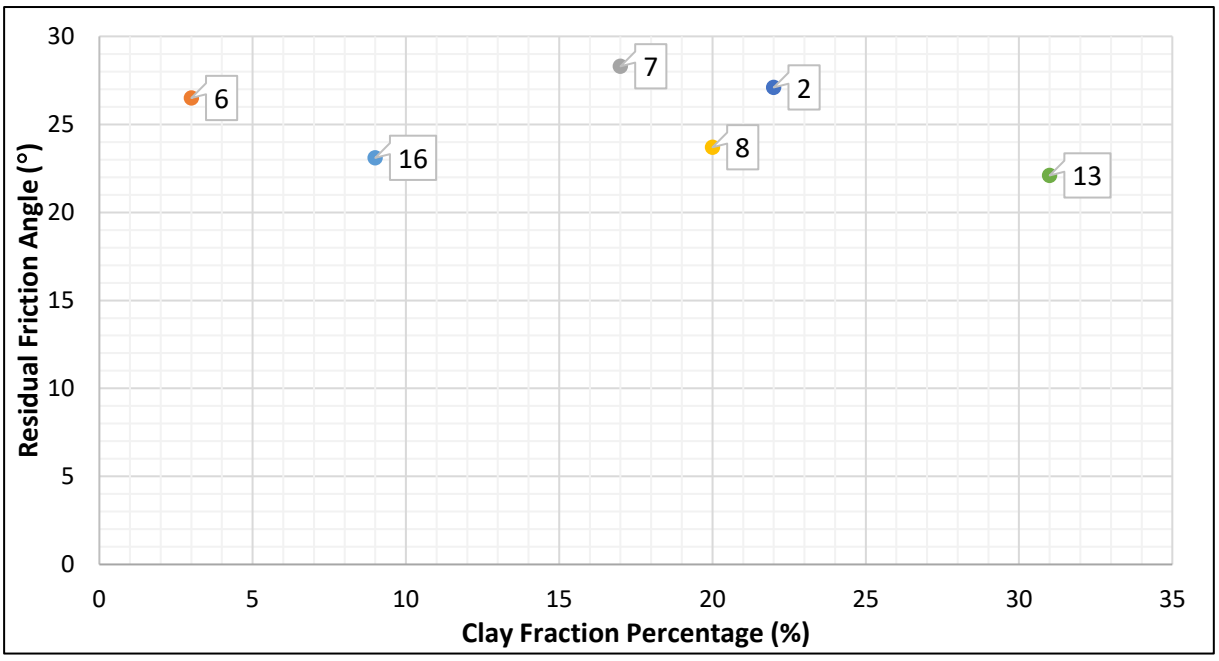

Figure 4.16: Correlation of clay fraction to residual friction angle for pre and 2018 soil samples.

The residual strength depends almost entirely on the clay particles where the clay fraction exceeds 50%. When the clay fraction is less than 20%, the clay minerals can have little effect on residual strength as the strength is then controlled largely by the sand and silt particles (Skempton, 1985). Out

of the six samples tested, three samples had a clay fraction of more than 20% (S2, S8, and S13) and all of them were collected from the 2018 debris flow source areas.

Wesley (2003) reviews the relationship between index properties and residual friction angle by looking at comprehensive strength data in studies by Lupini et al. (1981), Wesley (1992) and Townsend & Gilbert (1973). The paper by Lupini et al. (1981) states that the relationship between residual friction angle and the index properties of the soil cannot be generalised. Although reasonable correlations can be made by restricting correlations to certain types of soils, Wesley's research on a correlation between Atterberg limits and residual angle shows that neither plasticity index nor liquid limit alone is a good indicator, but relation to A line in the Casgrande chart. This correlation is applicable for soils above liquid 50, i.e. Samples 8, 13 and 16. The value of the residual friction angle is under 10° above the A line, whereas it is typically higher below the A line. As you go further from the A line, the greater the value for residual strength (Figure 4.17). The high residual strength can be related to the distance from the A line (Wesley, 2003).

The red square box outlines the area where S8, S13 and S16 would plot. The distances from the A-line calculated using the equation in Figure 4.17 were -13, -8, and -7 for S8, S13 and S16 respectively. This confirms that the residual friction angle is expected to be above 20 degrees. This estimated residual friction angle and measured residual friction angle are both above 20 degrees. The soils in the study area are predominantly silt with varying amounts of clay and sand, suggesting that the behaviour is mostly influenced by the silt.

Two samples (S8 and S13) were tested at two different shear rates, as shown in Table 4.17, to test the influence of shear speed on residual shear strength. The studies by Ramiah, Dayalu, and Purushothamaraj (1970) show that the influence of the displacement rate from 60mm/min to 0.02mm/min on the residual strength of silty clay (Plasticity index = 17) was found to be negligible. Vaughan et al. (1978) found that there was an increase in residual shear strength of the clay with Ip = 27 by 24%, when the displacement rate was changed from 0.015 mm/min to 15 mm/min (Lupini et al., 1981).

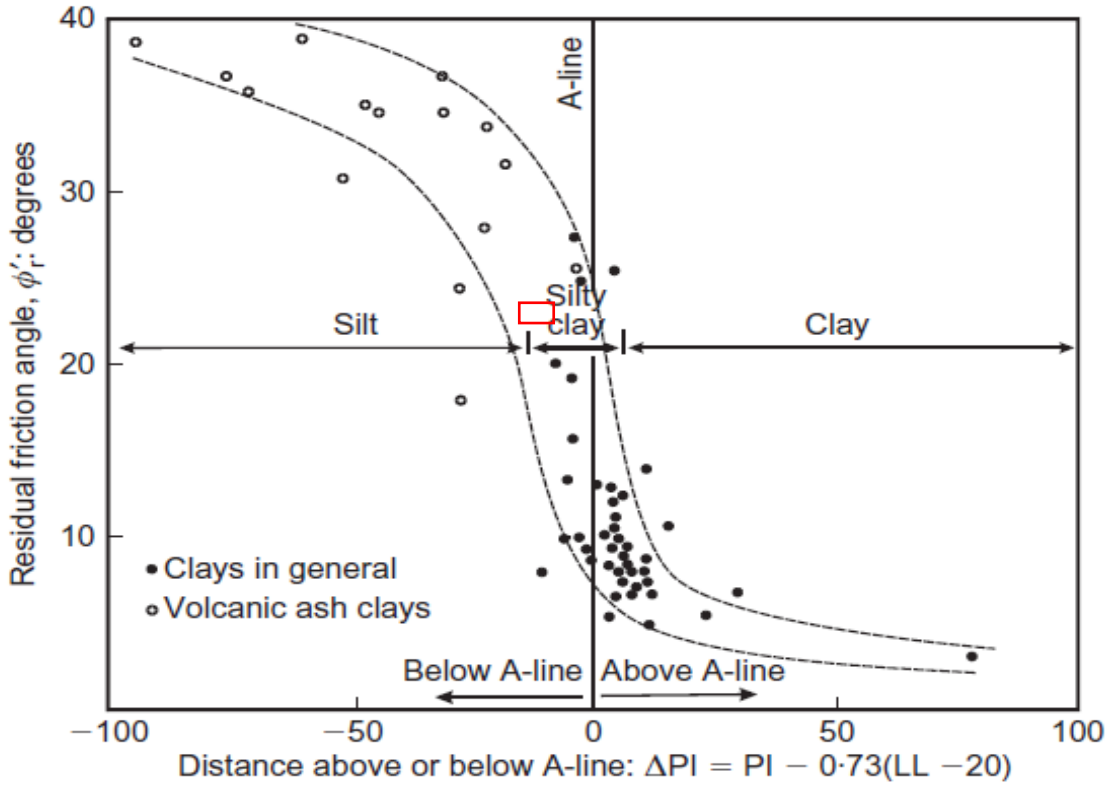

Figure 4.17: Residual friction angle plotted against distance above and below the A line, Sample 8, 13 and 16 plots in the red square box. Source: Wesley, (2003).

This study shows that soil (S8) with a plasticity Index of 15 showed an increase of 10% (i.e. 2 degree difference). Soil with a plasticity Index of 25 (S13), the residual angle differed by 19% (i.e. 4 degrees difference). The rest of the samples – sample numbers 2, 7 and 16 with plasticity index of 16, 17, and 19 respectively – sheared at 0.35 mm/min and may have been slightly over-estimated maybe by 1° or 2°. However, it does provide a good estimation.

4.9 Synthesis

The laboratory results have been summarised in Table 4.18. Soil samples collected from colluvium (both 2018 and pre-2018) had a moisture contents between 16.5% and 30.8% percent. Most of these samples were observed to be moist in the field.

Approximately 2 weeks prior to Ex-tropical cyclone Gita (20th February 2018), the Nelson region experienced another cyclone named Ex-tropical cyclone Fehi on February 1st and 2nd 2018. Heavy rainfall and flooding were recorded, but no landslide activity was observed for this region. A total of

35mm in 24 hours was recorded 5km from the study area, this being the nearest rain gauge data available for the cyclone Fehi event.

Table 4.18: Summary results for the study area.

Sample no.	Parent Bedrock	Cohesion (kPa)	Effective friction angle (°)	Residual friction angle (°)	Plasticity Index	Clay Fraction (%)	Hydraulic Conductivity (m/s)
2018 (Gita)							
2	SPG	5	37	27	16	22	
8	URIC	12	33	24	15	20	$3.38x10^{-6}$
13	OS	4	32	22	25	31	$1.94x10^{-6}$
Pre-2018							
6	SPG			27		3	
7	SPG	8	33	28	17	17	
16	URIC	13	31	23	19	9	
19	URIC					5	$2.07x10^{-5}$
Weathered Bedrock							
1	SPG	2	46			4	$7.79x10^{-6}$
4	SPG	2	42			3	$7.76x10^{-6}$
9	URIC	1	44			3	$9.25x10^{-5}$
14	OS	6	40			34	

On the 11thof February 2107, 117 mm of rainfall was recorded in 24 hours. Therefore, from the rainfall records the soil at the time of Ex-tropical cyclone Gita would have been in a wet state. The role of antecedent moisture content is important, and it is concluded that Ex-tropical cyclone Gita was the trigger for extensive landsliding in steep terrain underlain by 1 - 5 m of partially saturated colluvium.

The hydraulic conductivity measured for the colluvium was in the range 10^{-5} to 10^{-6} m/s which is typical of silt and is relatively low due to clay content. The rainfall intensity of Ex-tropical cyclone Gita on 20th February 2018 was 55mm/hour over 24 hours, whereas the 11th of February 2018 was only 12mm/hour (Figures 4.18 and 4.19). The hydraulic conductivity when converted to mm/hour is 76 mm/hour for Sample 19 (pre-2018 fan deposit), and for samples collected from 2018 debris flow source areas were 12 mm/hour and 7 mm/hour. The hydraulic conductivity of the source areas are significantly lower than the intensity of the 20th February Gita event. Experiments by Wu et al. (2015) has shown that the failure occurs due to low hydraulic conductivity, which makes it difficult for rainwater to infiltrate the deep areas of the slope. This leads to formation of shallow transient saturated zones with soil deformation where the pore-water pressure cannot dissipate resulting in sliding failure (Wu et al., 2015). There needs to be more hydraulic conductivity tests conducted to see the relationship between hydraulic conductivity and rainfall intensity. Other parameters to consider

would be slope angle and antecedent moisture level. More data is needed to develop the hydrogeological model, which was beyond the timeline of this thesis.

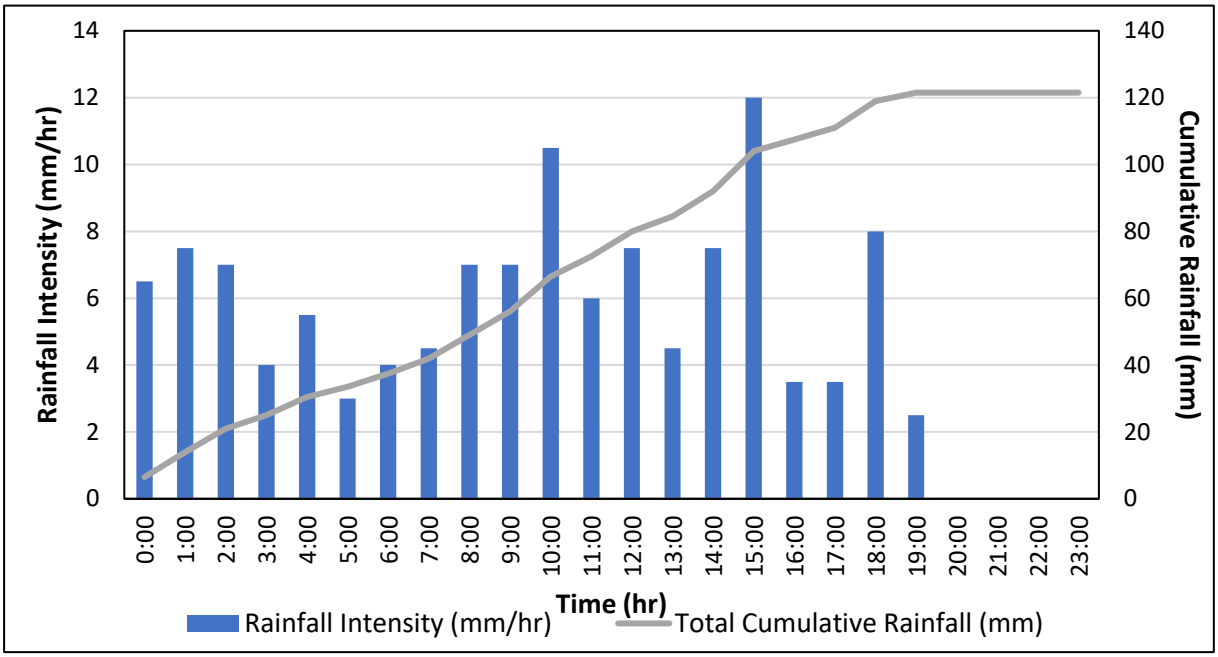

Figure 4.18: Rainfall intensity for 11th February 2018 storm. Blue indicates the total rainfall per hour while grey shows the total cumulative rainfall over the day.

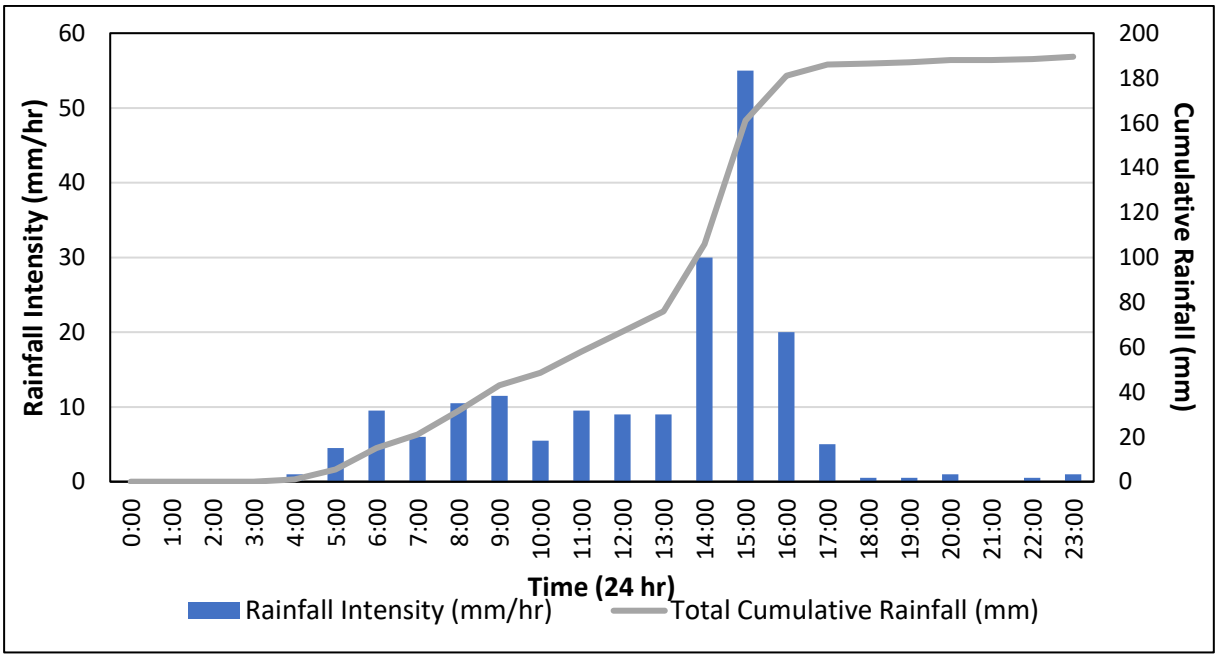

Figure 4.19: Rainfall intensity for 20th February 2018 (Ex-tropical cyclone Gita) storm. Blue indicates the total rainfall per hour while grey shows the total cumulative rainfall over the day.

To model the colluvium soil deposits and weathered bedrock, a range of tests were conducted. The particle size distribution was carried out on the fine fraction (excluding boulders and cobbles), as the

fine material controls the matrix properties. The clay content was of particular importance due to its low strength and high compressibility. Any soil finer than 0.002 mm is regarded as clay size, but it is noted that not all clay fractions are clay minerals. An XRD analysis needs to be conducted to identify the clay minerals, but this was beyond the scope of the study.

For the 3 soil samples tested, the average effective friction angle ($\phi_P{}'$) in the 2018 (Gita) source area was 34° and the average residual friction angle (ϕ_r)was 24°. There is a drop of 10° from peak to residual friction angle. For the 2 samples tested, the average peak friction angle for pre-2018 deposit is 32° and results for 3 samples tested (pre-2018), the average residual friction angle of 26°. There is no significant difference between effective friction angle and residual friction angle in 2018 (Gita) and pre-2018 soil collected and these values can be regarded as representative of the debris flow deposits irrespective of source bedrock lithology.

In comparison, for each of the weathered bedrock (highly to residual soil), the average effective friction angle was 43°, which is approximately 25% higher than colluvium soil, deposits tested. This confirms the field model that the colluvial failures occurred over weathered bedrock due to saturation of the near surface colluvial layers.

The soil in the study area is predominately silt with varying amounts of clay, sand and gravel. The strength of this material is reasonably high (>30° effective friction angle) which could explain why these materials fail only in extreme rainfall conditions (180mm / 24 hours) on average of 30 years. There is no major differences in soil properties of colluvium underlain by each different bedrock lithology. The only difference that was noted was the high clay content of highly weathered to residual soil Onekaka Schist bedrock and the overlying colluvium. The clay content of colluvium (debris flow source area) and underlying completely weathered to residual soil developed on Onekaka Schist comprised more than 30% clay size fraction, the highest recorded. The effective friction angle and residual friction angle of completely to residual soil Onekaka Schist and the overlying colluvium, is slightly lower than Undifferentiated Riwaka Igneous Complex and Separation Point Granite, but shear strength parameters do not appear to differ significantly between lithologies.

Figure 4.20 shows a schematic stratigraphic profile in Channel 2, which is underlain by Undifferentiated Riwaka Igneous Complex rocks. Undifferentiated Riwaka Igneous Complex is the dominant lithology along SH60, and the results are relevant for to batter design.

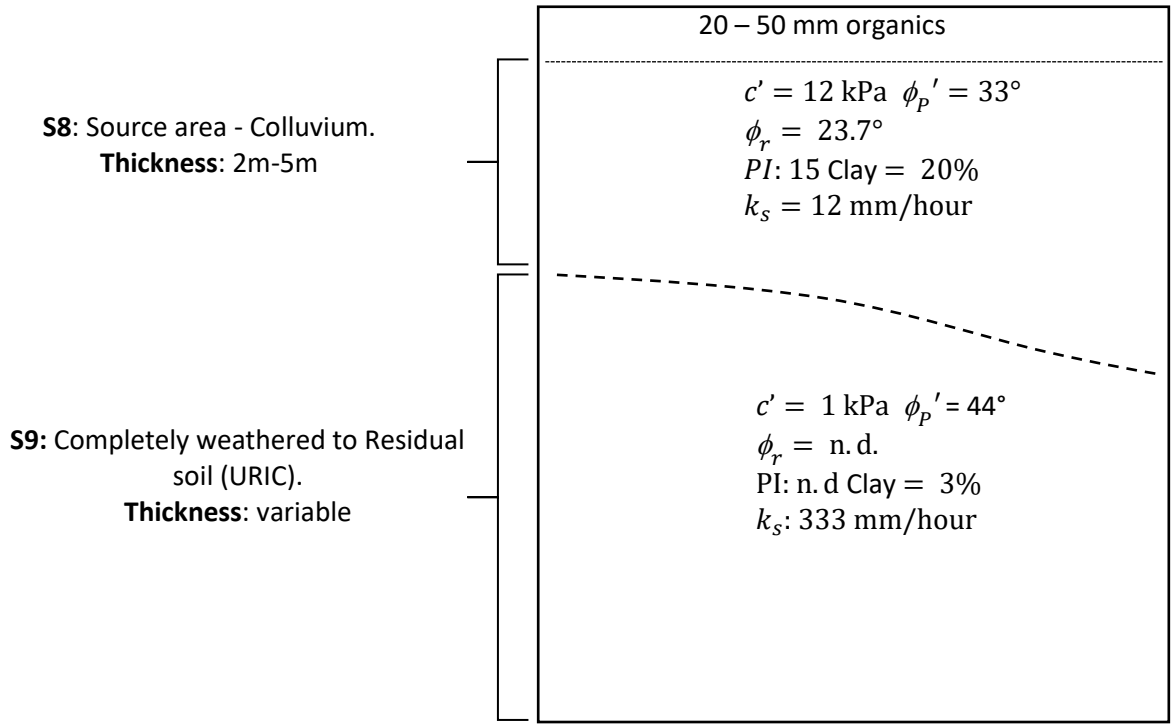

Figure 4.20: Schematic stereographic profile for slide source area in Channel 2 underlain by URIC rock. Diagram is not drawn to scale.

Chapter 5: Bedrock Weathering Profile Characterisation

5.1 Introduction

This chapter discusses the geotechnical characterisation of rock masses for each of three main lithologies studied in terms of the recognised weathering profiles (Chapter 1, Figure 1.9). To assess rock strength, Schmidt rebound hammer tests were conducted in the field, and point load (PLS) and unconfined compressive (UCS) strength testing was carried out in the laboratory. The samples were collected during detailed field investigation by the author, and from cores from drilling conducted by the engineering consultancy Beca Limited on behalf of the New Zealand Transport Agency (Refer to Figure 5.1 for location). The main objective of the tests was to estimate strength properties of rocks in the Takaka area as a function of weathering grade, as determined from outcrop and core logging using the New Zealand Geotechnical Society (NZGS) 2005 Guidelines.

The samples used for conducting UCS testing were from core recovered from drilling in March 2019 for remedial design works. Most of the drilling took place in areas underlain by Undifferentiated Igneous Riwaka Complex (URIC, Chapter 1) rocks, and the granite encountered in the drill holes was intruding into URIC bedrock. The samples used in laboratory point load testing were from core recovered from drilling, and from block samples collected during field investigations from exposure along road cuts and drainage channels. Thin sections were also prepared for each weathering grade of rock (slightly to completely weathered) from outcrop and drill core samples.

This chapter is divided into two parts: (1) a geological description of the weathering profiles from thin sections and outcrop; and (2) strength testing by various methods, with limited density results.

Thin section study was adopted as the main method for assessing weathering following the six category hand specimen descriptors (UW to RS) generally adopted (e.g. NZGS, 2005). Strength testing was used as the primary method for comparing intact rock variation as a function of weathering grade, in conjunction with thin section study providing additional data on fabric alteration for each lithology. Dry density was also calculated for the three UCS samples, which were derived from URIC lithology because of its dominance on the highway alignment. Slake durability testing was not undertaken because of time and sample limitations, and density determination was considered less important for weathering characterisation due to difficulty in obtaining representative samples.

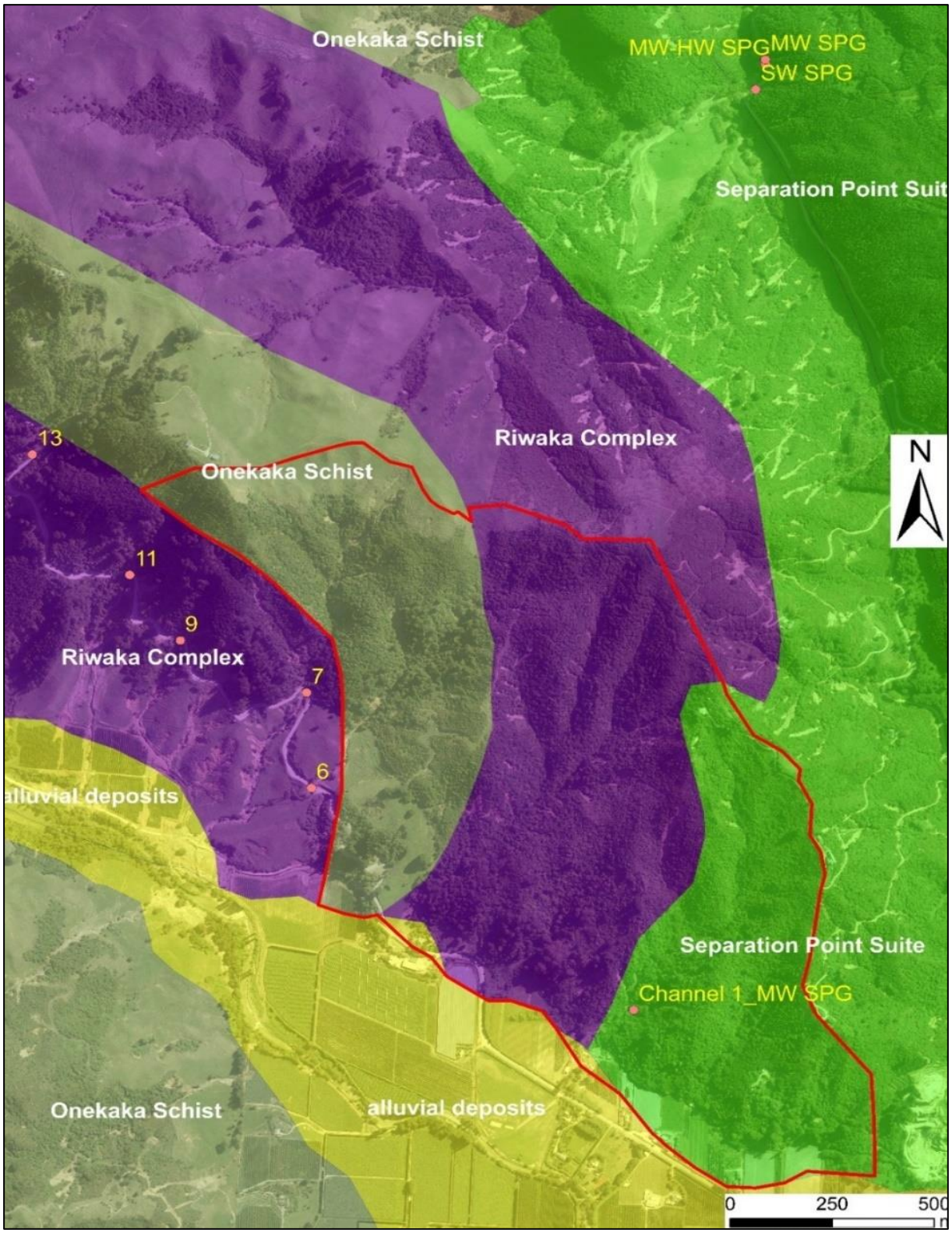

Figure 5.1: Location of all rock samples collected. The highway is underlain by mainly Undifferentiated Riwaka Complex, and there is therefore more drill core available for this bedrock unit. Sample locations are marked by pink dots. Red polygon outlines the area of detailed catchment analysis. Lithological units are shown on a bedrock geology overlay for the study area. The geology map is from 1: 250,000 published map (GNS Web Map, 2012).

5.2 Weathering Profiles

Comparative profiles from borehole logs for Sites 6, 7, 11, and 13 (Figure 5.2), as drilled and logged by Beca Ltd (Beca, 2019) in March 2019 with additional data from the author, are presented in Figure 5.2 at approximate horizontal distances from Borehole 6 as the zero datum. The objective of this figure is to show the well-developed and highly variable weathering profile along the highway within the URIC lithological unit. The description of the weathering profile is taken from observations by the site geologist, supplemented by personal observations for Boreholes 6i and 7i during completion of those holes. The soil and rock description follows New Zealand Geotechnical Society December 2005 Guidelines (New Zealand Geotechnical Society, 2005). Chapter 1 describes the six-fold weathering grade system adopted.

5.2.1 Beca Ltd Drill holes

Beca conducted a total of 7 boreholes at five locations shown in Figure 5.1. Sites 7 and 13 had both vertical and inclined boreholes, the latter being at 60° and 70° to horizontal respectively. The borehole log information and samples were kindly provided by Beca Limited (Beca, 2019). Table 5.1 shows the information on weathering grade in each inclined borehole, and Table 5.2 from the vertical boreholes. The data are presented as profiles only, with no attempt to incorporate road gradients.

In terms of bedrock lithology, it is apparent from Figures 5.2 and 5.3 that, although all five boreholes were collared in Undifferentiated Igneous Riwaka Complex (URIC), interlayering of the different lithologies has occurred as a result of the intrusive nature of both the URIC and the Separation Point Granite (SPG) in relation to the older Onekaka Schist (OS). As a consequence, shearing and accompanying alteration has occurred, and a simple ‘top down’ weathering profile is not present, reflecting prolonged exposure to climatically-controlled weathering.

In Boreholes 6, 11 and 13 a ~9-10m thick layer of colluvium overlies weathered bedrock, the colluvium containing clasts up to boulder size. As seen in both Tables 5.1 and 5.2, the weathering profile varies with depth. Sites 6 and 7, and Sites 9 and 11, are relatively close to each other (Figure 5.1), however the weathering grades change markedly over this short distance. Unweathered to slightly weathered bedrock starts at a depth of 10m or more below the colluvium in all boreholes.

Table 5.1: Summary of Beca drill log results for inclined boreholes ("i").

Borehole ID	Depth	Material Thickness (m)	Material Description	Tests
6i	27 m	0 - 1.1	Fill	
		1.1 - 10.7	Colluvium	
		10.7 - 12.7	HW-CW OS	
		12.7 – 14	HW OS	
		14 - 14.6	SW OS	
		14.6 - 17.5	HW URIC	
		17.5 - 18	SW- MW URIC	
		18 - 20.9	HW OS with UW-SW quartzite band	Point load
		20.9 - 22.2	SW-MW SPG	Point load
		22.2 - 25.1	MW-HW SPG	
		25.1 - 26	SW URIC	
		26 - 26.5	SW-MW URIC	
		26.5 - 27	UW URIC	
7i	15 m	0 - 4.2	Fill	
		4.2 - 7	HW OS	
		7 - 8.3	SW-MW URIC	Point load Thin section
		8.3 - 8.8.8	CW URIC	
		8.8 - 9	CW-RS URIC	
		9 - 10.2	HW OS	
		10.2 - 10.6	SW –MW URIC	
		10.6 - 11.5	HW-CW URIC	
		11.5 - 11.7	UW-SW SPG	
		11.7 - 12.4	MW-HW URIC	
		12.4 - 13.3	CW URIC	
		13.3 - 15	MW-HW URIC	
11i	17.6 m	0 - 3.7	Fill	
		3.7 - 13.5	Colluvium	
		13.5 - 15.5	HW URIC	Point load
		15.5 - 16	MW OS	
		16 - 16.6	SW OS	
		16.6 - 17.6	UW-SW URIC	UCS
13i	27.1 m	0 - 5.1m	Fill	
		5.1 - 19.8	Colluvium	
		19.8 - 24.8	MW URIC	
		24.8 - 25.8	HW URIC	
		25.8 - 27.1	SW URIC	UCS Point load

Table 5.2: Summary results of Beca drill log results for vertical boreholes ("v").

Borehole ID	Depth	Material Thickness (m)	Material Description	Tests
7v	9.45 m	0 - 2.2	Fill	
		2.2 - 3.3	RS OS	
		3.3 - 6.9	HW-CW OS	
		6.9 - 9.45	HW URIC	
9v	14.8 m	0 - 0.8	Fill	
		0.8 - 6.5	CW URIC	
		6.5 - 8	HW URIC	
		8 - 9.8	MW URIC	
		9.8 - 10.1	UW URIC	
		10.1 - 14.15	MW URIC	Point load
		14.15 - 14.4	UW-SW URIC	UCS Thin section
13v	14.8 m	0 - 9.7	Colluvium	
		9.7 - 10.8	HW URIC	
		10.8 - 14.8	MW-HW URIC	

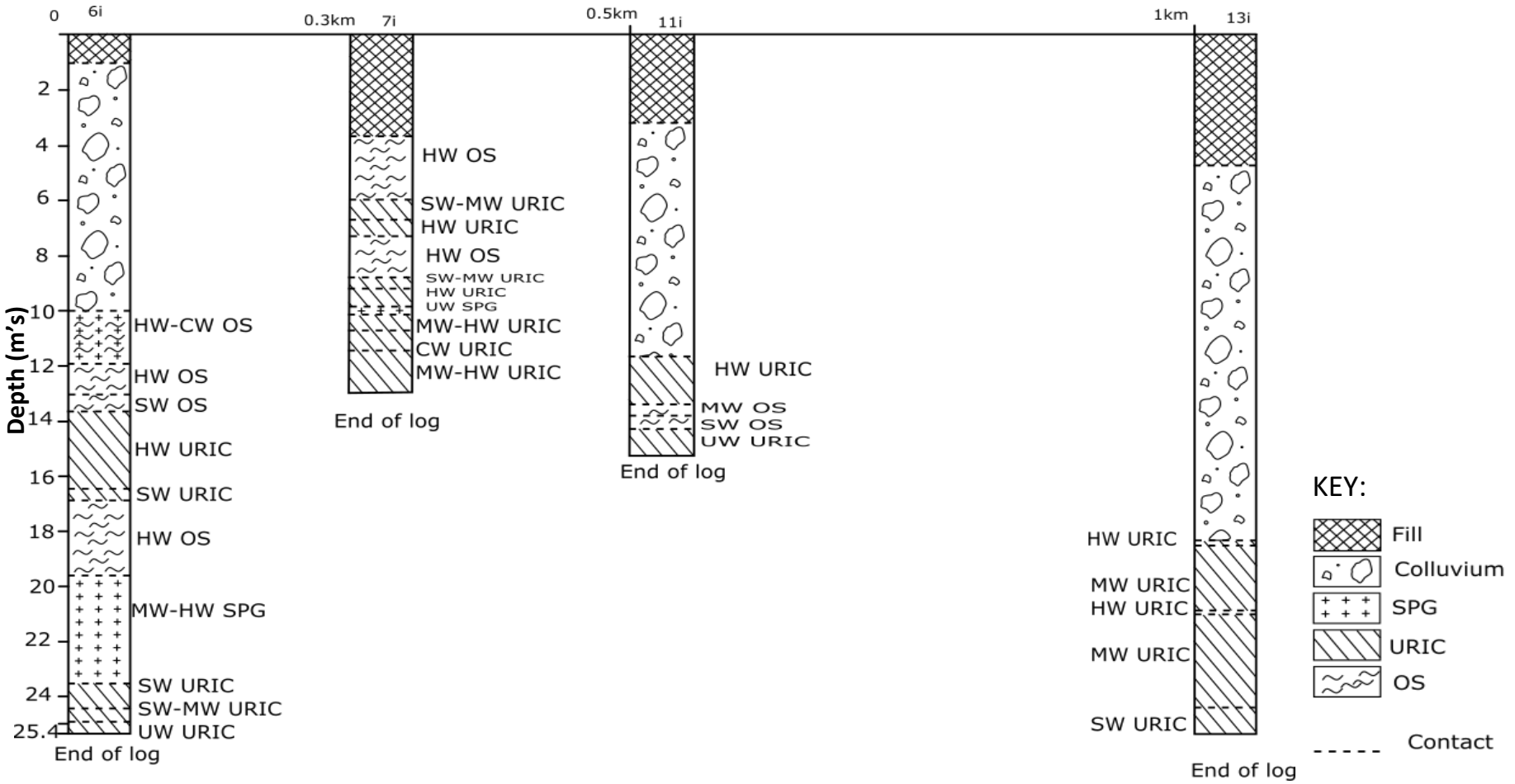

Figure 5.2: Borehole log summary (A)Inclined borehole log summary. Comparative set of profiles along the road alignment in mapped URIC at approximate horizontal scale from Borehole 6i as the zero datum. Figure 5.1 shows locations of the boreholes in plan. Inclined boreholes were projected to vertical. Weathering grades are as follows: UW - Unweathered, SW - Slightly weathered, MW - Moderately weathered, HW - Highly Weathered, CW - Completely Weathered, RS - Residual Soil. Bedrock lithologies are identified by the following codes: SPG – Separation Point Granite, URIC – Undifferentiated Riwaka Igneous Complex, OS – Onekaka Schist.

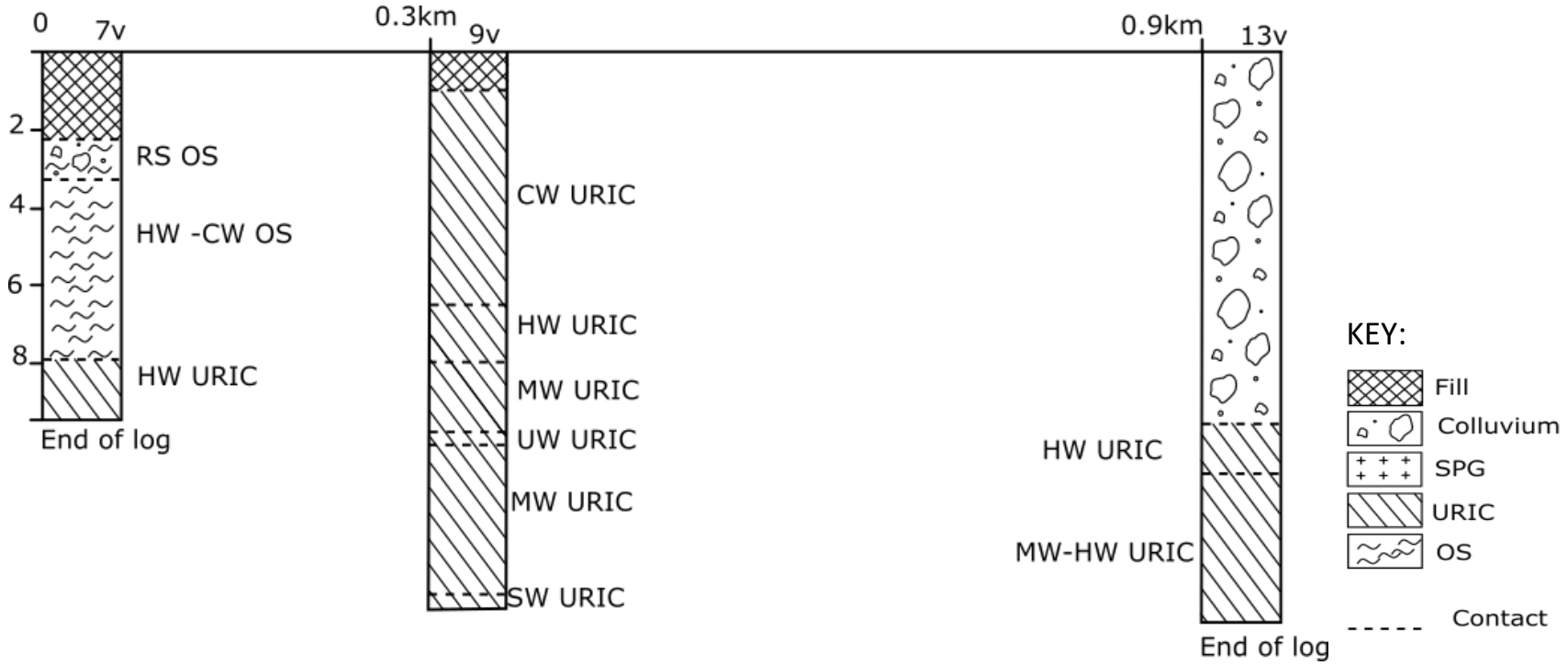

Figure 5.3: Vertical borehole logs summary. Comparative set of profiles along the road alignment in URC at approximate horizontal scale from borehole 7V as the zero datum. Refer to Figure 5.2 for weathering grade and rock mass acronyms.

5.3 Rock Mineralogy and Petrography

5.3.1 Introduction

The aim of this section is to describe the composition of the bedrock and how weathering processes have altered the mineralogy. Samples representing a range of weathering grades were collected from Separation Point Granite and Undifferentiated Igneous Riwaka Complex for thin sectioning. A point count of at least 250 grains at 1mm length was conducted using the Pelcon point counter with moving slide holder. Only limited study of weathered Onekaka Schist was possible.

5.3.2 Separation Point Granite (SPG)

Samples from each weathering profile were selected for thin section examination. The unweathered (UW) to slightly weathered (SW) bedrock was collected from road cuts, and moderately weathered (MW) and highly weathered (HW) material from Channel 1 (Figure 5.1). The slightly weathered SPG sample came from an area mapped as granite, and the moderately to completely weathered samples from mapped granodiorite (Rattenbury et al 1998). The moderately and completely weathered SPG samples can therefore be compared directly. Results are summarised in Table 5.3.

Table 5.3: Summary of point count results in each weathering grade of granite/granodiorite. All numbers are in Percentages. Refer to Figure 5.2 for weathering grade and rock mass acronyms.

Unit	Quartz	Plagioclase	Alkali feldspar	Biotite	Muscovite	Opaque	Ground mass	Degree of Alteration
SW Granite	47	16	29	4	1	1	2	Low
MW Granite	37	4	20	10	13	-	16	Moderate
CW Granite	10	3	9	5	3	-	70	High

The (UW) to (SW) granite consists of quartz (47%), plagioclase feldspar (16%) and alkali feldspar (29%), with biotite and muscovite as accessory minerals. The quartz displayed strong undulose extinction (Figure 5.4), and the alkali feldspar was characterised by perthite intergrowths. Myrmekitic textures were observed in thin section and the biotite had a pale green to brown pleochroism. In hand specimen pink alkali feldspar is abundant and up to 20mm in size, giving the rock a porphyritic texture. The thin sections showed that UW-SW granite is quartz rich.

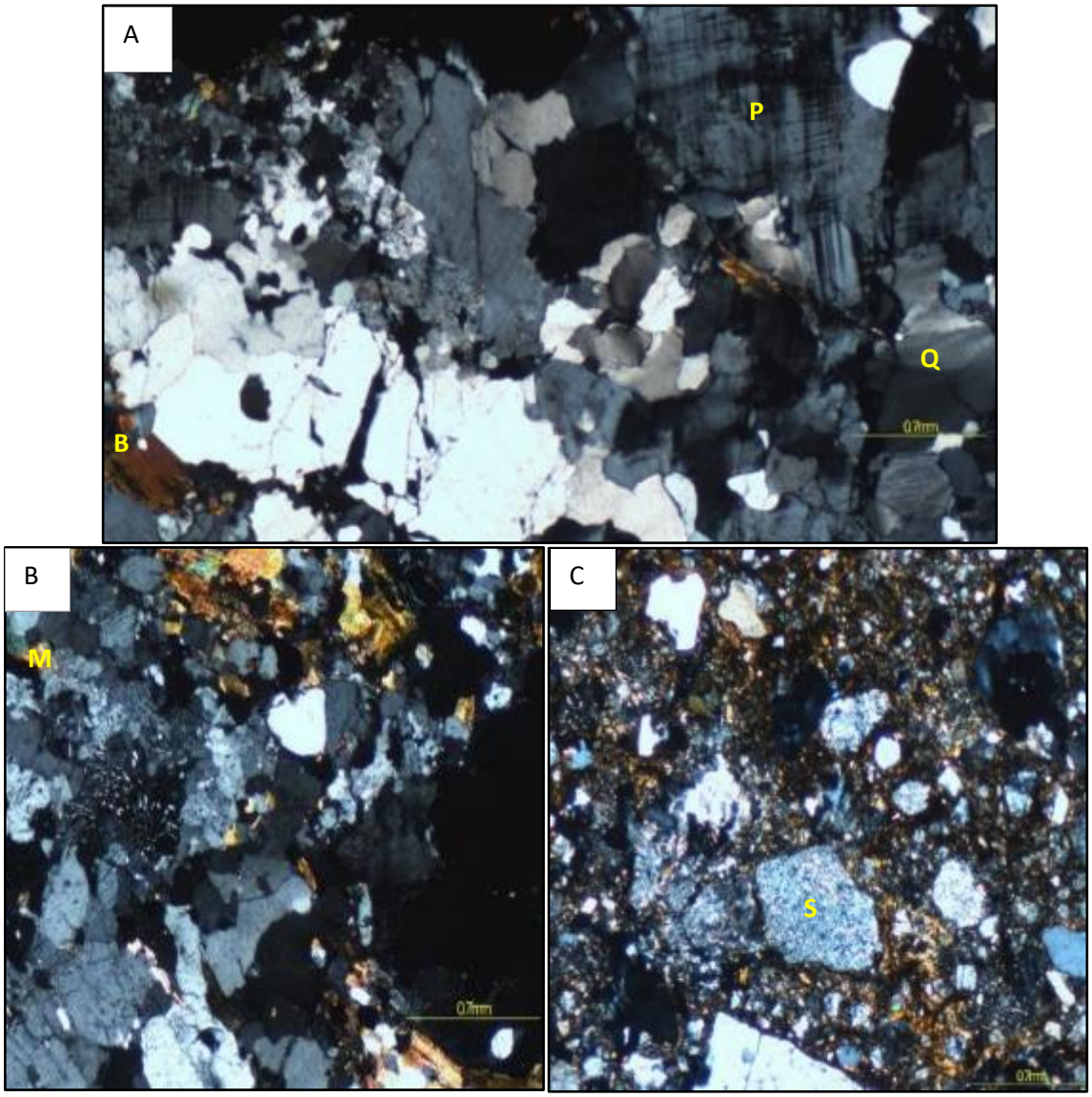

Figure 5.4: shows the different minerals present in selected granitic samples. As weathering grade increases, the Plagioclase (P) percentage decreases, as well as Biotite (B), and the plagioclase crystals exhibit sericite alteration. In the weathered granite, the groundmass is made of Quartz (Q), Sericite (S), Feldspar, Muscovite (M) and biotite.

5.3.3 Onekaka Schist (OS)

Unweathered Onekaka schist in altered bedrock near the contact in Channel 3 (angular gravel in a clay matrix) was collected to study the mineralogy of the OS. This was done to confirm that the bedrock was Onekaka Schist and not a granitic intrusion. The rock consisted of 80 % quartz, 17% muscovite and 3% biotite, and the mineralogy was typical of Onekaka Schist. The quartz displayed strong undulose extinction, and some crystal alignment (Figure 5.5).

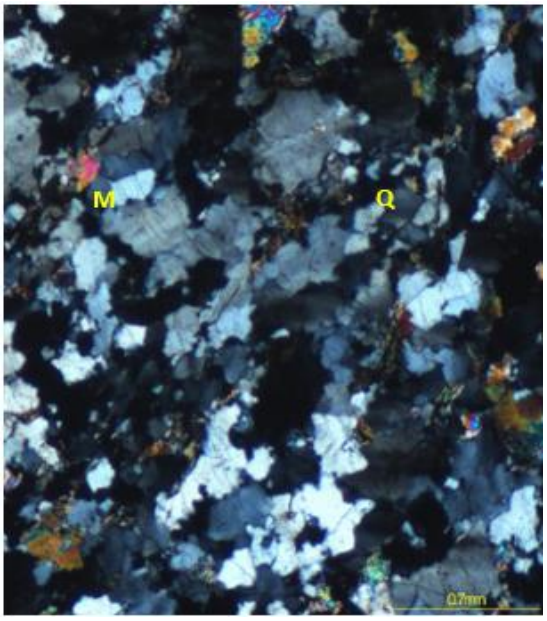

Figure 5.5: Photomicrographs of Onekaka Schist clast, under Cross Polarised Light (CPL). Quartz (Q) and Muscovite (M).

5.3.4 Undifferentiated Riwaka Igneous Complex (URIC)

Slightly weathered (SW) and moderately weathered (MW) URIC samples were collected from drill core, and highly weathered (HW) material from Channel 2. In hand specimen the SW URIC samples were coarse-grained and grey in colour, with black flecks and visible pyrite as opaques in thin section. The MW rock consisted of 31% chlorite and 20% groundmass, together with pyroxene, plagioclase, quartz and opaques (Table 5.4). In hand specimen, MW URIC bedrock was greenish grey, with visible quartz, feldspar and pyrite. The green colour is probably due to chlorite, which was present in high percentage in thin section (Figure 5.6).

Table 5.4: Summary of point count results for each weathering grade in URIC bedrock. All numbers are in percentages. Refer to Figure 5.2 for weathering grade and rock mass acronyms.

Rock mass Units	Quartz	Plagioclase	Chlorite	Pyroxene	Hornblende	Biotite	Opaque	Groundmass	Degree of alteration
SW	43	31	10	4	-	-	6	6	Low
MW URIC	15	8	31	15	4	2	5	20	Moderate
HW URIC	2	1	26	5	7	1	1	57	High

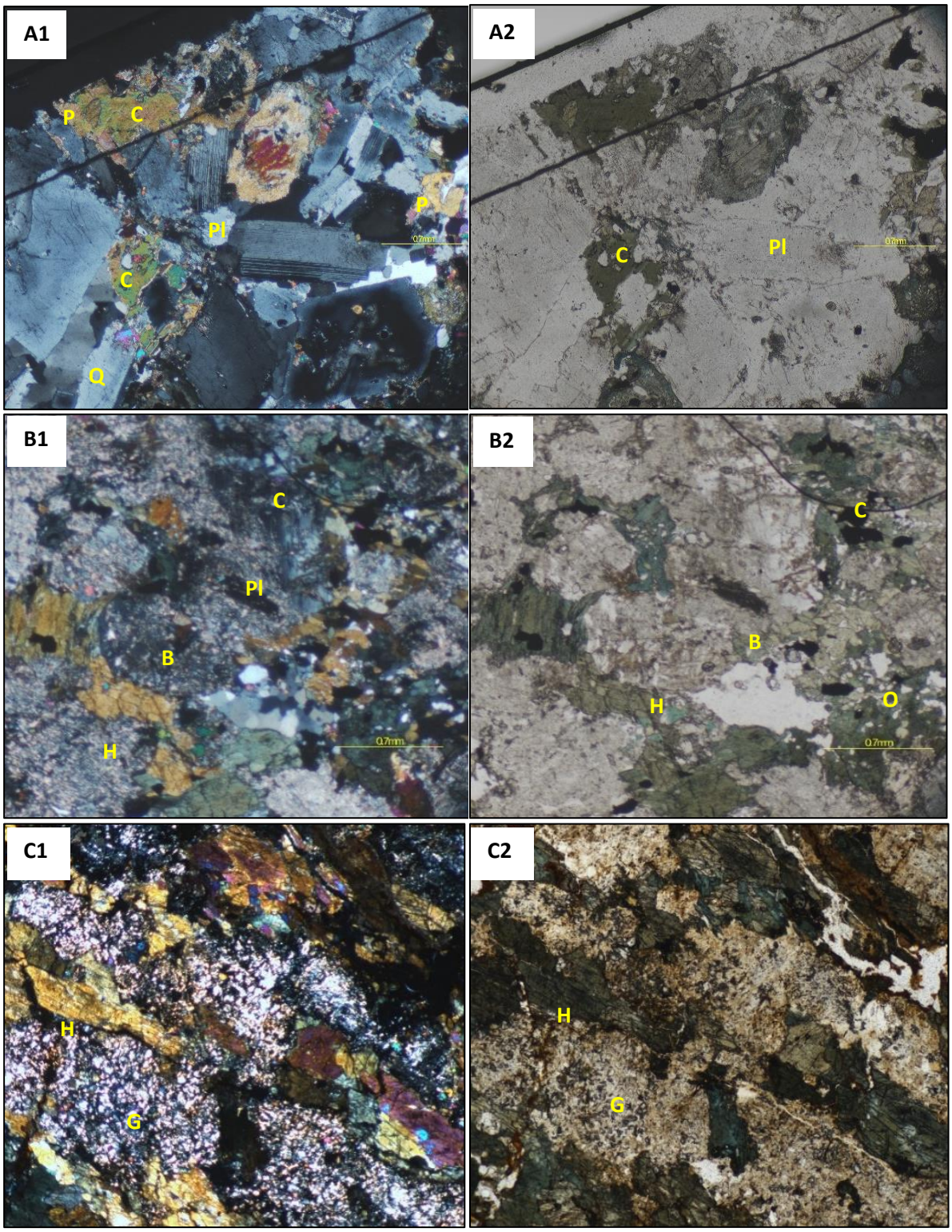

Figure 5.6: Photomicrographs of URIC. Opaque (O), Biotite (B), Muscovite (M), Hornblende (H), Groundmass (G), Plagioclase (PL), Pyroxene (P), and Quartz (Q). A1, B1 & C1 are all under Cross Polarised Light (CPL), and A2, B2 & C2 are under Plane Polarised Light (PPL). A1 and A2 are slightly weathered URIC, See figure 5.2 for explanation. The unaltered Plagioclase shows twinning. B1 and B2 are moderately weathered URIC. C1 and C2 are highly weathered URIC, where the groundmass is replaced by Sericite (S), Quartz, Pyroxene, Chlorite (CL) and Feldspar.

As weathering grade increases, the degree of mineral alteration increases. Plagioclase in moderately to completely weathered URIC has either completely or partially sericitised, and the pyroxene and amphibole have been replaced by chlorite. In Figure 5.6 (A) pyroxene is observed to be replaced by chlorite. The groundmass is made up of fine-grained sericite, quartz, feldspar, pyroxene and chlorite.

5.3.5 Discussion of Petrographic Changes with Weathering

Muir et al. (1995) reports that the mineralogy assemblage for Separation Point Granite in the study area showed 15 - 20% quartz, 30 - 35% plagioclase, 30 - 35% orthoclase, 5 - 10% microcline, 5 - 10% biotite, and 2-3% hornblende. The plagioclase was oligoclase composition displaying myrmekitic intergrowths and microperthic textures (Muir et al., 1995) This mineralogy and texture was similar to the current observations, however no hornblende was observed in the samples examined.

In granitic rocks plagioclase and biotite tend to weather first (Durgin, 1977), and they are observed as plagioclase and biotite composition decreasing with increasing weathering grade. The sequence of weathering is plagioclase feldspar, biotite, potassium feldspar, muscovite and quartz. In the weathering of granite, biotite is particularly important in breaking down the rock into grus, and it does this by expanding to form hydro-biotite. Hydrolysis and hydration processes break down feldspars into clay and colloids, while quartz and muscovite weather more slowly (Durgin, 1977).

More research has been done on granite and limestone weathering compared to other rock types (, 2010). It is well known that quartz has a low susceptibility to weathering and will be present as quartz grains. In a hand sample, completely weathered granite was observed to have sand and gravel-sized quartz minerals.

In Undifferentiated Igneous Riwaka Complex bedrock plagioclase was the commonly altered mineral. Pyroxene and hornblende (amphibole) were in lower percentage, and were altered to chlorite. Some pyroxene was of small crystal size, and appeared as remnant minerals.

5.4 Strength Characterisation of Weathered Bedrock

5.4.1 Uniaxial (Unconfined) Compressive Strength (UCS)

Uniaxial compressive strength (UCS) is commonly used for the design and characterisation of intact rock materials. UCS is one of the most important properties of a rock material. Ulusay and Hudson (2007) defines it as the failure strength of an intact rock specimen with a diameter of 48 mm to 54 mm, and having a length to diameter ratio of at least 2.0 as per the ISRM 2007 standard. The main objective

of testing for this thesis was to establish the strength properties of Undifferentiated Riwaka Igneous Complex rocks, and to correlate the results with the estimated strength obtained from point load testing and Schmidt hammer results. The only samples that were available for UCS testing were from Undifferentiated Riwaka Igneous Complex bedrock core drilling, as it was not practical to collect large blocks for coring in the laboratory.

The testing on all three samples of URIC was conducted in accordance with international standards. All samples had >50mm diameter, as required, although one sample did not fit the requirement of length to diameter ratio. The ISRM standard used does not give any correction factors for specimens that do not meet the standard size, and a correction equation was adapted from Protodyakonov (1969) in (Turk & Dearman, 1986):

$$\frac{\sigma_c}{\sigma_m} = \frac{1}{0.875+0.25\,(\frac{D}{L})} \qquad \text{Equation (7)}$$

Where, σ_c Corrected uniaxial compressive strength, recorded as a length to diameter ratio of 2.

Σm Measured uniaxial compressive strength of nonstandard size rock specimens.

D Diameter of the specimen.

L Length of the specimen.

Axial and radial strain gauges were placed on the samples to measure the deformability of the rock during UCS testing. Young's modulus and the Poisson ratio were derived from the stress-strain curves using standard procedures.

The test results are presented in Table 5.5, with raw data in Appendix C.1. The highest strength recorded was 128.6 MPa for sample 9v, which was described as unweathered. There were no visible planes of weakness along the failure surface, reflecting true overall strength of rock. Longitudinal splitting and steep failure surfaces were observed. In comparison the strength of samples collected from 11i and 13i were affected by weathering and microstructure. For specimen 11i, along the failure surface there was a reddish-brown colour observed indicating weathering. Micro-fracturing was also seen in the specimen, which failed along the axial length by longitudinal splitting into very sharp angular pieces.

Table 5.5: Summary of UCS results for Undifferentiated Riwaka Igneous Complex. All samples were collected from drill core. Note: UW = Unweathered. SW = slightly weathered.

Site ID	Depth (m)	UCS	Young's Modulus (GPa)	Poisson's ratio	Dry Density (kg/m^3)	Strength term	Weathering Grade
9v	14.16	128.6	31.85	0.31	2,913.26	Very Strong	UW
11i	16.84	97.5	42.15	0.18	3,082.47	Strong	SW
13i	26.8	23.2	7.54	0.21	2,723.40	Moderately Strong	SW

Figure 5.7: Displays core taken from site 9v, located at a depth of 14.15m. This is a photo of URIC before conducting a UCS test and B) is a photo post testing. Refer to Figure 5.2 for rock mass acronyms.

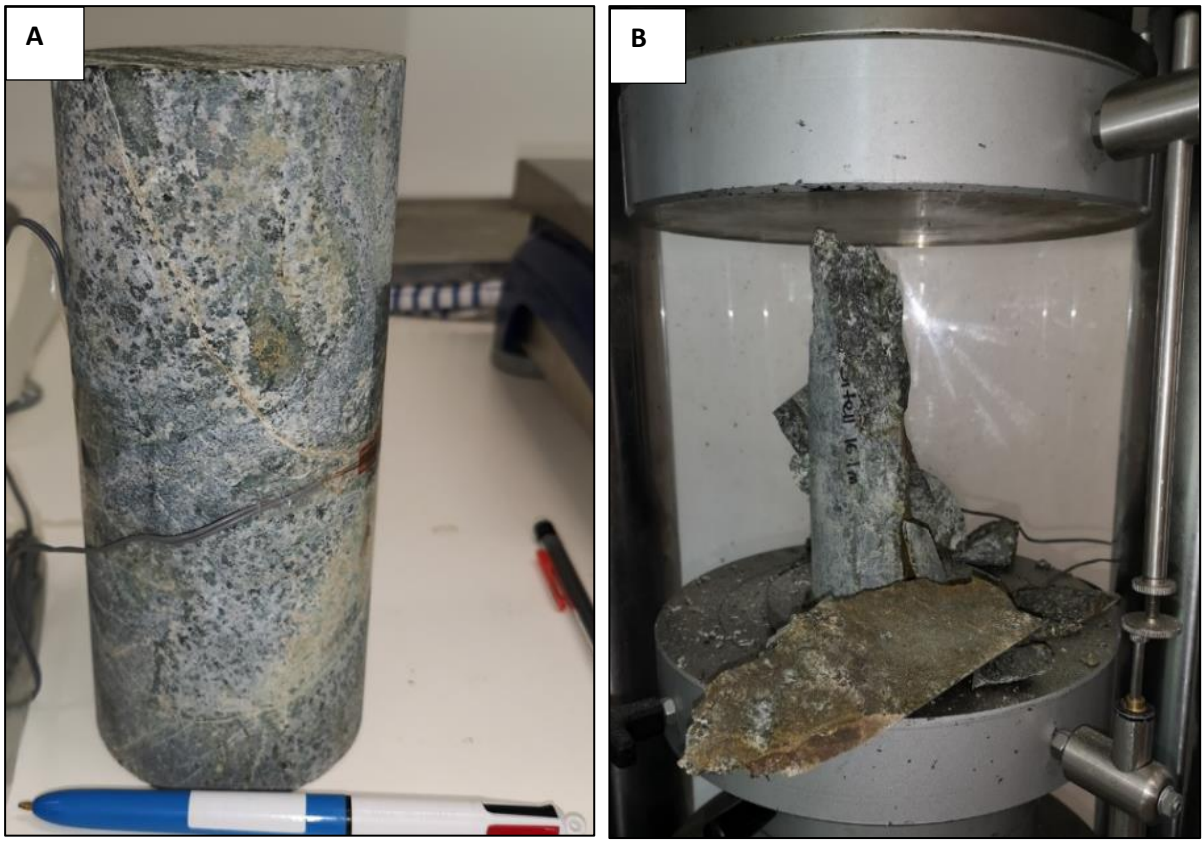

Figure 5.8: Displays core taken form site 11i. This core is recorded at a depth of 16.8m. A) is a photo of URIC before conducting a UCS test and B) is a photo post testing. Refer to Figure 5.2 for rock mass acronyms. Red brown colouring on the core indicates weathering.

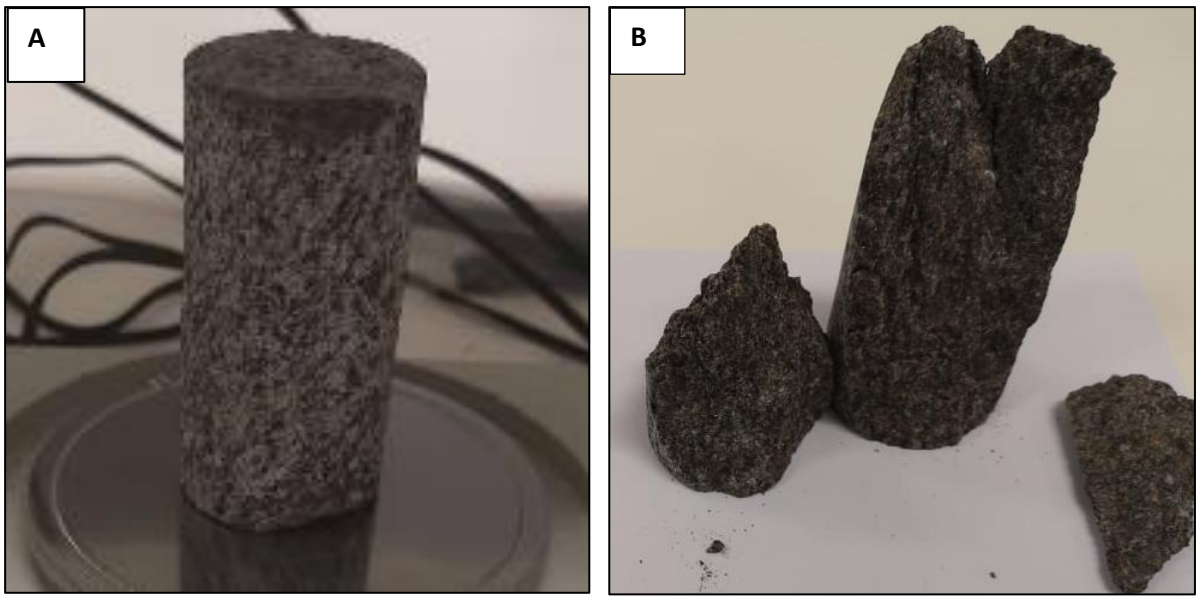

Figure 5.9: Displays core taken from site 13i. This core is recorded at a depth of 26.8m. A) is a photo of URIC before conducting a UCS test and B) is a photo post testing. Refer to Figure 5.2 for rock mass acronyms. Micro-cracking was observed oriented parallel to the failure plane.

For Sample 13i there were micro-cracks observed along the failure plane, which could have affected the overall strength of the rock leading to lower values for slightly weathered rock. The failures in all specimens occurred along the axial length of the specimen. Photographs of each specimen before and after the UCS test are shown in Figure 5.7 to Figure 5.9. Dry density values (Table 5.5) for three UCS samples tested are insufficient to establish trends but do indicate a density for fresh Undifferentiated Igneous Riwaka Complex bedrock of 3,000 ± 100 kg/m^3. The slightly lower dry density value for Sample 13i is consistent with significantly lower UCS strength.

5.4.2 Point-Load Strength (PLS) Testing

Point load strength was used as an index test for strength of Undifferentiated Riwaka Igneous Complex, quartzite (Onekaka Schist), and Separation Point granite rocks. "The test measures the Point Load Strength Index ($Is_{(50)}$) and their strength anisotropy which is the ratio of Point Load Strength in all directions giving the highest and lowest values" (Ulusay et al., 2007). It is a rapid and inexpensive way to determine the strength of rock. The values obtained from this test can also be used to estimate uniaxial compressive strength (UCS).

The test was conducted in accordance with ISRM guidelines, but, due to time and access limitations, it could not be performed in the field. All tests were conducted at natural moisture content and within 30 days of sample collection. Testing was performed on samples collected from drill cores, road cut exposures and channels. The specimens were in the form of core (diametral and axial tests) and irregular lumps. The rock specimens were broken by applying concentrated load through a pair of conical platens. All rock specimens tested had a distance between platen contact greater than 15mm. The core specimens used for diametral and axial tests were collected from Beca drill cores. Only a limited number of samples were brought back to the laboratory for testing. The core was selected based on weathering grade, with an emphasis on unweathered bedrock that would not be possible to collect using irregular lump field samples.

Tables 5.6 and 5.7 provide summaries of the results from the study area. The tables are divided into rock samples collected from drill core, and those collected during field investigations. The point load strength index was determined for various grade of weathered Undifferentiated Riwaka Igneous Complex and Separation Point Granite. A size correction factor was applied to all calculations, as stated in the ISRM standard. The mean value of Is(50) was calculated by deleting the two highest and two lowest values and then calculating the mean of the remaining values. There was an exception at Site 9v, where only 3 data points were possible.

The samples tested mostly appeared to be dry. All samples had water content of <2.5%, except for moderately weathered granite in Channel 2, which had about 3% water content.

The average corrected Point Load Index for slightly weathered irregular lumps of granite bedrock collected from road cuts ranged from 2.1 MPa (strong) to 1.11 MPa (moderately strong), with an average of 1.59 MPa (moderately strong). Similar results were obtained from drill core at site 6i, where values ranged between 2.02 MPa (moderately strong) and 0.46 MPa (weak), with an average of 1.31 MPa. The moderately weathered granite in Channel 1 had a range of values between 0.28 MPa (weak) and 0.14 MPa (very weak), with an average value of 0.21 MPa (weak). The strength term is based on the NZ rock classification (NZGS, 2005) system, and was confirmed in the field. Refer to Appendix C.2 to see the range of values obtained during the test.

Slightly weathered Undifferentiated Igneous Riwaka Complex rock ranged in value between 8.25 MPa and 6.2MPa, all being strong to very strong rock. The highly weathered rock cores in 9v and 11v were weak to very weak rocks. The quartzite band tested in Onekaka Schist bedrock (Site 6i in Table 5.7) should not be used as an indicative strength of the bedrock (Beca, 2019).

The conversion to estimate UCS from point load results were:

$$UCS = 24 \times I_s(50) \qquad \text{Equation (8)}$$

The conversion is based on the ISRM standard (Ulusay et al., 2007)

Table 5.6 Rock samples collected during field investigation for irregular lump point load strength testing. The raw data is presented in Appendix C.2. Both samples were tested using the Schmidt hammer.

Site ID	Rock type	Number of tests	Mean I_s(50)	Equivalent UCS	Strength Description	Weathering Grade
Road cut	SPG	10	1.59	38.2	MW	SW
Channel 1	SPG	10	0.21	5.0	W	MW

Table 5.7: Summary of Point Load strength results from samples collected from drill core. The raw data is presented in Appendix C.2. SPG = Separation Point Granite, URIC = Undifferentiated Riwaka Igneous Complex. The SPG are described as intrusion into URIC. OS represents quartzite band in Onekaka Schist.

Site ID	Depth (m)	Rock type	Number of tests	Mean I_s (50)	Equivalent (UCS)	Strength Description	Weathering Grade
6i	20.3	OS	10	5.84	140.2	Very Strong	SW
6i	21.05	SPG	13	1.31	31.5	Moderately strong	SW
6i	21.6	SPG	10	0.05	1.2	Very weak	HW
7i	7.6	URIC	10	6.97	167.4	Very strong	SW
7i	7.7	URIC	14	3.47	83.3	Strong	SW
7i	8.25	URIC	10	2.78	66.7	Strong	SW
9v	13.5	URIC	3	0.47	11.3	weak	MW
11i	15.5	URIC	12	0.08	1.9	Very weak	HW
13i	25.8	URIC	14	0.86	20.6	Moderately strong	SW

5.4.3 Schmidt Hammer Test Results

The Schmidt hammer was originally designed to test the strength of concrete, and it has also been widely used to measure the strength of rock. The spring-driven hammer was selected to test the strength of rock as it is a quick and simple test. The hammer was tested on different weathering grades. The N-type hammer was used in the field as it can provide data on strength from weak to very strong rock. At least 10 readings were taken from each rock surface, and from each joint set identified. The L type of hammer would have been more suitable for the highly weathered rock, however the hammer failed to work in the field.

The ranges of N Schmidt hammer "R" values for slightly weathered to highly weathered bedrock are given in Table 5.8. The values are average values of the readings, excluding the highest and lowest values and values that had a difference of more than 6. Soft rock, which is completely weathered rock to residual soil cannot be tested with an N type hammer. Because the L-type Schmidt hammer failed to work in the field, there is limited data available on characterising weathering grade of bedrock for this study.

The Schmidt Hammer was used to estimate the UCS values in two ways: (1) using the conversion chart that came with the hammer (Figure 5.10); and (2) for readings below 20, an empirical conversion equation of UCS = $0.308R^{1.327}$ (Saptono et al., 2013).

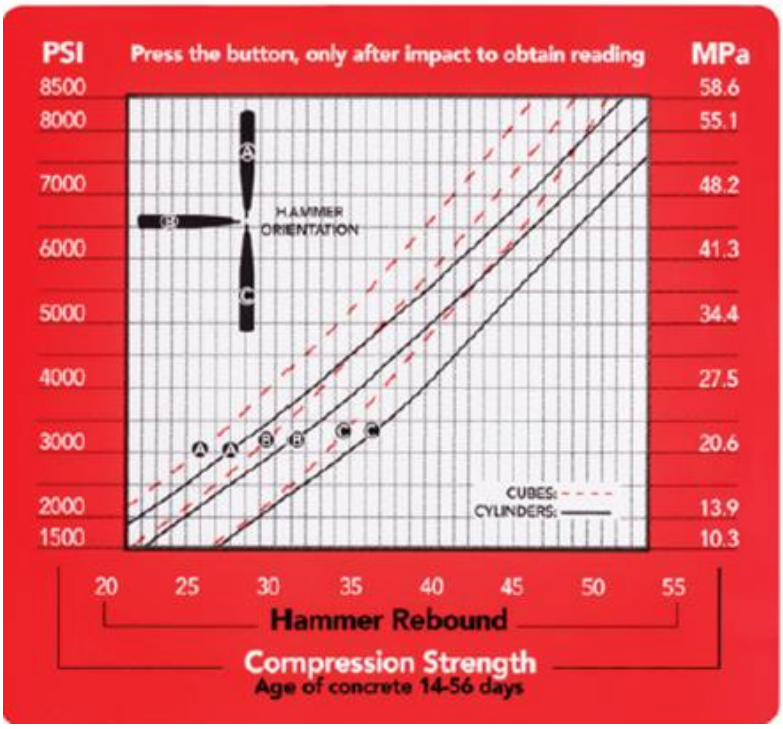

Figure 5.10: Concrete rebound hammer correlation curve provided by the company. Source: (Humboldt Mfg.Co., n.d.)

*Table 5.8: Summary of N-type Schmidt Hammer records. * indicates that the values are estimated using the Equation (UCS = 0.308R$^{1.327}$) for weak rock. ** are gathered using the conversion chart supplied with the N-Type Schmidt Hammer in Figure 5.10.*

Location	Rock type	Weathering grade	Joint set ID	Rebound number		*Estimated UCS (MPa)	**Estimated UCS (MPa)
				Range	Mean		
Channel 1	SPG	MW-HW	1	12-33	16	12.2	>10.3
		MW	2	10-46	16	12.2	>10.3
Road cut	SPG	SW	1	35-58	47	-	45
			2	40-55	48	-	42
	SPG	MW	-	15-28	20	16.4	>10.3
	SPG	MW-HW	-	12-18	18	14.3	>10.3
Channel 2	URIC	HW	-	1-12	8	4.9	>10.3

5.5 Weathering Grade Strength Variation

It was beyond the scope of the current project to test all geotechnical properties of rocks in the study area, and therefore only the strength of the three mapped lithologies was deemed important. The values obtained (Table 5.9) indicate the range in strengths for the various bedrock weathering grades, with particular emphasis on the Undifferentiated Igneous Riwaka Complex (URIC) and the Separation

Point Granite (SPG) as few suitable sites for sampling the Onekaka Schist were identified. The strength values obtained are considered useful for foundation design during further repairs along SH60, and as an indicator of strength reduction due to weathering in a temperate high rainfall environment. UCS values computed directly and indirectly gave reasonable correlation with field descriptions (Table 5.9).

The unweathered to slightly weathered Undifferentiated Riwaka Igneous Complex (URIC) rock was mostly in the very strong strength range, with point-load strength values between 2.8 and 7.0MPa. Measured UCS values of 98 and 128MPa were obtained, consistent the range in PLS data using the conventional multiplier of 24 x $Is_{(50)}$. The moderately weathered URIC was significantly weaker, with a measured UCS value of 23MPa: this corresponded to a range in UCS values computed from PLS of 11 to 21MPa.

Unweathered to slightly weathered Separation Point Granite samples were moderately strong. The Schmidt Hammer readings, and the Point Load Strength samples collected from the same outcrop, gave similar results as seen in Table 5.9: equivalent UCS values were in the range 32 to 38MPa from PLS testing, whilst Schmidt Hammer conversion suggested 45MPa. In general, the granite around the Takaka Hill is prone to chemical weathering and is weak to very weak in the weathered state. It was observed in reconnaissance around the study boundary that most exposures were highly to completely weathered granite with a sandy silt texture. The few places where moderately granite exposure was tested gave equivalent UCS values ≤5.0MPa from Point Load Strength testing, although Schmidt Hammer testing of outcrops suggested equivalent UCS values in the range 5 to 15MPa (Table 5.9).

The one site where Onekaka Schist was tested (Site 6i; Table 5.9) showed very strong rock, with equivalent UCS from Point Load Strength testing in excess of 100MPa. The lack of outcrop on the SH60 alignment was the principal reason for not completing more testing.

From the limited strength testing carried out, it can be said generally that the unweathered to slightly weathered Undifferentiated Igneous Riwaka Complex rocks are stronger than those of the Separation Point Granite of the same weathering grade by a factor of 2 to 3. This observation was made in the field as well. From personal communication with a local geologist, Paul Wopereis (personal communication, October 14, 2019) mentions “on the hills the granite is generally extremely weak to very weak due to chemical weathering, except at the coast where there is harder rock which in places would likely reach moderately strong”.

Unconfined compressive strength (UCS) is an important rock property that is used for foundation design. There were limitations on the number of tests that could be conducted for this thesis study,

and indirect tests (Point Load Strength; Schmidt Hammer) were therefore used to estimate the UCS. The Schmidt hammer was originally designed in 1948 for carrying out *in situ* non-destructive tests on concrete, and it has been widely used to test the strength of rock. It offers a relatively cheap, fast and easy method to use, and the N type hammer is the most commonly used type hammer to test rock although it is not reliable in weak rocks. The Schmidt Hammer test is sensitive to the presence of discontinuities in rock, as well as to water content in weak rock (Selby, 1980). Readings were taken 60mm from the joint edge as is recommended.

The point load test (PLS) was first developed in Russia and generates rapid results. The results from the point load test have been correlated with UCS, and the conversion for hard rock is based on the ISRM standard. In this project it has been assumed that the standard conversion of 24 x PLS was appropriate, and it is generally in the range 20-25. Slightly weathered (site 7i) Undifferentiated Riwaka Igneous Complex (URIC) rock has a higher equivalent UCS than unweathered measured UCS for Undifferentiated Riwaka Igneous Complex, probably PLS X 24 is not correct for that rock type.

Table 5. 9: Summary of all test results divided according to weathering grade and subdivided into rock types. The data are from boreholes, road cut (RC), and channels (C). Refer to Figure 5.2 for weathering grade and rock mass type acronyms.

Site ID	Weathering Grade	Point Load		Schmidt hammer		Measured UCS (MPa)	Strength term
		I_s(50)	Equivalent UCS (MPa)	Rebound Value	Equivalent UCS (MPa)		
Undifferentiated Riwaka Igneous Complex (URIC)							
9v	UW	-	-	-	-	127.5	Very Strong
11i	SW	-	-	-	-	97.5	Very Strong
7i	SW	6.97	167.4	-	-	-	Very Strong
7i	SW	3.47	83.3	-	-	-	Very Strong
7i	SW	2.78	66.7	-	-	-	Very Strong
13i	SW	-	-	-	-	23.2	Moderately Strong
13i	MW	0.86	20.6	-	-	-	Moderately Strong
9v	MW	0.47	11.3				Weak
11i	HW	0.08	1.9				Very Weak
C2	HW	-	-	8	5	-	Weak
Separation Point Granite (SPG)							
RC	SW	1.59	38.2	47	45	-	Moderately Strong
6i	SW	1.31	31.5	-	-	-	Moderately Strong
C1	MW	0.21	5.0	16	7	-	Weak
RC	MW	-	-	20	16	-	Weak
RC	MW-HW	-	-	18	14	-	Weak
6i	HW	0.05	1.2	-	-	-	Very Weak
Onekaka Schist (OS, Quartzite)							
6i	SW	4.38	105				Very Strong

5.6 Conclusions

Specimens were collected from drill core along SH60, and from outcrop, for petrographic analysis and strength testing to characterise the three lithologies present, these being Onekaka Schist (OS), Undifferentiated Riwaka Igneous Complex (URIC), and Separation Point Granite (SPG). Of these lithologies, URIC comprising gabbros and related mafic igneous rocks is the dominant geological unit along the highway alignment.

Each lithology displays a well-developed weathering profile in the near surface 10-20m, and colluvial deposits overlie either residual soil or highly to completely weathered bedrock. The weathering profile reflects the steep topography and prolonged chemical weathering under temperate climatic conditions, clearly influencing slope stability.

Unweathered to slightly weathered bedrock in Undifferentiated Riwakak Igneous Complex is moderately strong to very strong, and equivalent unconfined compressive strengths typically exceed 60 MPa. The Separation Point Granite shows lower intact strength in the range 30 – 40 MPa, although no unconfined testing was carried out due to sampling difficulties.

Moderately to highly weathered bedrock in the URIC lithology gave computed equivalent UCS values of up to 20 MPa, reducing with increased weathering grade. Computed UCS values for moderately to highly weathered Separation Point Granite were less than 5MPa, consistent with the lower intact strength for unweathered bedrock samples.

Onekaka Schist (OS) was not exposed along the SH60 corridor, and where identified in eroding catchments was typically strong to moderately strong. The high quartz and low mica contents contribute to a less well developed weathering profile.

Further study using XRD analysis of the clay mineral fractions is advised for all rock types.

Chapter 6: Summary and Conclusions

6.1 Project Objectives

To assess debris flow hazard to SH60 on the eastern side of Takaka Hill, and to gain a better understanding of the mechanisms of slope failure, the following objectives were established for this study:

- Identify and map landslides ("slips") and debris flows caused by Ex-tropical cyclone Gita
- Quantify the debris flow magnitude and frequency on Takaka Hill
- Determine pertinent geotechnical properties of the slope-forming materials
- Consider the implications of the ground models for future management of the SH60 corridor

To meet the objectives of the study a programme of field and laboratory investigations was carried out, including remote sensing analysis, geomorphological mapping, soil sampling, *in-situ* and laboratory geotechnical testing, together with geophysical profiling.

6.2 Geomorphic Setting

The author of this thesis published a conference paper during the master's programme (Prasad & Fenton, 2020) which describes the geomorphology of the study area as follows:

> "The study area is located on the eastern side of Takaka Hill. Takaka Hill is a prominent south-facing escarpment rising to over 900 m above sea level at the western end of Tasman Bay. The eastern side of the SH60 corridor that suffered the greatest impact from the 2018 debris flows, rises from sea level to over 360 m in approximately 4 km. SH60 is crossed by a series of south-flowing tributary streams of the Riwaka River. These tributaries, which occupy deeply incised valleys, have steep (15° to 40°) bedrock channel gradients. These tributary drainage courses were the primary transport routes for debris flow activity in 2018. The study area comprise a series of three main catchments in which debris was mobilised during Ex-tropical cyclone Gita. The main channels are fed by tributary channels." (p.894)

The slope failures during Ex-tropical cyclone Gita occurred on well-vegetated slopes, showing that the vegetation cover was not enough to prevent the failures. The uneven fan surfaces with large boulders at low elevations in the study area indicate a debris flow history, and stream channel banks exposures provided information on earlier debris flow activity. At least two pre-2018 debris flow events were recognised along each of the three main channels examined. The accumulated thickness of pre-2018 debris flow deposits identified is variable, ranging from 1 m to 6 m in total.

Since streambank exposures only provide a limited 2D view of these older deposits, geophysical surveys were carried out. The Multi Analysis Surface Waves (MASW) survey identified up to 10 m of accumulated colluvium thickness above weathered bedrock in some locations.

The area of the debris fan next to Channel 2 is approximately 42,000 m^2. The average thickness of colluvium determined from MASW was 6 m, giving a total volume of 250,000 m^3 of the pre-2018 debris flow deposit. Linear features in the Ground Penetrating Radar (GPR) data were interpreted to be past debris flow events. Figure 6.1 shows an idealised sketch of debris flow activity in the study area.

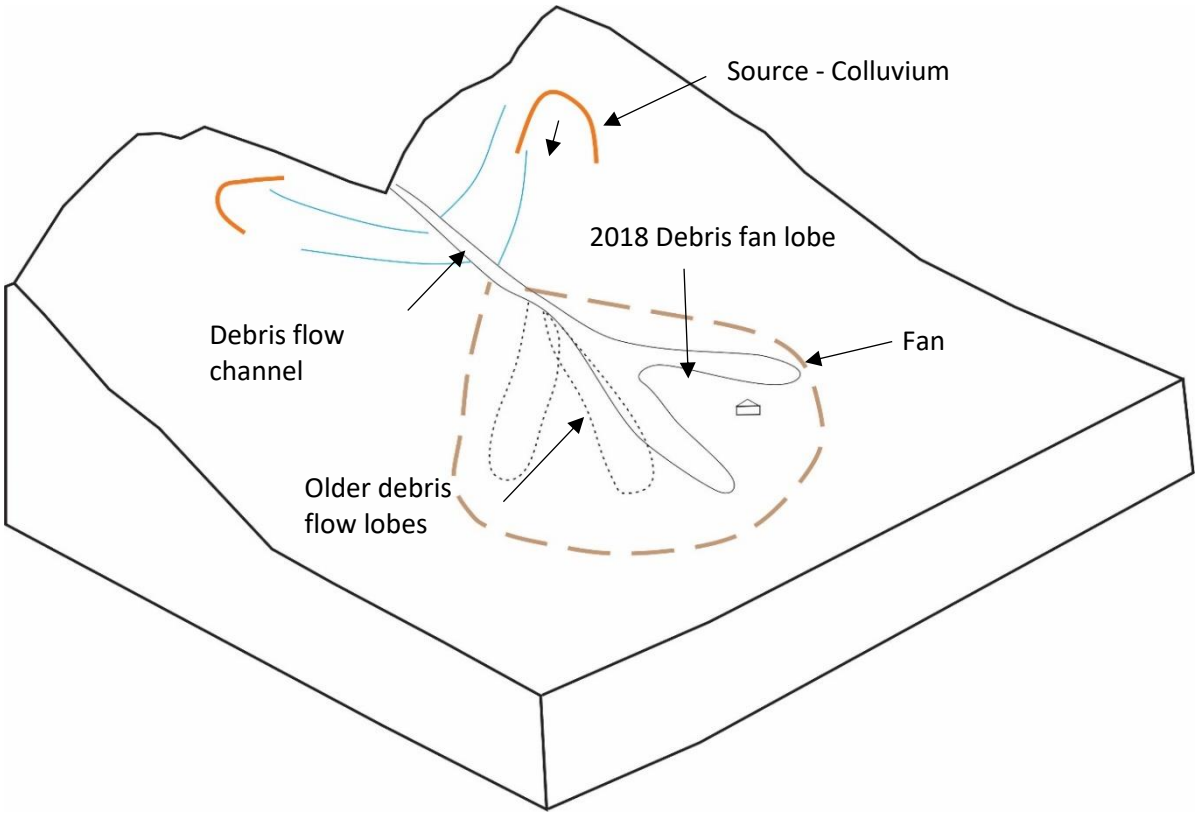

Figure 6.1: Schematic sketch of debris flow fan scenario.

6.3 Bedrock Geology and Geotechnics

Three different bedrock lithologies have been identified in the study area: Onekaka Schist, Undifferentiated Riwaka Igneous Complex, and Separation Point Granite. The main rock types are schist, gabbro, and granite/granodiorite respectively, and the unit contacts are broadly north-trending. The highway is underlain mainly by Undifferentiated Riwaka Igneous Complex. Hence, there is more surface data available than for Onekaka Schist and Separation Point Granite.

The three types of bedrock display a well-developed weathering profile up to 20 m deep in the near surface, and colluvial deposits overlie either residual or highly to completely weathered bedrock. The

thickness of each weathering profile varied along the highway. The completely weathered bedrock and residual soil is typically 1 m to 6 m thick. These weathering profiles are similar for all lithologies showing dominance of climatically-controlled temperate weathering.

The hydraulic conductivity of residual soil to highly weathered bedrock, which displays soil-like characteristics is in the range of 28 mm/hour to 333 mm/hour (i.e. the materials are semi-pervious). The rock characterisation included strength testing, and a linear relationship between weathering grade and strength was identified. The strength of the rock decreases with increasing weathering grade, i.e. from unweathered to completely weathered.

6.4 Surficial Deposits

The colluvial soils in the study area are divided into two categories: those soils activated as soil slides in 2018 (debris flow source areas), and pre-2018 debris flow deposits.

6.4.1 2018 Source Areas (Gita-related)

The thickness of colluvium in the debris flow source areas varied between 1 m and 5 m thick above weathered bedrock. Exposures in head and lateral scarps show the colluvium to be matrix-supported, with predominantly boulder and cobble-size clasts in a clayey to sandy matrix with fine gravel irrespective of source lithology. The particle size distribution analysis showed that the soil samples collected from debris flow source areas are predominantly silt, with varying amounts of clay, sand and gravel. The clay fraction, as determined by hydrometer and pipette methods, ranged from 20% to 31%. The colluvium in the debris flow source areas was described as stiff to hard in exposures. The hydraulic conductivity of colluvium was measured between 7 mm/hour and 12 mm/hour, which is in the intermediate range.

6.4.2 Pre-2018 Debris Flow Deposits

Pre-2018 debris flow deposits exposed on channel banks are also predominantly matrix-supported and contain boulders and cobbles in a fine-grained matrix. The clasts are sub angular to sub rounded, well or gap graded, with a chaotic structure (clast long axes show no preferred orientation). The fine-grained matrix is predominantly silt, with variable clay, sand and gravel fractions. The *in-situ* double ring infiltrometer test conducted on pre-2018 fan deposit sites gave an infiltration rate of 13 mm/hour. The values of infiltration rate suggested the soil to have sand and silt as the major fraction, and clay fraction to be low. This was confirmed by particle size distribution tests.

6.5 Translational Sliding and Debris Flow Generation

The field investigations identified two main types of slope movement in the 2018 Ex-tropical cyclone Gita event: translational shallow soil slides and channelised debris flows. The main soil slides were translational failures in colluvium at or near the bedrock–colluvium contact. The mechanism of failure is relatively rapid infiltration of rainwater into the semi-permeable colluvial slope-forming material, causing saturation above completely weathered bedrock and/or residual soil. This then increases pore water pressure, reducing effective stress and leading to failure. The soil slides enter the drainage channels and with addition of further water from excessive runoff during the rainstorm fluidise to form channelised debris flows.

The sources of debris in the channelised flows were colluvium (2018 soil slides), pre-existing boulders and cobbles in the channel bed, overlying vegetative material, and pre-2018 deposits on channel banks. The flows had a long runout distance, depositing material on the lower floodplain hundreds of metres from the source areas. There are clasts (mostly boulders) from 2018 (Gita) and pre -2018 debris flow present in the channels, as well tree debris from the 2018 events.

6.6 Impacts on SH60

A range of damage was observed that was triggered by Ex-tropical cyclone Gita in February 2018. The main damage was from translational shallow slides, channelised debris flows, and culvert blockage with debris and associated scouring.

The translational shallow soil slides feeding the debris flows impacted directly on the SH60 road corridor. The channelised debris flow had material up to 1 m in boulder size brought down during the Ex-tropical cyclone Gita. These flows inundated (buried) and eroded the road corridor, resulting in undermining of the road fill embankments.

The design of culverts was another factor contributing to the extensive damage to SH60. The size and design were not adequate for the large-scale debris flow events caused by Ex-tropical cyclone Gita, which led to overflowing of debris due to blockage, and caused extensive damage to the road. Undermining of culvert outfalls by flood scour in steep channels contributed to roading problems and requires long-term re-design of culvert intakes and outfalls.

A recurrence interval of approximately 30 years for extensive storm-triggered debris flow activity, at least over the past 70 years, has been established. This extensive damage is defined as a storm event

causing damage to SH60 such that the highway is completely closed for ≥5 days. SH60 is the only vehicular access to the Takaka Hill –Golden Bay area on the western side of Takaka Hill.

6.7 Geotechnical Ground Profiles

6.7.1 Geotechnical Test Data

The field observations and geotechnical laboratory data were integrated to develop a series of ground profile models representing each of the debris flow source areas. The face logging, borehole data and MASW showed highly varied weathering profiles. The depth to bedrock has been inferred from outcrop face logging and geophysical data. The shear strength parameters determined for the soil were apparent cohesion (c') and effective friction angle (ϕ'_p') as well as the residual friction angle (ϕ_r). The rock strength represented in these models is from Uniaxial Compressive Strength (UCS) testing and equivalent UCS calculated from point load testing and Schmidt hammer test results. A summary of results is provided in Table 6.1.

Table 6.1: Geotechnical summary table for Separation Point Granite, Undifferentiated Riwaka Igneous Complex and Onekaka Schist.

	Parameters	Unit	Separation Point Granite	Undifferentiated Riwaka Igneous Complex	Onekaka Schist
Colluvium	Clay fraction	%	22	20	22
	Plasticity Index	-	16	15	25
	Hydraulic conductivity	mm/hr	-	12	7
	Apparent cohesion	kPa	5	12	4
	Effective friction angle	(°)	37	33	32
	Residual friction angle	(°)	27	24	22
Completely weathered bedrock to residual soil	Clay fraction	%	3	3	34
	Hydraulic conductivity	mm/hr	28	333	-
	Apparent cohesion	kPa	2	1	6
	Effective friction angle	(°)	42	44	40
Highly weathered bedrock (soil description)	Clay fraction	%	4	-	-
	Hydraulic conductivity	mm/hr	28	-	-
	Apparent cohesion	kPa	2	-	-
	Effective friction angle	(°)	46		-
Highly weathered (rock description)	UCS	MPa	-	1.9-5	
Moderately weathered bedrock	UCS	MPa	7-16	11-21	-
Slightly weathered bedrock	UCS	MPa	31-45	67-98	105
Unweathered bedrock	UCS	MPa	-	128	-

6.7.2 Onekaka Schist (Figure 6.2)

Soil slides above the completely weathered bedrock and residual soil developed on Onekaka Schist were about 1-1.5 m thick in the mapped exposures. The colluvium had a high clay content (31%) and a relatively low saturated hydraulic conductivity (k_s). The underlying completely weathered bedrock also showed a high clay fraction (34%). The effective friction angle of the overlying colluvium was 25 % lower than the underlying completely weathered and residual soil on Onekaka Schist (ϕ_p '=32° and 40°, respectively).

Limited rock strength data exists for this bedrock unit. The point load testing results were for a quartzite band in Onekaka Schist bedrock. There are limited samples of highly to moderately weathered Onekaka Schist from boreholes by Beca, being present in only 2 boreholes where slightly weathered quartzite was encountered

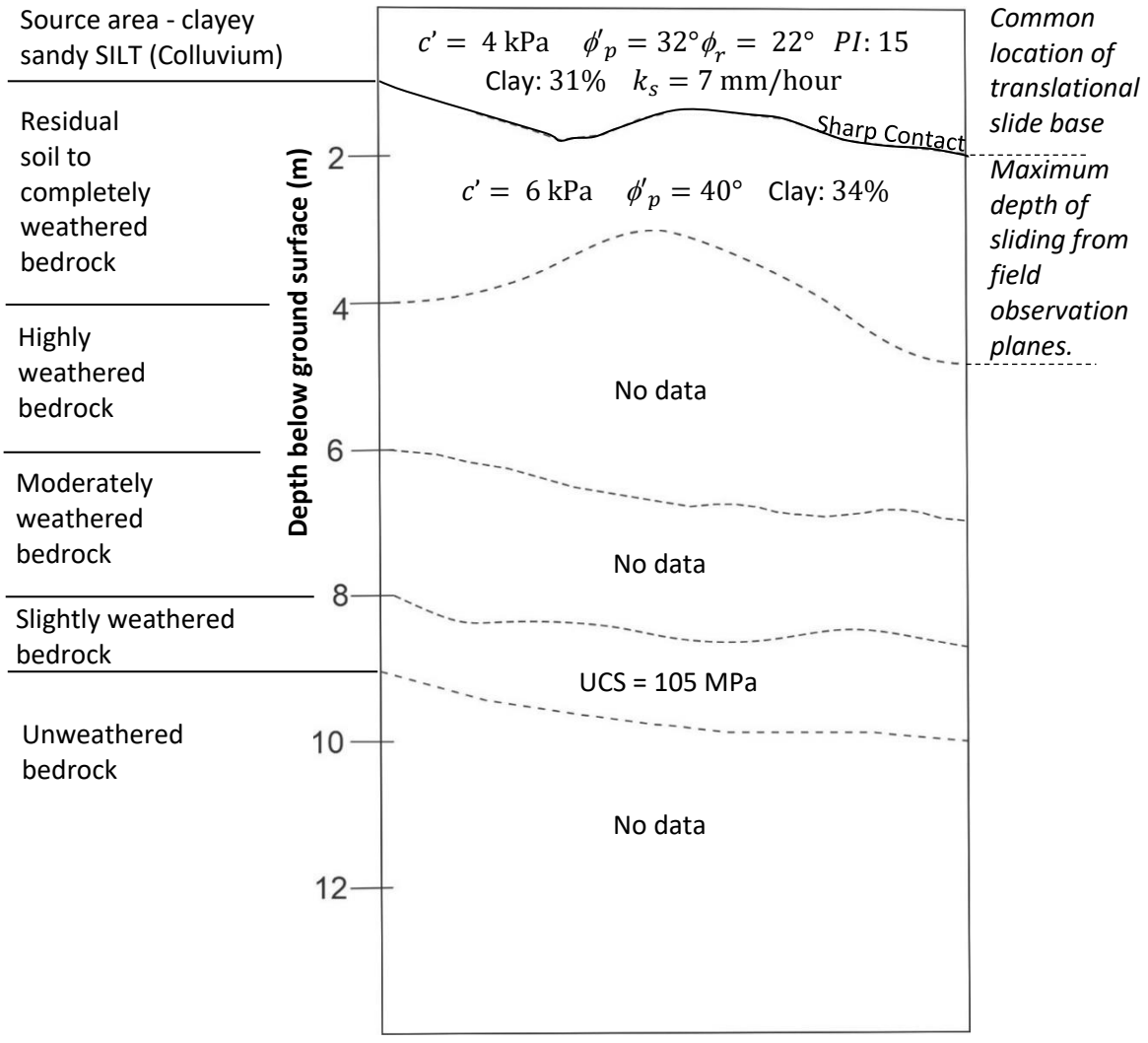

Figure 6.2: Generalised geotechnical ground profile in area underlain by Onekaka Schist.

6.7.3 Undifferentiated Riwaka Igneous Complex (Figure 6.3)

The shallow soil slide source area that was selected for detailed investigation was up to 5 m above the completely weathered bedrock/residual soil interface in Channel 2. The colluvium had a high clay content of 20%, and an intermediate saturated hydraulic conductivity (K_s) of 12 mm/hour. The underlying bedrock had a much lower clay fraction of 3%. The effective friction angle of the overlying colluvium was 33% lower than the underlying completely weathered bedrock to residual soil (ϕ_p'=33° and 44°, respectively).

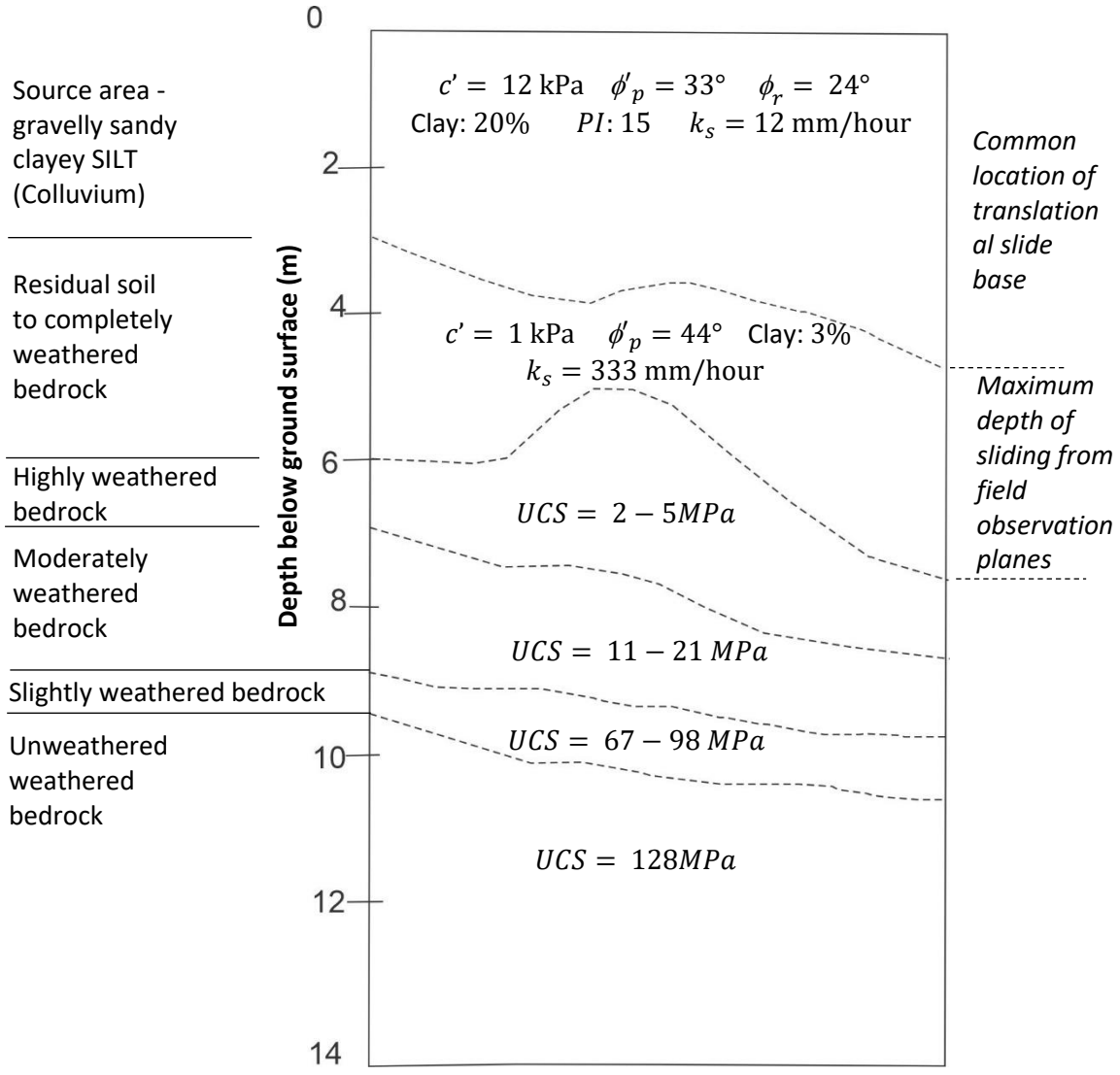

Figure 6.3: Generalised geotechnical ground profile in area underlain by Undifferentiated Riwaka Igneous Complex.

The underlying completely weathered to residual soil developed on Undifferentiated Riwaka Igneous Complex bedrock had a higher hydraulic conductivity than the overlying colluvium (k_s=333 mm/hour

versus 12 mm/hour respectively). This is due to the low clay content and a higher sand and silt content in the weathered rock compared to the colluvium, and possibly to the fracture flow.

The rock strength increases with decreasing weathering grade from 2 MPa (highly weathered bedrock) to over 100 MPa for unweathered bedrock. The unweathered UCS strength corresponds to the very strong rock strength term.

There is more data available for Undifferentiated Riwaka Igneous Complex than for the other two lithologies. This is due to the outcrop exposure, and the fact that Undifferentiated Riwaka Igneous Complex underlies most of SH60 as well as the lower slopes of Channels 2 and 3 selected for study. This made it easier to collect samples, given that the Beca drilling programme targeted the SH60 corridor.

6.7.4 Separation Point Granite (Figure 6.4)

In the exposures studied in detail, a shallow translational soil slide (~1-1.5 m deep) had occurred above the highly weathered bedrock to residual soil developed on Separation Point Granite. The colluvium had a high clay content of 22%, but the underlying bedrock had a low clay fraction of 3% to 4%. The highly to completely weathered Separation Point Granite contains a high proportion of quartz minerals which have a high resistance to weathering. The effective friction angle of the overlying colluvium and underlying completely to residual soil Separation Point Granite was ϕ'_p = 37° and 42° respectively.

As with the other two lithologies, UCS measured with depth below ground surface to a maximum of 45 MPa in slightly weathered Separation Point Granite.

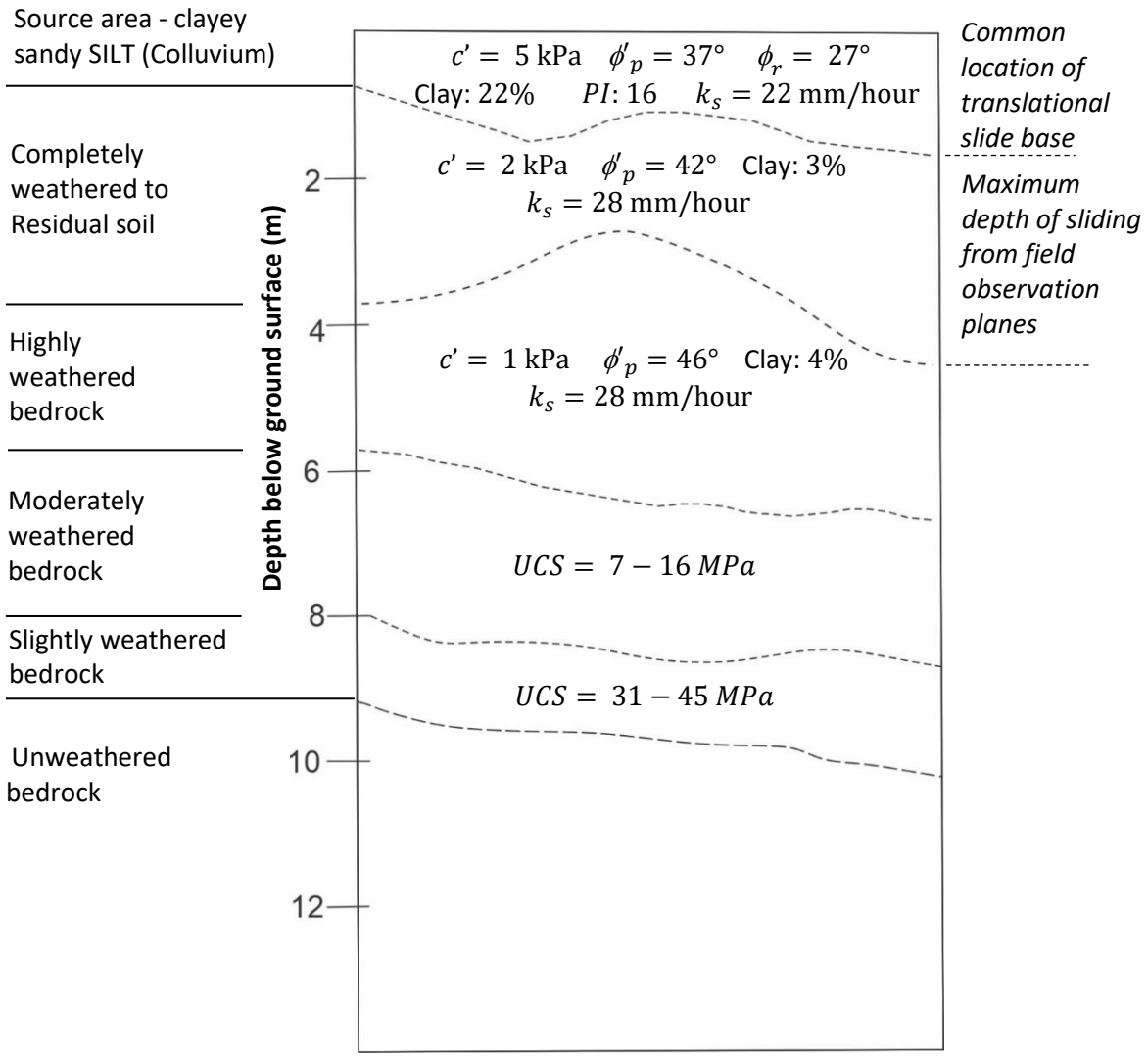

Figure 6.4: Generalised geotechnical ground profile in area underlain by Separation Point Granite.

6.8 Principal Conclusions

6.8.1 Ex – Tropical Cyclone Gita (February 2018)

- The passage of Ex-tropical Cyclone Gita on 20th February 2018 produced extreme rainfall, closing SH60 across Takaka Hill for more than 5 days due to shallow translational soil sliding and related debris flows, culvert blockage and scour, and cut and fill batter failures.
- Total rainfall recorded was ~180mm in 24 hours at the nearby Riwaka gauging station, and review of NIWA rainfall records showed similar extreme rainfall events in 1956/7 and 1990 causing highway closure for more than 5 days.

6.8.2 Eastern Takaka Hill

- The eastern side of Takaka Hill comprises a series of deeply incised steep gradient watercourses which are presently heavily vegetated. The slopes are underlain by three lithologies (Onekaka Schist, Undifferentiated Riwaka Igneous Complex, and Separation Point Granite), of which gabbro from the Undifferentiated Riwaka Igneous Complex is dominant along SH60.
- SH60 provides the only road access to the Golden Bay area (Takaka and Collingwood), and its closure affects a population of ~5000 together with tourists. In addition to the three extreme events recognised in the past 70 years, partial closure of SH60 for hours to days occurs on average 5 times annually.

6.8.3 Landslide Mechanisms

- Study of Ex-tropical cyclone Gita has shown that the source area for soil slides affecting the various catchments above SH60 is in the colluvium overlying all three lithologies. Failure depths are 3-5 m below the existing ground surface, and translational soil sliding typically occurs at the interface between colluvium and the underlying completely weathered bedrock/residual soil.
- Bedrock type appears to have a little influence on slope failure, the slope angle (15°- 40°) and deep weathering providing the primary controls on rainfall-triggered slope failures. Because of the level of shallow “soil “saturation, and the presence of cobble to boulder size material in the colluvium, channelised debris flows are generated by slope and bank collapse.
- Runout distances of several hundred metres have been identified for the debris flows, with debris fans forming at gully mouths below SH60 where watercourses discharge onto the flatter valley floor alluvium.

6.8.4 Past Debris Flow Activity

- The evidence for past debris flow events is present in the stream bank deposits of the mapped channels. Detailed geomorphological mapping identified at least 2 debris flow events in each of the three studied channels.
- Geophysical surveys provided an estimate for the volume of pre-2018 debris flow deposits. The volume was estimated to be ~250,000 m^3 for the fan deposit sourced from Channel 2. Further surveys would be required to refine debris flow volume estimates.

6.8.5 Geotechnical Properties of Colluvial Deposits and Weathered Bedrock

- In this research a database of geotechnical parameters (strength and index properties) and hydrological parameters (saturated hydraulic conductivity) has been created. The parameters are for colluvium (2018 debris flow source areas), pre-2018 debris flow deposits and weathered bedrock for the eastern part of Takaka Hill.
- The effective friction angle for source area colluvial deposits is ~30°, compared to 40° for completely weathered bedrock to residual soil. This confirms the field model that translational soil slide failures occur over weathered bedrock due to saturation of the near surface colluvium.
- Rock strength increases with decreasing weathering grade in the topmost 20m above unweathered bedrock and unweathered to slightly weathered bedrock is moderately strong to very strong.
- Equivalent unconfined compressive strengths typically exceed 60 MPa for unweathered to slightly Undifferentiated Riwaka Igneous Complex, and the Separation Point Granite shows lower intact strength in the range 30 – 40 MPa.

6.8.6 Implications for SH60 Management

- Because of the steep terrain along SH60, and the likelihood for slide-flow events under extreme rainfall, re-assessment of culvert intake and outfall design is a key requirement of future damage is to be minimised.
- Where fill batters have failed due to saturation, reinstatement using benched gabion basket or pole walls should be considered as part of the engineering design.

6.9 Further research

Future work should aim to use the ground models developed in this thesis as an aid to design. Recognition of the catchment history can be refined by dating older deposits where this is possible.

Detailed trenching on the geophysical lines, would improve volume estimates for individual recognised events from geomorphological mapping and geophysical surveys. Additional laboratory testing would capture variability and further develop the geotechnical ground model.

One of the tests recommended is infiltration testing to identify degree of saturation for strength reduction if quantitative stability analysis is required. However, the complexities of catchment geology may render quantitative stability analysis of limited value.

References

ASTM-D3080/D3080M. (2011). *Direct Shear Test of Soils Under Consolidated Drained Conditions*. ASTM International.

ASTM-D3385. (2019). *Standard Test Method for Infiltration Rate of Soils in Field Using Double-Ring Infiltrometer*. ASTM International.

ASTM D4318. (2017). *Standard Test Methods for Liquid Limit, Plastic Limit, and Plasticity Index of Soils*. ASTM International.

Barnes, G. (2000). *Soil mechanics: principles and practice* (2nd ed.). PALGRAVE.

Beca. (2019). *Takaka Hill Five Sites Remediation Geotechnical Investigations Factual Report*. NZ Transport Agency.

Bowles, J. E. (1979). *Physical and Geotechnical Properties of Soils* (2nd ed.). McGraw-Hill Inc.

British Standard Institution. (1990). *British Standard Methods of test of Soils for civil engineering purposes. Part 7. Shear Strength (Total Stress)*.

Calcaterra, D., & Parise, M. (, 2010). Weathering as a predisposing factor to slope movements: An introduction. *Geological Society Engineering Geology Special Publication, 23*, 1-4. https://doi.org/10.1144/EGSP23.1

Controls Group. (2018). *Instruction Manual: 27-WF21E80 Shearmatic*.

Cruden, D. M., & Varnes, D. J. (1996). Landslide Types and Processes. *Special Report, Transportation Research Board, U.S. National Academy of Sciences, 247*, 36-75.

de Vallejo, L. G., & Ferrer, M. (2011). *Geological engineering*. CRC Press.

Durgin, P. B. (1977). Landslides and the weathering of granitic rocks. *Reviews in Engineering Geology, 3*, 127-131.

Eid, H. T., Rabie, K. H., & Wijewickreme, D. (2016). Drained residual shear strength at effective normal stresses relevant to soil slope stability analyses. *Engineering Geology, 204*, 94-107. https://doi.org/10.1016/j.enggeo.2016.02.003

Eijkelkamp. (2018). *Double ring infiltrometer Operating Instructions*. Eijkelkamp. https://en.eijkelkamp.com/products/field-measurement-equipment/double-ring-infiltrometer.html

GEOadvice Limited. (2016). *Geotechnical Assessment Memo Report Upper Takaka Underslip, SH60 56/12.060. (Unpublished Work)*.

GNS Web Map. (2012). *1:250 000 Geological Map of New Zealand (QMAP)*. Retrieved February 21, 2019, from https://data.gns.cri.nz/geology/

Head, K. H., & Epps, R. J. (2014). *Manual of soil laboratory testing* (Third ed.). Whittles Publishing.

Humboldt Mfg.Co. (n.d.). *Concrete Rebound Hammer, Product Manual H-2987H*. https://www.humboldtmfg.com/

Jongens, R. (2006). Structure of the Buller and Takaka Terrane rocks adjacent to the Anatoki Fault, northwest Nelson, New Zealand. *New Zealand Journal of Geology and Geophysics, 49*(4), 443-461. https://doi.org/10.1080/00288306.2006.9515180

Land Information New Zealand. (1958). *Retrolens Historic Image Resource*. Retrieved February 1, 2019 from http://retrolens.nz/

Land Information New Zealand. (2018). *Tasman - Abel Tasman and Golden Bay LiDAR 1m DEM (2016)*. LINZ Data Service. Retrieved 20 February 2019, from https://data.linz.govt.nz/layer/95578-tasman-abel-tasman-and-golden-bay-lidar-1m-dem-2016/

Lewis, D. W., & McConchie, D. (1994). *Analytical sedimentology*. Chapman & Hall.

Macara, G. R. (2016). *The climate and weather of Nelson and Taman* (ISSN 1173-0382). https://doi.org/http://docs.niwa.co.nz/library/public/NIWAsts71.pdf

Muir, R. J., Weaver, S. D., Bradshaw, J. D., Eby, G. N., & Evans, J. A. (1995). The Cretaceous Separation Point Batholith, New Zealand: Granitoid magmas formed by melting of mafic lithosphere. *Journal of the Geological Society, 152*(4), 689-701. https://doi.org/10.1144/gsjgs.152.4.0689

MWH. (2009). *NZ Transport Agency, SH60 RP56/3.9-RP56/12.0 Western Takaka Hill,Geotechnical Risk Assessment Report. New Zealand. (Unpublished Work)*.

MWH. (2014). *Project Technical Memorandum for NZ Transport Agency: SH60 Takaka Hill RP 56/4.37 Failed Gabion Wall. (Unpublished Work)*. NZ Transport Agency.

National Institute of Water and Atmospheric Research [NIWA]. (n.d). *New Zealand Historic Weather Events Catalog*. Retrieved June 21, 2019, from https://hwe.niwa.co.nz/

New Zealand Geotechnical Society. (2003). *NZ Geomechanics News December 2003* [Press release]

New Zealand Geotechnical Society. (2005). *Field Description for Soil and Rock. Guideline for the Field Classification and Description of Soil and Rock for Engineering Purposes.* NZ Geotechnical Society Inc,. www.nzgeotechsoc.org.nz

New Zealand Standards 4402. (1986). *Methods of testing soils for civil engineering purposes*

Opus International Consultants Limited. (2001). *Takaka Hill Management Strategy. (Unpublished Work)*.

Opus International Consultants Limited. (2014). *SH60 Takaka Hill Structures Management Plan Contract 434PN. (Unpublished Work)*.

Opus International Consultants Limited. (2016). *Evaluation of Reinstatement Options. (Unpublished Work)*.

Page, M. J. (2013). Landslides and debris flows caused by the 15-17 June 2013 rain storm in the Marahau-Motueka area, and the fatal landslide at Otuwhero Inlet. *GNS Science Report 2013/44*.

Park Seismic LLC. (2006). *MultiChannel Analysis of Surface Waves (MASW)*. Retrieved August 29, 2018, from http://www.masw.com/

Prasad, C., & Fenton, C. H. (2020). Cyclone-triggered debris flow hazard on Takaka Hill, Tasman District, South Island, New Zealand. In *Geotechnics for Sustainable Infrastructure Development* (pp. 893-900). Springer.

Rattenbury, M. S., Cooper, R. A., & Johnston, M. R. (1998). Geology of the nelson area. *Institute of Geological and Nuclear Sciences 1:250,000 Geological Map, 9*, 1-73.

Sanders, L. L. (1998). *A manual of field hydrogeology*. Prentice Hall.

Saptono, S., Kramadibrata, S., & Sulistianto, B. (2013). Using the Schmidt hammer on rock mass characteristic in sedimentary rock at Tutupan coal mine. *Procedia Earth and Planetary Science, 6*, 390-395.

Sassa, K., Fukuoka, H., Wang, F., & Wang, G. (2007). *Progress in landslide science*. Springer Science & Business Media.

Selby, M. J. (1980). A rock mass strength classification for geomorphic purposes: With tests from Antarctica and New Zealand. *Zeitschrift fur Geomorphologie, 24*(1), 31-51.

Skempton, A. (1953). The colloidal activity of clays. *Selected papers on soil mechanics*, 106-118.

Stark, T. D., & Eid, H. T. (1994). Drained Residual Strength of Cohesive Soils. *Journal of Geotechnical Engineering, 120*(5), 856-871. https://doi.org/10.1061/(ASCE)0733-9410(1994)120:5(856)

Stuff.co.nz. (2018). *Escape coming for those stranded in Golden Bay by ex-Cyclone Gita*. Retrieved November 10, 2019, from https://www.stuff.co.nz/national/101727383/escape-coming-for-those-stranded-in-golden-bay-by-excyclone-gita

Tideman, E. (1996). *Watershed Management Guidelines for Indian Conditions*. Omega Scientific Publishers.

Turk, N., & Dearman, W. R. (1986). A correction equation on the influence of length-to diameter ratio on the uniaxial compressive strength of rocks. *Engineering Geology, 22*(3), 293-300. https://doi.org/10.1016/0013-7952(86)90030-X

Turley, C. (2009). *Rocks and hard places: The Takaka Hill*. River Press.

Turnbull, R. E., Size, W. B., Tulloch, A. J., & Christie, A. B. (2017). The ultramafic-intermediate Riwaka Complex, New Zealand: summary of the petrology, geochemistry and related Ni-Cu-PGE mineralisation. *New Zealand Journal of Geology and Geophysics, 60*(3), 270-295. https://doi.org/10.1080/00288306.2017.1316747

Ulusay, R. a., Hudson, J. A., & International Society for Rock Mechanics. Commission on Testing, M. (2007). *The complete ISRM suggested methods for rock characterization, testing and monitoring: 1974-2006*. Commission on Testing Methods,International Society of Rock Mechanics.

University of Otago. (n.d.). *Tectonic setting of New Zealand: Astride a plate boundary which includes the Alpine Fault.* https://www.otago.ac.nz/geology/research/structural-geology/alpine-fault/nz-tectonics.html

Wesley, L. D. (2003). Residual strength of clays and correlations using Atterberg limits. *Geotechnique, 53*(7), 669-672. https://doi.org/10.1680/geot.2003.53.7.669

Wu, L., Huang, R., Xu, Q., Zhang, L., & Li, H. (2015). Analysis of physical testing of rainfall-induced soil slope failures. *Environmental earth sciences, 73*(12), 8519-8531.

Appendices

Appendix A: Site Investigations

Appendix A.1 Reconnaissance Survey Data

A typical profile of the channels has been presented from the reconnaissance survey. The accumulated thickness of colluvium (pre-2018 debris flow deposit) and GPS measurements was taken every 20 m along the stream bank exposures in the three channels. The elevation is from GPS measurements.

The generalised cross sections shows the accumulated thickness of colluvium (pre-2018 debris flow deposit and 2018 soil slide source areas) from stream bank exposures and the contact to bedrock. This is a 2D estimation where the colluvium and bedrock contact are not known in some areas. In those areas the contact was interpreted.

In channel 3, it was easy to differentiate between the matrix supported deposit with occasional boulders or cobbles; and matrix deposits supported with more than 20% boulders or cobbles, therefore a distinction in the profile has been made. Whereas in channel 1 and 2, the distinction between different debris flow events was not as defined, hence only accumulated thickness was noted as part of the reconnaissance survey.

After the reconnaissance survey, two sites were selected for detailed face outcrop logging and sample collection.

Table A.1.1: start and end of the profile lines.

	Channel 1		**Channel 2**		**Channel 3**	
	lat	long	lat	long	lat	long
Start of line	-41.0568	172.9695	-41.0547	172.9641	-41.0509	172.9614
End of line	-41.0561	172.9708	-41.0525	172.966	-41.049	172.9632

Channel 1 Profile

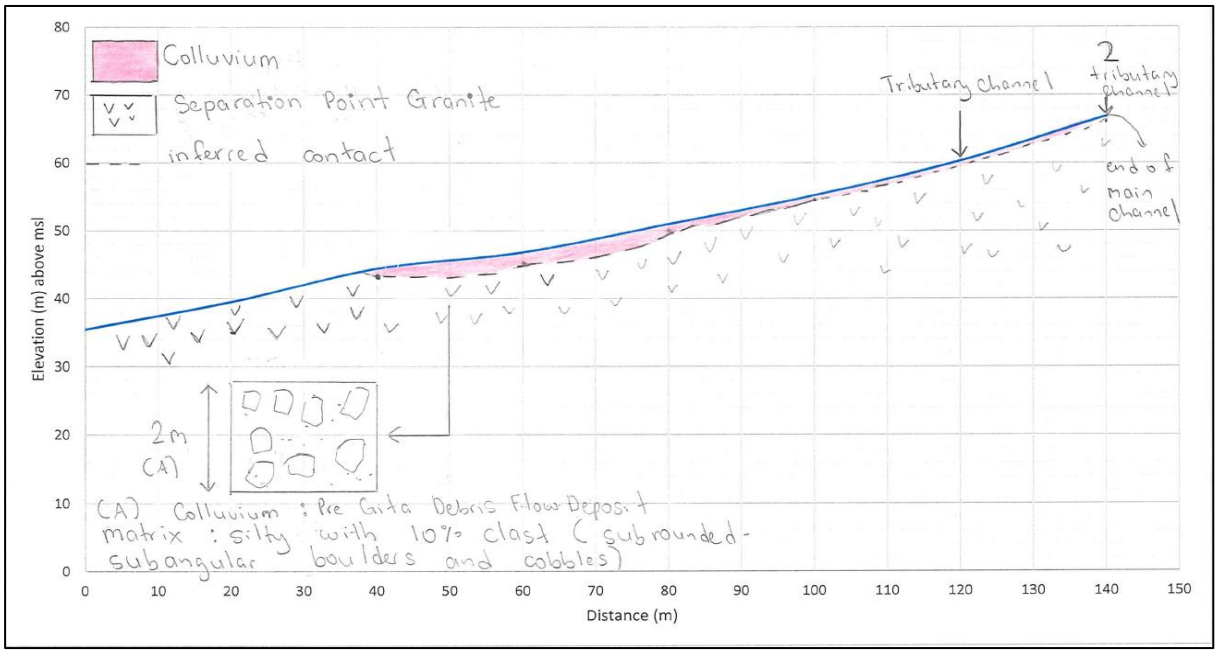

Channel 2 Profile

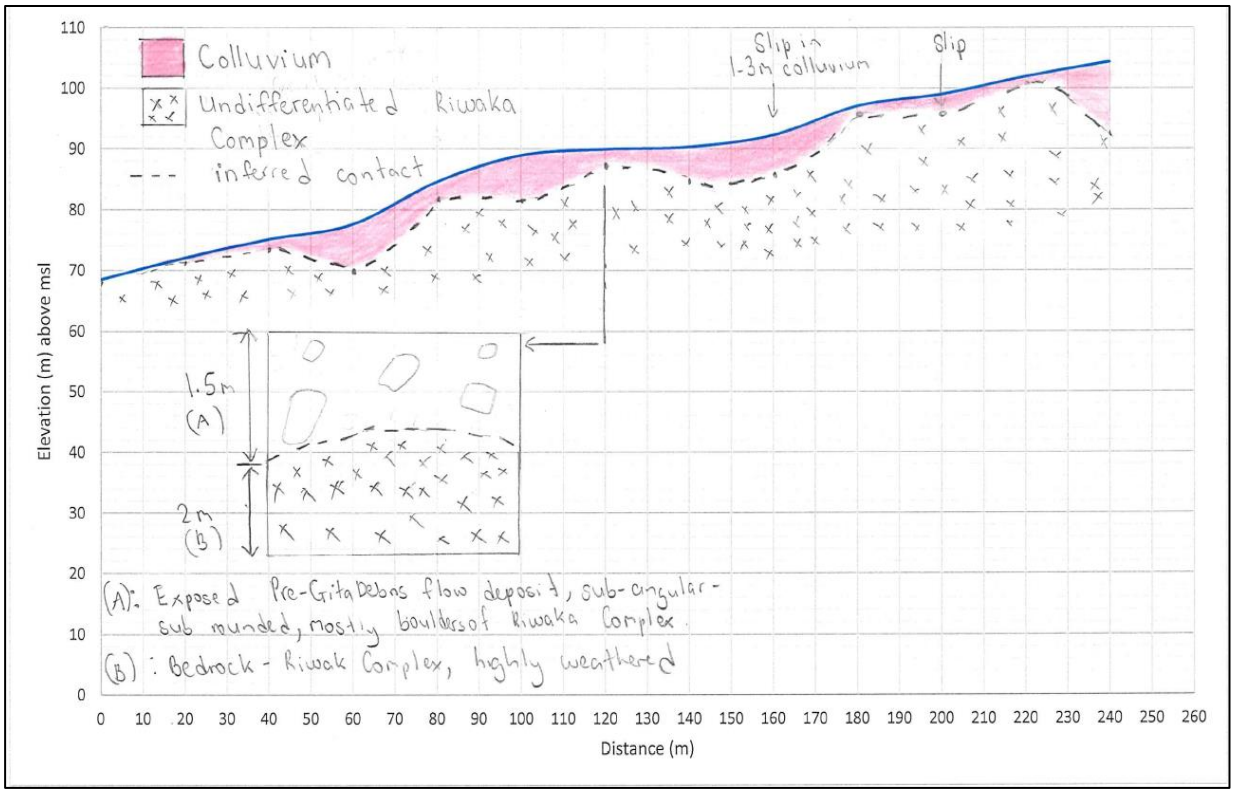

Channel 3 Profile

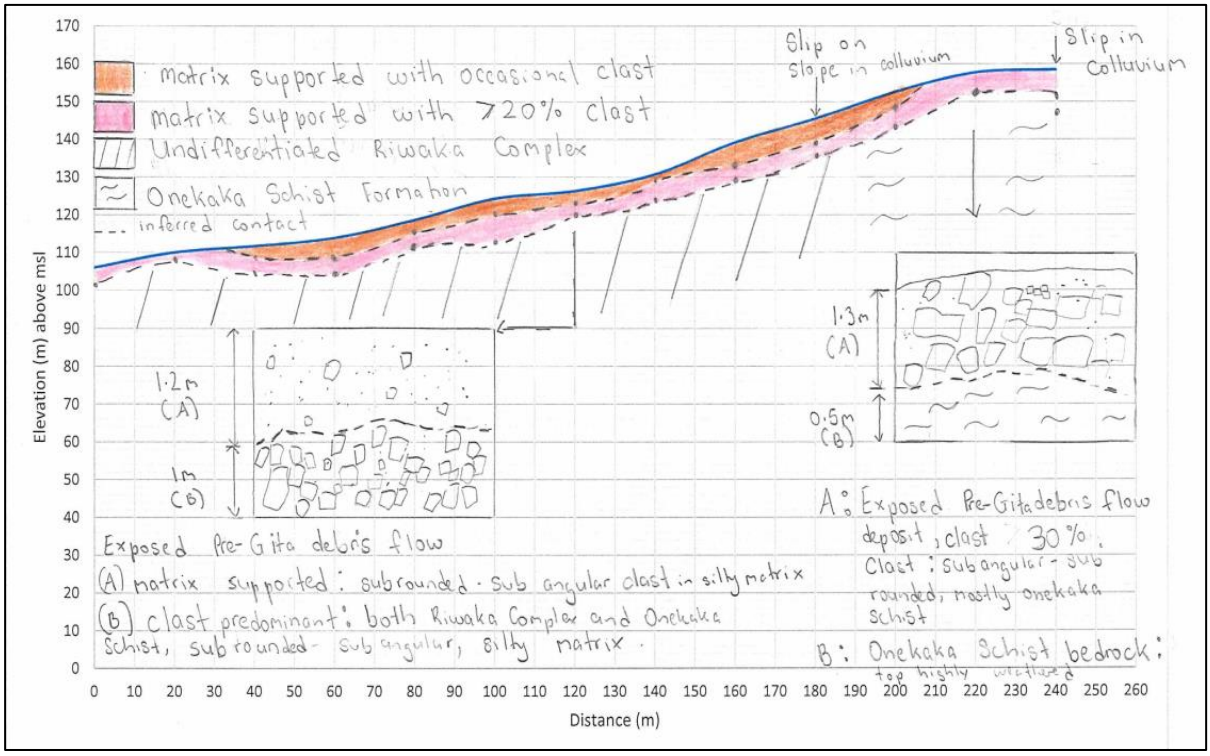

During field survey, channel depth, width and height were measured. The full length of main channel 1 and 2 was not surveyed due to accessibility. The total length was measured from aerial image (the active debris flow path length, Figure 3.1) and depth and width averaged from field measurement. The resulting analysis is an index measure of volume of channels. Assumptions made limit the average accuracy of these volumes, and they should be regarded as approximate only.

Table A.1.2: Ex-tropical cyclone Gita related debris volume

Channel	Area (m^2)	Average Thickness	Volume (m^3)
1	3200	2	6400
2	3300	4	13000
3	4800	3	14000

Appendix A.2 Outcrop Face Logging and Sample Locations

The field observations and interpretations are shown in this section. The sample collection locations for laboratory testing as well as *in-situ* test locations are shown with respect to outcrop exposure.

Table A.2.1: Field Mapping and sample locations

Sample number	Log number	Geomorphic setting	Latitude	Longitude
1		Riwaka-Kaiteriteri Road	-41.0502	173.010376
2		Riwaka-Sandy Bay Road	-41.025	172.979385
3	1	Channel 1	-41.0563	172.970688
4		Channel 1	-41.056	172.970459
5 and 6	2	Channel 1	-41.0565	172.970062
7	3	Channel 1	-41.0565	172.970001
8 and 9	4	Channel 2	-41.053	172.965836
10, 11, 12	5	Channel 2	-41.0534	172.964386
13, 14 and 15	6	Channel 3	-41.0493	172.96257
16 and 17	7	Channel 3	-41.0506	172.961823
18		Adjacent to Channel 3	-41.0506	172.963516
19		Adjacent to channel 2	-41.3135	172.574905

Note: SPG= Separation Point Granite

URIC= Undifferentiated Riwaka Igneous Complex

OS= Onekaka Schist

Road cut

Figure A.2.1: Riwaka –Kaiteriteri Road. Highly weathered, white with iron staining, porphyritic, SPG. Silty SAND, with some gravel and trace clay, moist, no plasticity, well graded. Gravel: sub angular to angular quartz and feldspar. Sample 1 –highly weathered SPG collected both as tube and bulk sample.

Figure A.2.2: Riwaka –Sandy Bay road. Shallow Soil slide. Failure in colluvial soil derived from SPG. The soil is described as silty clay with some gravel, orange brown, firm, moist, low plasticity. Gravel: angular to sub-angular, unweathered to moderately weathered granite gravel. Sample number 2. Both tube and bulk sample were collected.

Channel 1

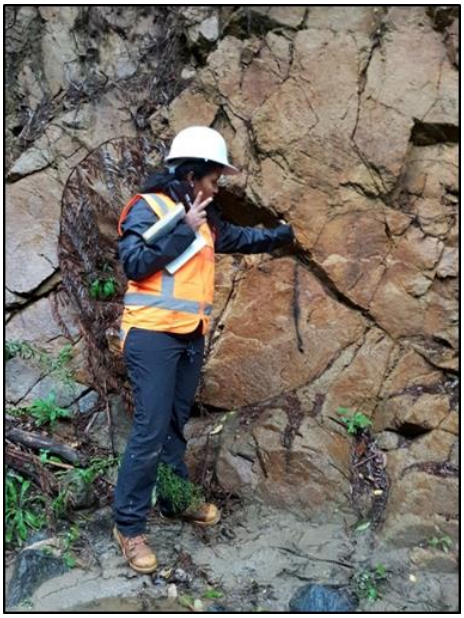

Figure A.2.3: SPG outcrop at the end of channel 1. Moderately weathered, white with iron staining, jointed, SPG, moderately strong to weak, moderately to closely spaced joint set, clay infilling along joints. Sample collected for point load test and thin section. Schmidt hammer test was also conducted.

Figure A.2.4: end of channel 1. Two steep tributary drainage scouring the underlying bedrock.

Figure A.2.5: Completely weathered granite (silty sand with minor gravel) supplying sediment to the channel. The inset picture shows enlarged picture of the weathered bedrock.

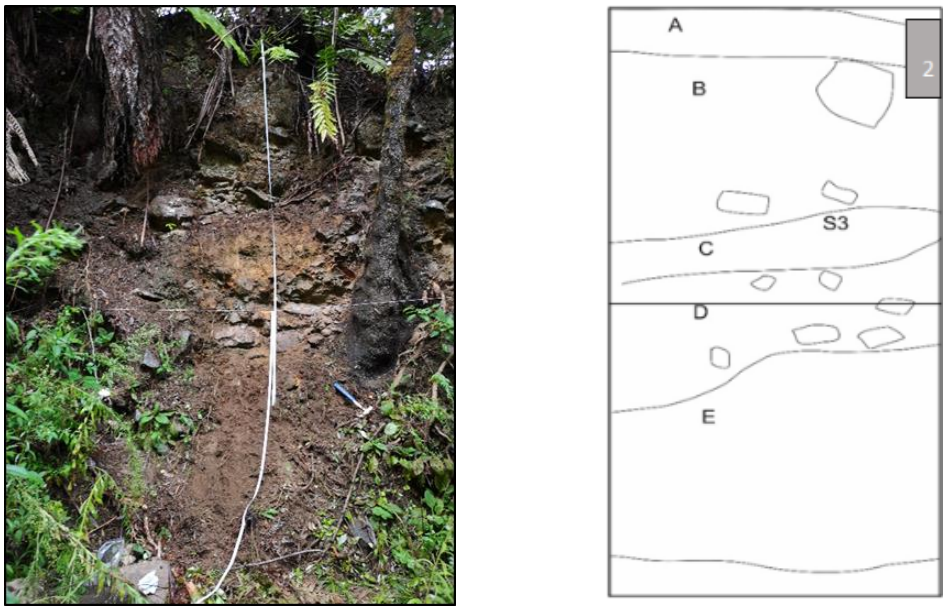

Figure A .2.6: Log 1-Pre-2018 debris flow deposit. 1 is without interpretation and 2 is with interpretation. (A) matrix supported (B) clast supported deposit, clast is angular to sub angular, random orientation (C) matrix supported –sandy silty, brown, moist, low plasticity and poorly graded. Bulk Sample collected (S3). (D) Clast supported, sub angular to sub rounded cobbles and boulders up to 50cm.

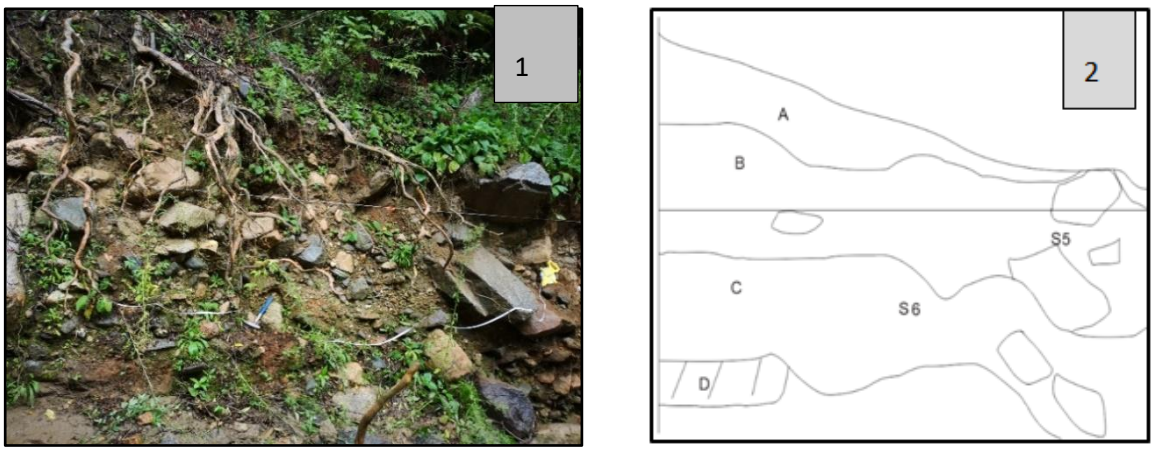

Figure A.2.7: Log 2- Pre-2018 debris flow deposit above weathered SPG. 1 is without interpretation and 2 is with interpretation. The weathered granodiorite (D) is overlain by at least 3 different debris flow activity recognized (A-C). (A) Clayey Silt with some gravel. (B) 15% clast (cobbles and boulders). Matrix: sandy with some fine gravel, dark orange brown, moist, no plasticity. Clast: up to 1m diameter, felsic and mafic igneous rock. Sub rounded to sub angular granite and diorite. (C) 20% clast (cobbles and boulders) Matrix: sandy Gravel, dark brown, moist, no plasticity. Bulk sample collected: S5 and S6.

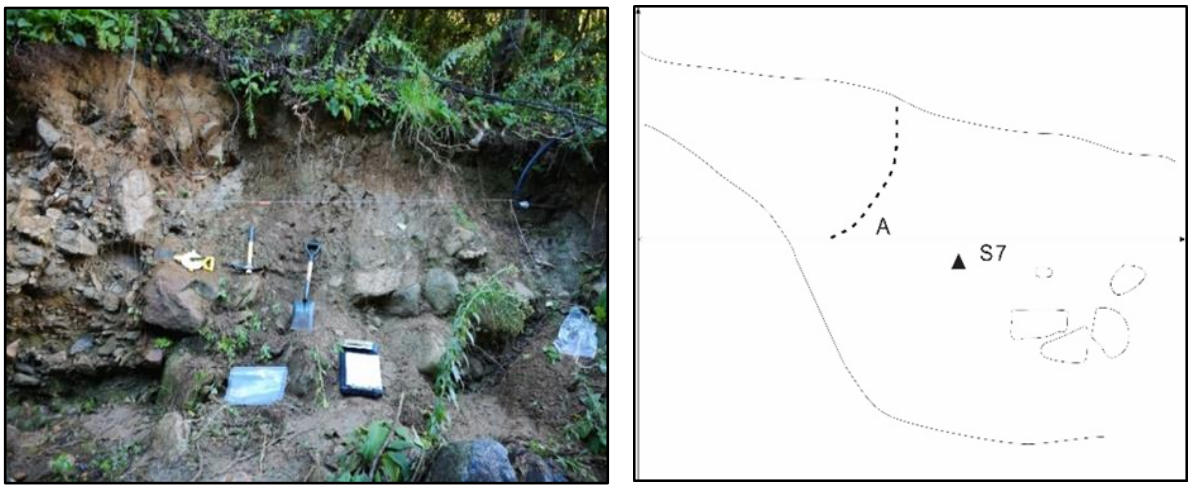

Figure A.2.8: Log 3-Pre-2018 debris flow deposit (A) 5% clast (boulders and cobbles). Matrix: clayey silt with some gravel, firm, moist, medium plasticity. Clast: sub rounded, unweathered to slightly weathered diorite and granite. Tube and bulk sample collected: S7. Shear vane measurement taken.

Channel 2

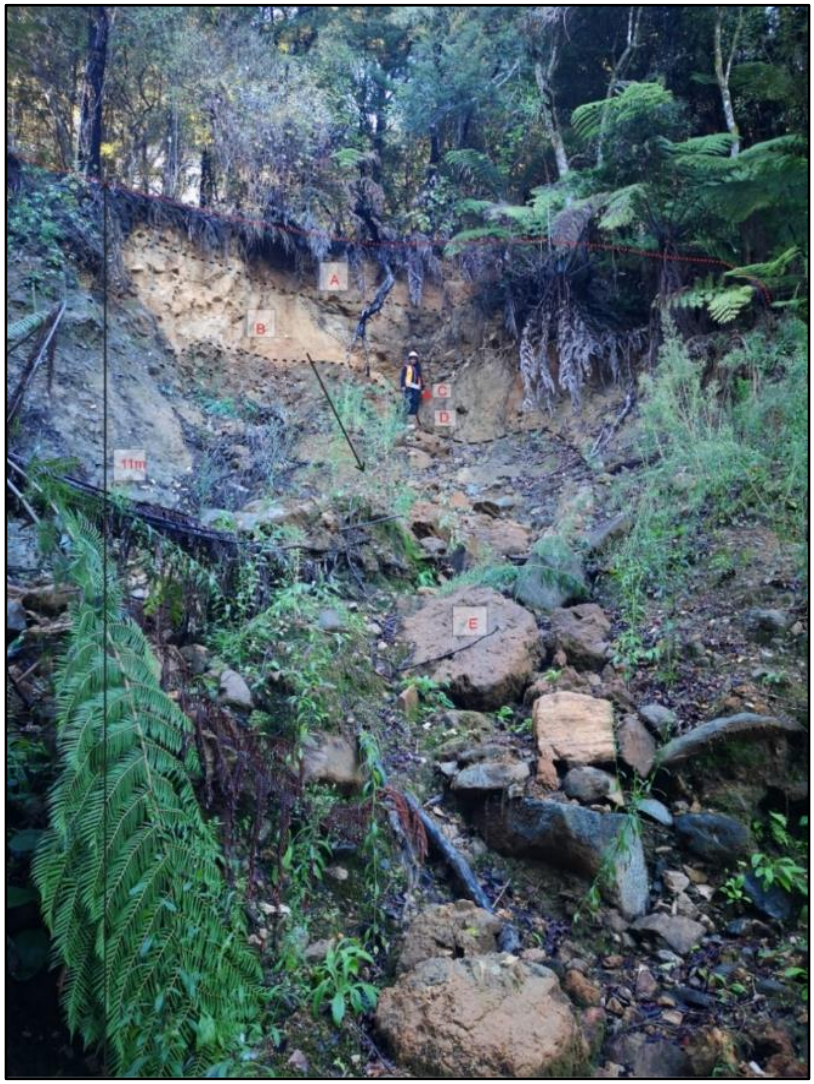

Figure A.2.9: Log 4-Soil slide in approximately 5 m thick colluvium (A and B) located in Channel 2. Failure is translational on a slip plane subparallel to the ground surface at the contact with completely weathered bedrock to residual soil(C) and highly weathered bedrock (D). The failed material has fallen into the active drainage channel (E). Shear vane measurements taken on completely weathered bedrock to residual soil. The colluvium was too hard to drive the vane in. The sample locations are numbered. The colluvium (A) is described as silty clayey with minor coarse gravel, orange, soft, moist, medium plasticity. (B) 2% boulders and cobbles. Matrix: sandy clayey Silt with minor fine gravel, orange brown, loose, dry. Too hard to drive shear vane. Bulk sample and tube sample collected with difficulty, S8. (C) Weathered bedrock: completely weathered to residual soil, brown orange with black and white specks (minerals), URIC. Silty SAND with some gravel and trace clay, moist, low plasticity. Bulk and tube sample collected, S9.

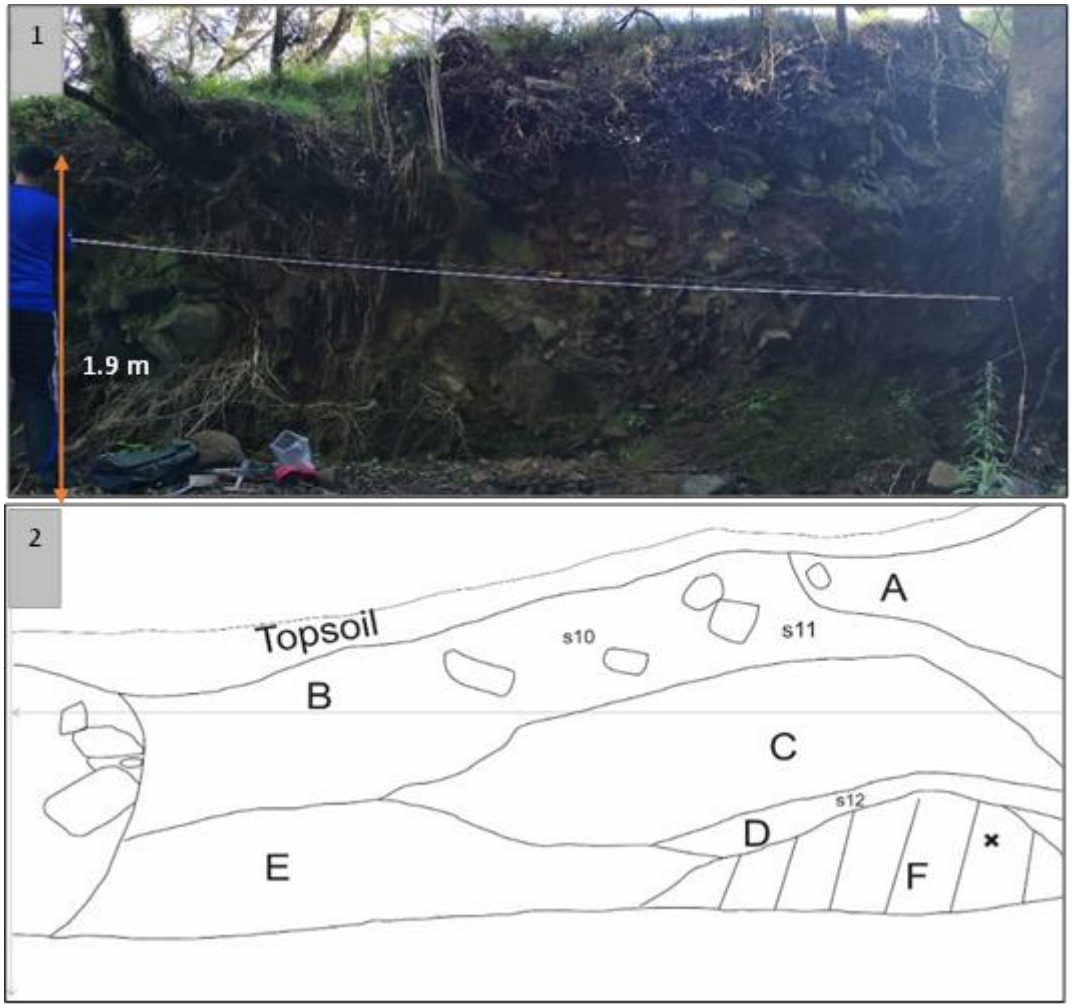

Figure A.2.10: Log 5- Pre 2018 debris flow deposit-1 is without interpretation and 2 is with interpretation. At least 4 debris flow events (A-D) has been identified above weathered bedrock (F). (A) 50 % boulders of felsic and mafic igneous rock, sub rounded to sub angular, unweathered to slight weathered in a sandy matrix. (B) 7% boulders and cobbles of mafic and felsic igneous rock sub angular to sub rounded. Matrix supported: silty Sand with minor gravel, moist, no plasticity, very stiff. Bulk sample 11 and 12 collected. (C) 30% to 40 % boulders and cobbles, mostly mafic rock with some quartzite, sub angular to sub rounded, unweathered to slightly weathered in sandy matrix. D) Stratified gravelly debris flow deposit in a sandy silty matrix. Gravels: unweathered to moderately gravels of mafic and quartzite rocks. Bulk sample collected, S12. (E): 30% boulder and cobbles, sub rounded to sub angular igneous rock, mostly gabbro in a sandy matrix.

Channel 3

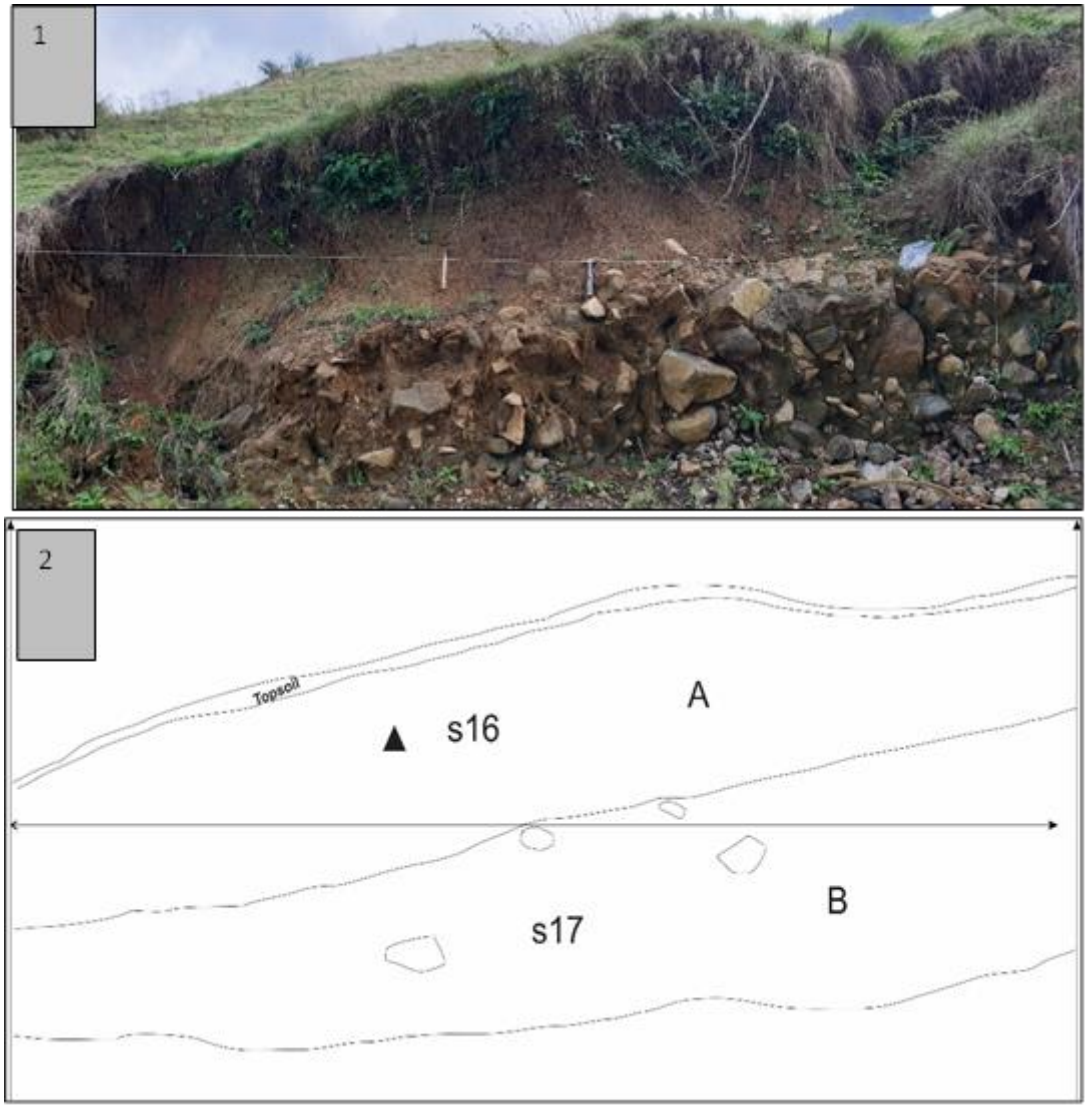

Figure A.2.11: Log-7 Pre -2018 debris flowdeposit-1 is without interpretation and 2 is with interpretation. (A) Clayey Silt with some sand and trace gravel, soft, moist, high plasticity. Bulk and tube sample collected, S16. Shear vane test performed (B) 30% to 40% boulder and cobbles of sub rounded diorite, and sub angular Onekaka schist. Matrix: silty with some gravel and minor clay, moist, low plasticity. Bulk sample collected, S17.

Figure A.2.12: Log -6 .2018 Shallow soil slide in approximately 1m thick colluvium located in Channel 3. Failure is translational on an undulating surface. The contact between Onekaka schist (OS) and Undifferentiated Riwaka Igneous Complex (URIC) is seen. The colluvium (S13) consist of 12% cobbles. Matrix silty clay, dark brown, soft, moist, high plasticity. The Onekaka Schist (S14): completely weathered to residual soil, orange brown, silty CLAY with some gravel, moist, high plasticity. Gravel: angular, slightly weathered schist. The URIC (S15): completely weathered to residual soil, dark brown with some visible black minerals, clayey SILT, moist, low plasticity. Tube and bulk samples were collected for colluvium and both weathered bedrocks.

Figure A.2.13: Soil creep on slope next to channel 3.

Figure A.2.14: Reactivation of colluvium material. 7% cobbles clast mostly sub angular Onekaka schist, and few URIC rocks. Matrix silty gravelly sand with trace clay, orange brown, moist, low plasticity. P.S. Ignore the happiest field assistant.

Figure A.2.15: Surface deformation- Tunnel gully up to 1 m deep, next to channel 3.

Appendix A.3 Drone Survey

Channel 2 Drone Image

Figure A.3.1: Drone image captured above channel 2. No new slides were identified. Image taken on August 2019

Channel 1

Figure A.3: Drone image captured above Channel 1. No new slides were identified. Image taken on August 2019.

Appendix B: Soil Laboratory Testing

Appendix B.1 Particle Size Distribution

Introduction

The samples were tested in accordance to NZ 4402 1986. All samples were wet sieved to ensure that coarser particles are free from finer particles. The silt and clay (fines) were further tested using hydrometer and pipette method. The hydrometer method required specific gravity of silt and clay only. The procedure to determine specific gravity is discussed in the next section. Both hydrometer and pipette testing required addition of Calgon (sodium hexametaphosphate at 9% by weight) to disperse the grains. A correction factor was applied as Calgon has a slightly higher unit weight than water.

In addition, particle size analysis was also determined using a laser scanner (Micromeritics Saturn Digisizer II 520). Particles smaller than 2mm were used for this analysis.

Laser Sizer Method

The following are the steps followed at University of Canterbury laboratory

- A small amount of sample ("pea size") is stirred in beaker of Calgon (Sodium hexametaphosphate) 50g/L on magnetic stirrer so all particles are in suspension.
- A representative sample is extracted using disposable pipette
- Sample deposited in liquid sampling handler until desired obscuration achieved (14%)
- Diffraction-only Fraunhofer theory was used as refractive index of the sample was not determined (University of Canterbury Geology Department, n.d.).

Sieve and Pipette method

The PSD using pipette followed method outlined by (Lewis & McConchie, 1994) in accordance with NZS4402: 1986. The pipette method determines size of silt and clay particles. According to the standards, a representative sample of material needs to be obtained, which is then carefully "wet sieved" using 0.063mm sieve to remove coarser fractions (sand and gravel). The separated sand and gravel is then oven dried followed by "dry sieving" in accordance to NZGS4402: 1986, Test 2.8.2.

The silt and clay passing the 0.063mm sieve is transferred to a 1L-measuring cylinder and topped with water and calgon to make the volume up to 1000ml. At a specified time and depths, a specific volume is extracted from suspension and the weight of each dried subsamples is representative of the

proportion of the total silt and clay (Lewis & McConchie, 1994). The sample was extracted at a time interval of 20sec, 2min, 4 min, 8min, 15 min, 30min, 2 hrs and 8 hrs. For full method refer to (Lewis & McConchie, 1994) “Analytical Sedimentology” pages 103 – 109.

Sieve and Hydrometer method

The PSD using hydrometer was conducted in accordance with NZ4402:1986, Test 2.8.4. This method also determines fraction of silt and clay. According to the standards, a representative sample of material needs to be obtained, which is then carefully “wet sieved” using 0.063mm sieve to remove coarser fractions (sand and gravel). The separated sand and gravel is then oven dried followed by “dry sieving” according to NZGS4402: 1986, Test 2.8.2.

The soil passing through the 0.063m sieve is poured into a 1L-measuring cyclinder and topped with water to make the volume up to 1000ml. Calgon was added to the solution during preparation. This solution will have a unit weight higher than that of water resulting in a higher hydrometer reading. A blank solution using water and calgon was prepared and hydrometer reading taken and was used in the calculation for correction factor.

Results

The results for each sample is presented below:

Sample 1: Highly weathered Separation Point Granite

Test method: wet sieve, hydrometer and dry sieve results

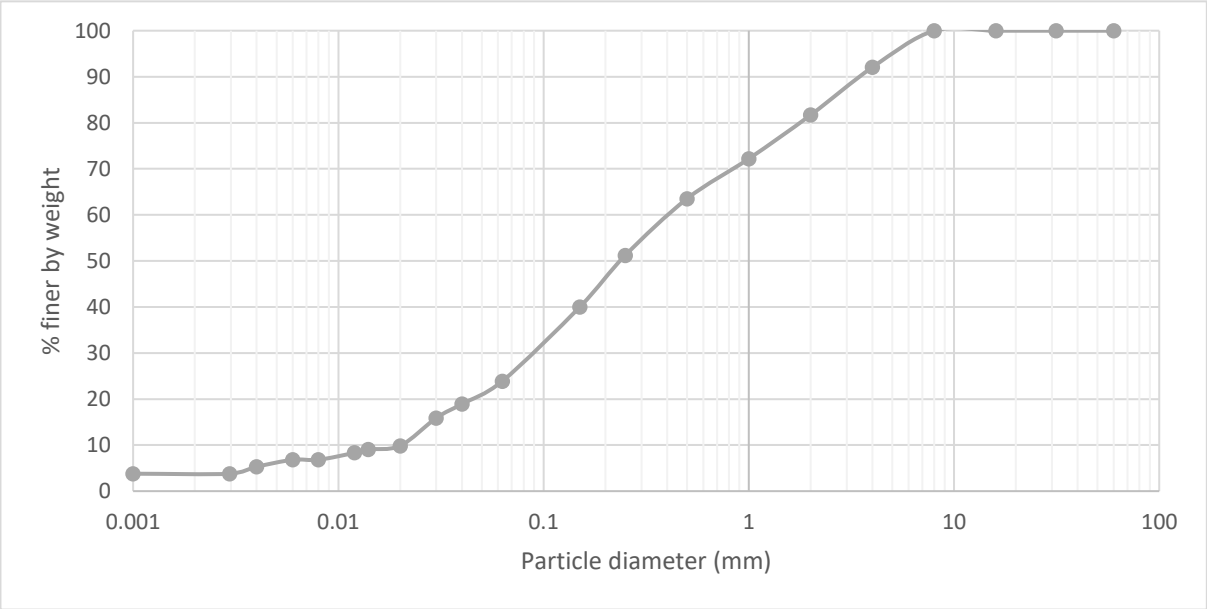

Test Sieve (mm)	% finer by weight
60	100
31.5	100
16	100
8	100
4	92
2	82
1	72
0.5	64
0.25	51
0.15	40
0.063	24
0.04	19
0.03	16
0.02	10
0.014	9
0.012	8
0.008	7
0.006	7
0.004	5
0.003	4
0.001	4

Sample 2: 2018 (Gita) Colluvial soil_ Separation Point Granite

Test method: wet sieve, hydrometer and dry sieve results

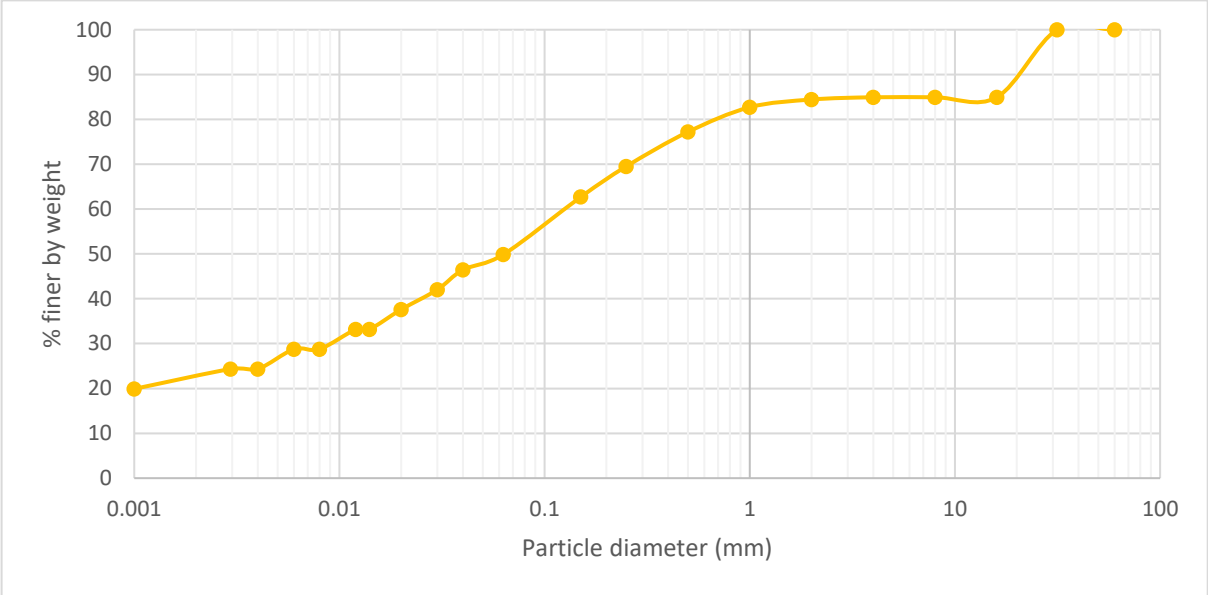

Test Sieve (mm)	% finer by weight
60	100
31.5	100
16	85
8	85
4	85
2	84
1	83
0.5	77
0.25	70
0.15	63
0.063	50
0.04	46
0.03	42
0.02	38
0.014	33
0.012	33
0.008	29
0.006	29
0.004	24
0.003	24
0.001	20

Sample 3: Pre-2018 debris flow deposit

Test method: wet sieve, hydrometer and dry sieve results

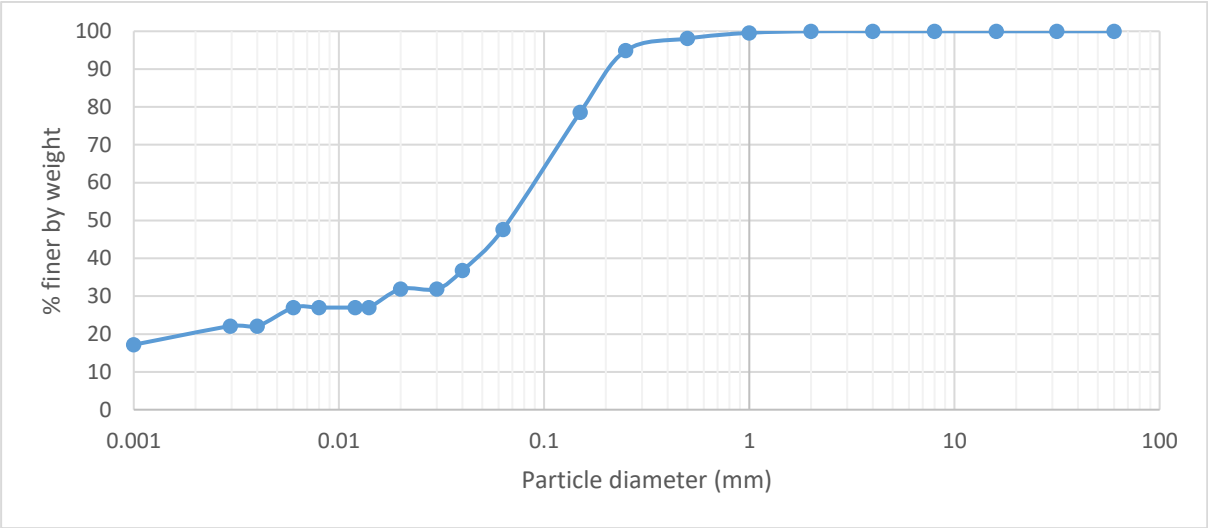

Test Sieve (mm)	% finer by weight
60	100
31.5	100
16	100
8	100
4	100
2	100
1	100
0.5	98
0.25	95
0.15	79
0.063	48
0.04	37
0.03	32
0.02	32
0.014	27
0.012	27
0.008	27
0.006	27
0.004	22
0.003	22
0.001	17

Sample 4: Completely weathered to residual soil Separation Point Granite

Test method: wet sieve, hydrometer and dry sieve results

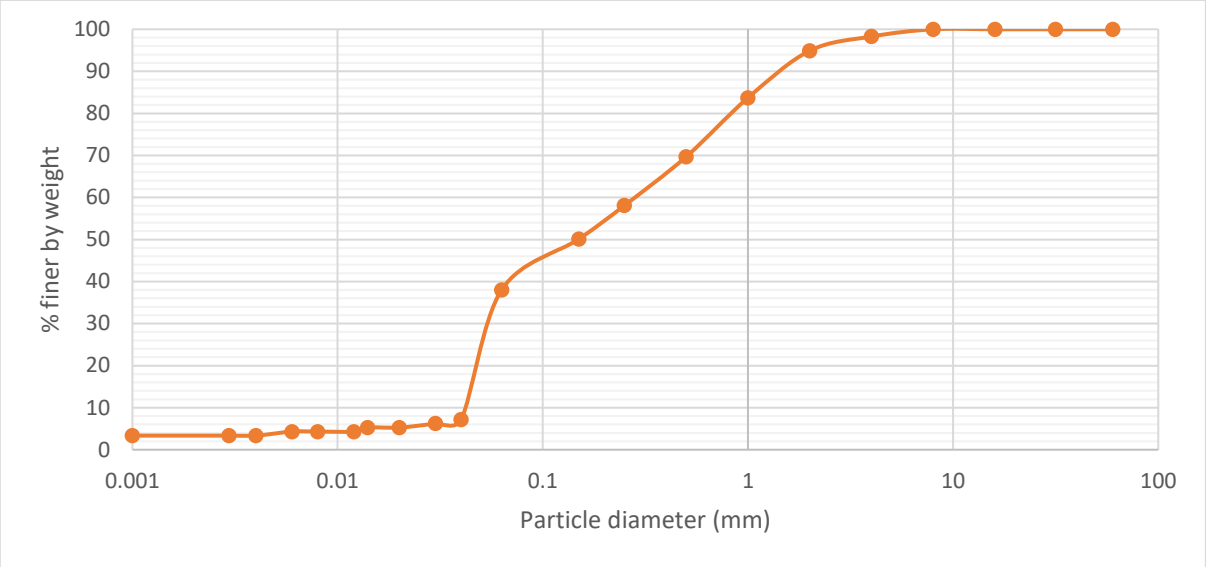

Test Sieve (mm)	% finer by weight
60	100
31.5	100
16	100
8	100
4	98
2	95
1	84
0.5	70
0.25	58
0.15	50
0.063	38
0.04	7
0.03	6
0.02	5
0.014	5
0.012	4
0.008	4
0.006	4
0.004	3
0.003	3
0.001	3

Sample 5: Pre-2018 debris flow deposit

Test method: wet sieve, hydrometer and dry sieve results

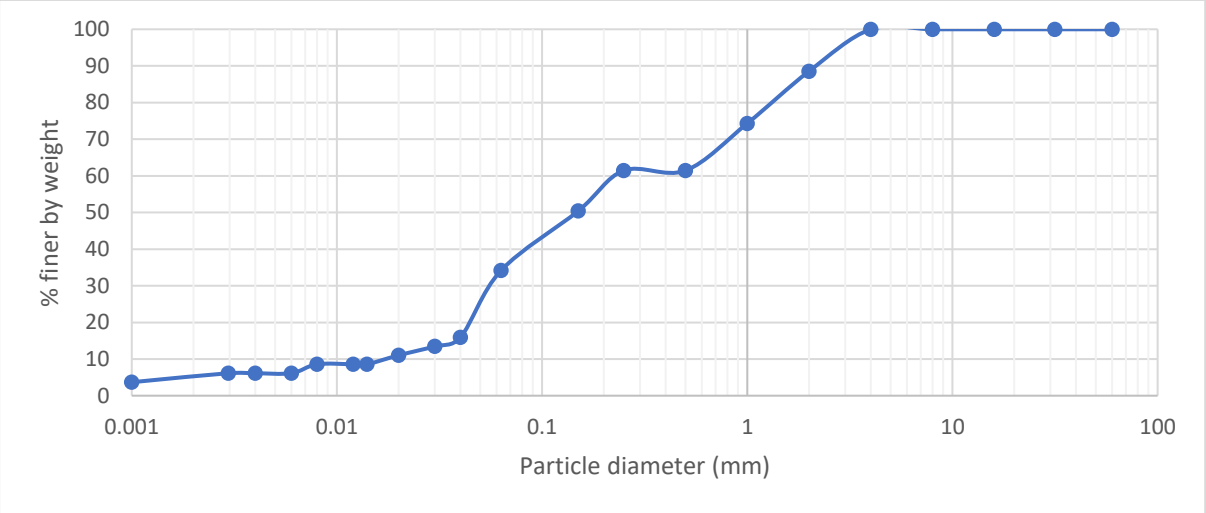

Test Sieve (mm)	% finer by weight
60	100
31.5	100
16	100
8	100
4	100
2	89
1	74
0.5	61
0.25	61
0.15	50
0.063	34
0.04	16
0.03	13
0.02	11
0.014	9
0.012	9
0.008	9
0.006	6
0.004	6
0.003	6
0.001	4

Sample 6: Pre-2018 debris flow deposit

Test method: wet sieve, pipette and dry sieve result

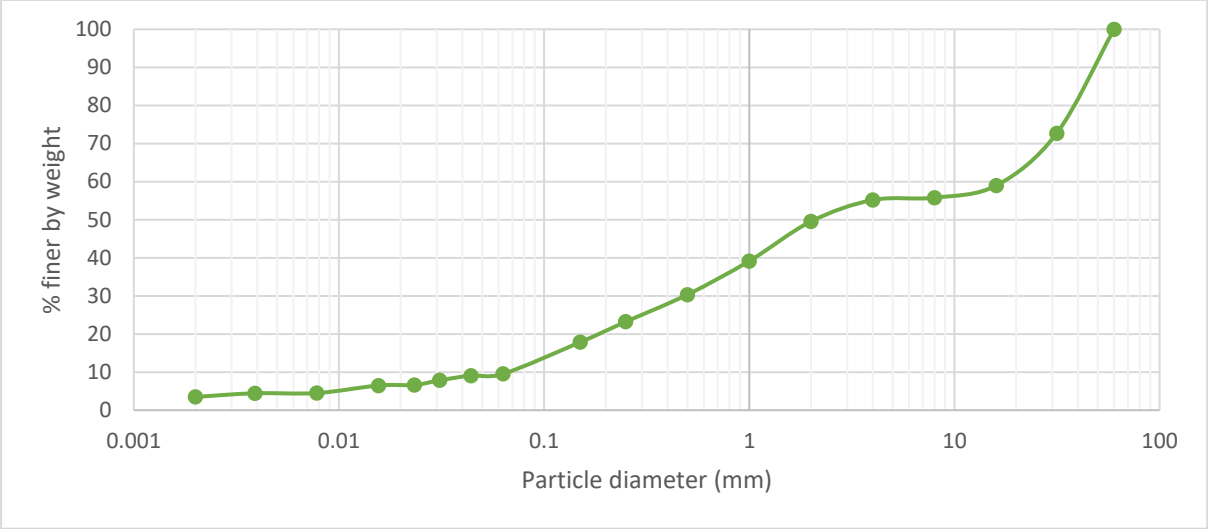

Test Sieve (mm)	% finer by weight
60	100
31.5	73
16	59
8	56
4	55
2	50
1	39
0.5	30
0.25	23
0.15	18
0.063	10
0.04	9
0.03	8
0.02	7
0.016	6
0.008	5
0.004	4
0.002	3

Sample 7: Pre-2018 debris flow deposit
Test method: wet sieve, hydrometer and dry sieve results

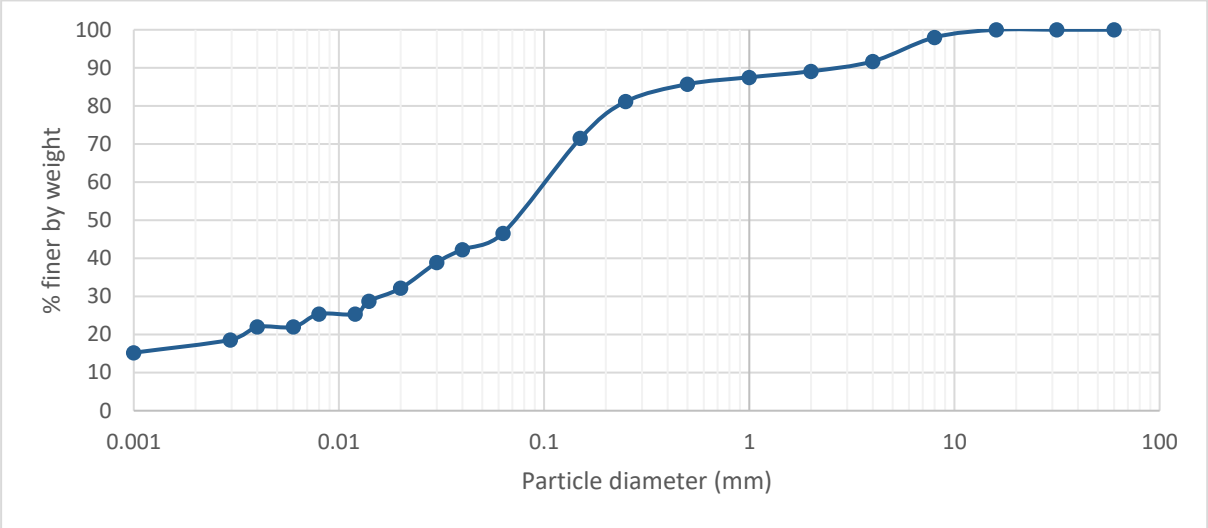

Test Sieve (mm)	% finer by weight
60	100
31.5	100
16	100
8	98
4	92
2	89
1	88
0.5	86
0.25	81
0.15	71
0.063	47
0.04	42
0.03	39
0.02	32
0.014	29
0.012	25
0.008	25
0.006	22
0.004	22
0.003	19
0.001	15

Sample 8: 2018 debris flow source area

Test method: wet sieve, hydrometer and dry sieve results

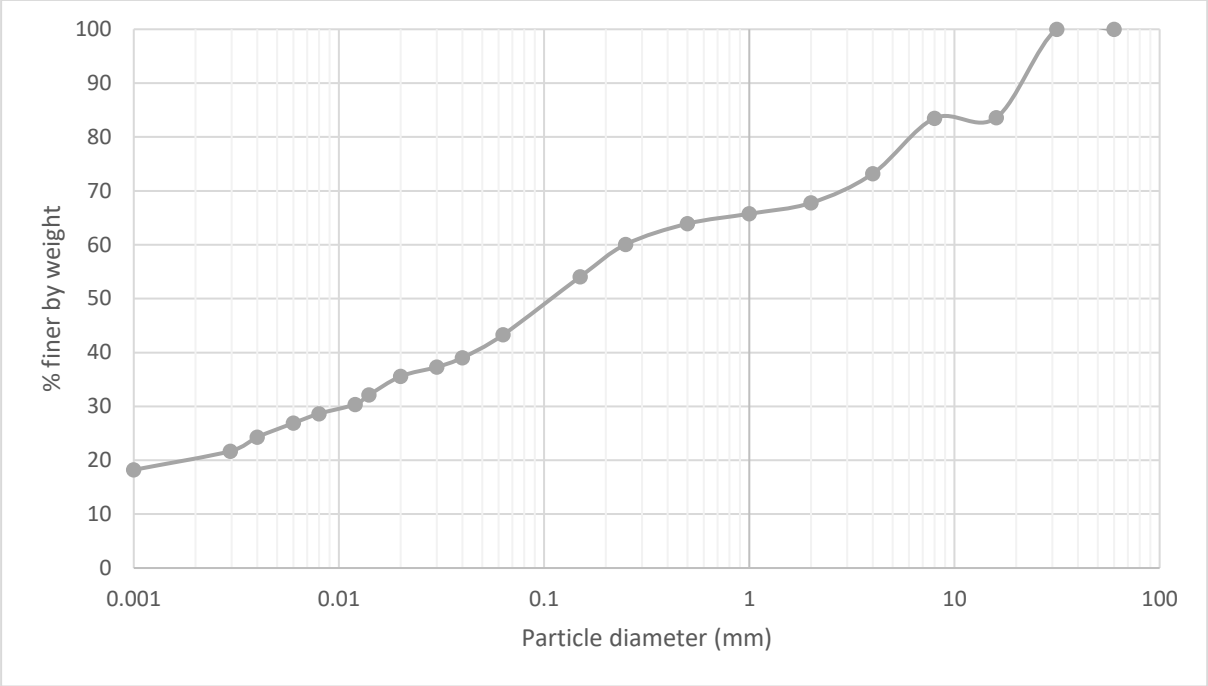

Test Sieve (mm)	% finer by weight
60	100
31.5	100
16	84
8	84
4	73
2	68
1	66
0.5	64
0.25	60
0.15	54
0.063	43
0.04	39
0.03	37
0.02	36
0.014	32
0.012	30
0.008	29
0.006	27
0.004	24
0.003	22
0.001	18

Sample 9: Completely weathered to residual soil (Undifferentiated Riwaka Igneous Complex)

Test method: wet sieve, hydrometer and dry sieve results

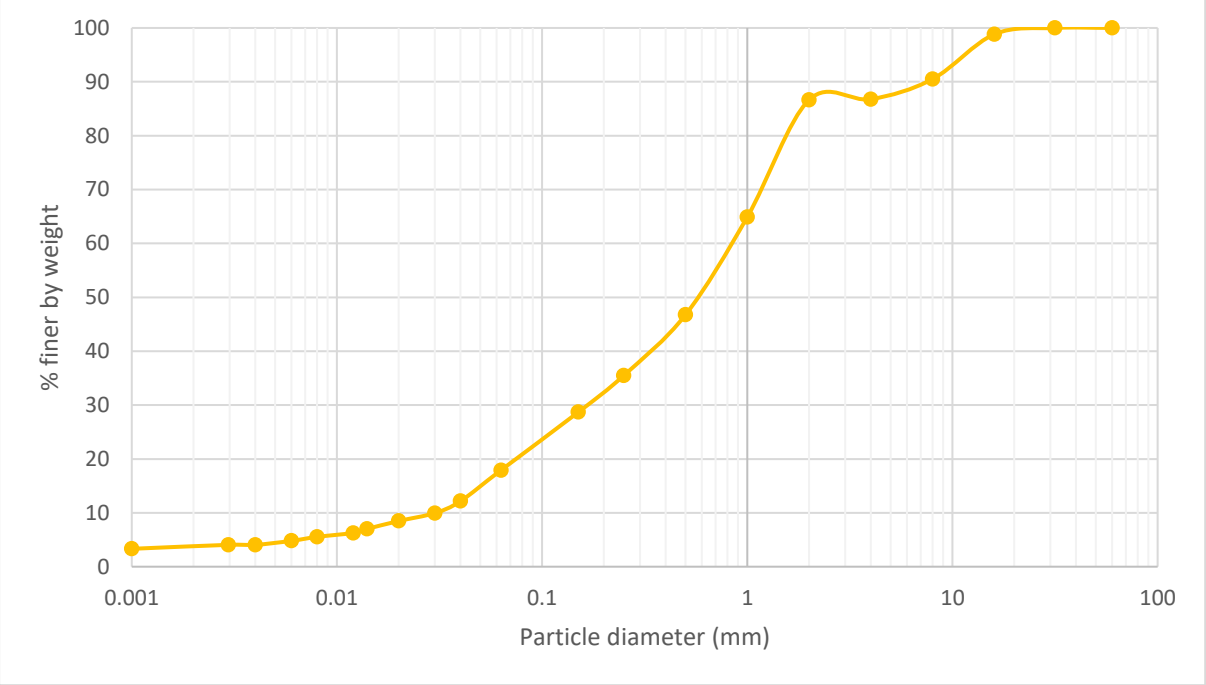

Test Sieve (mm)	% finer by weight
60	100
31.5	100
16	99
8	91
4	87
2	87
1	65
0.5	47
0.25	35
0.15	29
0.063	18
0.04	12
0.03	10
0.02	8
0.014	7
0.012	6
0.008	6
0.006	5
0.004	4
0.003	4
0.001	3

Sample 10: Pre-2018 debris flow deposit

Test method: wet sieve, hydrometer and dry sieve results

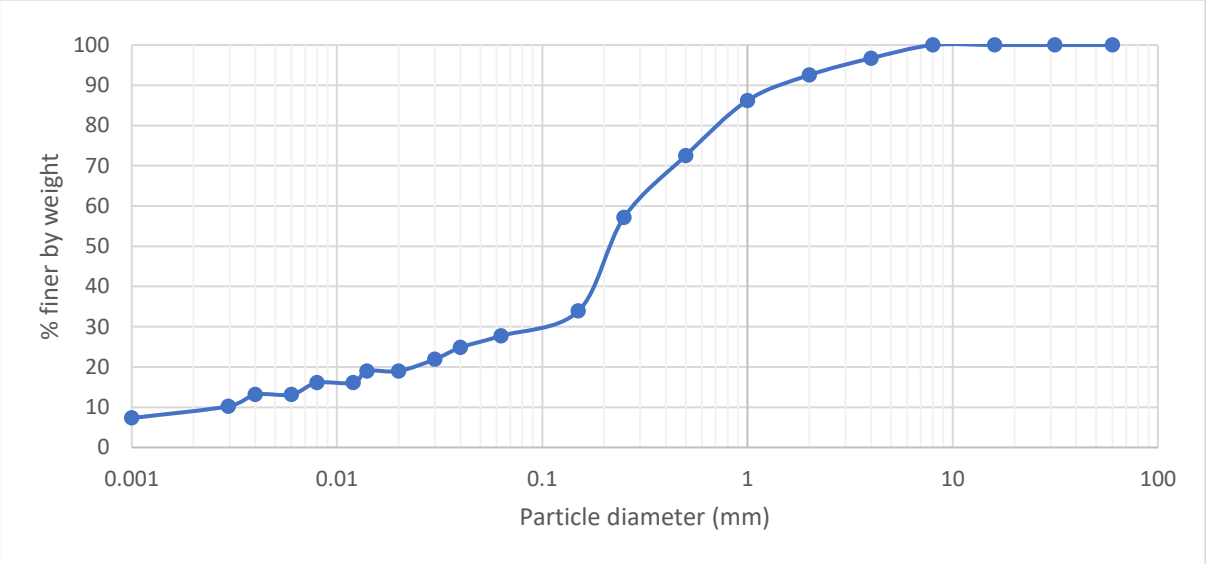

Test Sieve (mm)	% finer by weight
60	100
31.5	100
16	100
8	100
4	97
2	93
1	86
0.5	73
0.25	57
0.15	34
0.063	28
0.04	25
0.03	22
0.02	19
0.014	19
0.012	16
0.008	16
0.006	13
0.004	13
0.003	10
0.001	7

Sample 10: Pre-2018 debris flow deposit

Test method: wet sieve, pipette and dry sieve results

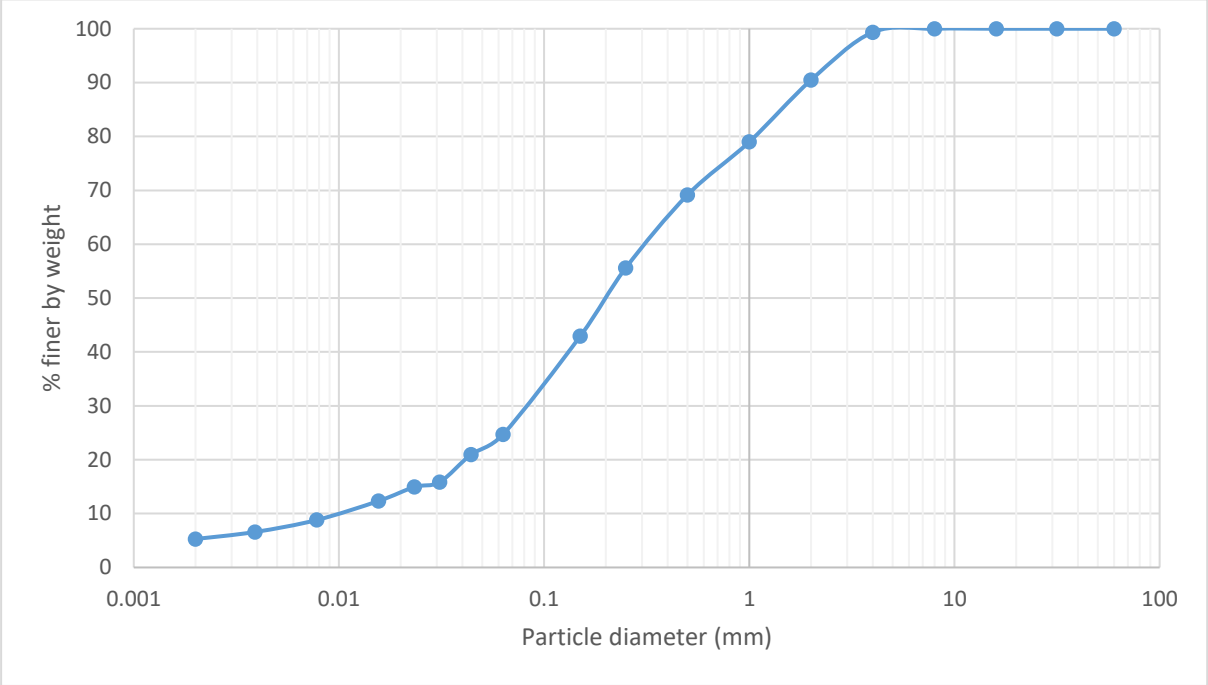

Test Sieve (mm)	% finer by weight
60	100
31.5	100
16	100
8	100
4	99
2	90
1	79
0.5	69
0.25	56
0.15	43
0.063	25
0.044	21
0.031	16
0.0233	15
0.0156	12
0.0078	9
0.0039	7
0.002	5

Sample 11: Pre-2018 debris flow deposit

Test method: wet sieve, hydrometer and dry sieve results

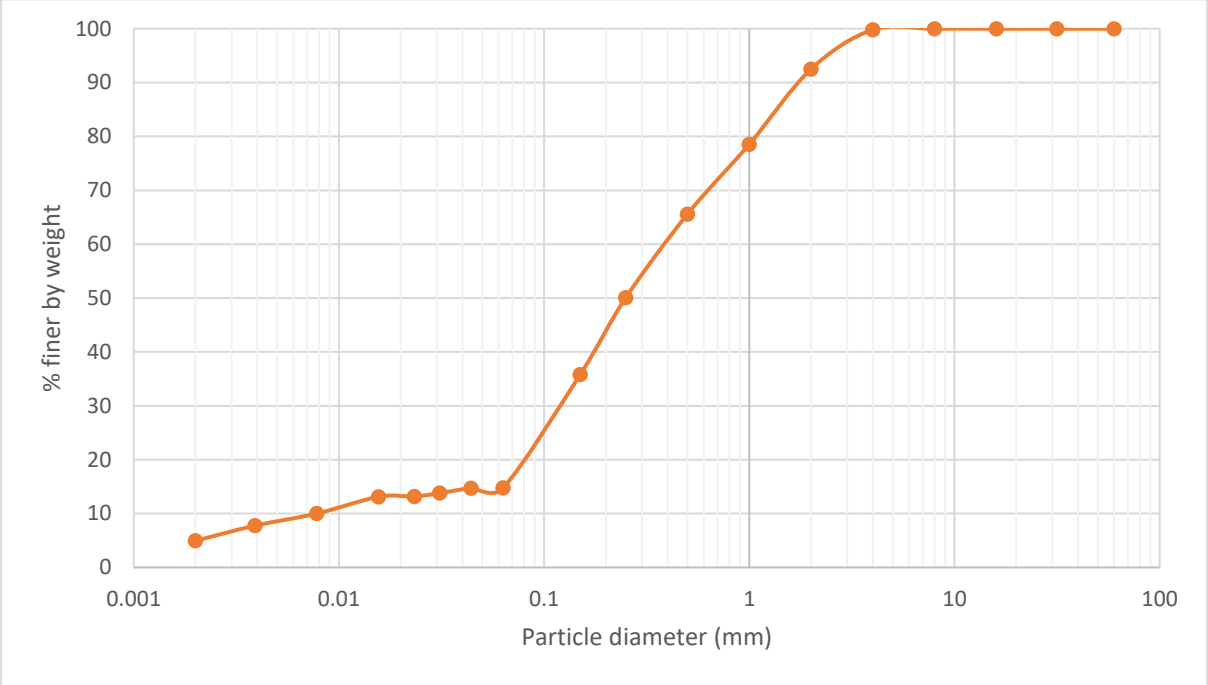

Test Sieve (mm)	% finer by weight
60	100
31.5	100
16	100
8	100
4	100
2	93
1	79
0.5	66
0.25	50
0.15	36
0.063	15
0.044	15
0.031	14
0.0233	13
0.0156	13
0.0078	10
0.0039	8
0.002	5

Sample 13: 2018 debris flow source area

Test method: wet sieve, hydrometer and dry sieve results

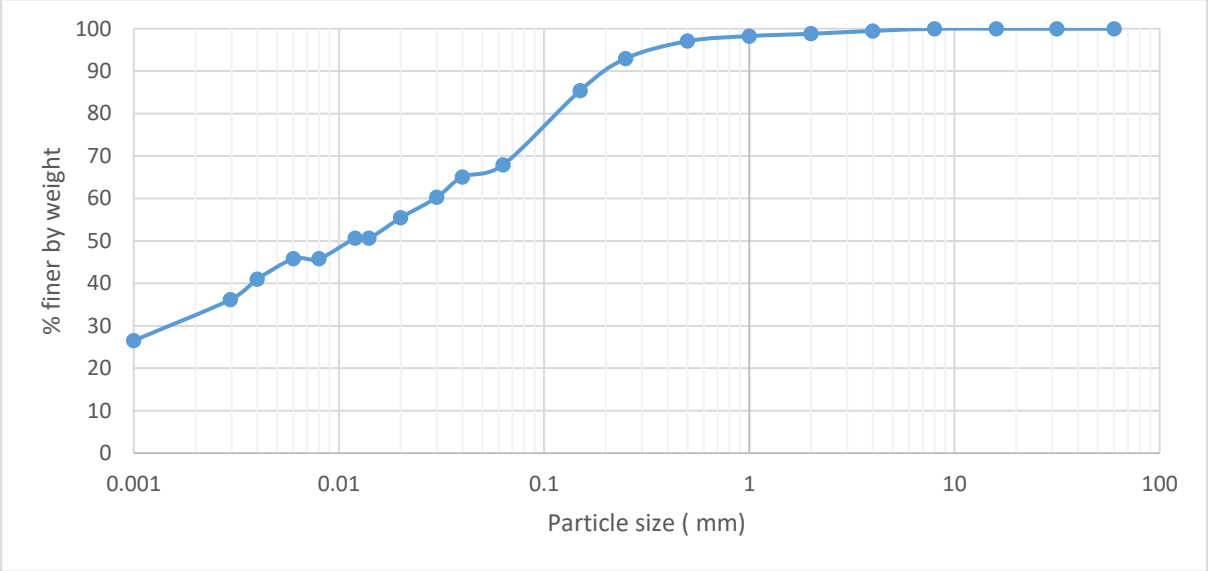

Test Sieve (mm)	% finer by weight
60	100
31.5	100
16	100
8	100
4	99
2	99
1	98
0.5	97
0.25	93
0.15	85
0.063	68
0.04	65
0.03	60
0.02	55
0.014	51
0.012	51
0.008	46
0.006	46
0.004	41
0.003	36
0.001	27

Sample 14: Completely weathered to residual soil Onekaka schist

Test method: wet sieve, hydrometer and dry sieve results

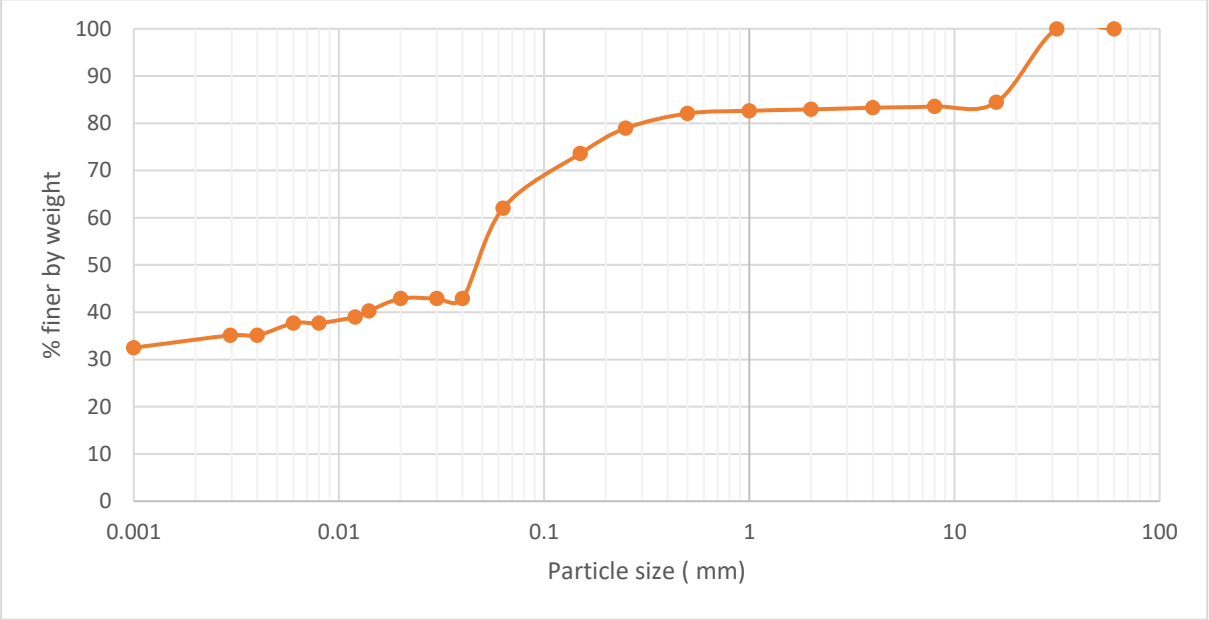

Test Sieve (mm)	% finer by weight
60	100
31.5	100
16	84
8	84
4	83
2	83
1	83
0.5	82
0.25	79
0.15	74
0.063	62
0.04	43
0.03	43
0.02	43
0.014	40
0.012	39
0.008	38
0.006	38
0.004	35
0.003	35
0.001	32

Sample 15: Completely weathered to residual soil Undifferentiated Riwaka Igneous Complex

Test method: wet sieve, hydrometer and dry sieve results

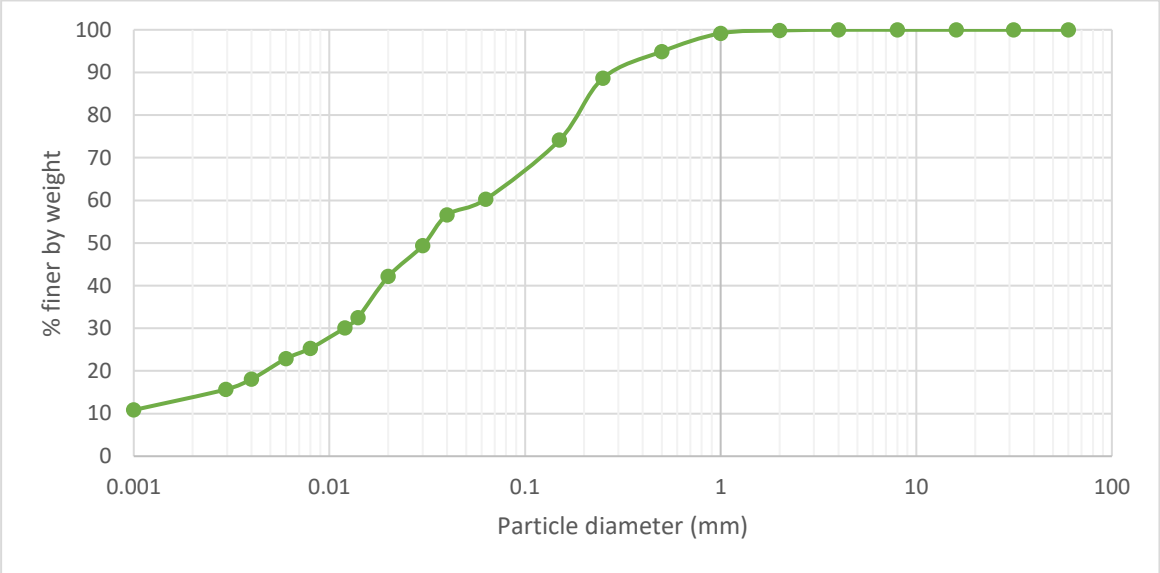

Test Sieve (mm)	% finer by weight
60	100
31.5	100
16	100
8	100
4	100
2	100
1	99
0.5	95
0.25	89
0.15	74
0.063	60
0.04	57
0.03	49
0.02	42
0.014	33
0.012	30
0.008	25
0.006	23
0.004	18
0.003	16
0.001	11

Sample 16: Pre-2018 debris flow deposit

Test method: wet sieve, hydrometer and dry sieve results

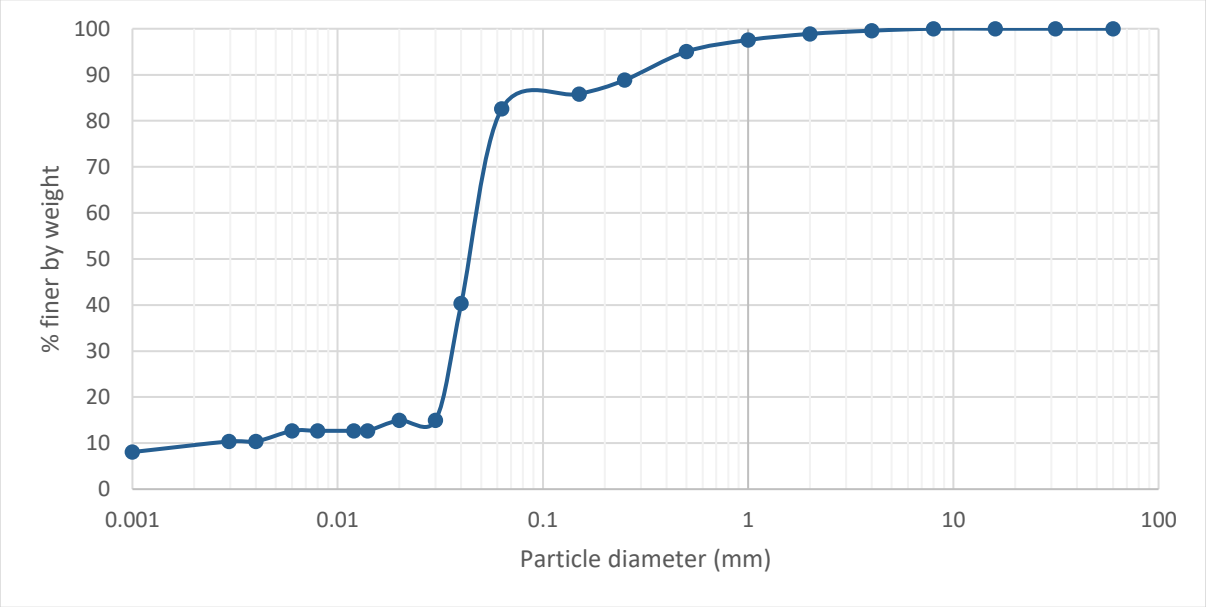

Test Sieve (mm)	% finer by weight
60	100
31.5	100
16	100
8	100
4	100
2	99
1	98
0.5	95
0.25	89
0.15	86
0.063	83
0.04	40
0.03	15
0.02	15
0.014	13
0.012	13
0.008	13
0.006	13
0.004	10
0.003	10
0.001	8

Sample 18: 2018 Reactivated Landslide

Test method: wet sieve, hydrometer and dry sieve results

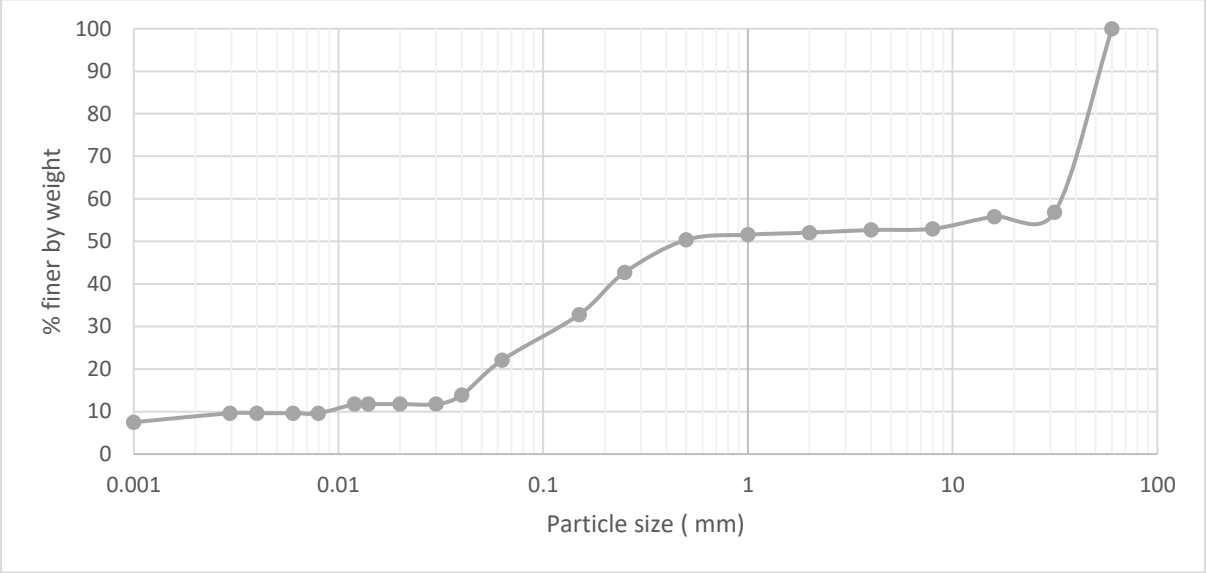

Test Sieve (mm)	% finer by weight
60	100
31.5	57
16	56
8	53
4	53
2	52
1	52
0.5	50
0.25	43
0.15	33
0.063	22
0.04	14
0.03	12
0.02	12
0.014	12
0.012	12
0.008	10
0.006	10
0.004	10
0.003	10
0.001	7

Sample 19: Fan deposit (Geophysical survery area)

Test method: wet sieve, hydrometer and dry sieve results

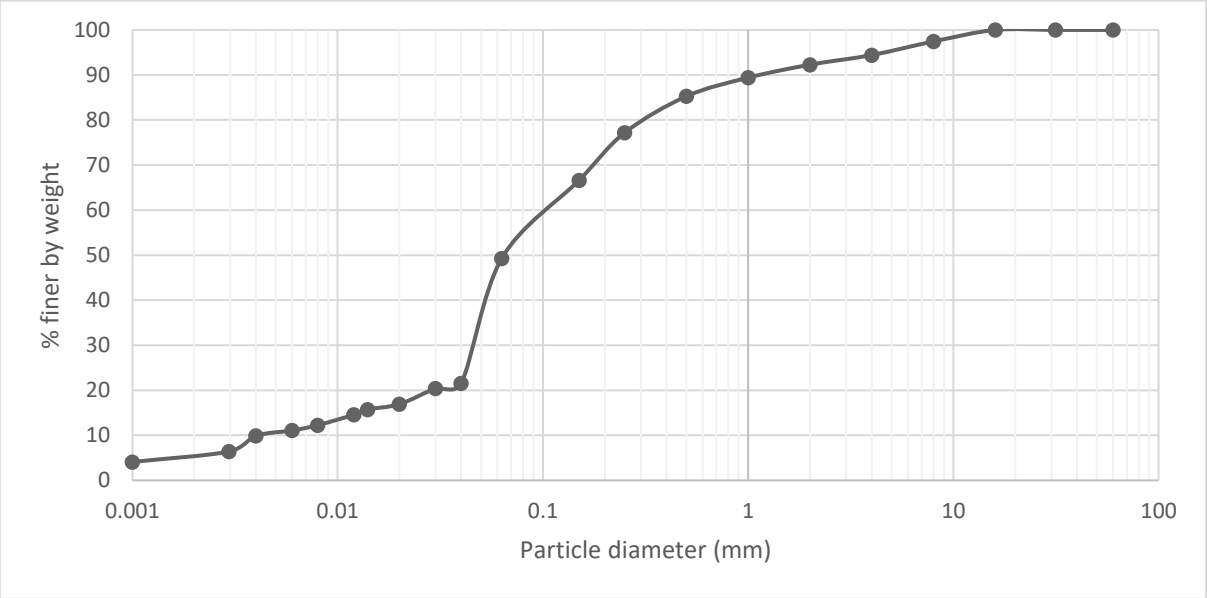

Test Sieve (mm)	% finer by weight
60	100
31.5	100
16	100
8	97
4	94
2	92
1	89
0.5	85
0.25	77
0.15	67
0.063	49
0.04	22
0.03	20
0.02	17
0.014	16
0.012	15
0.008	12
0.006	11
0.004	10
0.003	6
0.001	4

Appendix B.2 Hydraulic Conductivity

Hydraulic conductivity tests of soil was conducted in two ways: Constant Head and Falling Head tests.

Constant Head Test

A 63 mm cell was used for the test. Sample was placed using hand tamping method. The test was repeated four times at same hydraulic gradient at a temperature of 20°C. All tests were performed using de-ionised water.

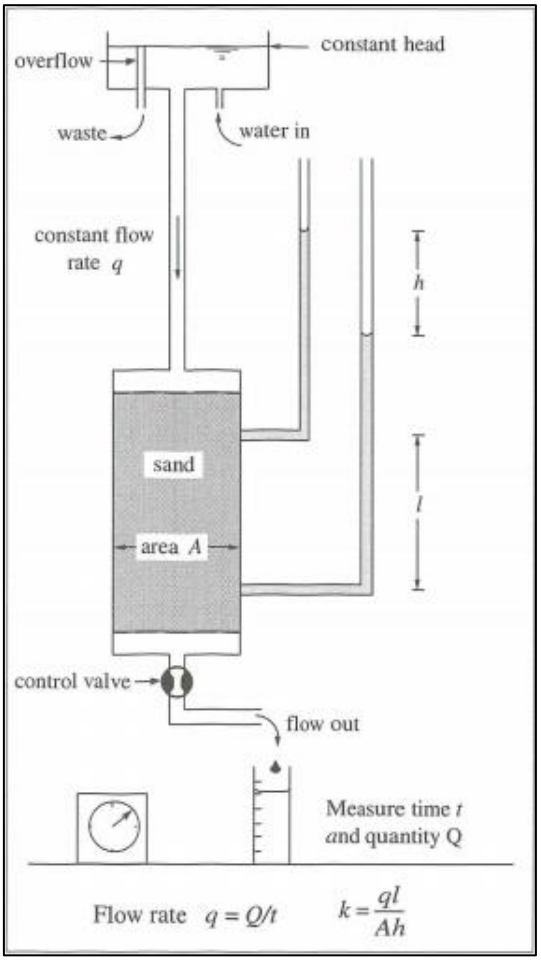

Figure B.2.1: Constant Head test setup (Barnes, 2000).

The equation used to calculate hydraulic conductivity was:

$$k=\frac{LQ}{Ath} \qquad \text{Equation (1)}$$

k=hydraulic conductivity (cm/sec)

Q=Quantity of Flow, taken as average of Inflow and Outflow (cm^3)

L=Length of sample in cm

A= Cross-sectional area of specimen, cm^2

t=Interval of time, over which the flow Q occurs, seconds

h=Difference in Hydraulic Head across the Specimen, cm of water

Sample details	**Sample 1: Completely weathered Separation Point Granite**			
Measurements				
Radius (cm)	3.15	3.15	3.15	3.15
L (cm)	6	6	6	6
z1 (cm)	5	5	5	5
z2 (cm)	11	11	11	11
z2-z1(cm)	6	6	6	6
hp1 (cm)	66	66	66	66
hp2 (cm)	2	2	2	2
h1 (cm)	77	77	77	77
h2 (cm)	7	7	7	7
V (cm3)	51	51	50	51
t (sec)	180	180	180	180
Δh=h2-h1	70	70	70	70
A	3.12E+01	3.12E+01	3.12E+01	3.12E+01
k	7.79E-04	7.79E-04	7.64E-04	7.79E-04
Average (k)	7.79E-04			

Falling Head Test

The setup of the test is shown in Figure B.2.2.

The equation used to calculate hydraulic conductivity for falling head permeameter is:

$$K=\frac{aL}{At}\ln\left(\frac{h0}{h}\right) \qquad \text{Equation (2)}$$

a = standpipe area

A = specimen area

t = elapsed time

L = specimen height

h = height of water in standpipe

h0 = initial height of water in standpipe

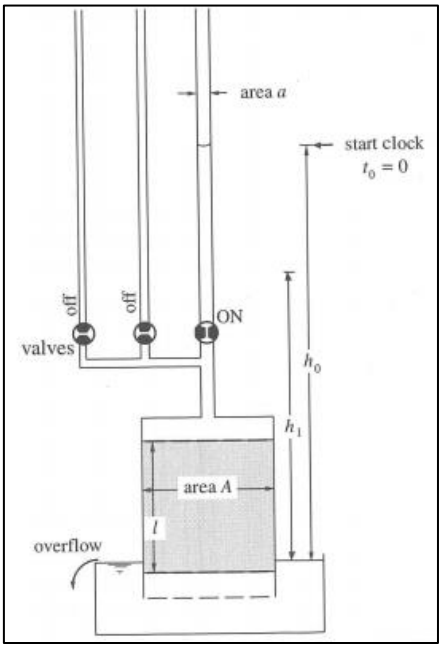

Figure B.3.2: Falling headset up (Barnes, 2000)

Sample no.	**4_Completely to residual soil Separation Point Granite**
L (cm2)	10.82
a (cm2)	0.28
A (cm2)	88.58
ho (cm)	162

Trial	1		2		3	
Time (sec)	h (cm)	k (cm/sec)	h (cm)	k (cm/sec)	h (cm)	k (cm/sec)
0	160	0.00E+00	160	0	160	0
10	118	1.08E-03	118	1.08E-03	119	1.06E-03
20	100	8.25E-04	100	8.25E-04	110	6.62E-04
30	88	6.96E-04	88	6.96E-04	88	6.96E-04
40	74.5	6.64E-04	76.5	6.42E-04	75.5	6.53E-04
50	64	6.35E-04	65.5	6.19E-04	65	6.25E-04
60	56	6.06E-04	56.5	6.00E-04	56	6.06E-04
	Average	8.68E-04		7.44E-04		7.16E-04
	K average	7.76E-04				

Sample no.	8_2018 debris flow source area
L (cm2)	12.5
a (cm2)	0.28
A (cm2)	0
ho (cm)	163

Trial	1		2		3	
Time (sec)	h (cm)	k (cm/sec)	h (cm)	k (cm/sec)	h (cm)	k (cm/sec)
0	163	0.00E+00	163	0	160	0
10	137	6.76E-04	149	3.50E-04	140	5.92E-04
20	125	5.17E-04	128	4.70E-04	122	5.64E-04
30	117	4.30E-04	120	3.97E-04	119	4.08E-04
40	112	3.65E-04	110	3.83E-04	108	4.01E-04
50	105	3.42E-04	102	3.65E-04	100	3.80E-04
60	94	3.57E-04	96	3.43E-04	92	3.71E-04
70	90	3.30E-04	89	3.36E-04	87	3.49E-04
80	86	3.11E-04	83	3.28E-04	82	3.34E-04
90	80	3.08E-04	78	3.19E-04	77	3.24E-04
100	73	3.13E-04	73	3.13E-04	72	3.18E-04
110	69	3.04E-04	67	3.15E-04	65	3.25E-04
120	64	3.03E-04	62	3.14E-04	61	3.19E-04
Average		3.51E-04		3.26E-04		3.90E-04
Average		3.56E-04				

Sample no.	9_completely weathered to residual soil URIC
L (cm2)	11.1
a (cm2)	0.28
A (cm2)	82.033
ho (cm)	160

Trial	1		2		3	
Time (sec)	h (cm)	k (cm/sec)	h (cm)	k (cm/sec)	h (cm)	k (cm/sec)
0	160	0.00E+00	160	0	160	0
1	131	7.58E-03	123	9.96E-03	129	8.16E-03
2	110	7.10E-03	90	1.09E-02	99	9.09E-03
3	78	9.07E-03	72	1.01E-02	79	8.91E-03
4	57	9.78E-03	52	1.06E-02	57	9.78E-03
Average		8.38E-03		1.04E-02		8.99E-03
Average	9.25E-03					

Sample no.	13_2018 debris flow source area
L (cm2)	13.25
a (cm2)	0.28
A (cm2)	89.92
ho (cm)	162

Trial	1		2		3	
Time (sec)	h (cm)	k (cm/sec)	h (cm)	k (cm/sec)	h (cm)	k (cm/sec)
0	162	0.00E+00	162	0	162	0
10	135	7.52E-04	136	7.37E-04	137	6.92E-04
20	128	4.86E-04	131	4.38E-04	133	4.07E-04
30	125	3.57E-04	128	3.24E-04	128	3.24E-04
40	121	3.01E-04	124	2.80E-04	125	2.67E-04
50	115	2.83E-04	120	2.49E-04	121	2.41E-04
60	114	2.42E-04	116	2.30E-04	119	2.12E-04
70	110	2.29E-04	113	2.12E-04	114	2.07E-04
80	106	2.17E-04	109	2.04E-04	111	1.95E-04
90	104	2.03E-04	106	1.94E-04	109	1.82E-04
100	102	1.93E-04	104	1.85E-04	105	1.79E-04
110	99	1.85E-04	100	1.83E-04	102	1.74E-04
120	96	1.80E-04	98	1.75E-04	98	1.73E-04
130	94	1.73E-04	96	1.68E-04	96	1.66E-04
140	91	1.70E-04	94	1.62E-04	95	1.57E-04
150	90	1.63E-04	91	1.60E-04	92	1.57E-04
160	87	1.60E-04	89	1.56E-04	91	1.50E-04
170	85	1.57E-04	87	1.52E-04	89	1.47E-04
180	83	1.54E-04	84	1.51E-04	86	1.45E-04
190	81	1.51E-04	82	1.47E-04	84	1.43E-04
200	79	1.49E-04	81	1.43E-04	82	1.41E-04
210	77	1.46E-04	78	1.43E-04	80	1.39E-04
220	76	1.43E-04	76	1.42E-04	78	1.37E-04
230	74	1.41E-04	74	1.40E-04	77	1.35E-04
240	72	1.39E-04	73	1.37E-04	74	1.35E-04
250	70	1.38E-04	71	1.36E-04	74	1.30E-04
260	69	1.37E-04	70	1.34E-04	71	1.32E-04
270	67	1.34E-04	68	1.33E-04	69	1.30E-04
280	66	1.33E-04	66	1.32E-04	67	1.30E-04
290	65	1.31E-04	65	1.30E-04	66	1.28E-04
300	64	1.29E-04	64	1.29E-04	65	1.26E-04
Average		2.02E-04		1.94E-04		1.86E-04
Average	1.94E-04					

Sample no.	19_Fan deposit
L (cm2)	12.14
a (cm2)	0.28
A (cm2)	90.93
ho (cm)	162

Trial	1		2		3	
Time (sec)	h (cm)	k (cm/sec)	h (cm)	k (cm/sec)	h (cm)	k (cm/sec)
0	162	0.00E+00	162	0	162	0
5	121	2.18E-03	120	2.24E-03	121	2.18E-03
10	90	2.20E-03	91	2.16E-03	91	2.16E-03
15	74	1.95E-03	75	1.92E-03	74	1.95E-03
20		-	59	1.90E-03	59	1.89E-03
Average		2.11E-03		2.06E-03		2.04E-03
Average		2.07E-03				

Appendix B.3 Direct Shear Box Testing

Introduction

The direct shear testing is relatively simple and inexpensive. The soil specimen is consolidated and sheared along a mechanically induced horizontal shear plane while being subjected to a pressure applied normally to that plane.

The direct shear testing was conducted on 27-WF21E80 SHEARMATIC EmS by controls group. This automatic standalone machine allows determination of the shear strength of cohesive or granular soils in drained conditions by creating a failure plane through the application of horizontal displacement. The 100mm by 100mm square shearbox has a maximum horizontal travel of 25mm and maximum vertical travel of 10mm.

Figure B.3.1: Shearmatic machine used for direct shear testing. SHEARMATIC EmS is standalone machine by Controls Group.

There are 3 graphs presented for each test: The consolidation curve plot, direct shear testing plot, and peak shear stress versus normal stress used to determine effective friction angle and apparent cohesion. A table of index properties is presented for each soil sample.

Pre-2018 debris flow deposit (soil sample)

Sample 7:

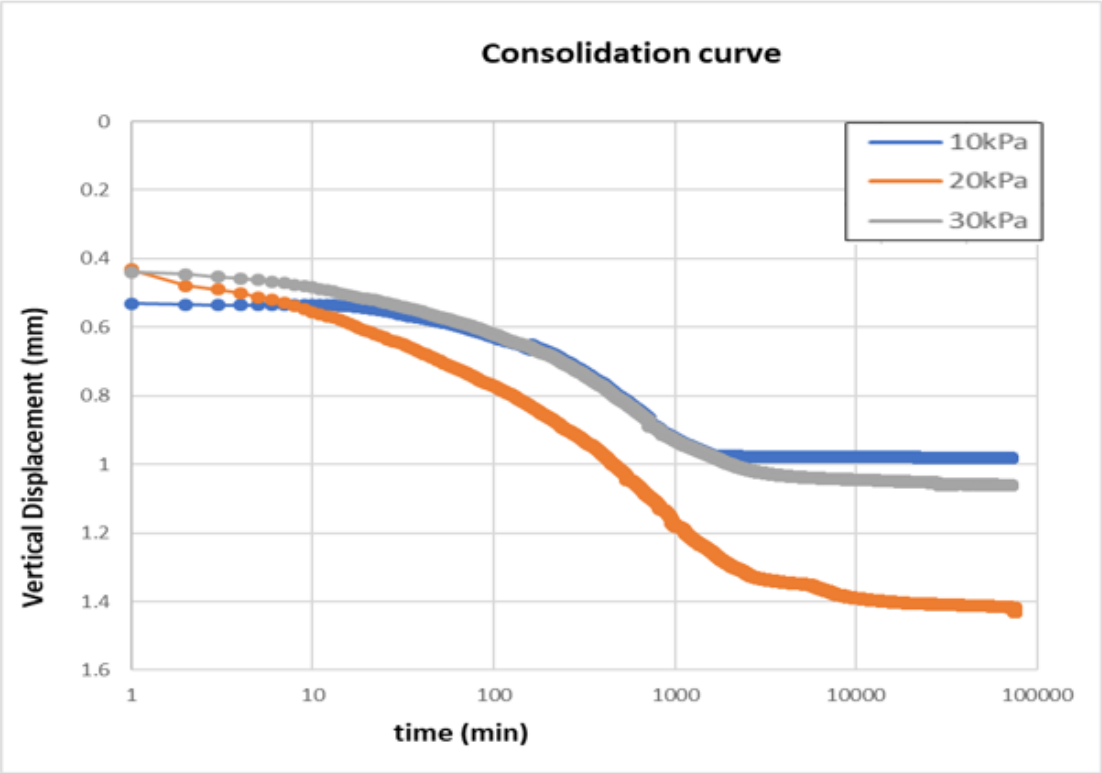

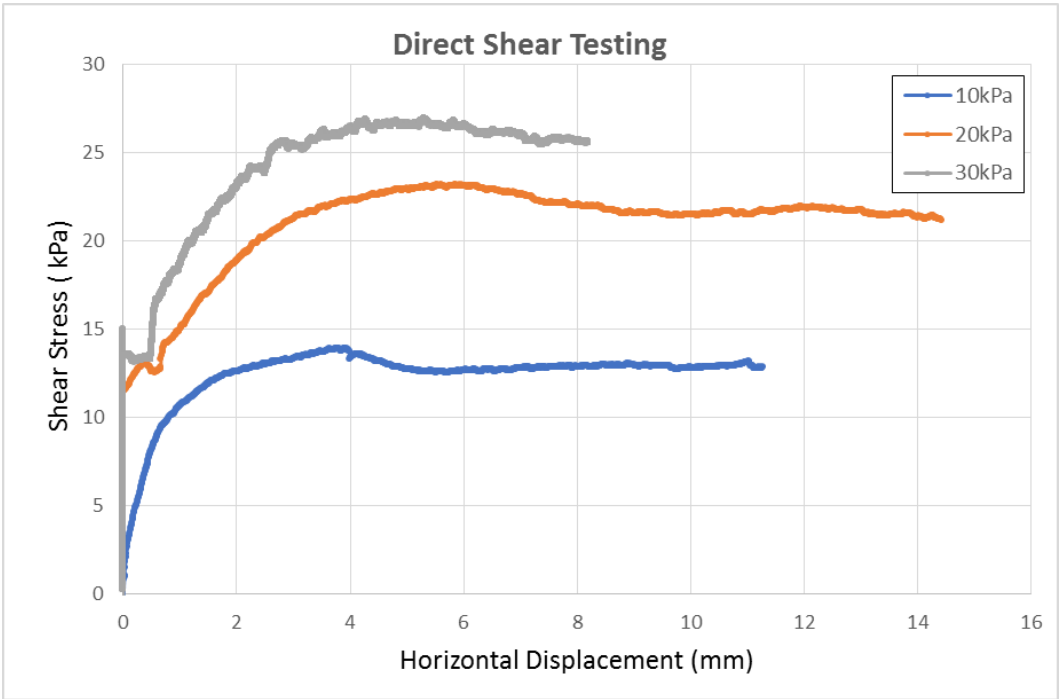

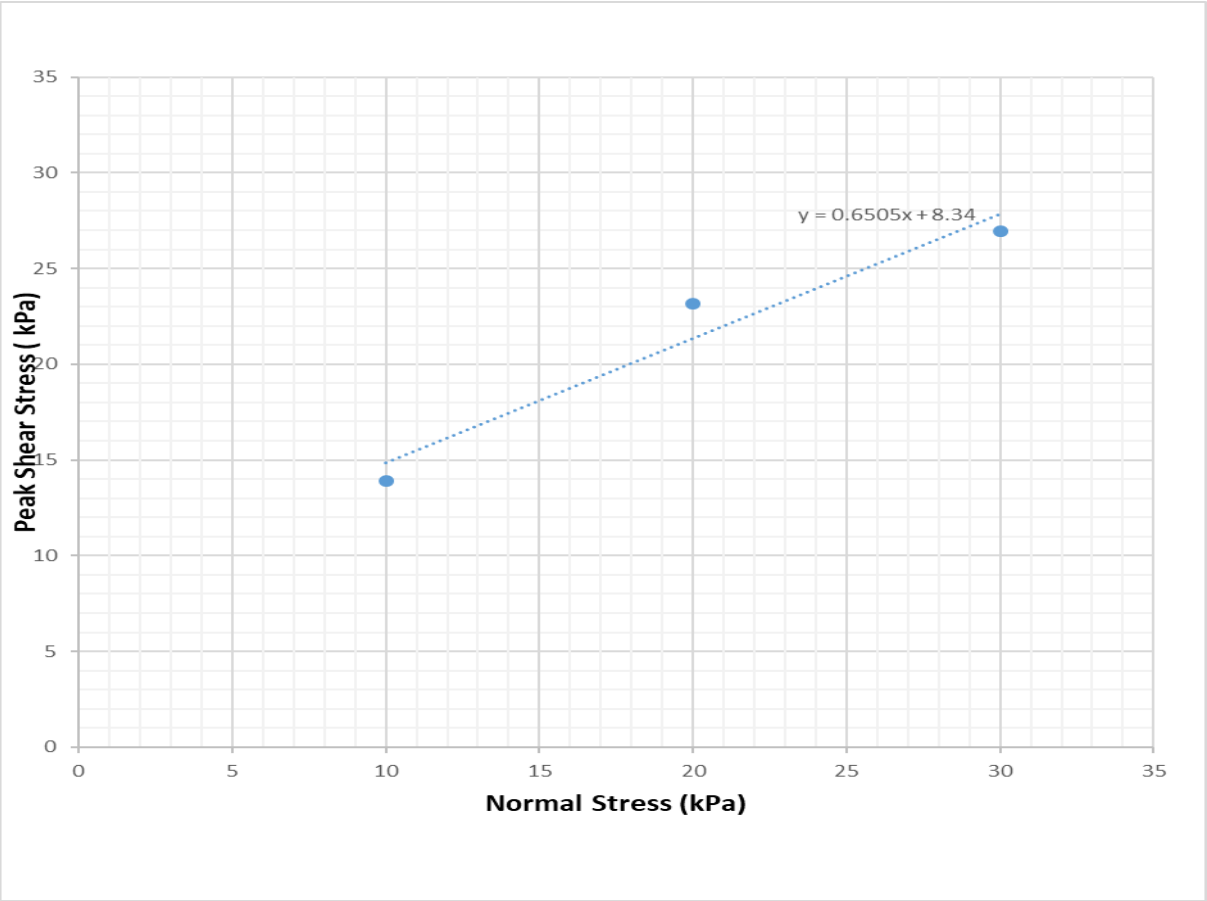

Specie-men no.	Normal stress (kPa)	Specific Gravity	Bulk density (t/m3)	Initial void ratio	Initial dry density (t/m3)	Degree of saturation	Initial water content %	Pre-shear void ratio	Final Water content %	Final void ratio
3	30	2.64	2.13	0.57	1.68	1.24	27.0	0.50	33.5	0.48
2	20	2.64	2.06	0.62	1.62	1.14	27.0	0.53	33.5	0.46
1	10	2.64	2.03	0.65	1.60	1.10	27.0	0.60	33.5	0.60

Sample 16

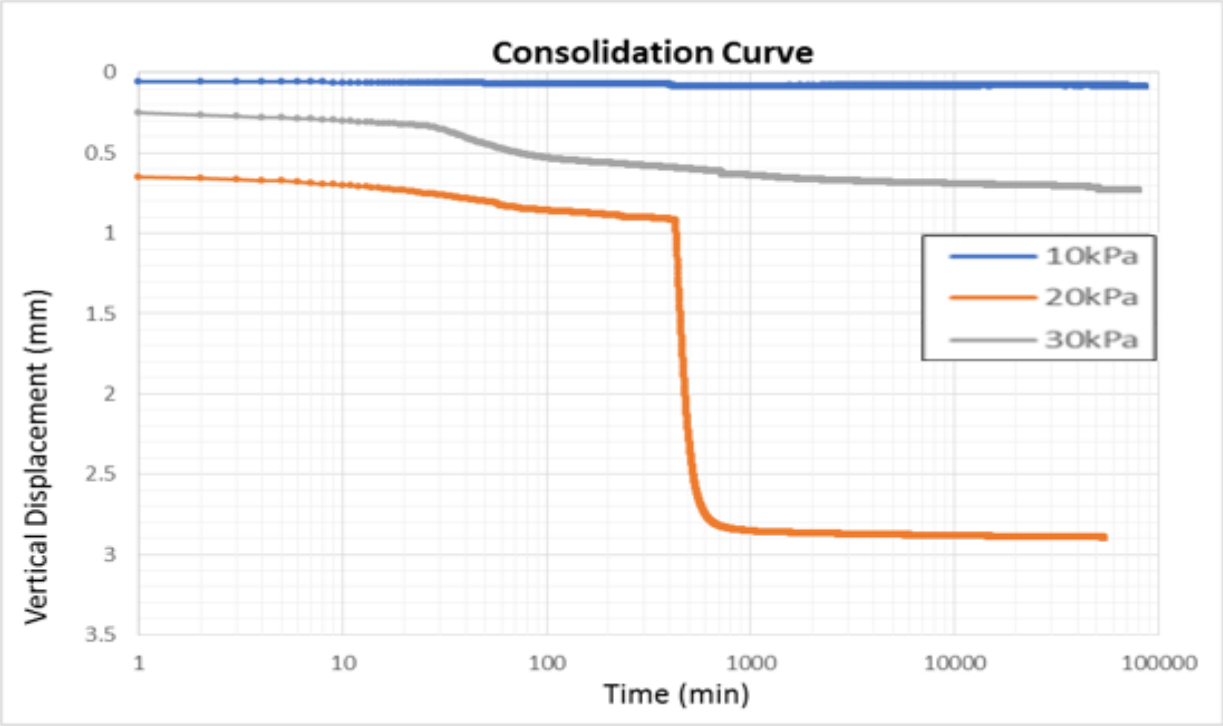

Note: Specimen number 2 (20kPa) collapsed during the test. 20kPa data has not been used in the calculation for effective friction angle and apparent cohesion.

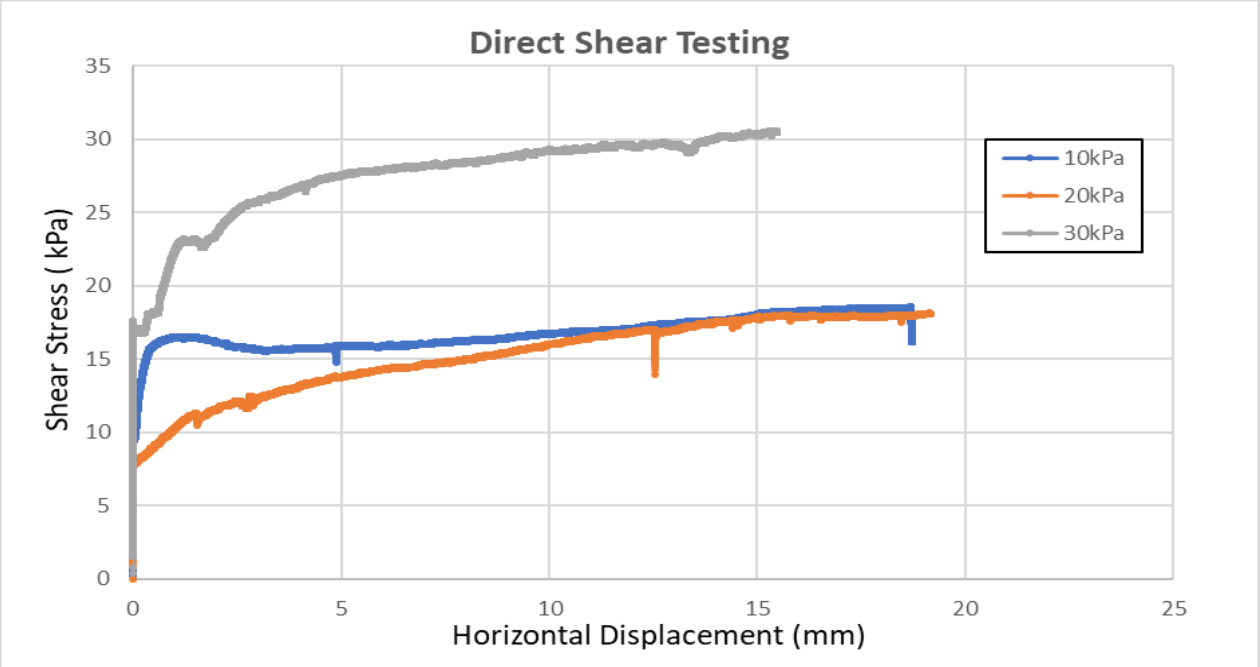

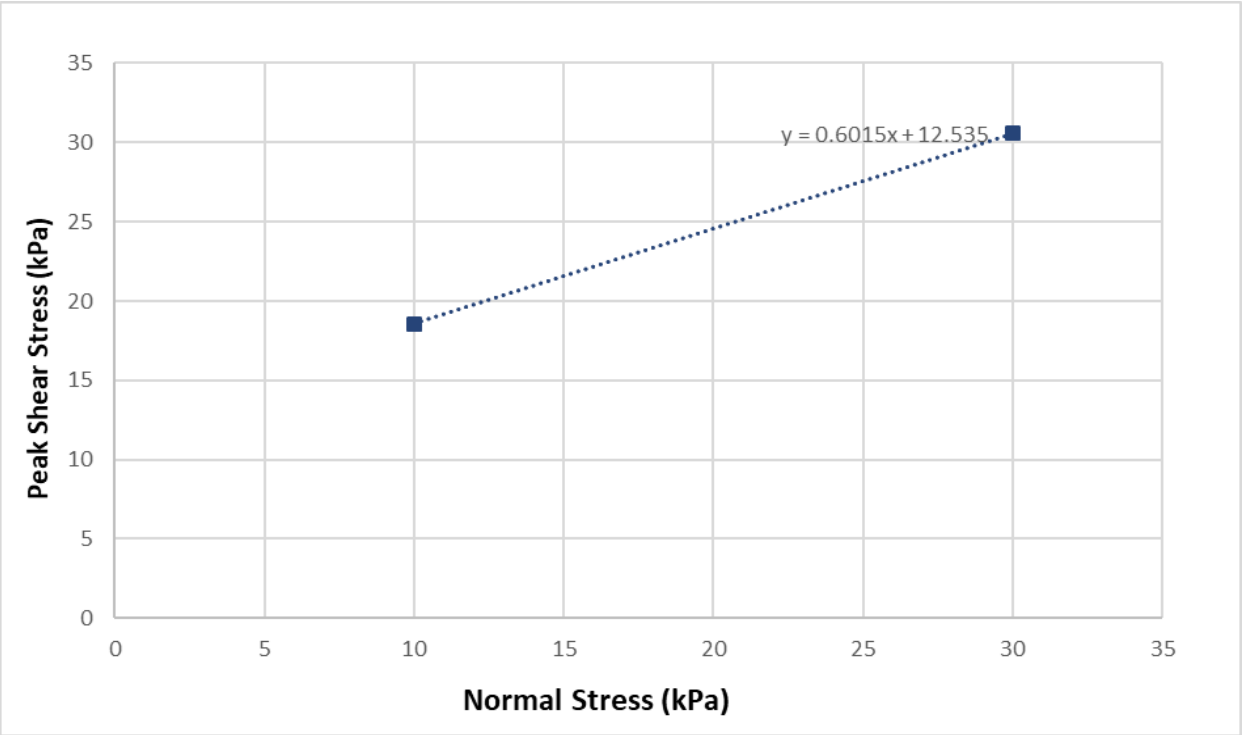

Specie-men no.	Normal stress (kPa)	Specific Gravity	Bulk density (t/m3)	Initial void ratio	Initial dry density (t/m3)	Degree of saturation	Initial water content %	Pre-shear void ratio	Final Water content %	Final void ratio
3	30	3.03	1.71	1.34	1.30	0.72	31.6	1.27	33.0	1.16
2	20	3.03	1.36	1.94	1.03	0.49	31.6	1.54	33.0	1.28
1	10	3.03	1.82	1.19	1.38	0.80	31.6	1.19	33.0	1.15

2018 (Gita) Soil Samples

Sample 2

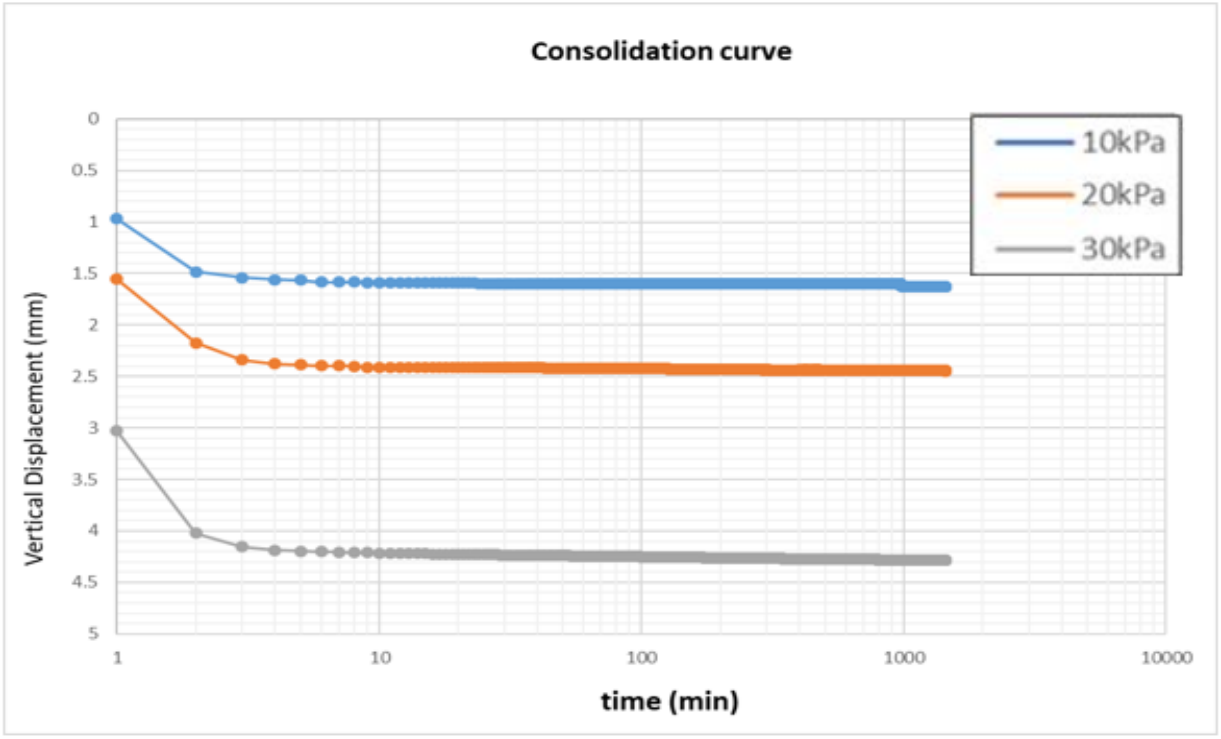

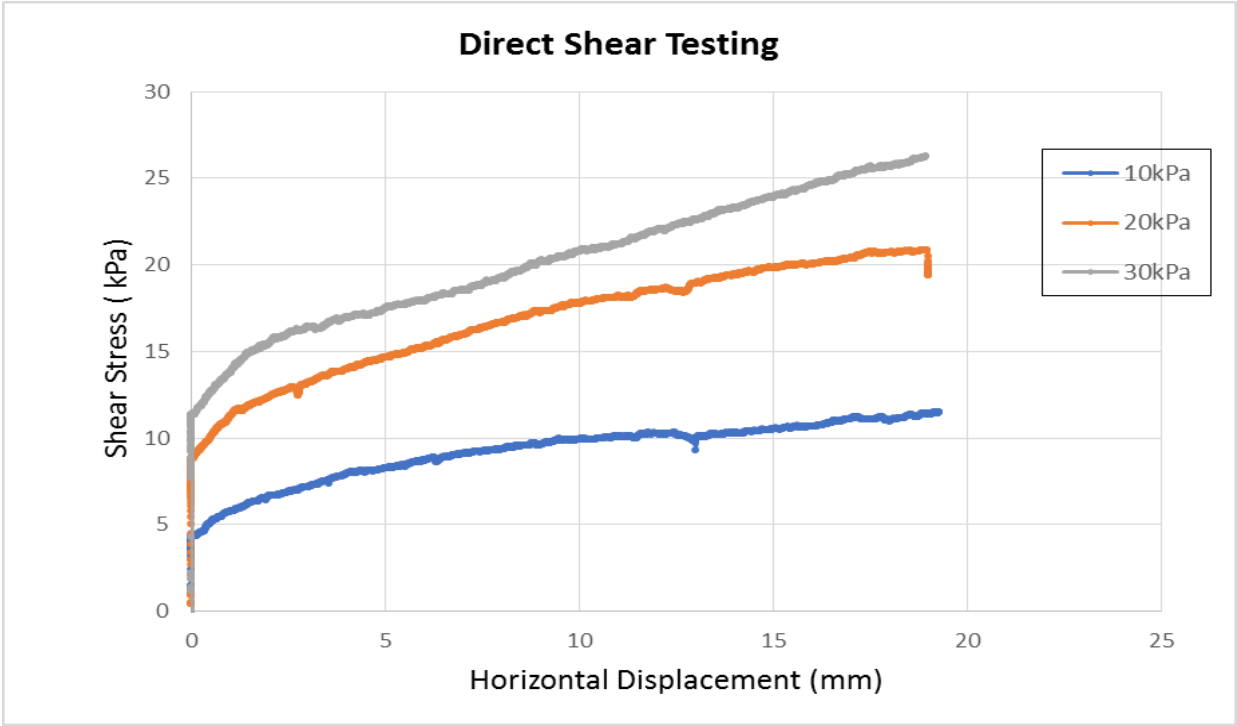

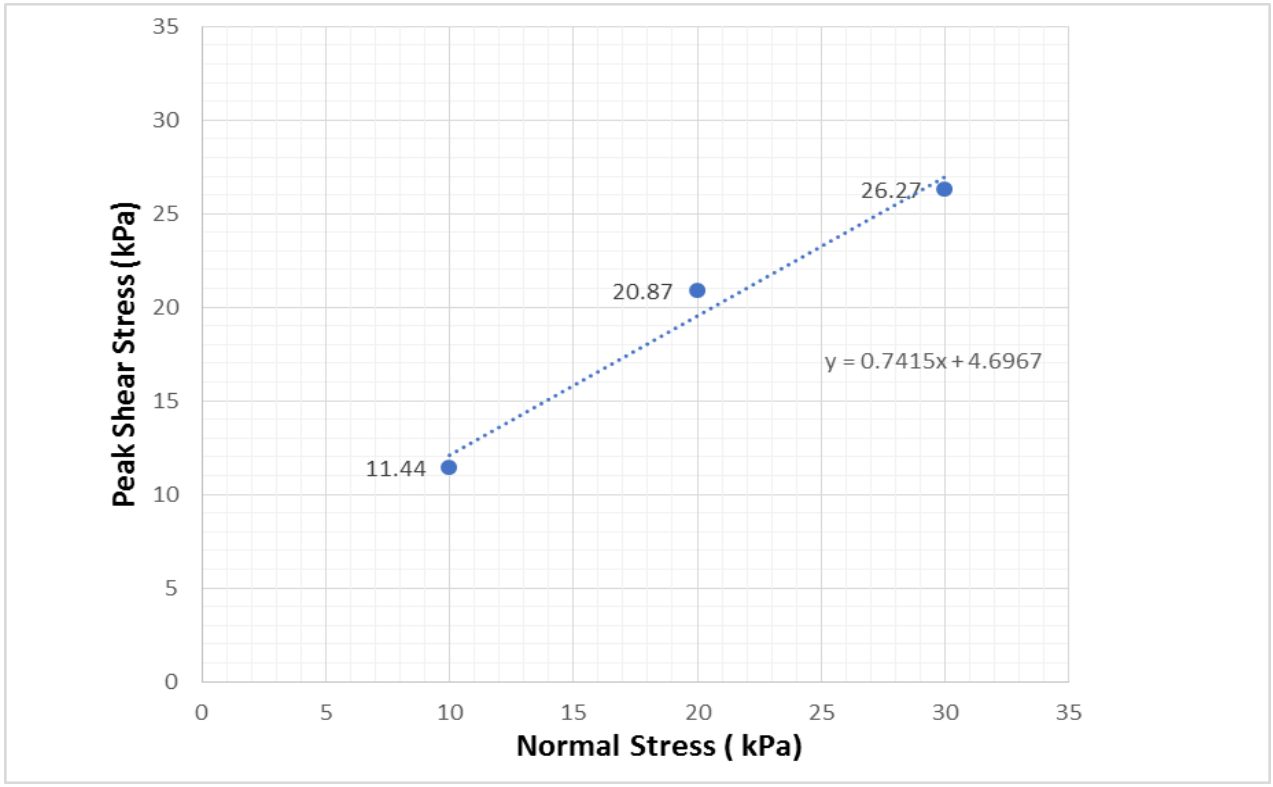

Specie-men no.	Normal stress (kPa)	Specific Gravity	Bulk density (t/m3)	Initial void ratio	Initial dry density (t/m3)	Degree of saturation	Initial water content %	Pre-shear void ratio	Final Water content %	Final void ratio
3	30	2.64	1.47	1.18	1.21	0.48	21.7	0.80	40.2	0.60
2	20	2.64	1.44	1.23	1.19	0.47	21.7	1.00	40.2	0.84
1	10	2.64	1.48	1.17	1.22	0.49	21.7	1.02	40.2	0.78

Sample 8

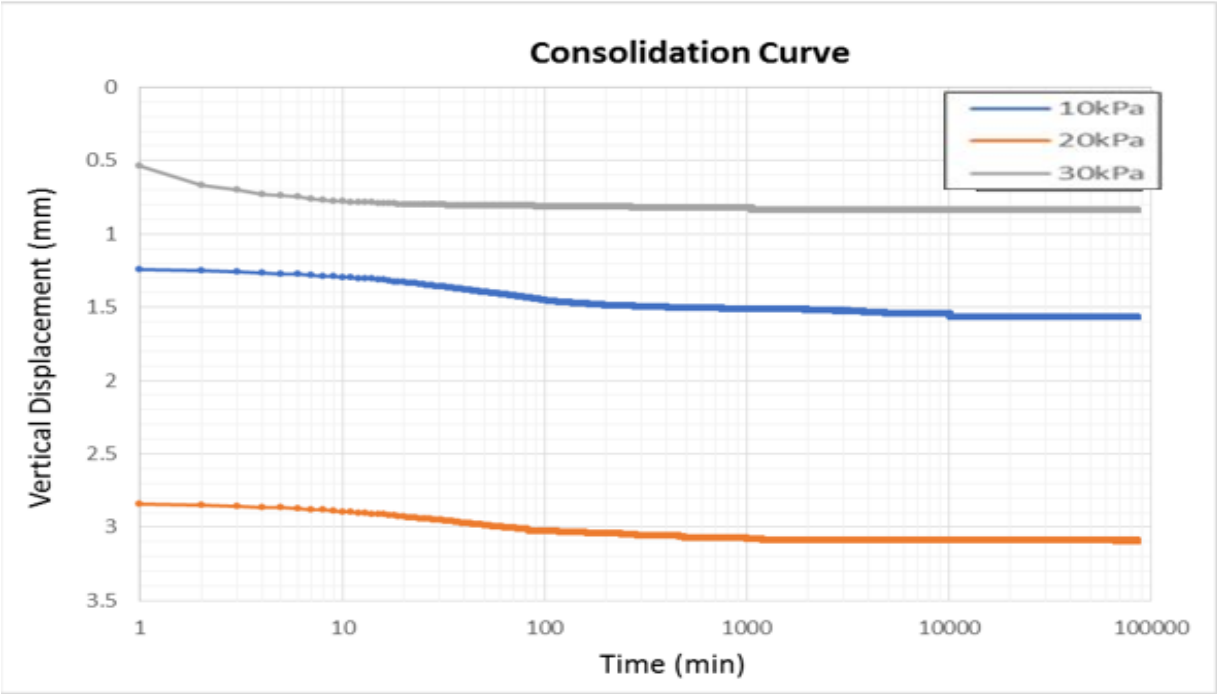
Consolidation Curve
Vertical Displacement (mm)
0
0.5
1
1.5
2
2.5
3
3.5
1
10
100
1000
10000
100000
Time (min)
10kPa
20kPa
30kPa

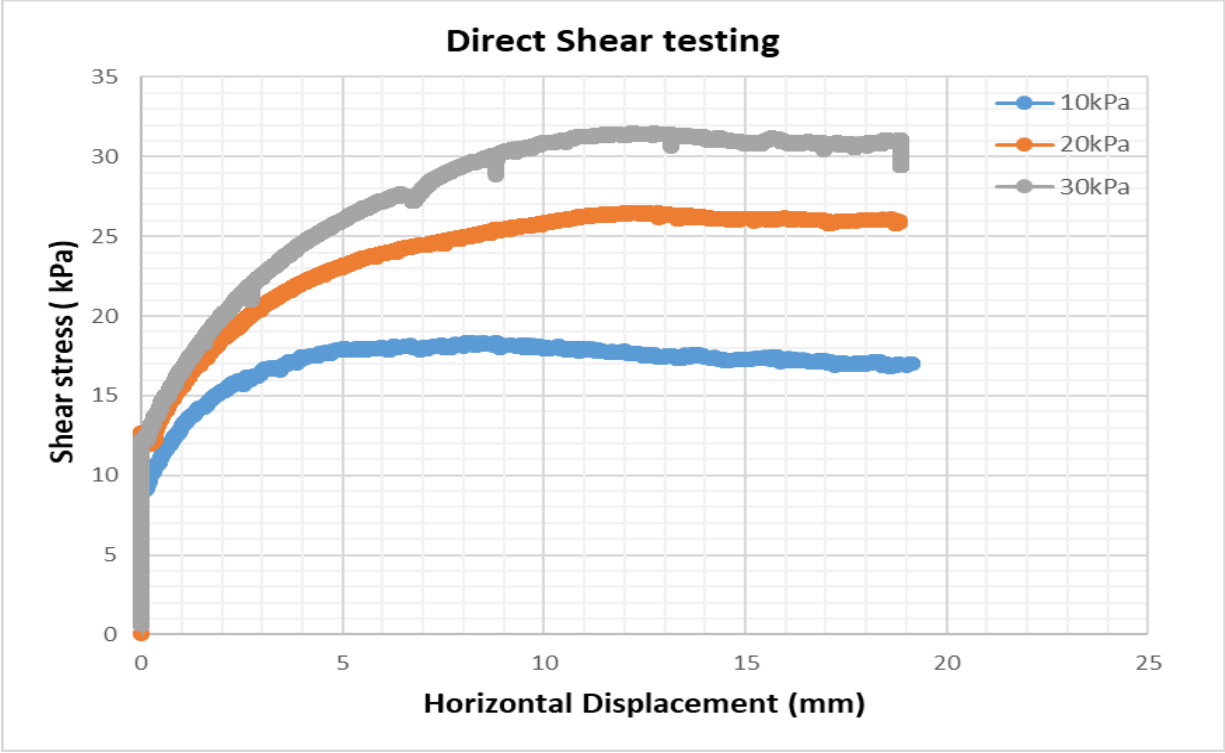
Direct Shear testing
Shear stress (kPa)
35
30
25
20
15
10
5
0
0
5
10
15
20
25
Horizontal Displacement (mm)
10kPa
20kPa
30kPa

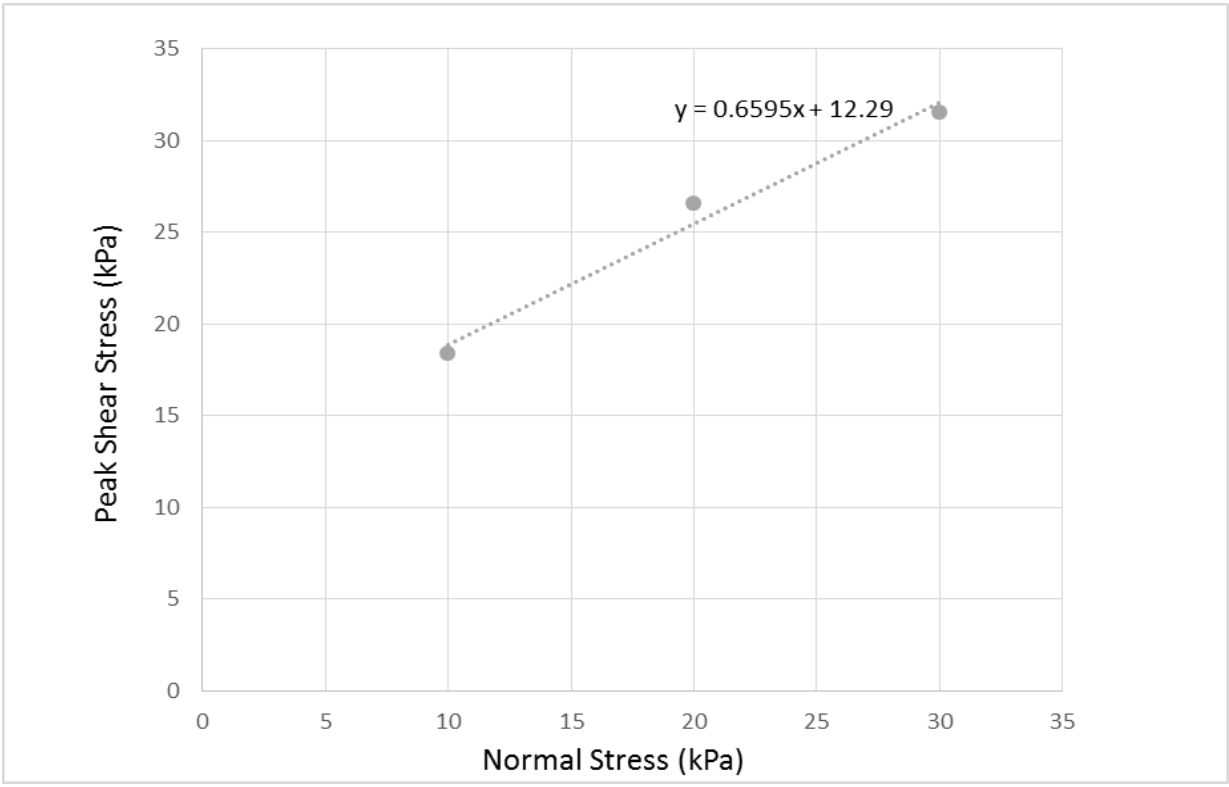

Specie-men no.	Normal stress (kPa)	Specific Gravity	Bulk density (t/m3)	Initial void ratio	Initial dry density (t/m3)	Degree of saturation	Initial water content %	Pre-shear void ratio	Final Water content %	Final void ratio
3	30	3.03	1.12	1.93	1.03	0.14	8.9	1.56	40.2	1.36
2	20	3.03	1.08	2.04	1.00	0.13	8.9	1.85	40.2	1.65
1	10	3.03	1.08	2.06	0.99	0.13	8.9	1.95	40.2	1.88

Sample 13

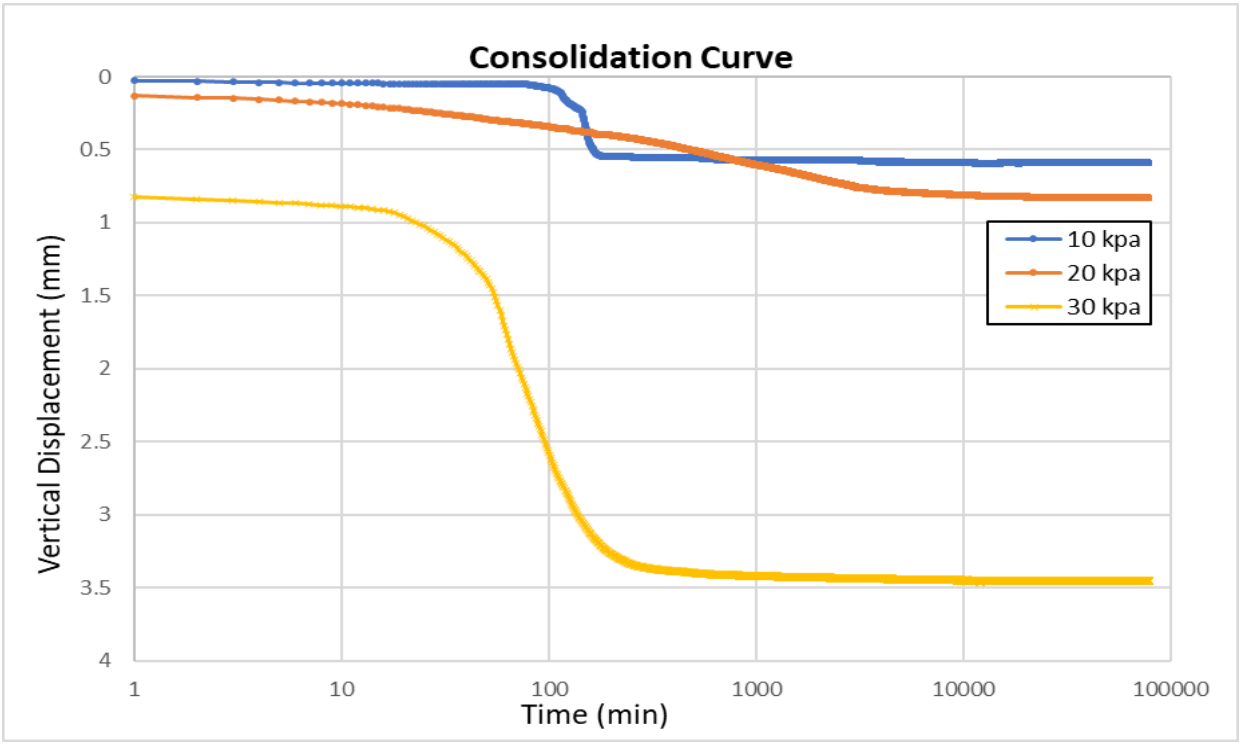
Consolidation Curve
Vertical Displacement (mm)
0
0.5
1
1.5
2
2.5
3
3.5
4
1
10
100
1000
10000
100000
Time (min)
10 kpa
20 kpa
30 kpa

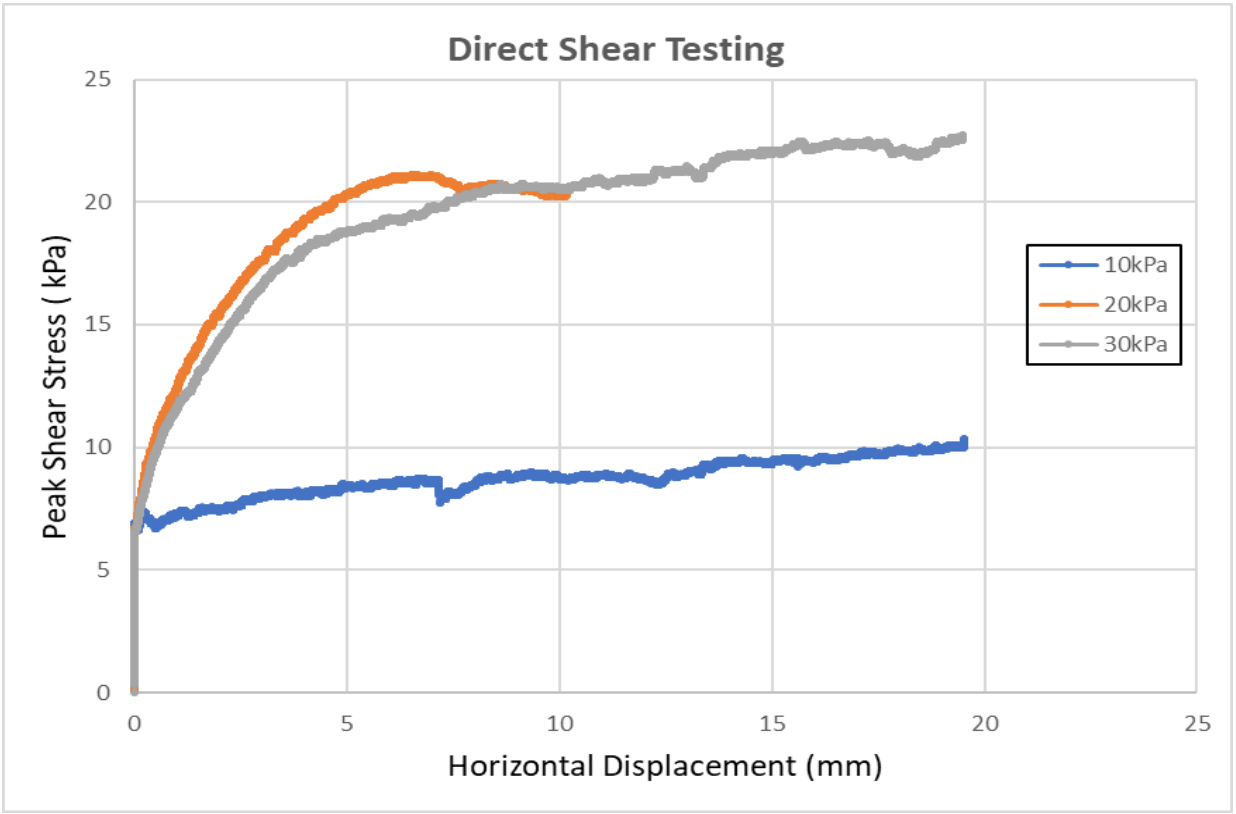
Direct Shear Testing
Peak Shear Stress (kPa)
25
20
15
10
5
0
0
5
10
15
20
25
Horizontal Displacement (mm)
10kPa
20kPa
30kPa

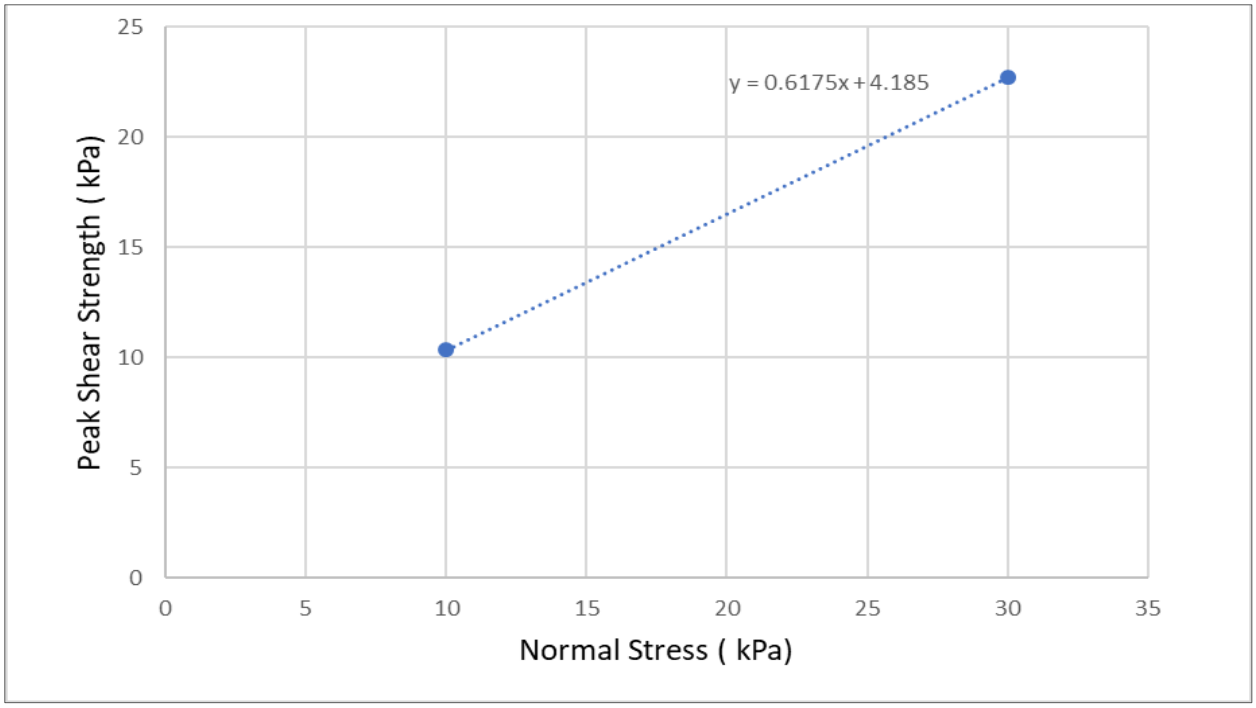

Specie-men no.	Normal stress (kPa)	Specific Gravity	Bulk density (t/m3)	Initial void ratio	Initial dry density (t/m3)	Degree of saturation	Initial water content %	Pre-shear void ratio	Final Water content %	Final void ratio
3	30	3.05	1.31	2.09	0.99	0.48	32.9	2.06	40.2	1.83
2	20	3.05	1.71	1.37	1.28	0.73	32.9	1.30	40.2	1.28
1	10	3.05	1.41	1.88	1.06	0.53	32.9	1.73	40.2	1.50

Weathered Bedrock

Sample 1: Highly weathered Separation Point Granite

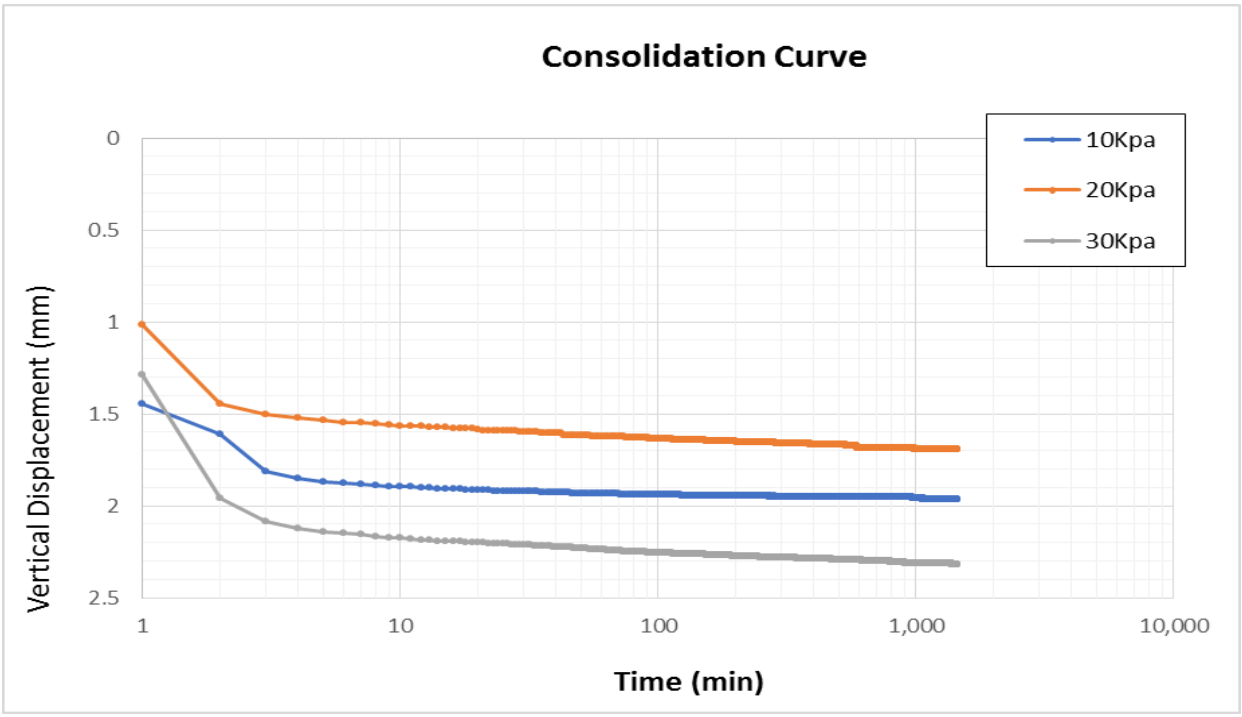

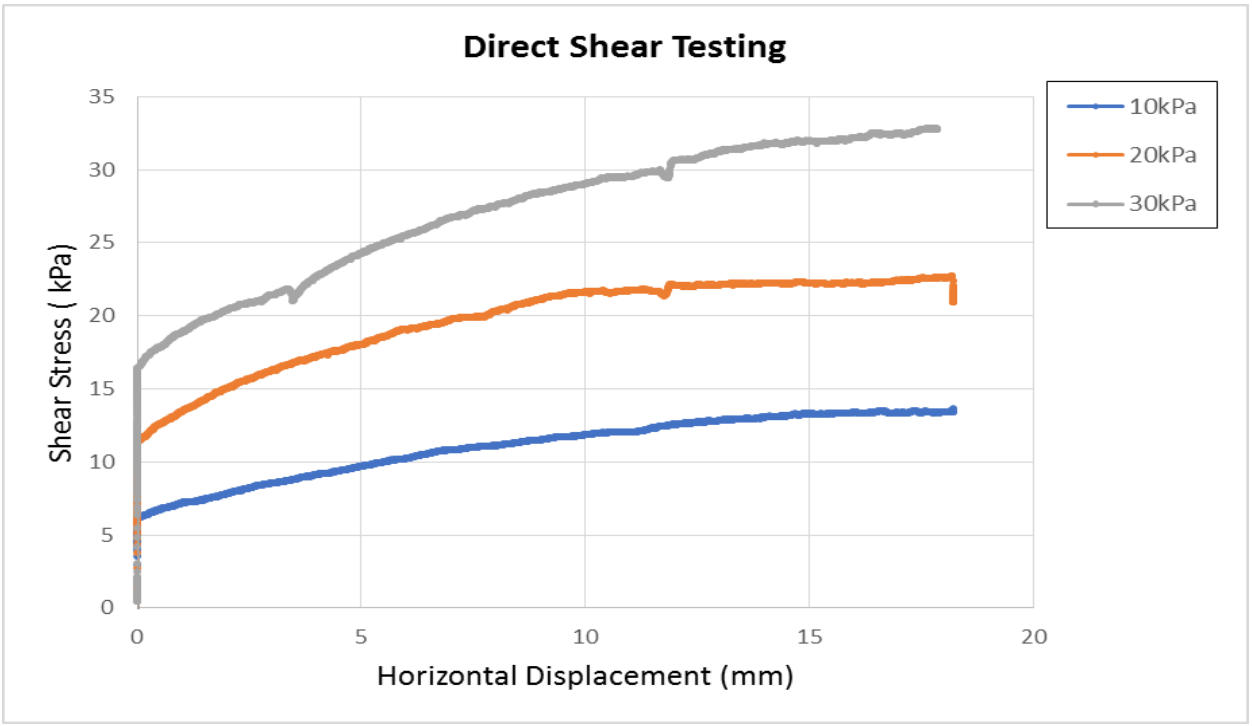

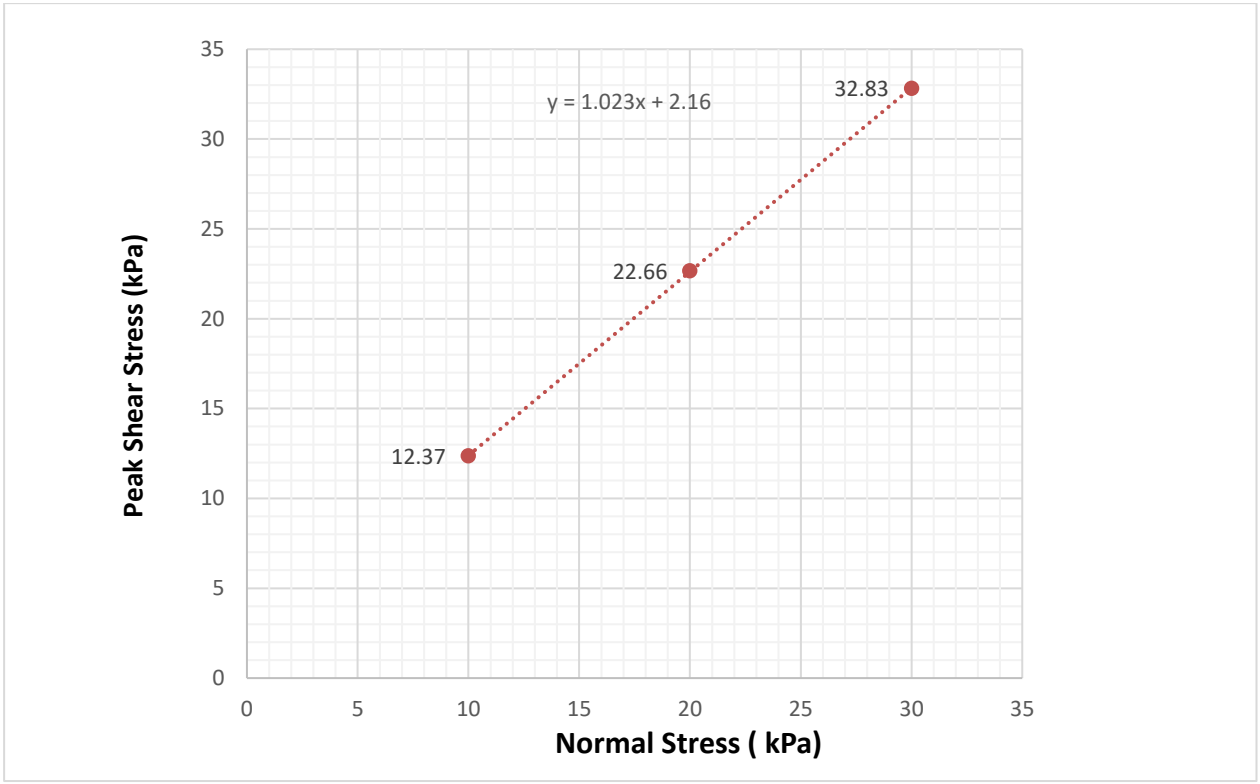

Specie-men no.	Normal stress (kPa)	Specific Gravity	Bulk density (t/m3)	Initial void ratio	Initial dry density (t/m3)	Degree of saturation	Initial water content %	Pre-shear void ratio	Final Water content %	Final void ratio
3	30	2.64	1.47	1.07	1.39	0.38	15.3	0.72	35.5	0.68
2	20	2.64	1.44	1.11	1.25	0.36	15.3	0.96	35.5	0.89
1	10	2.64	1.46	1.08	1.27	0.37	15.3	0.91	35.5	0.87

Sample 4: Completely weathered to Residual soil Separation Point Granite

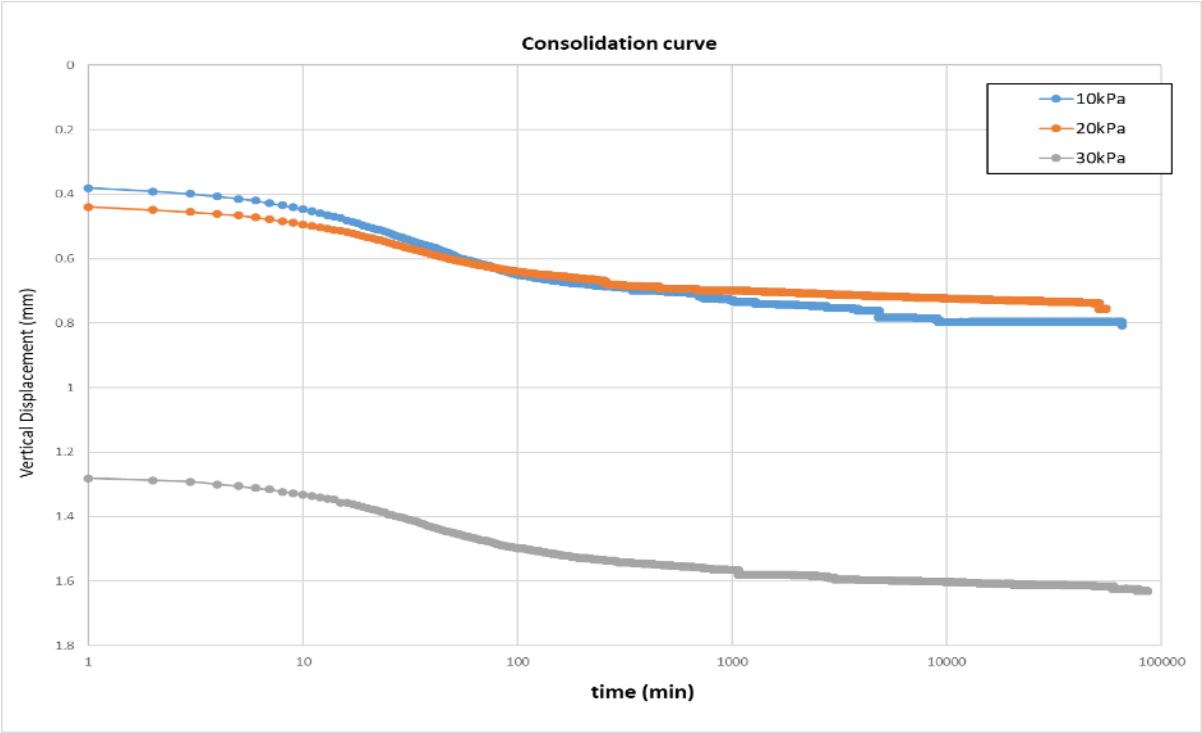

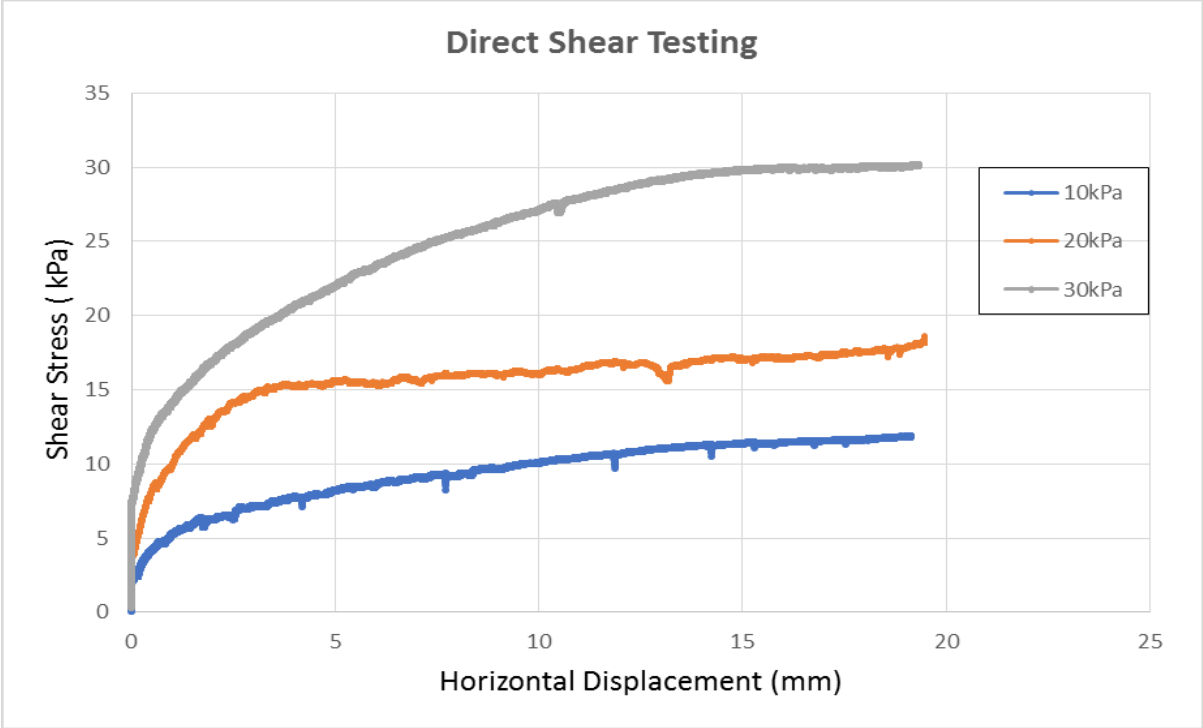

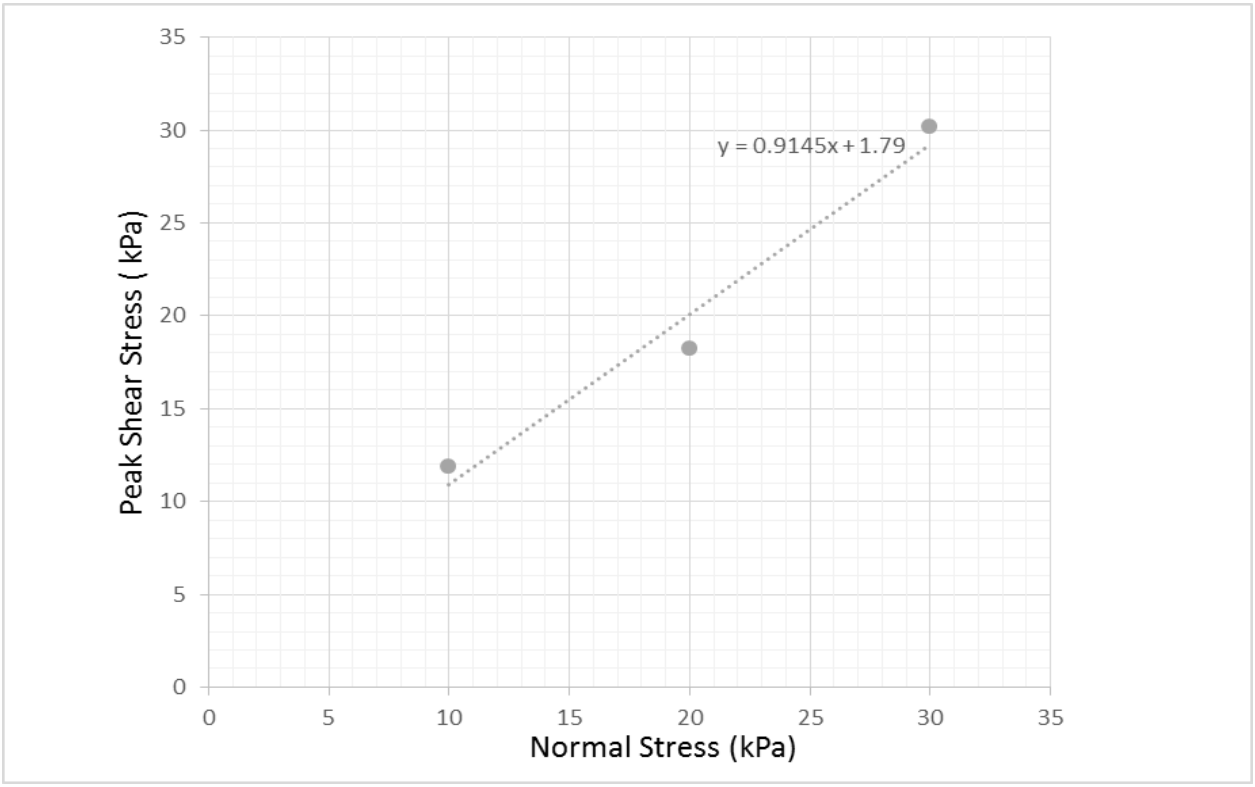

Specie-men no.	Normal stress (kPa)	Specific Gravity	Bulk density (t/m3)	Initial void ratio	Initial dry density (t/m3)	Degree of saturation	Initial water content %	Pre-shear void ratio	Final Water content %	Final void ratio
3	30	2.64	1.62	0.84	1.44	0.41	13.1	0.71	26.6	0.58
2	20	2.64	1.66	0.80	1.46	0.43	13.1	0.74	26.6	0.53
1	10	2.64	1.46	1.04	1.29	0.33	13.1	0.93	26.6	0.86

Sample 9: Completely weathered to residual soil Undifferentiated Riwaka Igneous Complex

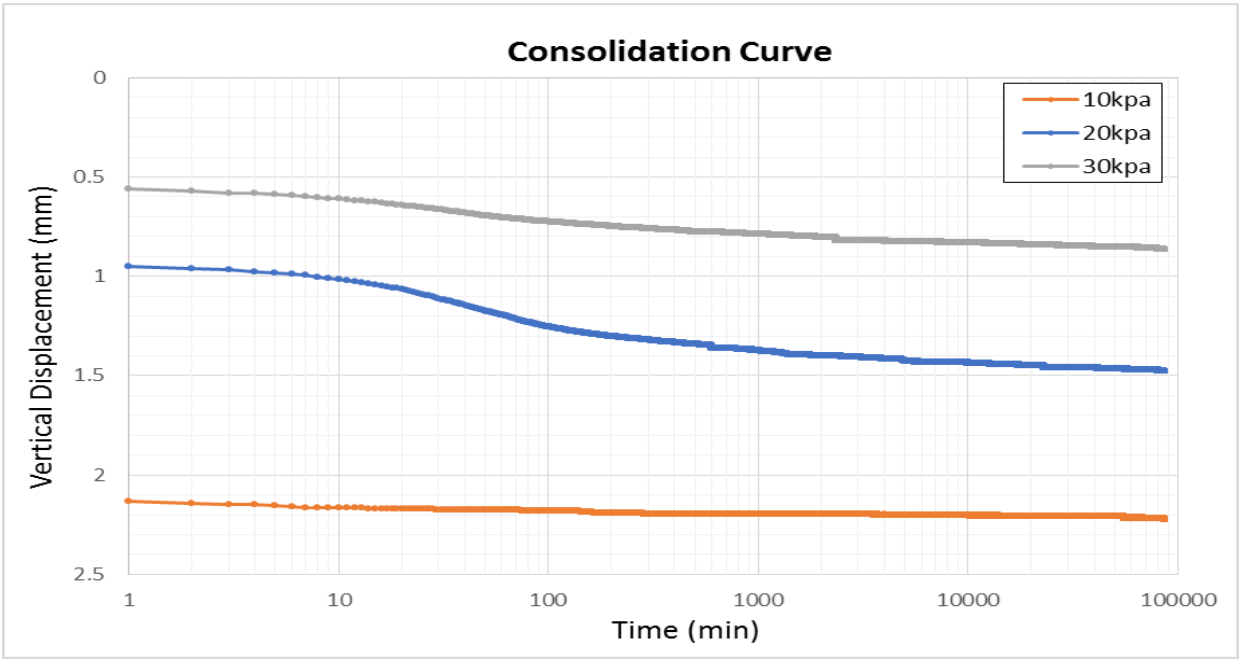

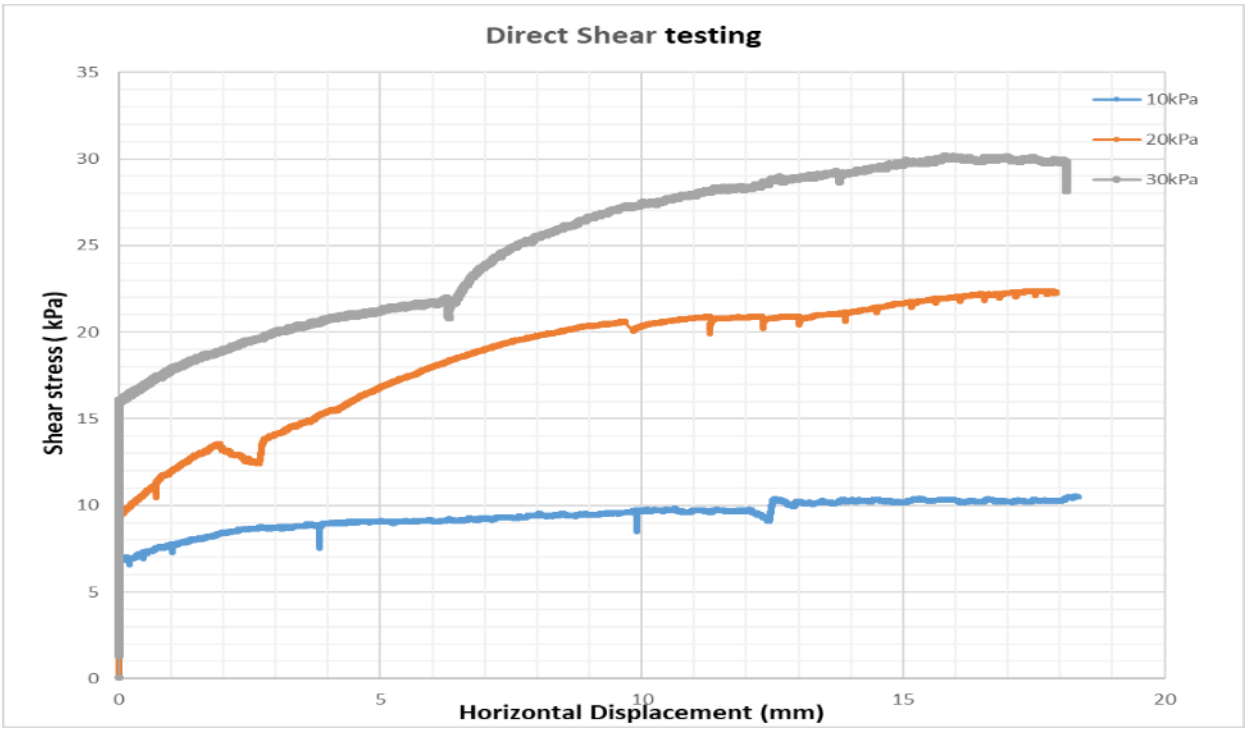

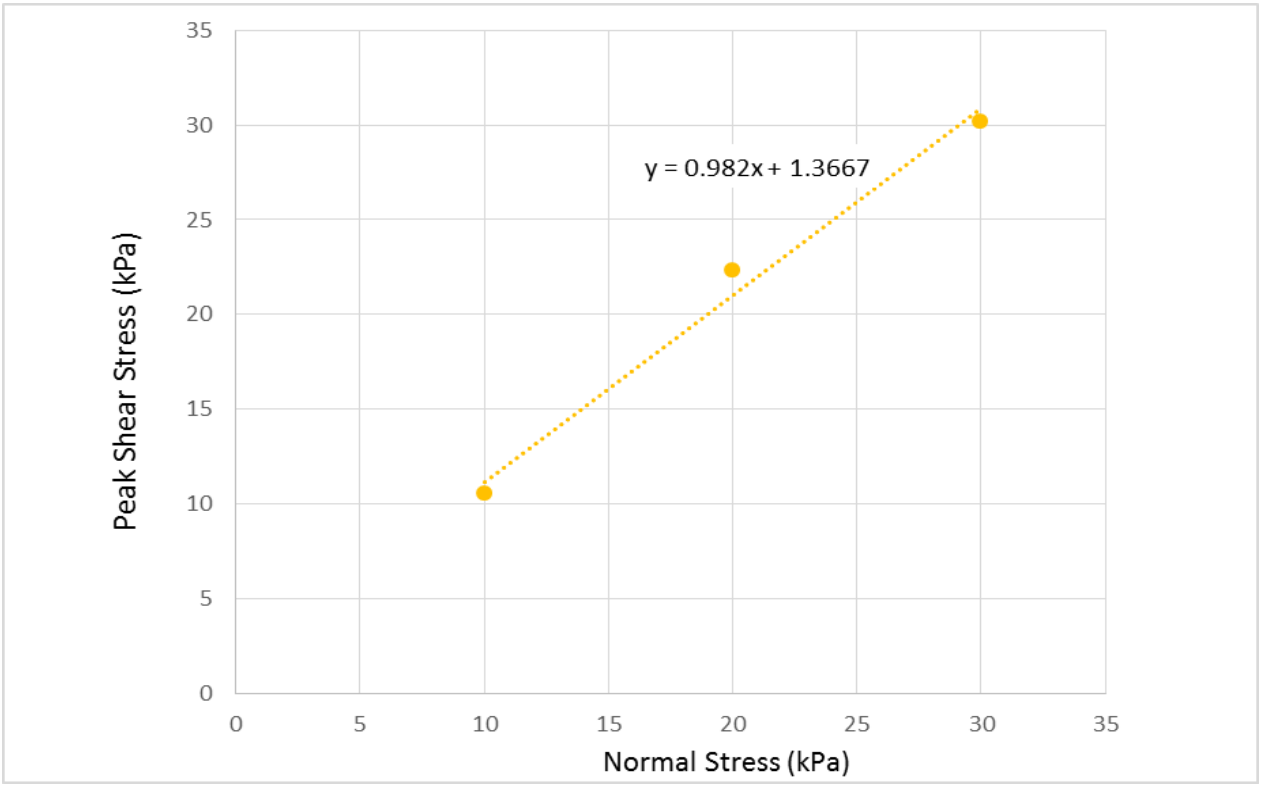

Specie-men no.	Normal stress (kPa)	Specific Gravity	Bulk density (t/m3)	Initial void ratio	Initial dry density (t/m3)	Degree of saturation	Initial water content %	Pre-shear void ratio	Final Water content %	Final void ratio
3	30	3.03	1.54	1.43	1.24	0.50	23.5	1.35	39.8	1.19
2	20	3.03	1.59	1.36	1.29	0.53	23.5	1.22	39.8	1.02
1	10	3.03	1.43	1.62	1.16	0.44	23.5	1.37	39.8	1.26

Sample 14: Completely Weathered to Residual Soil Onekaka Schist

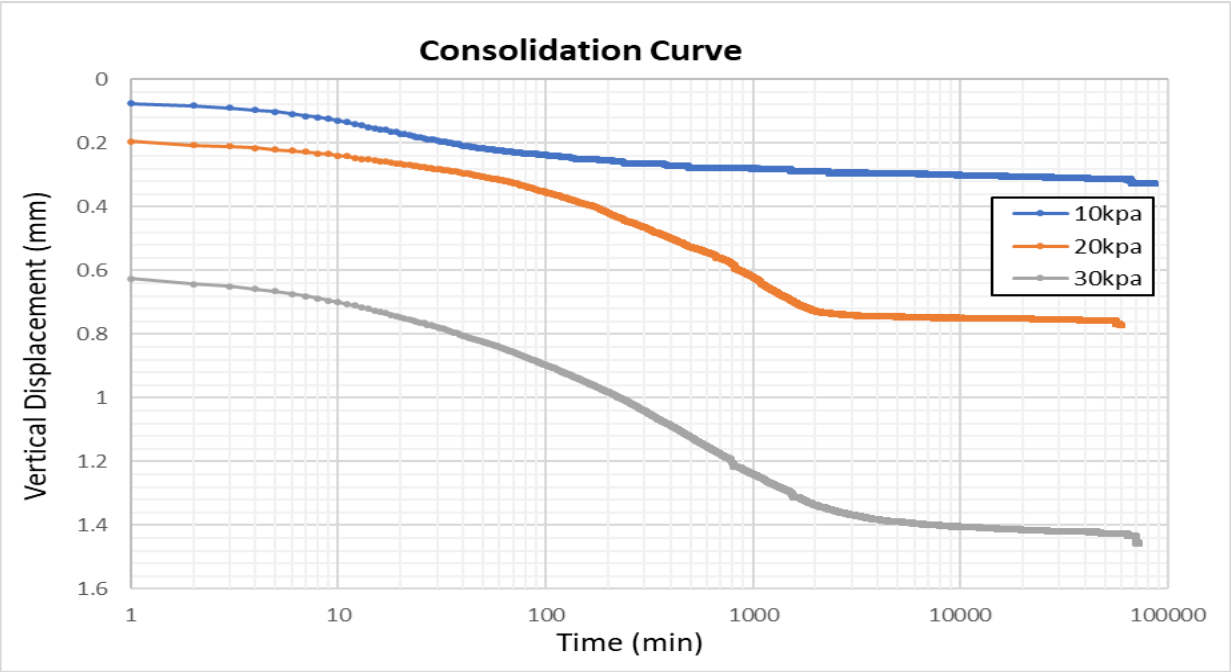

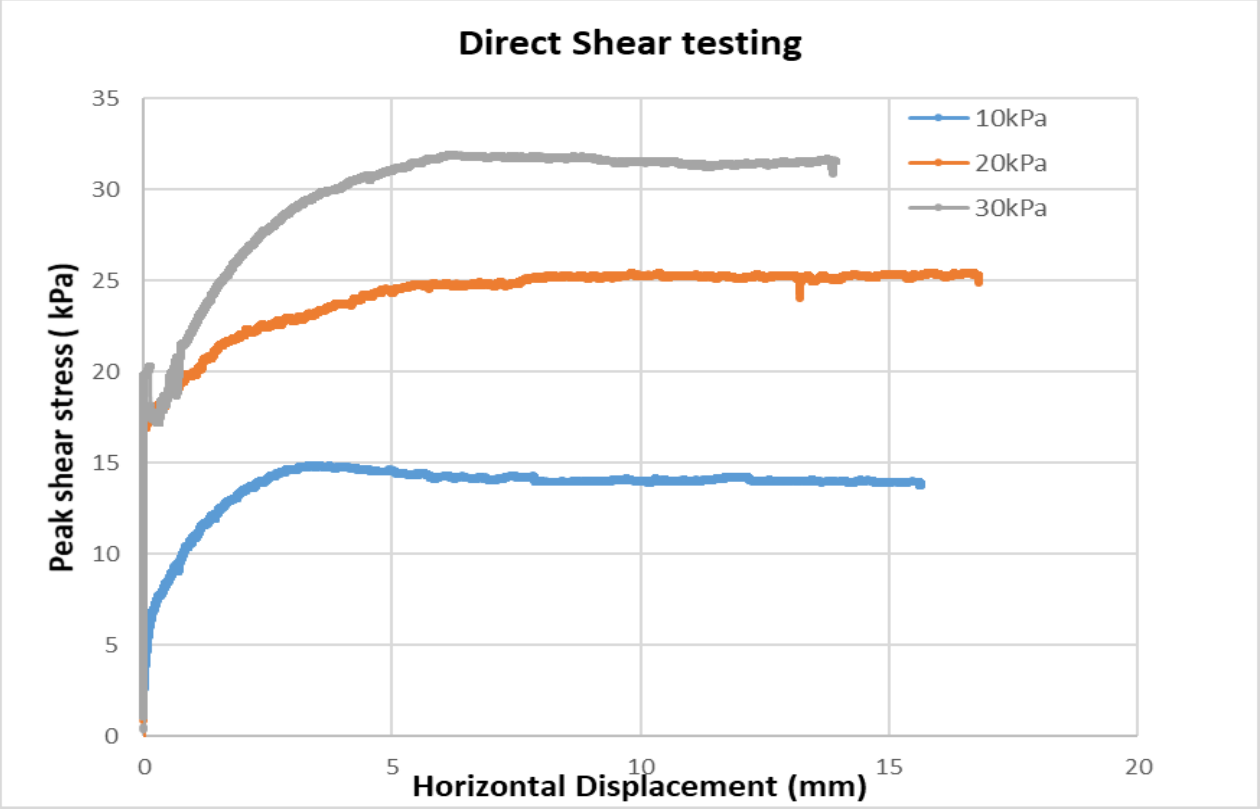

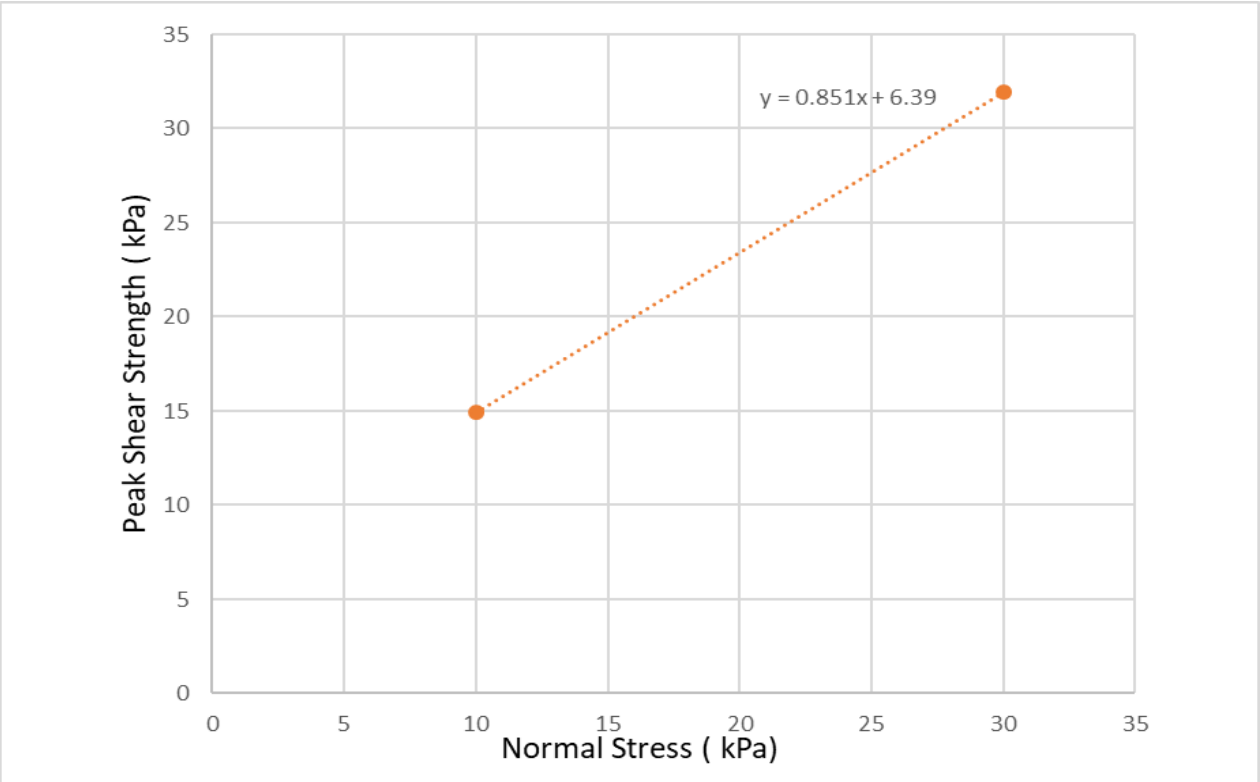

Specie-men no.	Normal stress (kPa)	Specific Gravity	Bulk density (t/m3)	Initial void ratio	Initial dry density (t/m3)	Degree of saturation	Initial water content %	Pre-shear void ratio	Final Water content %	Final void ratio
3	30	3.05	1.23	2.26	0.94	0.42	30.8	2.06	33.7	1.98
2	20	3.05	1.46	1.73	1.12	0.54	30.8	1.65	33.7	1.60
1	10	3.05	1.29	2.10	0.98	0.45	30.8	2.06	33.7	2.05

Appendix B.4 Ring Shear

Introduction

Residual shear strength was conducted using ring shear apparatus (Figure B.4.1). This apparatus measures residual shear strength on remoulded soil (silt and clay). The angular ring shape specimen has a thickness of 5mm. The ring shear test was conducted with accordance to BS1377: Part 7 1990. The test was run under 3 different loads of 2kg, 3kg and 4kg which is equivalent to 52 kPa, 76 kPa and 100 kPa.

Figure B.5.1: Ring Shear setup for residual shear strength

The normal stress was calculated using:

Normal stress, $\sigma'_n = \frac{torque\ arm\ mass + (mass\ on\ hanger \times 10) \times 9.806}{Sample\ area \times 1000}$ Equation (3)

Where: torque arm mass = 1.55kg

: Sample area= 4.006×10^{-3} m^2

The residual shear stress was calculated using:

$\tau_r = \frac{3 \times \mathrm{Pr} \times L}{2\pi(R_2^3 - R_1^3)}$ Pa Equation (4)

Where P_r=average residual force in N

L= distance between the load cell points (0.15m for outer position)

R_2=outer radius of sample=0.05m

R_1=inner radius of sample=0.035m

From the three different normal stress, a graph was plotted of the residual shear stress versus normal stress and a line of best fit was drawn. It is assumed that the effective residual cohesion c'_r=0.

From the relationship: $\tau_r = c'_r + \sigma'_n \tan \phi'_r$ Equation (5)

Where ϕ'r is the effective residual friction angle and is represented by the slope of the graph.

Pre-2018 debris flow deposit (soil sample)

Table B.4.1: Sample 6, summarized ring shear test data

Sample	6
Bedrock	SPG
Shear rate	0.35mm/min
Ring Shear	
Normal	**Shear**
0.0	0.0
51.7	28.6
76.2	43.6
100.7	48.0
Moisture Content (%)	
Before test	16.1
After test	66.6
residual friction angle	27.4

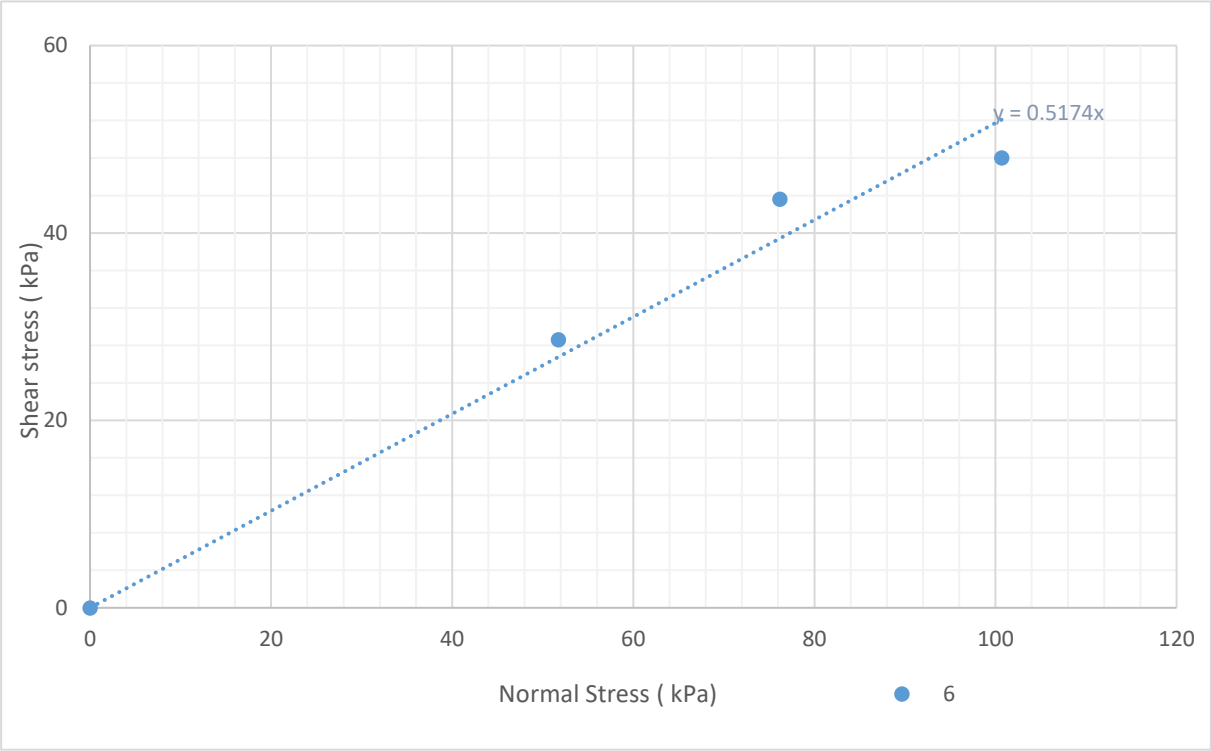

Figure B.4.2: residual shear stress versus normal stress, sample 6

Table B.4.2: Sample 7 summarised ring shear data

Sample	7
Bedrock	SPG
Shear rate	0.35 mm/min
Ring Shear	
Normal	Shear
0.0	0.0
51.7	30.1
76.2	45.3
100.7	53.1
Moisture Content (%)	
Before test	26.0
After test	49.4
residual friction angle	27.6

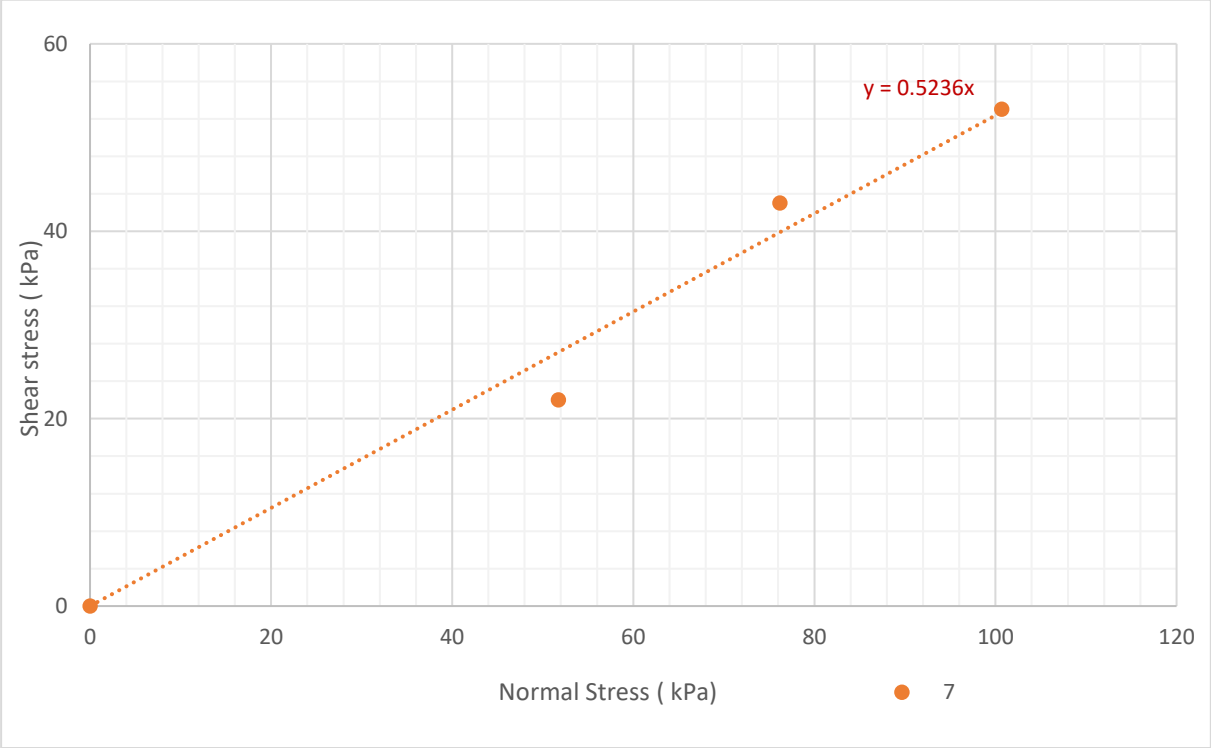

Figure B.4.3: residual shear stress versus normal stress, sample 7

Table B.4.3: Sample 16 summarised ring shear data

Sample	16
Bedrock	URIC
Shear rate	0.35 mm/min
Ring Shear	
Normal	Shear
0.0	0.0
51.7	24.2
76.2	26.2
100.7	46.3
Moisture Content (%)	
Before test	35.6
After test	40.6
residual friction angle	22.8

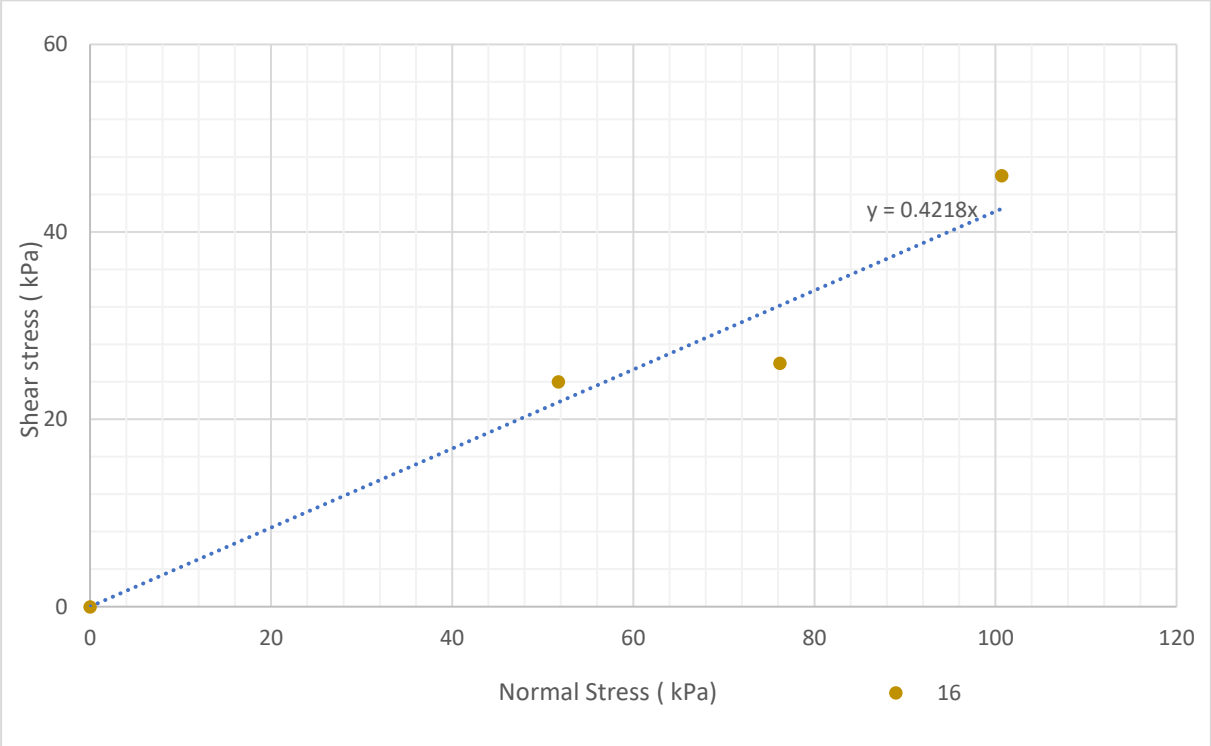

Figure B.4.4: residual shear stress versus normal stress, sample 16

2018 (Gita) soil sample

Table B.4.4: Sample 2 summarised ring shear data

Sample	2
Bedrock	SPG
Shear rate	0.02 mm/min
Ring Shear	
Normal	Shear
0.0	0.0
51.7	26.4
76.2	40.5
100.7	50.8
Moisture Content (%)	
Before test	20.5
After test	40.3
residual friction angle	27.2

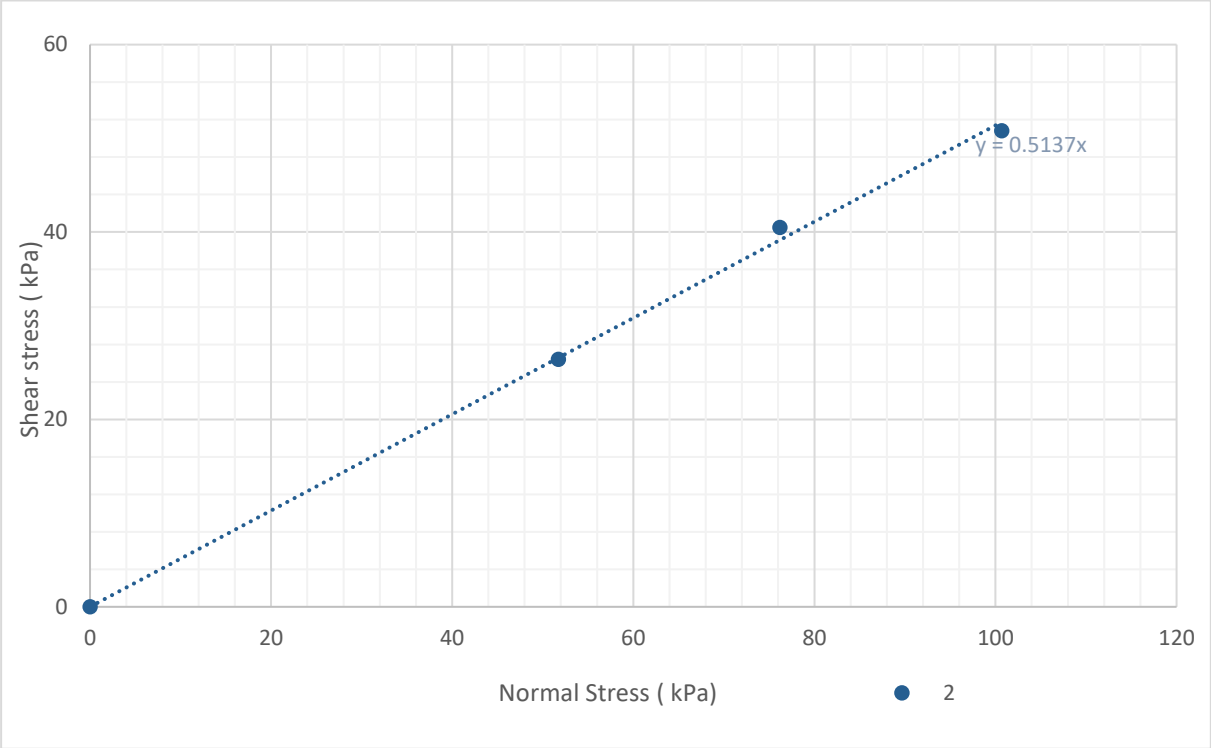

Figure B.4.5: residual shear stress versus normal stress, sample 2

Table B.4.5: sample 8 summarised ring shear data. Shear rate: 0.035616 mm/min

Sample	8
Bedrock	URIC
Shear rate	0.35 mm/min
Ring Shear	
Normal	Shear
0.0	0.0
51.7	27.0
76.2	36.0
100.7	50.0
Moisture Content (%)	
Before test	33.7
After test	39.0
residual friction angle	26.2

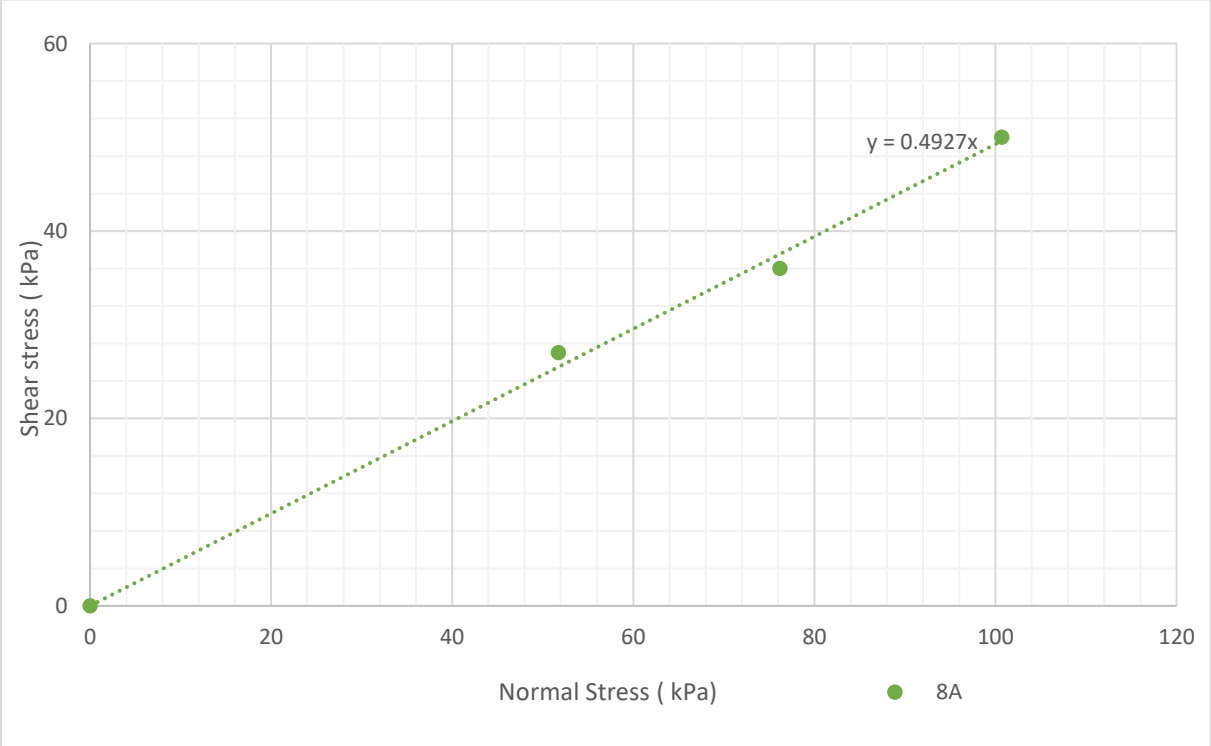

Figure B.4.6: residual shear stress versus normal stress, sample 8

Table B.4.6: sample 8 summarised ring shear data. Shear rate: 0.02mm/min

Sample	8
Bedrock	URIC
Shear rate	0.02 mm/min
Ring Shear	
Normal	Shear
0.0	0.0
51.7	22.3
76.2	36.1
100.7	43.4
Moisture Content (%)	
Before test	33.7
After test	40.3
residual friction angle	23.8

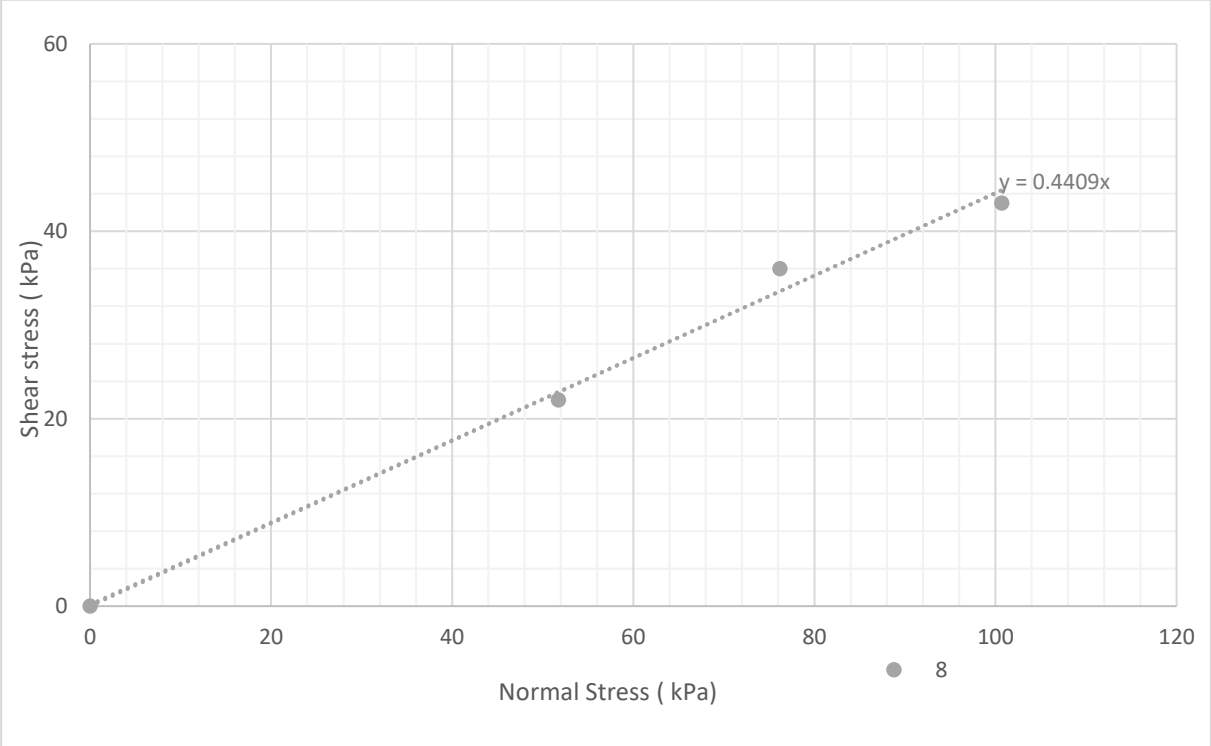

Figure B.4.7: residual shear stress versus normal stress, sample 8.

Table B.4.7: Sample 13 summarised ring shear data. Shear rate: 0.35 mm/min

Sample	13
Bedrock	OS
Shear rate	0.35 mm/min
Ring Shear	
Normal	Shear
0.0	0.0
51.7	29.3
76.2	42.1
100.7	51.2
Moisture Content (%)	
Before test	35.0
After test	43.1
residual friction angle	26.7

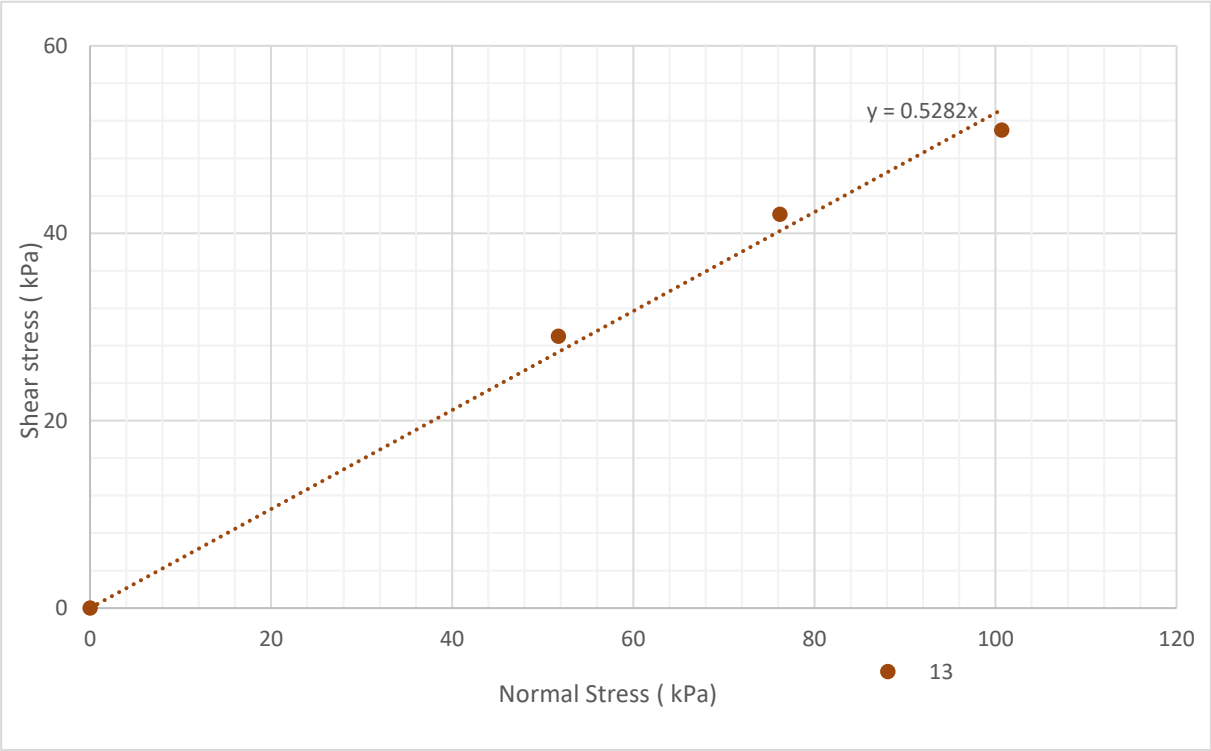

Figure B.4.8: residual shear stress versus normal stress, sample 13

Table B.4.8: sample 13summarised ring shear data. Shear rate: 0.01708 mm/min

Sample	13
Bedrock	OS
Shear rate	0.02 mm/min
Ring Shear	
Normal	Shear
0	0
51.7	23
76.2	31
100.7	41
Moisture Content (%)	
Before test	26.5
After test	36.7
residual friction angle	22.4

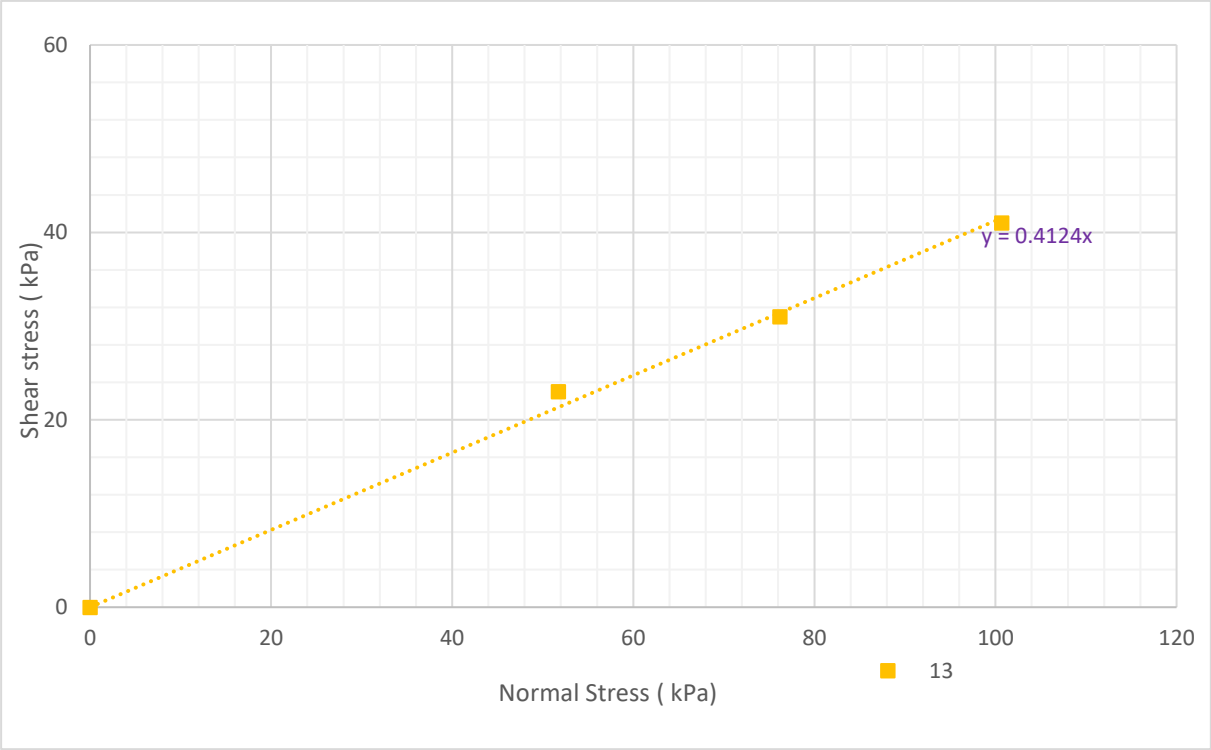

Figure B.4.9: residual shear stress versus normal stress, sample 13

Appendix C: Rock Laboratory Testing

Appendix C.1 UCS

Apparatus

The loading frame used to conduct Uniaxial (Unconfined) compressive strength was a tecnotest, Machine series: KE300/ECE.

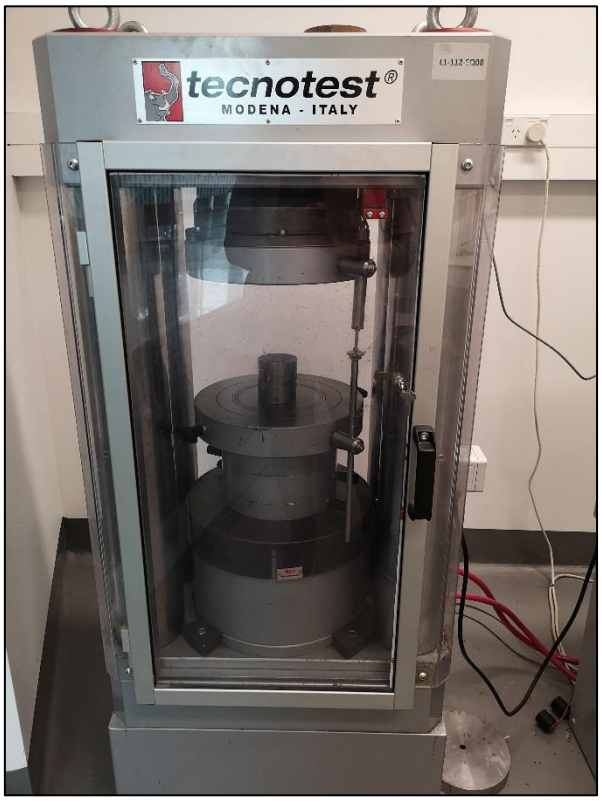

Figure C.1.1: Photograph of the UCS test apparatus

Results

The first graph for each specimen shows stress versus time relationship and second graph shows strain gauge analysis (axial and radial strain).

Specimen 9v

Note: The maximum stress data has been corrected as the specimen didn't meet the length to diameter ratio

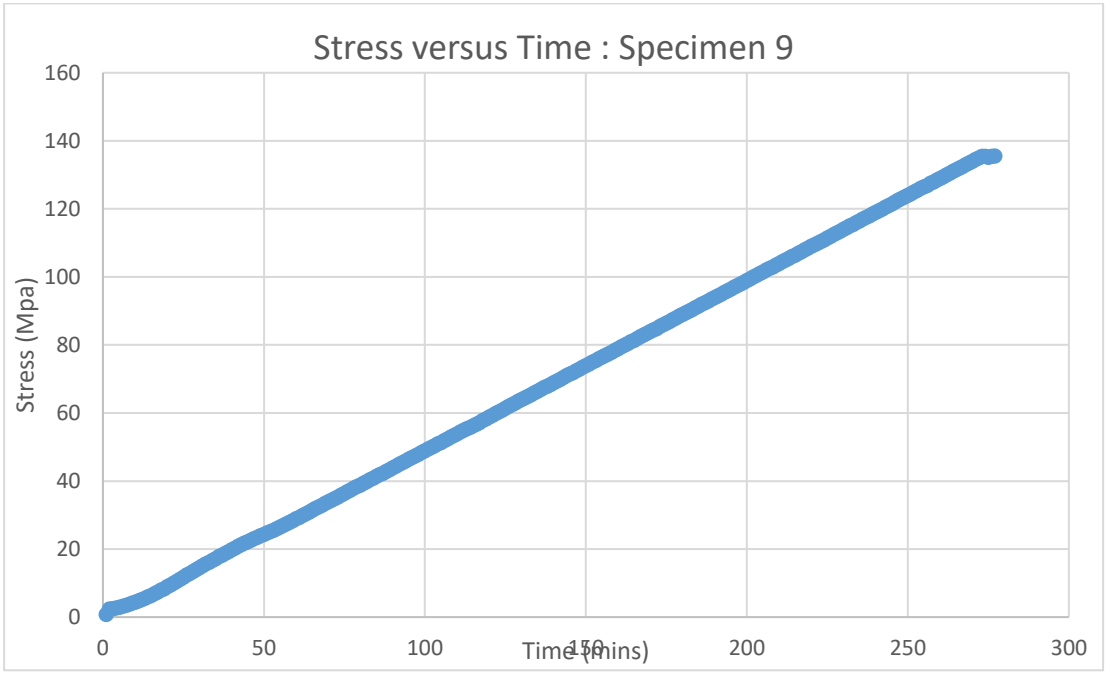

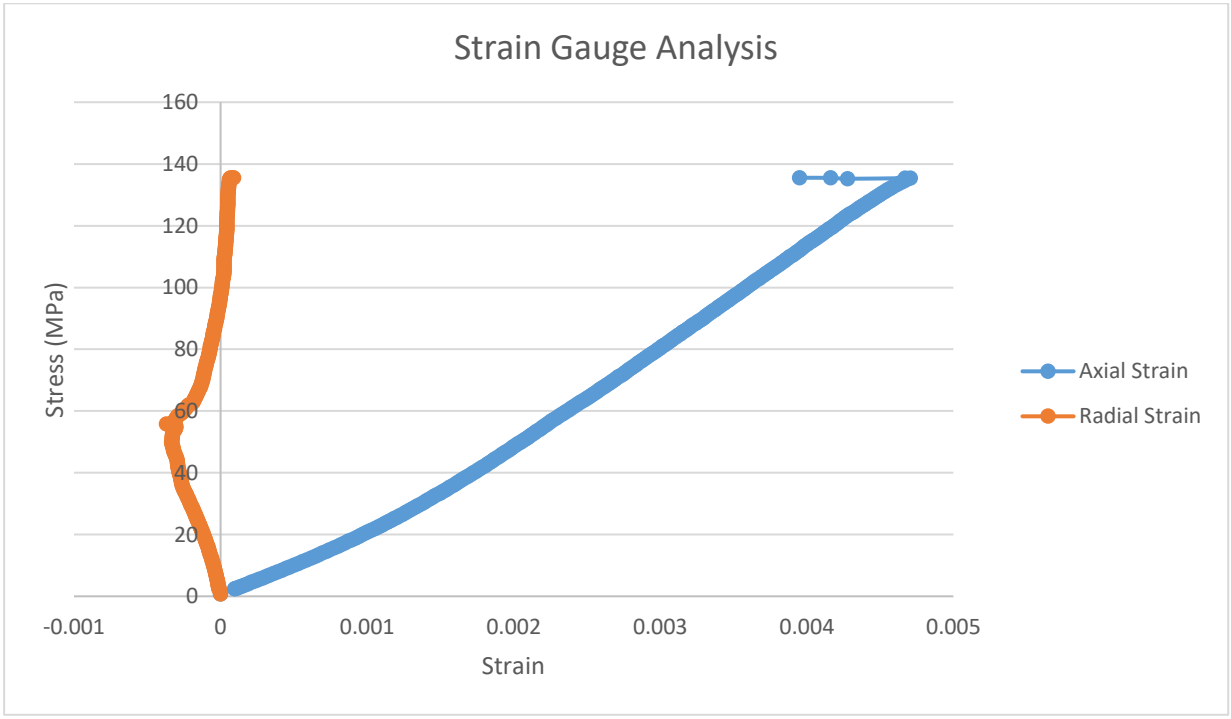

Specimen 11i:

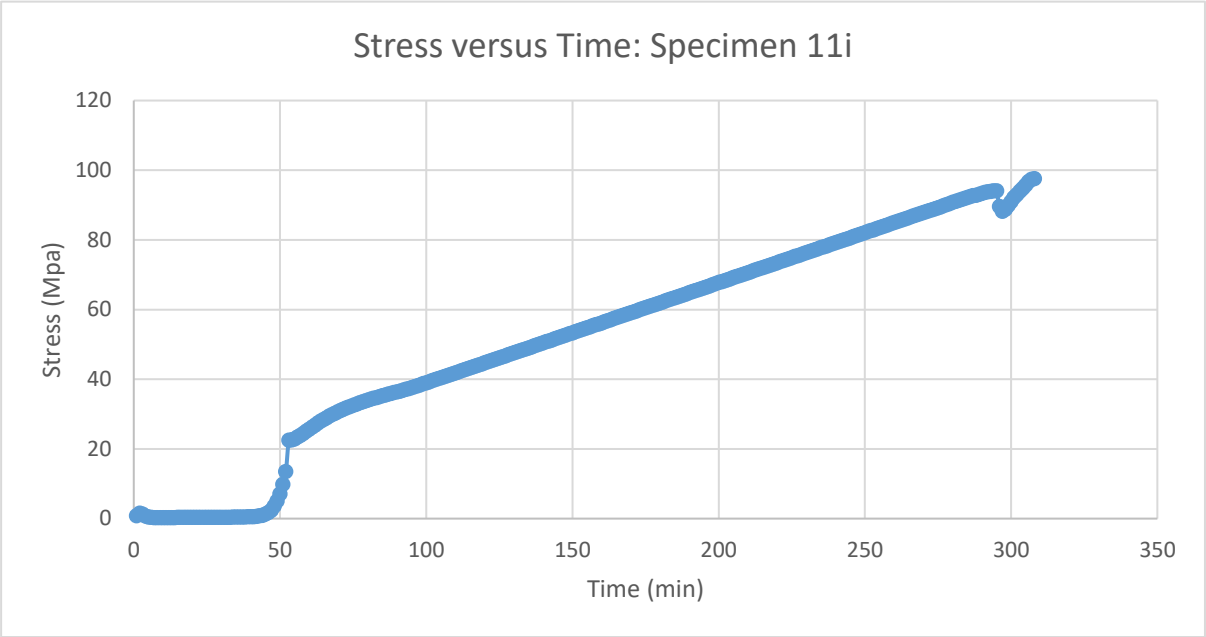

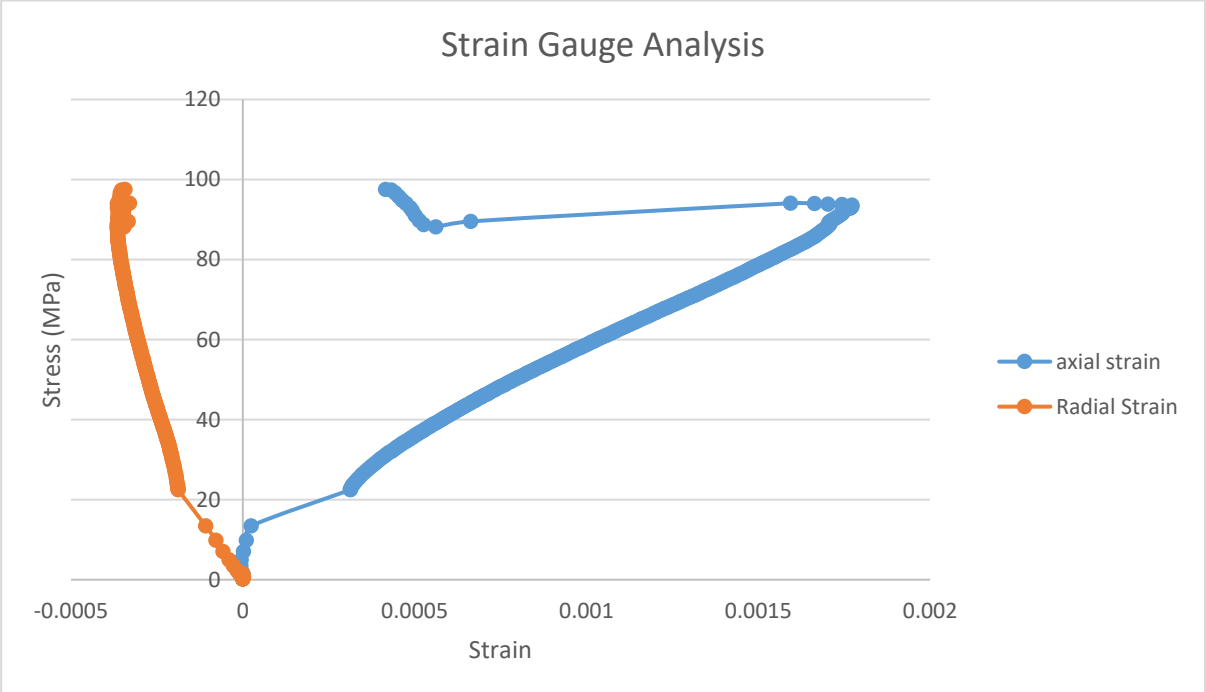

Specimen 13i:

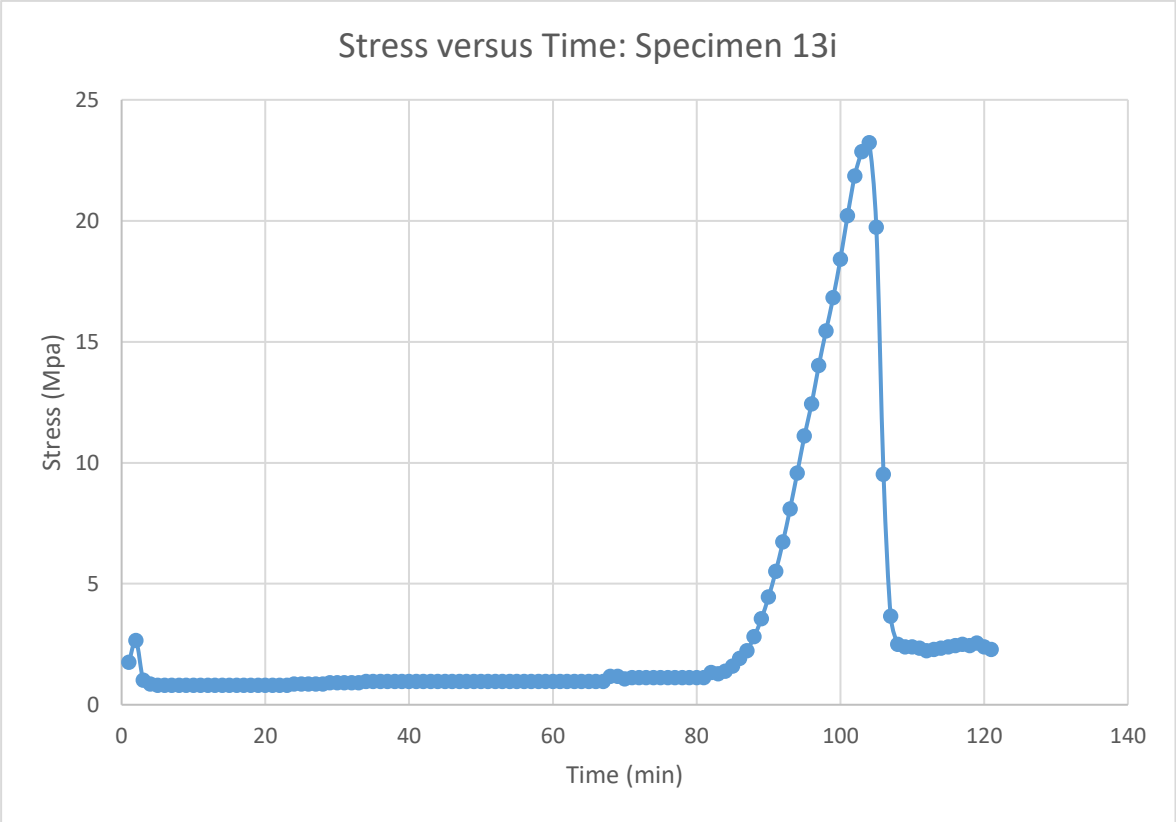

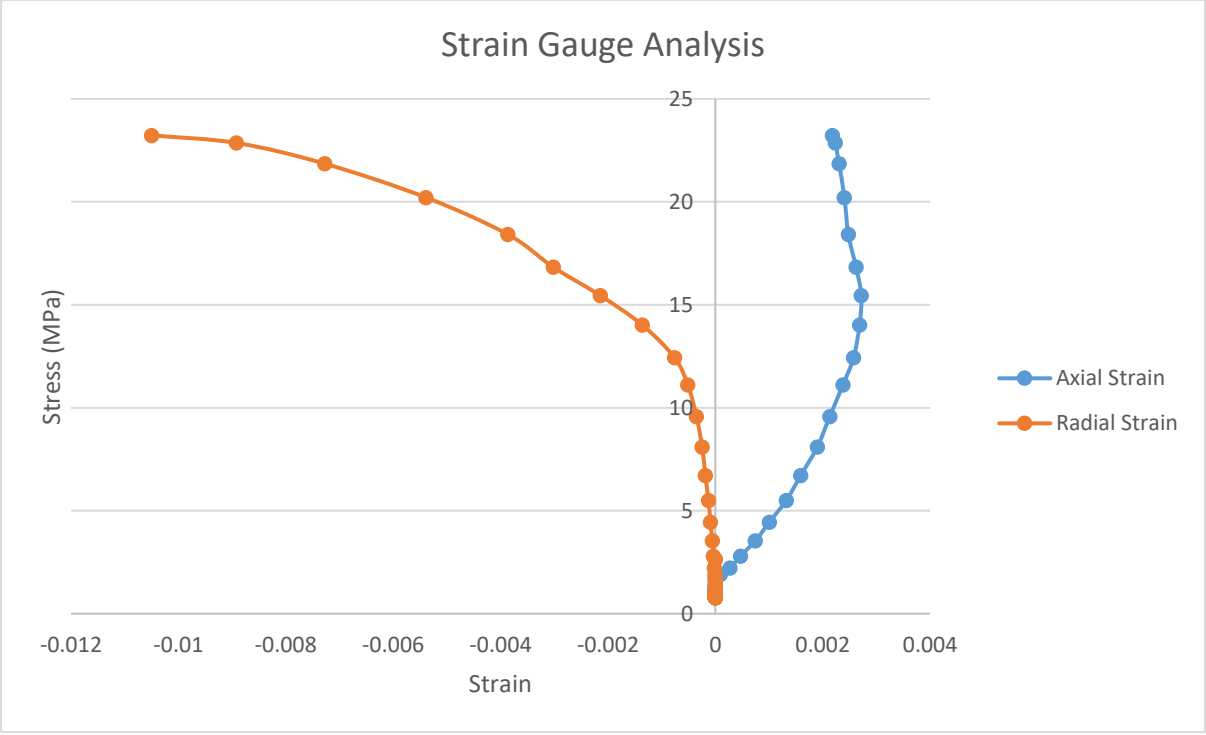

Appendix C.2 Point Load results

Apparatus

The loading frame used to conduct point load test was point load tester by Geotechnical Systems Australia, model 6500. It is a portable apparatus.

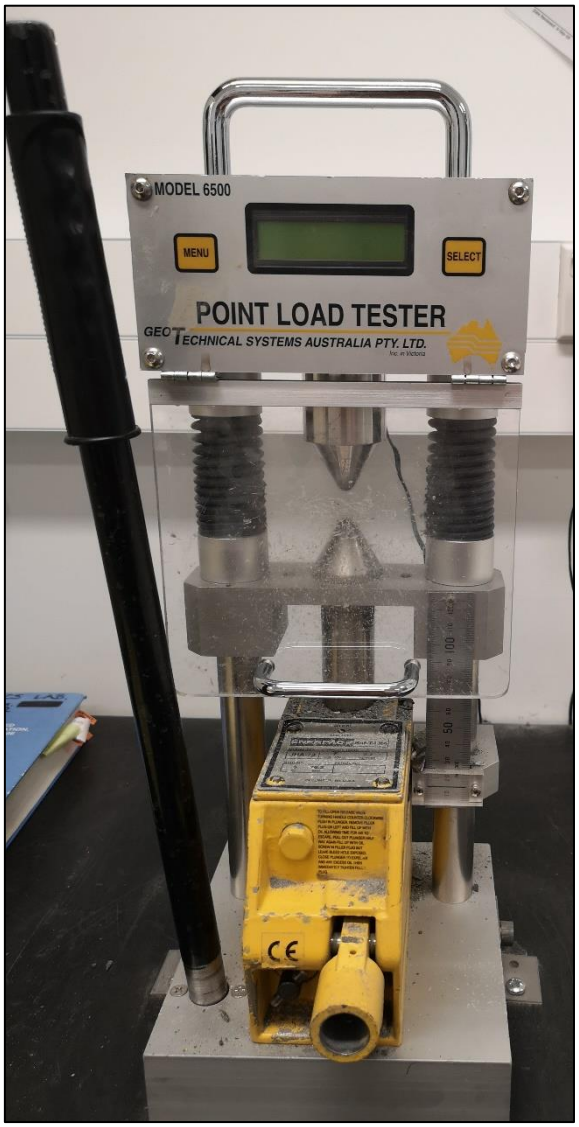

Figure C.2. 1: Photograph of Point load tester apparatus.

Site	6i										
Depth	20.3										
Material	Quartzite	fine grained	Slightly Weathered								
Test No.	**Type**	**Type**	**P (kN)**	**D (mm)**	**W (mm)**	**A = WD (mm^2)**	**D_e^2**	**D_e**	**I_s**	**F**	**$I_{s(50)}$ (MPa)**
1	L	r	9	45	65	2925	3724	61	2.42	1.094	2.64
2	L	r	6	46	41	1886	2401	49	2.5	0.991	2.48
3	L	r	14.94	33	28.75	949	1208	34.8	12.37	0.849	10.5
4	L	r	16.14	29	38.5	1117	1422	37.7	11.35	0.881	10
5	L	r	10.22	37	44	1628	2073	45.5	4.93	0.959	4.73
6	L	r	16.58	36	42	1512	1925	43.9	8.61	0.943	8.12
7	L	r	7.41	33	35.5	1172	1492	38.6	4.97	0.89	4.42
8	L	r	8.06	23	42.5	978	1245	35.3	6.48	0.855	5.54
9	L	r	7.59	19	38.5	732	931	30.5	8.15	0.801	6.53
10	L	r	4.47	22	20	440	560	23.7	7.98	0.714	5.7
Rejecting 2lowest and 2 highest results, the mean Is(50) =											**5.84**
i=	irregular lump								UCS	24xIs(50)	140.2
d=	diametral										
a=	axial										
⊥	perpendicular										
//	parallel										
r	random orientation										

Site	6i										
Depth	21.05										
Material	SPG	coarse grained	Slightly Weathered								
Test No.	**Type**	**Type**	**P (kN)**	**D (mm)**	**W (mm)**	**A = WD(mm^2)**	**D_e^2**	**D_e**	**I_s**	**F**	**$I_{s(50)}$ (MPa)**
1	a	r	1.26	36	61	2196	2796.03	52.88	0.45	1.03	0.46
2	a	r	0.54	53	62.4	3307.2	4210.86	64.89	0.13	1.12	0.14
3	a	r	2.08	52	64	3328	4237.34	65.09	0.49	1.13	0.55
4	i	r	5.3	54	55	2970	3781.52	61.49	1.40	1.10	1.54
5	i	r	3.98	30	52	1560	1986.25	44.57	2.00	0.95	1.90
6	i	r	5.66	29	41.5	1203.5	1532.34	39.15	3.69	0.90	3.31
7	i	r	0.66	34	46	1564	1991.35	44.62	0.33	0.95	0.31
8	i	r	2.77	23	40.35	928.05	1181.63	34.37	2.34	0.84	1.98
9	i	r	1.44	25	37.41	935.25	1190.80	34.51	1.21	0.85	1.02
10	i	r	7.36	28	40.6	1136.8	1447.42	38.04	5.08	0.88	4.50
11	i	r	1.41	29	32.63	946.27	1204.83	34.71	1.17	0.85	0.99
12	i	r	1.34	15.5	38.5	596.75	759.81	27.56	1.76	0.76	1.35
13	i	r	1.93	18	31.54	567.72	722.84	26.89	2.67	0.76	2.02
Rejecting 2lowest and 2 highest results, the mean Is(50) =											**1.31**
									UCS	24xIs(50)	31.5
i=	Irregular lump										
d=	diametral										
a=	axial										
⊥	perpendicular										
//	parallel										
r	random orientation										

Sample details	Site 6i										
	Depth:21.6										
	SPG	coarse grained		Highly Weathered							
Test No.	**Type**	**Type**	**P (kN)**	**D (mm)**	**W (mm)**	**A = WD (mm2)**	**De2**	**De**	**Is**	**F**	**Is(50) (MPa)**
1	a	r	0.15	49	83	4067	5178.27	71.96	0.03	1.18	0.03
2	a	r	0.04	42	81	3402	4331.56	65.81	0.01	1.13	0.01
3	i	r	0.04	44	73.8	3247.2	4134.46	64.30	0.01	1.12	0.01
4	i	r	0.08	25	46	1150	1464.23	38.27	0.05	0.89	0.05
5	i	r	0.17	23	50	1150	1464.23	38.27	0.12	0.89	0.10
6	i	r	0.16	19	50	950	1209.58	34.78	0.13	0.85	0.11
7	i	r	0.06	15	50	750	954.93	30.90	0.06	0.81	0.05
8	i	r	0.04	20	55	1100	1400.56	37.42	0.03	0.88	0.03
9	i	r	0.1	30	45	1350	1718.87	41.46	0.06	0.92	0.05
10	i	r	0.09	20	44	880	1120.45	33.47	0.08	0.83	0.07
Rejecting lowest and highest results, the mean Is(50) =											**0.05**
									UCS	24xIs(50)	1.2
i=	irregular lump										
d=	diametral										
a=	axial										
⊥	perpendicular										
//	parallel										
r	random orientation										

Sample details	Site 7i Depth:7.6 URC	medium grained		Slightly Weathered						
Test No.	**Type**	**Type**	**P (kN)**	**D (mm)**	**W (mm)**	**A = WD (mm2)**	**De2**	**De**	**Is**	**F**	**Is(50) (MPa)**
1	a	r	4.53	15.0	32	480	611	24.7	7.41	0.728	5.40
2	a	r	8.34	23.5	36.545	859	1093	33.1	7.63	0.830	6.33
3	i	r	7.51	20.0	46.035	921	1172	34.2	6.41	0.843	5.40
4	i	r	8.06	19.0	30.75	584	744	27.3	10.83	0.761	8.25
5	i	r	9.50	18.5	55.75	1031	1313	36.2	7.23	0.865	6.26
6	i	r	16.91	29.0	36.06	1046	1331	36.5	12.70	0.868	11.02
7	i	r	6.86	18.0	28.19	507	646	25.4	10.62	0.738	7.83
8	i	r	13.54	24.0	29.11	699	890	29.8	15.22	0.793	12.06
9	i	r	5.40	18.0	28	504	642	25.3	8.41	0.736	6.20
10	i	r	6.14	20.0	25.53	511	650	25.5	9.44	0.739	6.98
Rejecting lowest and highest results, the mean Is(50) =											**6.97**
									UCS	Is(50)*24	167.4
Rejecting lowest and highest results, the mean Is(50) =											
i=	irregular lump										
d=	diametral										
a=	axial										
⊥	perpendicular										
//	parallel										
r	random orientation										

Sample details	Site 7i Depth:7.7m URC	medium grained		Slightly Weathered						
Test No.	**Type**	**Type**	**P (kN)**	**D (mm)**	**W (mm)**	**A = WD (mm2)**	**De2**	**De**	**Is**	**F**	**Is(50) (MPa)**
1	d	r	9.68	60.00			3600.00		1.09	1.09	2.92
2	d	r	25.56	58.00			3364.00		1.07	1.07	8.12
3	a	r	6.77	39.00	69.67	2717.13	3459.56	58.82	1.96	1.08	2.11
4	a	r	3.52	22.00	46.42	1021.24	1300.28	36.06	2.71	0.86	2.34
5	i	r	5.75	19.00	43.50	826.50	1052.33	32.44	5.46	0.82	4.50
6	i	r	10.68	31.00	56.50	1751.50	2230.08	47.22	4.79	0.97	4.67
7	i	r	12.10	35.00	45.50	1592.50	2027.63	45.03	5.97	0.95	5.69
8	i	r	7.86	30.00	39.63	1188.75	1513.56	38.90	5.19	0.89	4.64
9	i	r	3.83	23.00	32.90	756.70	963.46	31.04	3.98	0.81	3.21
10	i	r	2.43	19.50	27.50	536.25	682.77	26.13	3.56	0.75	2.66
11	i	r	3.60	17.50	34.63	605.94	771.50	27.78	4.67	0.77	3.58
12	i	r	3.91	24.50	32.61	798.95	1017.25	31.89	3.84	0.82	3.14
13	i	r	1.41	23.00	26.20	602.49	767.11	27.70	1.84	0.77	1.41
14	i	r	3.00	21.00	27.53	578.03	735.96	27.13	4.08	0.76	3.10
Rejecting lowest and highest results, the mean Is(50) =											**3.47**
i=	irregular lump								UCS	Is(50)*24	83.3
d=	diametral										
a=	axial										
⊥	perpendicular										
//	parallel										
r	random orientation										

Sample details	Site 7i										
	Depth:8.25m										
	URC	medium grained		Slightly Weathered							
Test No.	**Type**	**Type**	**P (kN)**	**D (mm)**	**W (mm)**	**A = WD (mm2)**	**De2**	**De**	**Is**	**F**	**Is(50) (MPa)**
1	a	r	1.19	37.0	37.5	1388	1767	42.0	0.67	0.925	0.62
2	a	r	11.51	41.0	52.5	2153	2741	52.4	4.20	1.021	4.29
3	i	r	6.54	26.0	24.5	637	811	28.5	8.06	0.776	6.26
4	i	r	3.09	28.0	31.5	882	1123	33.5	2.75	0.835	2.30
5	i	r	0.53	26.0	75	1950	2483	49.8	0.21	0.998	0.21
6	i	r	6.02	17.0	38	646	823	28.7	7.32	0.779	5.70
7	i	r	2.17	15.0	36	540	688	26.2	3.16	0.748	2.36
8	i	r	4.78	15.0	36.7	551	701	26.5	6.82	0.751	5.12
9	i	r	1.88	16.0	35	560	713	26.7	2.64	0.754	1.99
10	i	r	0.76	25.0	38	950	1210	34.8	0.63	0.849	0.53
Rejecting lowest and highest results, the mean Is(50) =											**2.78**
									UCS	Is(50)*24	66.7
Rejecting lowest and highest results, the mean Is(50) =											
i=	irregular lump										
d=	diametral										
a=	axial										
⊥	perpendicular										
//	parallel										
r	random orientation										

Sample details	Site 9v										
	Depth:13.5m										
	URC	medium grained		Moderately Weathered							
Test No.	**Type**	**Type**	**P (kN)**	**D (mm)**	**W (mm)**	**A = WD (mm2)**	**De2**	**De**	**Is**	**F**	**Is(50) (MPa)**
1	d	r	2.32	76.00			5776.00		0.40	1.21	0.48
2	d	r	1.67	39.00	82.00	3198.00	4071.82	63.81	0.41	1.12	0.46
3	a	r	0.61	52.00	82.00	4264.00	5429.09	73.68	0.11	1.19	0.13
Rejecting lowest and highest results, the mean Is(50) =											**0.47**
i=	irregular lump								UCS	Is(50)*24	11.3
d=	diametral										
a=	axial										
⊥	perpendicular										
//	parallel										
r	random orientation										

*Note: only 3 tests possible: 0.13 seemed to be an outlier and was excluded from the average.

Sample details	Site 11i										
	Depth:15.5m										
	URC	medium grained		Highly Weathered							
Test No.	**Type**	**Type**	**P (kN)**	**D (mm)**	**W (mm)**	**A = WD (mm2)**	**De2**	**De**	**Is**	**F**	**Is(50) (MPa)**
1	a	r	0.24	46.0	81.14	3732	4752	68.9	0.05	1.155	0.06
2	a	r	0.15	59.0	82.83	4887	6222	78.9	0.02	1.228	0.03
3	i	r	0.11	36	82	2952.00	3758.60	61.31	0.03	1.10	0.03
4	i	r	0.1	22	45	990.00	1260.51	35.50	0.08	0.86	0.07
5	i	r	0.11	25	36	900.00	1145.92	33.85	0.10	0.84	0.08
6	i	r	0.1	23	44	1012.00	1288.52	35.90	0.08	0.86	0.07
7	i	r	0.13	19	38	722.00	919.28	30.32	0.14	0.80	0.11
8	i	r	0.14	25	43	1075.00	1368.73	37.00	0.10	0.87	0.09
9	i	r	0.1	17	31.3	532.10	677.49	26.03	0.15	0.75	0.11
10	i	r	0.05	18	35	630.00	802.14	28.32	0.06	0.77	0.05
			0.11	25	39	975.00	1241.41	35.23	0.09	0.85	0.08
			0.09	18	50	900	1145.92	33.85	0.08	0.84	0.07
Rejecting lowest and highest results, the mean Is(50) =											0.08
									UCS	Is(50)*24	1.92
i=	irregular lump										
d=	diametral										
a=	axial										
⊥	perpendicular										
//	parallel										
r	random orientation										

Sample details	Site 13i										
	Depth:25.8m										
	URC	medium grained		Slightly Weathered							
Test No.	**Type**	**Type**	**P (kN)**	**D (mm)**	**W (mm)**	**A = WD (mm2)**	**De2**	**De**	**Is**	**F**	**Is(50) (MPa)**
1	a	//	1.72	21.0	82.95	1742	2218	47.1	0.78	0.973	0.75
2	a	//	2.62	33.5	82.95	2779	3538	59.5	0.74	1.081	0.80
3	i	//	1.63	33.5	71.165	2384	3035	55.1	0.54	1.045	0.56
4	i	//	1.62	33.0	45.545	1503	1914	43.7	0.85	0.942	0.80
5	i	//	1.89	20.5	42.65	874	1113	33.4	1.70	0.834	1.42
6	i	//	1.37	21.0	38.47	808	1029	32.1	1.33	0.819	1.09
7	i	//	0.24	20.0	54.1	1082	1378	37.1	0.17	0.875	0.15
8	i	//	0.58	33.0	51.575	1702	2167	46.6	0.27	0.968	0.26
9	i	//	1.04	20.0	58.21	1164	1482	38.5	0.70	0.889	0.62
10	i	//	2.39	32	43.005	1376.16	1752.18	41.86	1.36	0.92	1.26
11	i	//	0.7	21	28.035	588.74	749.60	27.38	0.93	0.76	0.71
Rejecting lowest and highest results, the mean Is(50) =											0.86
									UCS	Is(50)*24	20.6
i=	irregular lump										
d=	diametral										
a=	axial										
⊥	perpendicular										
//	parallel										
r	random orientation										

Site	Road cut										
Depth											
Material	SPG	coarse grained		Slightly weathered							
Test No.	**Type**	**Type**	**P (kN)**	**D (mm)**	**W (mm)**	**A = WD (mm2)**	**De2**	**De**	**Is**	**F**	**Is(50) (MPa)**
1	i	r	8.5	35.00	56.31	1970.85	2509.36	50.09	3.39	1.00	3.39
2	i	r	2.22	26.00	56.90	1479.40	1883.63	43.40	1.18	0.94	1.11
3	i	r	4.9	52.50	68.10	3575.25	4552.15	67.47	1.08	1.14	1.23
4	i	r	0.89	25.00	36.39	909.75	1158.33	34.03	0.77	0.84	0.65
5	i	r	2.71	20.00	36.78	735.60	936.60	30.60	2.89	0.80	2.32
6	i	r	1.61	25.00	35.00	875.00	1114.08	33.38	1.45	0.83	1.20
7	i	r	0.7	30.00	33.00	990.00	1260.51	35.50	0.56	0.86	0.48
8	i	r	2.02	29.00	30.50	884.50	1126.18	33.56	1.79	0.84	1.50
9	i	r	3.65	33.00	37.00	1221.00	1554.63	39.43	2.35	0.90	2.11
10	i	r	1.26	24.00	27.00	648.00	825.06	28.72	1.53	0.78	1.19
Rejecting 2lowest and 2 highest results, the mean Is(50) =											1.59
i=	irregular lump								ucs	24xIs(50)	38.2
d=	diametral										
a=	axial										
⊥	perpendicular										
//	parallel										
r	random orientation										

Site	channel 1										
Depth											
Material	SPG	medium grained		Moderately weathered							
Test No.	**Type**	**Type**	**P (kN)**	**D (mm)**	**W (mm)**	**A = WD (mm2)**	**De2**	**De**	**Is**	**F**	**Is(50) (MPa)**
1	i	r	0.36	36.00	38.47	1384.92	1763.33	41.99	0.20	0.92	0.19
2	i	r	0.24	29.00	42.00	1218.00	1550.81	39.38	0.15	0.90	0.14
3	i	r	0.7	35.00	54.95	1923.25	2448.76	49.48	0.29	1.00	0.28
4	i	r	0.74	36.00	40.00	1440.00	1833.46	42.82	0.40	0.93	0.38
5	i	r	0.29	26.00	51.70	1344.20	1711.49	41.37	0.17	0.92	0.16
6	i	r	0.2	29.00	37.71	1093.59	1392.40	37.31	0.14	0.88	0.13
7	i	r	0.51	35.00	36.15	1265.25	1610.97	40.14	0.32	0.91	0.29
8	i	r	0.32	39.00	43.33	1689.87	2151.61	46.39	0.15	0.97	0.14
9	i	r	0.36	26.00	40.50	1053.00	1340.72	36.62	0.27	0.87	0.23
10	i	r	0.38	25.00	42.00	1050.00	1336.90	36.56	0.28	0.87	0.25
Rejecting 2lowest and 2 highest results, the mean Is(50) =											0.21
i=	irregular lump								ucs	24x Is(50)	5.04
d=	diametral										
a=	axial										
⊥	perpendicular										
//	parallel										
r	random orientation										